Asymptotically Correct Isoenergetic Formulation of Geometrically Nonlinear Anisotropic Inhomogeneous Stiffened Plates

Doctoral Thesis

by

Anup Kumar Pathak

(2018MEZ0015)



DEPARTMENT OF MECHANICAL ENGINEERING INDIAN INSTITUTE OF TECHNOLOGY ROPAR

November, 2024

Asymptotically Correct Isoenergetic Formulation of Geometrically Nonlinear Anisotropic Inhomogeneous Stiffened Plates

A Thesis

Submitted in partial fulfillment

of the requirements for the degree of

DOCTOR OF PHILOSOPHY

by

Anup Kumar Pathak

(2018MEZ0015)



DEPARTMENT OF MECHANICAL ENGINEERING Indian Institute of Technology Ropar

November, 2024



Dedicated to

My Family and Friends

Declaration of Originality

I hereby declare that the work which is being presented in the thesis entitled **Asymp**totically Correct Isoenergetic Formulation of Geometrically Nonlinear Anisotropic Inhomogeneous Stiffened Plates has been solely authored by me. It presents the result of my own independent investigation/research conducted during the time period from January 2019 to April 2024 under the supervision of Dr. Srikant Sekhar Padhee, Assistant Professor, Department of Mechanical Engineering, Indian Institute of Technology Ropar and Dr Satwinder Jit Singh, Assistant Professor, Department of Mechanical Engineering, Indian Institute of Technology Ropar. To the best of my knowledge, it is an original work, both in terms of research content and narrative, and has not been submitted or accepted elsewhere, in part or in full, for the award of any degree, diploma, fellowship, associateship, or similar title of any university or institution. Further, due credit has been attributed to the relevant state-of-the-art collaborations (if any) with appropriate citations and acknowledgments in line with established ethical norms and practices. I also declare that any idea/data/fact/source stated in my thesis has not been fabricated/falsified/misrepresented. All the principles of academic honesty and integrity have been followed. I fully understand that if the thesis is found to be unoriginal, fabricated, or plagiarized, the Institute reserves the right to withdraw the thesis from its archive and revoke the associated Degree conferred. Additionally, the Institute also reserves the right to appraise all concerned sections of society of the matter for their information and necessary action (if any). If accepted, I hereby consent for my thesis to be available online in the Institute's Open Access repository, inter-library loan, and the title & abstract to be made available to outside organizations.

A) Patlak 13/ No1/2029

Name: Anup Kumar Pathak Entry Number: 2018MEZ0015

Program: PhD

Department: Mechanical Engineering Indian Institute of Technology Ropar

Rupnagar, Punjab 140001

Date:

Certificate

This is to certify that the thesis entitled "Asymptotically Correct Isoenergetic Formulation of Geometrically Nonlinear Anisotropic Inhomogeneous Stiffened Plates" submitted in partial fulfilment of the requirements for the award of the degree of Doctor of Philosophy to Department of Mechanical Engineering, Indian Institute of Technology Ropar, is an authentic record of the work carried out by Mr. Anup Kumar Pathak during a period from January, 2019 to November, 2024 under our supervision. The matter presented in this dissertation has not been submitted in part or full to any other University/Institute for the award of any degree.

Date 13th Nov. 2024

Dr. S.S. Padhee

Assistant Professor Department of Mechanical Engineering Indian Institute of Technology Ropar

Date 13-11-24

Dr. S.J. Singh

Assistant Professor Department of Mechanical Engineering Indian Institute of Technology Ropar

Acknowledgements

First and foremost, I would like to express my sincere gratitude to Dr. S.S. Padhee and Dr. S.J. Singh for their invaluable guidance and support throughout my doctoral studies. Their belief in my potential and their willingness to supervise my research on a challenging problem in applied mechanics are deeply appreciated.

Dr. S.S. Padhee's excellent mentorship and personal support were instrumental in my development. His expertise in solid and variational calculus proved highly beneficial. I am also grateful to Dr. S.J. Singh for providing me with a strong foundation in mathematics and continuum mechanics, which has been crucial to my research.

I would like to thank my doctoral committee members, Dr. Ekta Singhla, Dr. Prabhat Agnihotri, Dr. Rakesh Kumar Maurya, and Dr. S. Das Gupta, for their valuable suggestions and insights. Additionally, I am grateful to the other faculty and staff members of the Department of Mechanical Engineering for their support. I am also grateful to IIT Ropar for providing a platform for research.

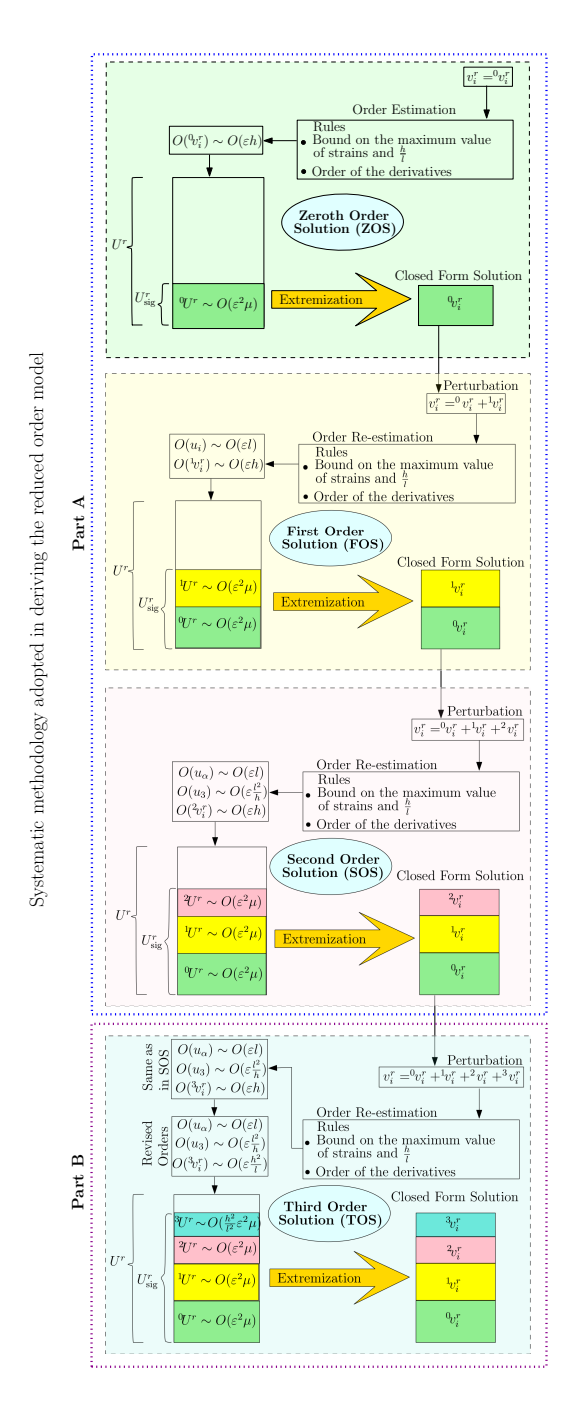
I am fortunate to have had a supportive lab environment. I thank Ajinkya Sir, Nishant Sir, Amandeep Sir, Arnav, and Josil for helping me navigate challenging workloads. My PhD journey wouldn't have been the same without my friends. Sudhendu Tiwari, Roshan, Shiva, Neeraj, Arshpreet, Himanshu, Gagan, Jasnoor and Rajat thank you for the endless memories, beautiful times, and unwavering support.

Finally, I express my heartfelt gratitude to my family. To my late grandmother, Mrs. Ramwati Pathak, for her love and support. To my parents, Mr. S.C. Pathak and Mrs. Sharda Pathak, for their unconditional love and support. To my mother-in-law, Mrs. Usha Devi, for her belief in me. To my brother-in-law, Mr. Sharad Tiwari, Mr. Ankur Shridhar, and Mr. Ankit Shridhar, for their consistent backing and encouragement. To my Sister Mrs. Alka Tiwari and my brothers Mr. Vinay Pathak and Mr. Vinod Shankar Pathak, for their constant support and encouragement. To my sister in laws Mrs. Shalini Pathak and Mrs. Shrishti Pathak for making my family complete. To my wife, Mrs. Khushbu Pathak, for her love and understanding during challenging times. To my daughters, Kavya and Ananya, and my niece Shreya and Misha and nephews Shubh, Ramcharan and Cheeku, for bringing joy and laughter into my life.

This dissertation is a culmination of the efforts and encouragement of many individuals. I am truly grateful to all of you.

Anup Kumar Pathak

Graphical Abstract



Structures with one dimension significantly smaller than the other two Single Layer Anisotropic Plate Symmetric Stiffened Plate Multilayered Composite Plate Asymmetric Stiffened Plate Functionally Graded Plate Dimension Reduction Asymptotically Correct Axiomatic through the thickness through the thickness Deformation Pattern Deformation Pattern Isoenergetic Deformed Reference plane Deformed Reference plane Outcome Outcome Modified Asymptotically Transverse Shear Force Correct ESL Plate Model Resultants Q_1 and Q_2

Simplification done using the concept of isoenergetics

Abstract

Stiffener Reinforced structures are widely used in many engineering disciplines like aerospace, marine, civil and automotive. By adding reinforcement to a structure in the form of a stiffener, the mechanical properties of the structure especially stiffness and fracture toughness are greatly improved without much increase in weight and cost. However, stiffened structures undergo a localized shift in the neutral plane due to the geometric discontinuities introduced by the stiffener. This shift necessitates careful attention when analyzing these structures.

Conducting full-scale 3D finite element analyses (FEA) for such structures can be computationally expensive, particularly during the design optimization phase. To address this computational burden, reduced-order models are often favored. The literature employs various approaches utilizing reduced-order models for plates and beams to analyze stiffened structures efficiently. However, selecting appropriate reduced-order beam and plate models is crucial, as the accuracy and efficiency of the analysis heavily rely on this selection. Furthermore, ensuring compatibility between the beam and plate models and accounting for geometric discontinuities pose challenges in accurately modeling stiffened plates. Most of the approaches found in the literature are based on ad hoc and a priory assumptions and have their own advantages and shortcomings.

This research addresses this challenge by developing a reduced-order model for the stiffened plates that captures their deformation behavior accurately with significantly reduced computational cost. The primary objective is to create a systematic and mathematically sound approach for analyzing various stiffened plate configurations, enabling efficient design optimization.

The core of the work lies in establishing an asymptotically correct reduced-order plate theory for anisotropic plates. This is achieved by leveraging variational calculus and the concept of isoenergetics. The theory was derived using first principles avoiding any ad hoc and a priory assumptions. The derived model accurately captures the deformation characteristics while significantly reducing computational complexity compared to full-scale 3D finite element analysis (FEA).

The framework developed for the single-layer anisotropic plates is then extended to handle more complex scenarios. The plate theory is modified to incorporate analysis of multilayered composite plates and functionally graded plates, reflecting real-world engineering structures with tailored properties. This allows for the analysis of plates with varying stiffness and strength profiles throughout their thickness.

Finally, the developed the developed reduced order plate theory is equipped to handle stiffened plates, a crucial component in many engineering applications. The model can analyze both symmetric and asymmetric stiffener configurations, providing valuable insights into the influence of stiffener orientation, size, and number on the overall plate behavior.

Key contributions of the present work are (a) First principles-based derivation of the reduced order 2D model from the 3D model energy (b) No dependency on the preassumed kinematics, (c) A systematic ordering scheme is employed utilizing the geometry of the structure and a bound on the maximum value of the strains. (d) The plane stress condition is a natural outcome of the present mathematical framework (e). The higher-order derivatives appearing during the dimensional reduction process were dealt with by a novel isoenergetic approach, reducing the computational complexities.

Overall, this research work presents a powerful tool for engineers by providing a mathematically rigorous and computationally efficient framework for analyzing and optimizing stiffened plates. The developed reduced order model allows for a deeper understanding of plate deformation behavior under various loading conditions, ultimately leading to improved design decisions for a diverse range of engineering applications.

Publications

Research Articles

- 1. Pathak, A. K., Singh, S. J., & Padhee, S. S. (2024). Asymptotically correct isoenergetic formulation of geometrically nonlinear anisotropic plates. Mechanics of Advanced Materials and Structures. https://doi.org/10.1080/15376494.2024.2319106
- 2. Pathak, A. K., Singh, S. J., & Padhee, S. S. Asymptotically Accurate Shear Correction Factors for Laminated Composite Plates. (Under Review)
- 3. Pathak, A. K., Singh, S. J., & Padhee, S. S. Asymptotically correct isoenergetic formulation of geometrically nonlinear Symmetric Multilayered Composite plate. (Under Review)
- 4. Pathak, A. K., Singh, S. J., & Padhee, S. S. Analysis of Functionally Graded Plates Using Novel Isoenergetic Formulation (Manuscript under preparation)
- 5. Pathak, A. K., Singh, S. J., & Padhee, S. S. Asymptotically correct isoenergetic formulation of geometrically nonlinear stiffened plates. (Manuscript under preparation)

Conference Proceedings

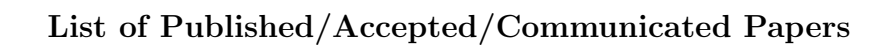
- 1. Pathak, A. K., Padhee, S. S. Asymptotically correct isoenergetic formulation of geometrically nonlinear stiffened plates. (Manuscript under production by AIP conference proceedings)
- 2. Pathak, A. K., Singh, S. J., & Padhee, S. S. An Energy based perspective into deformation of plates with anisotropic material properties. (Accepted for publication in Lecture Notes in Mechanical Engineering)

Contents

	List	of Figures xvii
	List	of Tables xxii
1	Intr	oduction 1
	1.1	Motivation
	1.2	Objective
	1.3	Literature Survey
	1.4	Outline of the Thesis
2	Asy	nptotically Correct Isoenergetic Formulation of Geometrically Non-
	line	r Anisotropic Plates 12
	2.1	Introduction
	2.2	Analytical Development
	2.3	Part A: Development of a CLPT type plate theory
		2.3.1 Order Estimation Scheme
		2.3.2 Constitutive Relations and Strain Energy
		2.3.3 Dimensional Reduction
		2.3.4 Zeroth Order Solutions (ZOS)
		2.3.5 First Order Solution (FOS)
		2.3.6 Second Order Solution (SOS)
		2.3.7 Summary of Part A
		2.3.8 Displcement Field Obtained in Part A $\dots \dots $
		2.3.9 Strains Obtained in Part A $\dots \dots $
	2.4	Part B: Refinement of Part A
		2.4.1 Third Order Solution (TOS)
		2.4.2 A Discussion on the Displacement Field
		2.4.3 A Discussion on the Strains, Stresses and Stiffness Matrix 31

	2.5	Part C: Elimination of Higher Order Derivatives	33
		2.5.1 Simplified Model Based on Isoenergetics	35
	2.6	Results and Discussion	37
	2.7	Conclusion	46
3	Asy	emptotically Accurate Geometrically Nonlinear Isoenergetic Analysis	
	of N	Aultilayered Composite plates	51
	3.1	Introduction	51
	3.2	Analytical Development	52
	3.3	Part A: Development of a reduced order model	54
		3.3.1 Order Estimation Scheme	55
		3.3.2 Constitutive Relations and Strain Energy	55
		3.3.3 Dimensional Reduction	56
		3.3.4 Zeroth Order Solutions (ZOS)	57
		3.3.5 First Order Solution (FOS)	60
		3.3.6 Second Order Solution (SOS)	63
		3.3.7 Summary of Part A	65
		3.3.8 Displcement Field Obtained in Part A	66
		3.3.9 Strains Obtained in Part A	67
	3.4	Part B: Refinement of Part A	68
		3.4.1 Third Order Solution (TOS)	68
		3.4.2 A Discussion on the Displacement Field	71
		3.4.3 A Discussion on the Strains, Stresses and Stiffness Matrix	73
	3.5	Part C: Elimination of Higher Order Derivatives	75
	3.6	Results and Discussion	77
		3.6.1 Validation of the SCFs	78
		3.6.2 Validation of the Deformation of Plates	79
	3.7	Conclusion	87
4	Ana	alysis of Functionally Graded Plates Using Novel Isoenergetic For-	
	mul	ation	90
	4.1	Introduction	90
	4.2	Analytical Formulation	92
	4.3	Part A: CLPT-type plate theory	94
		4.3.1 Ordering Scheme	94
		4.3.2 Constitutive Relations and Strain Energy	94
		4.3.3 Dimensional Reduction	05

		4.3.4 Zeroth Order Solutions (ZOS)	95
		4.3.5 First Order Solution (FOS)	
		4.3.6 Second Order Solution (SOS)	100
		4.3.7 Summary of Part A	101
		4.3.8 Displcement Field of Part A	
		4.3.9 Strains of Part A	103
	4.4	Part B: Refinement of Part A	104
		4.4.1 Third Order Solution (TOS)	104
		4.4.2 A Discussion on the Displacement Field	108
		4.4.3 A Discussion on the Strains, Stresses and	Stiffness Matrix 110
	4.5	Part C: Elimination of the Higher Order Derivative	ves
		4.5.1 Simplified Model Based on Isoenergetics	
	4.6	Results and Discussion	
		4.6.1 Material Gradation-1	
		4.6.2 Material Gradation-2	
	4.7	Conclusion	
5	Ana	alysis of Stiffened Plates	127
	5.1	Introduction	
	5.2	Methodology Used	
	5.3	Results and discussion	
	5.4	Conclusion	
6	Con	nclusion and Future Scope	139
	6.1	Summary	
	6.2	Key highlights of present work	
	6.3	Scope of Future Research	142
	Bibl	oliography	143
A	PPE	ENDICES	160
\mathbf{G}	Exp	pressions g_2, g_3, f_2 and f_3	160
н		1 32) 33) 32 - 33	
	Con	mparison of strain components	164



169

List of Figures

1.1	Decomposition of the complex $3D$ problem in through-the-thickness $1D$ problem and in-plane $2D$ problem	4
1.2	Literature summary with contribution of present work	9
1.3	Different solution approaches employed for the solution of the reduced order	
		11
2.1	Schematic of the plate deformation (a) Undeformed state (b) Deformed state	14
2.2	Systematic methodology adopted in deriving the reduced order model	24
2.3	Deformation of lines AB and CD lying along direction \hat{e}_3 and \hat{e}_1 respec-	
	tively. (a) Undeformed configuration (b) Configuration after zeroth per-	
	turbation (c) Configuration after first perturbation (d) Configuration after	
	second perturbation (e) Configuration after third perturbation	31
2.4	The isoenergetic approach	34
2.5	(a) Geometry, loading, and material orientation details for all numerical	
	examples. (b) Specific material orientation used in Example-1 ($\theta = 45^{\circ}$).	
	(c) Material orientation used in the remaining examples ($\theta = 0^{\circ}$)	38
2.6	Boundary conditions used in different numerical examples	38
2.7	Convergence plot for the out of plane deflection u_3 for Example-1 under	
	uniform Pressure of $P=25~\mathrm{kN/m^2}$ applied at the top face	39
2.8	Load-deflection curves for the central point of the plate considered in	
	Example-1 under uniform Pressure P applied at its top face $\dots \dots$	40
2.9	Load-deflection curves for the central point of the plate considered in	
	Example-2 under uniform Pressure P applied at its top face $\dots \dots$	41
2.10	Out of plane deflection of the plate considered in Example-1 along center-	
	line parallel to x_1 axis under uniform Pressure of $P=25\mathrm{kN/m^2}$ applied at	
	its top face	41

2.11	Out-of-plane deflection of the plate considered in Example-1 subjected to	
	a uniform pressure of $P=13~\rm kN/m^2$ applied on its top face. Deflections	
	are obtained using: (a) 3D Finite Element Analysis (FEA) and (b) present	
	ACI-ESL plate theory	42
2.12	Percentage error in the out of plane deflection u_3 for Example-1 under	
	uniform Pressure of $P=13~\mathrm{kN/m^2}$ applied at the top face	42
2.13	Out-of-plane deflection of the plate considered in Example-2 subjected to	
	a uniform pressure of $P = 400 \text{ kN/m}^2$ applied on its top face. Deflections	
	are obtained using: (a) 3D Finite Element Analysis (FEA) and (b) present	
	ACI-ESL plate theory.	43
2.14	Percentage error in the out of plane deflection u_3 for Example-2 under	
	uniform Pressure of $P = 400 \text{ N/m}^2$ applied at the top face	43
2.15	Through-thickness variation of the nondimensionalized transverse shear	
	stress components in a thin orthotropic square plate $(\frac{a}{h} = 50)$ considered	
	in Example-3 based on $3D$ FEA, Present Work (ACI-SEL), FSDT, CLPT	
	and Reddy's TSDT (R-TSDT)	45
2.16	Comparison of out of plane deflection u_3 along the centerline parallel to x_1	
	and stress components at point B (shown in Fig. 2.5(a)) for an orthotropic	
	square plate considered in Example-4	47
2.17		
	(b) annular plate considered in Example-6	48
2.18	Comparison of out-of-plane deflection u_3 along the centerline parallel to	
	x_1 axis for the circular and annular plates considered in Example-5 and	
	Example-6, respectively	48
3.1	Schematic of the plate (a) Undeformed state of the plate (b) r^{th} lamina of	
	the plate (c) through-the-thickness lay-up sequence (d) Deformed state of	
	the plate	54
3.2	Continuity of displacements and transverse stresses at the interface of two	
	consecutive laminae	59
3.3	Systematic methodology adopted in deriving the reduced order model	66
3.4	Progression of Deformation in lines AB and CD : (a) Undeformed config-	
	uration. (b) Configuration after zeroth-order perturbation. (c) Configu-	
	ration after first-order perturbation. (d) Configuration after second-order	
	perturbation. (e) Configuration after third-order perturbation	72
3.5	Variation of SCFs with number of plies	79

3.6	Variation of SCFs with $\frac{G_{13}}{G_{23}}$	79
3.7	Geometry of the plate examined in the numerical examples (a) in-plane dimensions of the plate (b) through the thickness structure of the plate in	
	Example-1 (c) through the thickness structure of the plate in Example-2	
	(d) through the thickness structure of the plate in Example-3 (e) through	
	the thickness structure of the plate in Example-4, (f) through the thickness	
	structure of the plate in Example-5	81
3.8	Boundary conditions used in different numerical examples	82
3.9	Load-deflection curves for the central point of the plate considered in	
	Example-1 under uniform Pressure P applied at its top face	82
3.10	Out-of-plane deflection of the plate considered in Example-1 subjected to	
	a uniform pressure of $P = 400 \text{ N/m}^2$ applied on its top face. Deflections	
	are obtained using: (a) 3D Finite Element Analysis (FEA) and (b) present	
	ACI-ESL plate theory.	83
3.11	Percentage error in the out of plane deflection u_3 obtained using $3D$ FEA	
	and present approach under uniform Pressure of $P = 400 \text{N/m}^2$ applied at	
	the top face	83
3.12	Load-deflection curves for the central point of the plate considered in	
	Example-2 under uniform Pressure P applied at its top face $\dots \dots \dots$	84
3.13	Variation of out of plane non-dimensionalized deflection \overline{w} along the cen-	
	terline parallel to x_1 and non-dimensionalized stress components $\overline{\sigma}_{ij}$ along	
	the thickness of the plate considered in Example-3	85
3.14	Variation of out of plane non-dimensionalized deflection \overline{w} along the cen-	
	terline parallel to x_1 and non-dimensionalized stress components $\overline{\sigma}_{ij}$ along	
	the thickness of the plate considered in Example-5	88
4.1	Schematic of the plate deformation (a) Undeformed state (b) Coordinate	
	system (c) Deformed state	93
4.2	Systematic methodology adopted in deriving the reduced order model	
4.3	Deformation of lines AB and CD lying along direction \hat{e}_3 and \hat{e}_1 respec-	
	tively. (a) Undeformed configuration (b) Configuration after zeroth per-	
	turbation (c) Configuration after first perturbation (d) Configuration after	
	second perturbation (e) Configuration after third perturbation	109
4.4	The isoenergetic approach	113
4.5	Variation of the Young's modulus along the thickness of the plate for the	
	first and second examples	117

4.6	Variation of the shift of the reference plane η and shear correction factor
	K with $\frac{Y_t}{Y_b}$ for the first and second examples
4.7	Geometry of the plate
4.8	Load-deflection curves for the central point of the plate considered in the
	first example under uniform Pressure P applied at its top face
4.9	Variation of the non-dimensionalized displacement \overline{w} along the center-
	line of the plate and through-the-thickness variation of the different non-
	dimensionalized stress components $\overline{\sigma}_{ij}$ evaluated at point B (shown in Fig.
	4.7) for an orthotropic square plate considered in the second example 120
4.10	Through-the-thickness variation of the volume fraction V and Young's
	modulus Y of the plate considered in the third example
4.11	Variation of the shift of the reference plane η and shear correction factor
	K with volume fraction index n
4.12	Variation of the non-dimensionalized quantities with volume fraction index
	for the third example. The non-denationalized displacement \overline{w} , normal
	stress $\overline{\sigma}_{11}$ and transverse shear stress $\overline{\sigma}_{23}$ are calculated at points $(x_1 =$
	$\frac{a}{2}, x_2 = \frac{b}{2}, y_3 = 0$, $(x_1 = \frac{a}{2}, x_2 = \frac{b}{2}, y_3 = \frac{h}{2})$ and $(x_1 = \frac{a}{2}, x_2 = 0, y_3 = 0)$
	respectively
4.13	Through-the-thickness variation of the volume fraction V and Young's
	modulus Y of the plate considered in the second example
4.14	Variation of $\frac{\eta}{h}$ and K with volume fraction index n
4.15	Variation of the non-dimensionalized normal stresses $\overline{\sigma}_{11}$ along the thick-
	ness of the plate for the different values of the volume fraction index n . $\overline{\sigma}_{11}$
	is calculated at the middle point of the plate in the fourth example 124
4.16	Variation of the non-dimensionalized normal stresses $\overline{\sigma}_{13}$ along the thick-
	ness of the plate for the different values of the volume fraction index n . $\overline{\sigma}_{13}$
	is calculated at $x_1 = a$, and $x_2 = 0$
5.1	Approach used for the analysis of the symmetric stiffened plates (a) sym-
	metric stiffened plate (b) splitting of the analysis in through-the-thickness
	1D analysis and in-plane $2D$ analysis
5.2	Approach used for the analysis of the asymmetric stiffened plates (a) asym-
	metric stiffened plate with its reference plane (b) splitting of the analysis
	in through-the-thickness $1D$ analysis and in-plane $2D$ analysis 130

5.3	Approach used for the analysis of the symmetric stiffened plates (a) sym-
	metric stiffened plate (b) splitting of the analysis in through-the-thickness
	1D analysis and in-plane $2D$ analysis
5.4	Geometry of the plate with symmetric stiffeners considered in the first
	example
5.5	Load deflection curve for the mid point of the plate with symmetric stiff-
	eners considered in the first example
5.6	Geometry of the plate with an asymmetric stiffener considered in the second
	example
5.7	Deflections along the centerlines of the plate parallel to the x_1 and x_2 axis 134
5.8	(a) Dimensions (b) Loading conditions
5.9	Deflection in x_3 direction (a) present work (b) 3-D FEA result 135
5.10	Comparison of result with 3-D FEA and present result
5.11	Percentage error
5.12	Stiffened plate analyzed in the fourth example (a) in plane geometry of the
	plate (b) through-the-thickness structure of the plate and loading condition
	(c) boundary conditions
5.13	Out-of-plane deflection of the plate considered in the fourth example. The
	results are obtained using (a) $3D$ FEA approach (b) present approach 137
5.14	Percentage error in the out of plane deflection u_3 for the fourth example 138

List of Tables

2.1	Material properties used in different numerical examples	37
2.2	Geometry, Material Properties and boundary conditions for the numerical	
	examples	39
2.3	Nondimensionalized deflections and stresses in the plate considered in Example) -
	3 under sinusoidal transverse loads[122]	46
3.1	Material properties used in different numerical examples	78
3.2	SCFs for different symmetric lay-up sequences	80
3.3	Geometry, Material Properties and boundary conditions for the numerical	
	examples	80
3.4	Comparison of the dimensionless quantities (Max Value) computed in Example) -
	4	86
H.1	Comparison of normal strains $\sigma_{\alpha\alpha}$ in different plate models for cases in-	
	volving small displacements and rotations only	164
H.2	Comparison of transverse shear strains $\sigma_{\alpha 3}$ in different plate models for	
	cases involving small displacements and rotations only	165
Н.3	Comparison of in-plane shear strains σ_{12} in different plate models for cases	
	involving small displacements and rotations only	165

Chapter 1

Introduction

Stiffened structures are frequently used in many engineering disciplines like aerospace, marine, civil and automotive. These structures strategically integrate stiffeners to enhance their mechanical performance, particularly stiffness and fracture toughness. The reinforcement of structures by stiffeners provides significant improvements with minimal weight and cost penalties. The design of stiffened structures involves numerous parameters that influence their performance for a specific application. These include

- 1. Sizing of the plate and stiffeners
- 2. The cross-section and material of the stiffeners
- 3. The spacing and orientation of the stiffeners

Adjusting these parameters is crucial for achieving the most suitable structure for a given application. This necessitates a mathematically robust, accurate, and computationally efficient model of such structures for selecting the optimal design. This becomes even more critical in the present scenario, where weight reduction and structural efficiency are highly desirable.

The approaches used for analyzing stiffened plates fall into three main categories:

- 1. Experimental approaches
- 2. 3D elasticity based approaches
- 3. Reduced order-based approaches

Suitably and carefully designed experimental approaches are accurate. However, performing experiments at a very large scale for the selection of the best suitable structure for a given application is tedious, cumbersome, and very cost-effective. Also, there are numerous reasons for the experiments to go wrong, which can cause wastage of material and time. Thus, numerical and analytical approaches are preferred over experimental analysis. The experimental analysis can be performed after proper numerical and analytical analysis. Among the numerical and analytical approaches, the 3D elasticity-based approach is the most fundamental; however, its applicability is limited as they are computationally intensive. The reduced order-based approaches are simpler and more efficient. The reduced order models not only offer the analyst the flexibility to alter the geometrical or material parameters but also provide quick results. Three prominent methods based on reduced order theories of beams and plates are given below.

- 1. Orthotropic Plate Approximation [24, 23]
- 2. Grillage Approximation [41, 40]
- 3. Separate Analysis and Compatibility [39, 38, 37]

The orthotropic Plate Approximation method simplifies the structure by distributing the effect of the stiffeners across the plate, treating it as an orthotropic material. This approach works well when stiffeners are closely spaced. The Grillage Approximation method incorporates the influence of the plate into the stiffeners by increasing their effective second moment of area. However, determining the effective width in this method can be challenging. Separate Analysis and Compatibility is a more general approach. It analyzes the plate and stiffeners independently. Compatibility is then ensured by enforcing equilibrium and continuity conditions along their connection line.

Stiffened plates incorporate plates as a fundamental component. The accuracy and efficiency of analyzing these stiffened plates with reduced-order models depend heavily on the chosen reduced-order plate theory. This work addresses this by developing an asymptotically accurate theory for the plates, which is then implemented for the analysis of stiffened plates. The following sections outline the motivation, objectives, and a literature review to identify existing research gaps and justify the need for this new theory

1.1 Motivation

Plate-like structures, characterized by one dimension that is significantly smaller than the other two, are predominant in engineering applications. Analyzing their behavior in full 3D detail can be computationally expensive and often unnecessary. To address this challenge, engineers have developed reduced-order theories. These theories aim to capture the essential mechanical behavior of plates with a lower computational expense.

Traditionally, these reduced-order theories rely on ad-hoc (made for a particular purpose or need) and a priori (based on an assumed principle or fact, rather than on actual observed facts) simplifications. These simplifications limit the suitability of these theories for specific cases, making them unreliable for others. As a result, engineers may find themselves constantly switching between different reduced-order theories depending on the specific application, which can be inefficient, time-consuming, and sometimes unscientific.

Among the reduced-order plate theories, Equivalent Single-Layer (ESL) theories, particularly First-order shear deformation plate theory, are known for their computational efficiency and simplicity. However, their reliance on ad hoc and a priori assumptions about material behavior or displacement patterns limits their applicability. This motivates the author to develop an ESL plate theory on mathematically rigorous grounds, avoiding any ad hoc and a priori assumptions. The aim is to remove the limitations/shortcomings of the ESL theories while maintaining computational cost comparable to the FSDT plate theory. This is done using the Variational Asymptotic Method (VAM).

VAM offers a more rigorous alternative for developing reduced-order plate theories. VAM leverages the energy aspect of the problem: the total potential energy of the deformed structure. By utilizing the asymptotic expansion of the energy functional (total potential energy) associated with the plate, VAM allows us to decompose the complex 3D problem into two simpler ones:

- A **Through-the-thickness** 1D **analysis**: This analysis focuses on how the plate deforms in the direction of its smallest dimension (thickness).
- A **In-plane** 2D **analysis**: This analysis focuses on how the plate deforms in its larger (in-plane) dimensions.

This decomposition, as illustrated in Fig. 1.1, leads to a more reliable reduced-order 2D plate theory. The resulting theory captures the details of plate deformation more

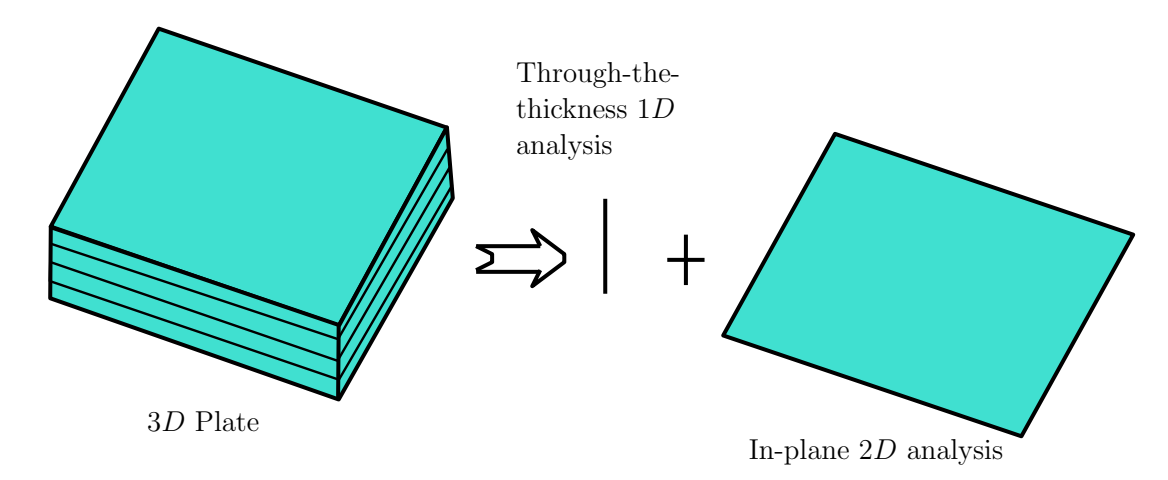


Figure 1.1: Decomposition of the complex 3D problem in through-the-thickness 1D problem and in-plane 2D problem

accurately than assumption-based plate theories while being significantly more computationally efficient than a full 3D analysis.

However, VAM-derived theories include higher-order derivatives of displacements and/or strains in their governing equations. These higher-order terms increase the complexity of the analysis significantly, making it difficult to solve for the unknown quantities. The existing literature addresses this by employing mathematically complex extremization processes. This process eliminates the higher-order terms at the expense of the asymptotic correctness of the theory. This limitation becomes even more problematic for plates with non-uniform thickness, such as stiffened plates. The existing VAM approaches struggle to handle the varying through-the-thickness geometry of these structures effectively.

These limitations of existing VAM approaches motivate us to develop an alternative procedure. The presented method eliminates the higher-order derivatives from the analysis while preserving the asymptotic correctness of the VAM framework. The key elements of the present approach are as follows.

- Strategic selection of a reference plane: The choice of the reference plane of the plate significantly impacts the resulting equations. The present work selects the reference plane of the plate suitably to result in the elimination of the higher-order derivatives from the analysis.
- Isoenergetic approach: This innovative approach ensures that the asymptotically correct plate theory and the commonly used First-order Shear Deformation Theory (FSDT) represent the same energy density for a specific deformation pattern of

CHAPTER 1 1.2. OBJECTIVE

the reference plane. This strategy effectively eliminates the higher-order derivative terms from the analysis while maintaining accuracy.

This improved approach offers a more robust and efficient framework for analyzing plate structures, particularly those with complex geometries. Furthermore, existing VAM approaches often rely on pre-assumed plate kinematics and an assumed ordering of the quantities involved. This work presents a first-principles-based VAM that avoids these assumptions. The VAM framework employed in this work does not rely on the pre-assumed kinematics of the plate. It determines the order of relevant quantities utilizing the plate geometry and a bound on the maximum values of strains, leading to a more robust foundation for the analysis.

1.2 Objective

The objectives of the present work include the development of a reduced-order Equivalent Single Layer (ESL) plate model using a systematic and mathematically robust approach, free from ad-hoc and a priori assumptions. Such a model is developed using VAM. The present work equips VAM with a mathematically rigorous and robust framework by eliminating its dependency on pre-assumed kinematics and introducing a systematic ordering scheme for the asymptotic expansion of the energy functional. This work eliminates the complications arising from the higher-order derivatives inherent with the VAM-based reduced-order model from the analysis using the concept of isoenergetics and by choosing a suitable reference plane for the plate. The developed framework is tailored to deal with different scenarios as follows.

- 1. Development of asymptotically correct isoenregetic formulation for geometrically nonlinear analysis of Anisotropic Plates.
- 2. Development of asymptotically accurate approach to find out shear correction factors for Laminated Composite Plates.
- 3. Development of asymptotically correct isoenergetic formulation for geometrically nonlinear analysis of Symmetric Multilayered Composite Plate.
- 4. Development of asymptotically correct isoenergetic formulation for geometrically nonlinear analysis of Functionally Graded Plates.

5. Development of asymptotically correct isoenergetic formulation for geometrically nonlinear analysis of symmetric and asymmetric Stiffened Plates.

1.3 Literature Survey

The study of the mechanics of solids finds its roots in the mathematically rigorous 3D continuum elasticity theory. However, solving the resulting set of differential equations for various loading and boundary conditions may be tedious [78, 66, 99, 79, 94]. In most of cases, analytical strategies may not be applicable, hence numerical methods become essential. Implementation of numerical methods requires a balance between accuracy and computational cost, which might be quite expensive in certain cases [142]. In order to provide an acceptable preliminary design solution, reduced order models have been developed. Researchers have developed reduced order theories for beams, plates and shells by approximating behavior in smaller dimensions [136].

To formulate reduced order models, fundamentally, three approaches have been adopted based on the choice of primary variables [92, 97, 93, 94, 65]:

- a. Displacement formulation, wherein the primary variables are the displacements of the reference surface
- b. Stress formulation, wherein the primary variables are the membrane stresses of the reference surface
- c. *Mixed formulation* involves the displacements of the reference plane and the traverse stresses as the primary variables.

Each formulation has its own advantages and disadvantages. However, the displacement formulation is the most commonly used approach for the analysis of thin and moderately thick plates because of its simplicity and intuitiveness.

The above-mentioned formulations can be adapted to model anisotropic and/or multilayered structures using presupposition-based modeling strategies such as Equivalent Single Layer (ESL) theories [100, 101, 102], Layer-Wise (LW) theories [106, 90, 91, 140] and unified formulations [7, 93, 8]. The ESL approach, which is the most popular method for analyzing anisotropic [135, 134, 133] and/or multilayered panels, simplifies the analysis by assuming that the plate is composed of a single layer and expresses primary variables associated with the whole domain of the plate in terms of primary variables associated

with the reference plane of the plate reducing the degree of freedom of the analysis and thereby increasing computational efficiency. The LW theories consider each layer separately with appropriate boundary conditions at the layer interfaces, resulting in a larger number of unknowns, which are directly proportional to the number of layers. Building on the foundation of classical plate theories, Carrera and his team introduced a unified formulation for laminated plates, now known as the Carrera Unified Formulation (CUF) [7, 8]. This approach was further extended by Demasi into a more general framework, termed the Generalized Unified Formulation (GUF) [6]. Similarly, Caliri et al. proposed their own unifying approach, Caliri's Generalized Formulation (CGF) [93]. Despite the simplifying assumptions made in the ESL approach, it has been shown to be effective in investigating the global response of multilayered thin and moderately thick plates. However, its performance significantly deteriorates for thick plates.

Several types of ESL plate theories have been developed to analyze the behavior of plates. A comprehensive review can be found in [100, 101, 80, 93]. In such theories, the 3D displacement field is represented in terms of the deformation of the reference plane. The ESL theories are broadly classified into three categories (a) the polynomial theories [71, 72, 73, 74, 75] (b) the non-polynomial theories [87, 88, 89, 69, 70] and (c) zig-zag (ZZ) theories [104, 105, 103, 143]. Polynomial theories are developed by expanding the displacements in a power series of transverse coordinates involving simple orthogonal polynomials, such as Legendre, Hermite or Chebyshev. Examples of polynomial theories include Classical Laminated Plate Theory (CLPT), First-order Shear Deformation Theory (FSDT), Reddy's Third Order Shear Deformation Plate Theory (R-TSDT), etc. In non-polynomial theories, the displacement field of the plate is expressed in terms of trigonometric, hyperbolic or exponential function of the thickness coordinates. The underlying principle of ZZ theories is to assume that the displacement field is a superposition of a global first-order, second-order, or higher-order displacement field and a local ZZ function [104, 95].

ESL plate theories offer several advantages over LW and 3D plate theories. Their key strengths lie in their low computational cost, ease of implementation, and overall simplicity. These attributes make them highly desirable for analyzing large structures and facilitating efficient iteration within optimization algorithms. Among ESL theories, the classical laminate plate theory (CLPT) and first-order shear deformation theory (FSDT) stand out for their remarkable simplicity. Computational efficiency and ease of use make FSDT a popular choice for thin and moderately thick plates. While higher-order ESL theories boast increased accuracy, their computational burden often outweighs the marginal

improvement in results, especially for multilayered composite materials.

While FSDT offers the appealing advantage of computational efficiency, it comes with limitations. Notably, it relies on a shear correction factor and struggles to accurately predict transverse shear stresses, particularly crucial for laminated composites prone to delamination. This limitation extends to higher-order ESL theories when dealing with composite laminates. To address this, the present work introduces a computationally efficient approach comparable to FSDT but with significantly improved accuracy in predicting transverse shear stresses.

The present work adopts the Variational Asymptotic Method (VAM) as a tool to derive a displacement-based, asymptotically correct, reduced-order plate theory. The computational complexities involved with this reduced order plate theory, due to its inherent higher order derivatives, were eliminated using a novel isoenergetic approach. Berdichevsky [107] introduced the VAM by combining asymptotic [150, 141, 149] and variational approaches [148] wherein, the small geometric and material parameters are used to reduce the dimensionality of the problem in hand. When applied to the plate problem, it decouples the 3D problem into a 1D through the thickness analysis and a 2D planar problem. This approach has been used by many researchers to solve plate problems [108, 113, 109, 86, 111, 112, 155], a detailed review of such theories is available in [110]. It is worth mentioning here that similar strategies have been successfully applied by researchers in various studies. Rajagopal et al. [64] utilized these strategies to analyze planar deformation of initially curved isotropic strips, Harusampath et al. and Liu et al. [63, 151, 147] applied them to model composite beams, Amandeep et al. [82, 67] used them to find analytical solutions for functionally graded beams, and Shakya et al. [81] employed them to investigate elastic coupling in anisotropic-homogeneous beams.

Yu introduced a new unified approach named Mechanics of Structure Genome (MSG) in 2016 for the multiscale constitutive modeling [?, 2]. This approach was built upon previous research using the Variational Asymptotic Method (VAM), which has been applied to beams, plates, shells, and unit cell homogenization. MSG establishes a unified framework for constructing constitutive models across multiple length scales. The core concept is the "structure genome," defined as the smallest fundamental mathematical unit of a structure. MSG bridges the gap between the microstructure and macroscopic levels of composite materials, providing essential information to develop constitutive models for a wide range of structural components, including 3D structures, beams, plates, and shells.

To the best of the author's knowledge, the existing plate models based on VAM typi-

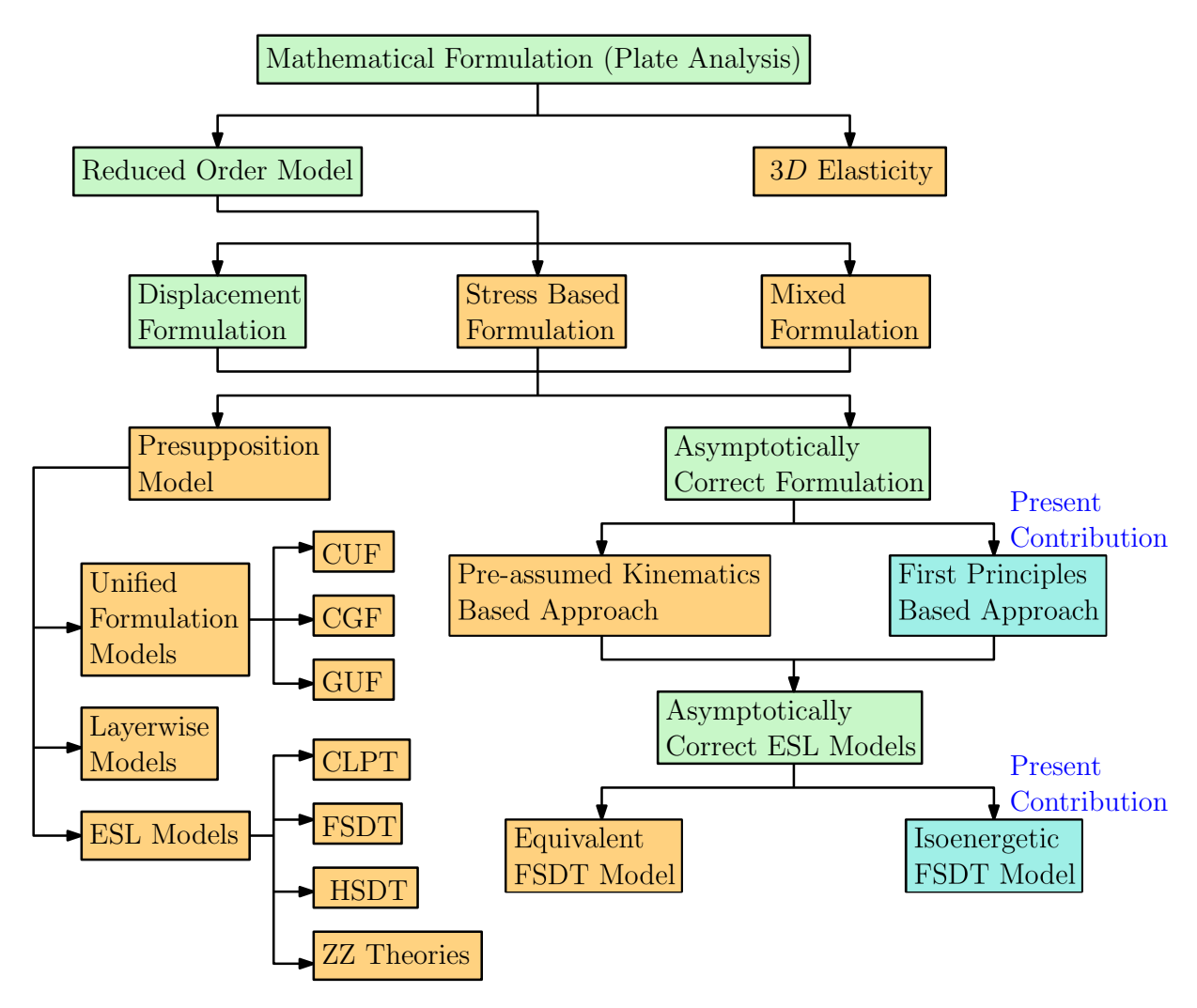


Figure 1.2: Literature summary with contribution of present work

cally begin with a priori assumptions about the 2D strains/displacements and refine them by considering a warping vector. In other words, VAM has mainly been used to improve existing reduced-order plate models by making perturbations rather than creating the reduced-order model by itself considering the 3D plate model. VAM-based plate theories, while accurate, are mathematically complex and computationally inefficient due to the involvement of higher-order derivatives of generalized 2D strains or 2D displacement variables. Consequently, these theories are often less practical to apply. In an effort to address this challenge in many VAM-based theories [112, 62, 108, 113], the plate model is transformed into a Reissner-like model, leading to a distortion of the model. Unfortunately, this distortion compromises the asymptotic correctness of the approach, which is

a key advantage of using VAM.

In this study, 1D through-the-thickness analysis is conducted for the plate problem, employing a first-principles-based derivation to obtain a reduced-order 2D plate model from the energy of the 3D model. Unlike traditional methods, the Present approach avoids pre-assumed plate kinematics and ordering of variables. Instead, This work proposes a systematic ordering scheme that assigns orders to different quantities of interest and improves them progressively. The final order obtained through this scheme aligns perfectly with established literature, demonstrating its robustness. Furthermore, the present approach does not require an a priori reference plane. Instead, the analysis methodology naturally yields a reference plane as an outcome. Similarly, the position of this plane is not pre-assumed but determined logically to eliminate higher-order derivatives. Overall, the present work has the following novel contributions

- i. First principles-based derivation of the reduced order 2D plate model from the 3D model energy,
- ii A systematic ordering approach is used utilizing bounds on the maximum value of the strains and the maximum thickness-to-length ratio.
- iii. Elimination of higher order derivatives of 2D displacement variables using isoenergetic principle.

A summary of the literature, along with the contribution of the present work, is illustrated in Fig. 1.2. The unification of the first principles-based displacement solutions with the isoenergetic approach results not only in an asymptotically correct theory but also in computationally efficient and robust solutions. The reduced order 2D plate theory can be analyzed using the analytical solutions approaches like Navier or Levy solution [119] or Numerical approaches like Finite Element Method (FEM). Different solution approaches highlighting the adapted solution approaches (shown in green colored blocks) are presented in Fig. 1.3

1.4 Outline of the Thesis

This thesis is organized into six chapters, each aligned with the defined objectives of the research.

Chapter 2 presents a novel asymptotically accurate equivalent single layer (ESL) geometrically nonlinear plate theory for anisotropic materials. This development builds

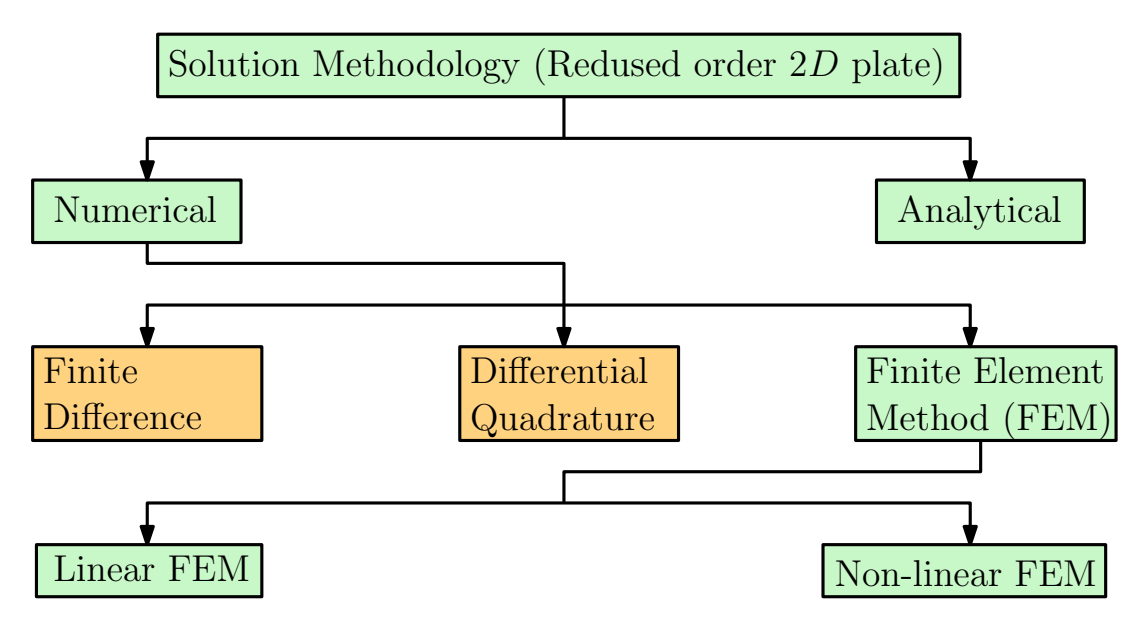


Figure 1.3: Different solution approaches employed for the solution of the reduced order 2D plates

upon a critical review of existing ESL plate theories in **Chapter 1**, which highlights the limitations of current approaches due to their reliance on *ad hoc* and *a priori* assumptions.

Chapter 3 extends the work done in Chapter 2 to analyze multilayered symmetric composite plates. It focuses on the continuity of displacements and transverse stresses at layer interfaces during the 1D through-the-thickness analysis. This chapter introduces asymptotically accurate shear correction factors. These factors make FSDT plate theory isoenergetic to the asymptotically correct plate theory. This innovation reduces the complexity of the analysis while maintaining high accuracy in the results.

Chapter 4 addresses functionally graded plates (FG plates) with different gradation models. Unlike symmetric plates, the reference plane for FG plates does not coincide with the mid-plane. This chapter determines the optimal reference plane position and develops an ESL theory for FG plates using VAM and the concept of isoenergetics.

Chapters 5 and 6 leverage the theories developed in previous chapters. Chapter 5 presents a systematic approach for analyzing symmetric stiffened plates, while Chapter 6 tackles asymmetric stiffened plates. Chapter 7 concludes the thesis by summarizing the key findings and outlining potential avenues for future research. This final chapter explores how the present work could be extended or modified to tackle a broader range of engineering challenges.

Chapter 2

Asymptotically Correct Isoenergetic Formulation of Geometrically Nonlinear Anisotropic Plates

2.1 Introduction

This chapter presents a displacement-based ESL plate theory for anisotropic materials derived using Variational Asymptotic Method (VAM) and further simplified using a novel isoenergetic approach. Unlike the available VAM-based plate theories, the present work does not rely on any pre-assumed kinematics of plates, thus establishing a more systematic and rigorous framework for VAM. Additionally, the present work introduces a systematic scheme leveraging the geometry of the plate and a bound on the maximum value of strains to assign an order to different quantities of interest, which play a crucial role in the asymptotic expansion of the 3D model energy functional associated with the plate. The asymptotic expansion results in the decoupling of the 3D plate problem into a 1Dthrough the thickness analysis and a 2D planar problem. The through-the-thickness 1Danalysis, which is conducted first, yields a 2D reduced-order model for plates. It is to be emphasized here that the classical reduced order model 2D plate model, as well as the through-the-thickness analysis, is a natural outcome of the methodology adopted in the present work. However current approach also results in the higher order derivatives of 2Ddisplacement terms. To circumvent this issue, an innovative isoenergetic approach has been developed by enforcing the condition that the asymptotically correct plate theory and FSDT plate theory represent identical energy densities for a given deformation pattern of the reference plane. This strategy, referred to as the isoenergetic approach, results in

the elimination of higher-order derivative terms.

The unification of the first principles-based displacement solutions with the isoenergetic approach results not only in an asymptotically correct theory but also in computationally efficient and robust solutions. Henceforth, this theory will be referred to as the Asymptotically Correct Isoenegetic Equivalent Single Layer (ACI-ESL) plate theory. The reduced order ACI-ESL plate theory can be analyzed using the analytical solutions approaches like Navier or Levy solution [119] or Numerical approaches like Finite Element Method (FEM).

In what follows, the detailed derivation and validation of the proposed ACI-ESL plate theory is presented.

2.2 Analytical Development

Consider a homogeneous anisotropic plate of length a, width b and thickness h, with a right-handed orthogonal cartesian coordinate system $x=(x_1,x_2,x_3)$ and unit vectors \hat{e}_i along the axes x_i as shown in Fig. 2.1. The x_3 -axis is oriented in the downward direction. For plate-like structures, the plate thickness h is much smaller than other dimensions a and b. Defining a and b to be of the order l, the ratio $\frac{h}{l}$ becomes a small parameter i.e. $\frac{h}{l} < 1$. The interior region of the plate is denoted by Ω and the boundary comprises of the top surface $\partial \Omega_{\text{top}}$, the bottom surface $\partial \Omega_{\text{bot}}$ and the side surfaces $\partial \Omega_{\text{side}}$ with $\partial \Omega_{\text{tb}} = \partial \Omega_{\text{top}} \cup \partial \Omega_{\text{bot}}$. The position vector of any arbitrary point P in this domain is given by $\vec{x} = x_i \hat{e}_i$. Throughout this work, Roman indices (i, j, k, \ldots) range from 1 to 3, while Greek indices $(\alpha, \beta, \gamma, \ldots)$ range from 1 to 2 unless their values are specified.

The point P deforms to point P' through displacement $\vec{v} = v_i \hat{e}_i$. For a deformation with small strains and moderate rotations, the Green–St. Venant strain tensor [128, 127, 119, 139] is given as

$$\underline{\underline{E}} = \frac{1}{2} \left[\left(\vec{\nabla}_x \vec{v} \right) + \left(\vec{\nabla}_x \vec{v} \right)^T + \left(\vec{\nabla}_x \vec{v} \right)^T \left(\vec{\nabla}_x \vec{v} \right) \right]$$
(2.1)

In the subsequent sections, we present a novel and intriguing strategy for developing a reduced-order plate theory. This theory is based on the generalized strain tensor defined in Eq. (2.1) with a limit on the maximum value of strains. Additionally, it utilizes the geometrical dimensions of the plate with a limit on the maximum value of $\frac{h}{l}$ to develop a reduced order plate model in a mathematically rigorous way, avoiding any a priori or ad hoc assumptions. It would be interesting to observe that the successive perturbations of

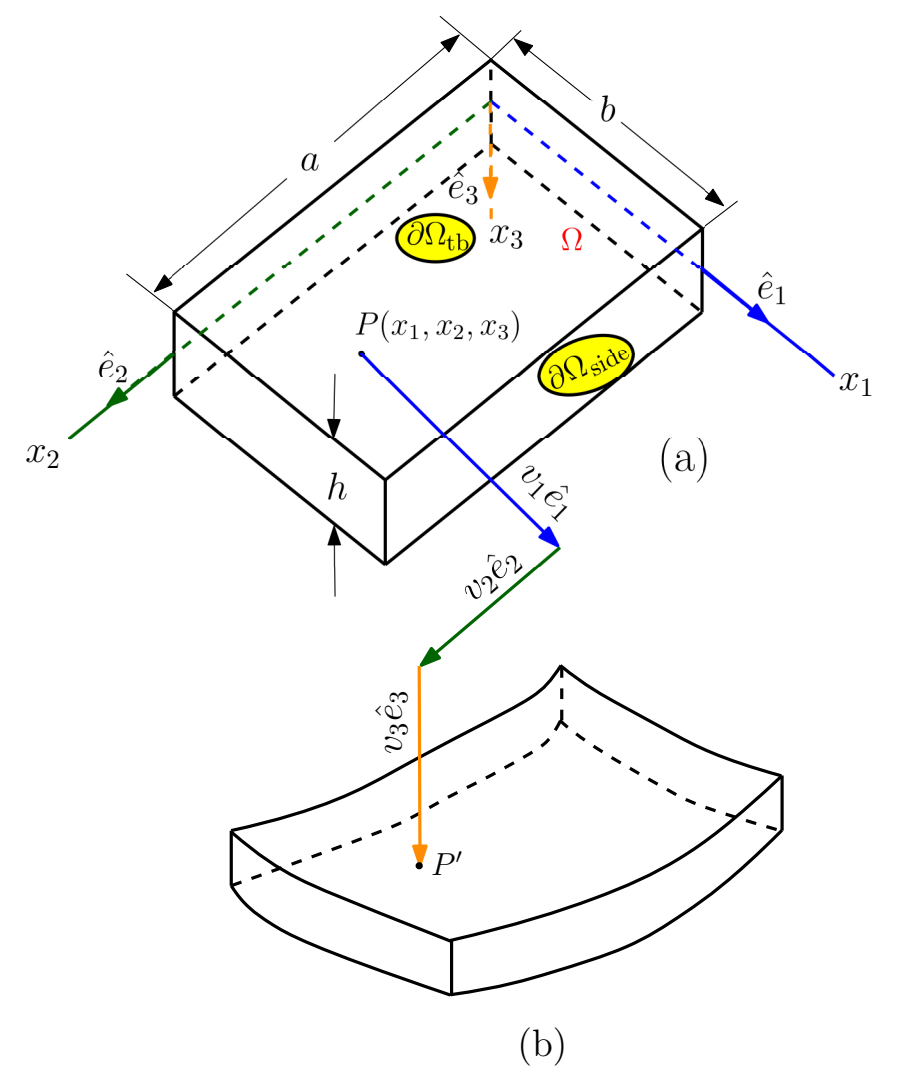


Figure 2.1: Schematic of the plate deformation (a) Undeformed state (b) Deformed state

the reduced order plate model, as will be demonstrated in this work, lead to increasingly improved plate theories encompassing the CLPT and higher order plate theories. The analytical development is divided into three parts: Part A develops a CLPT type plate theory, Part B refines the model presented in Part A considering the contribution of higher-order energy, and Part C presents a novel isoenergetic approach to eliminate the higher-order derivatives present in the plate theory developed in Part A and B to reduce the computational complexities and computational cost.

2.3 Part A: Development of a CLPT type plate theory

By leveraging the geometry of the plate and a bound on the maximum value of strains, a scheme has been established to estimate and re-estimate the order of the different quantities of interest. The ordering scheme is presented in the following section.

2.3.1 Order Estimation Scheme

With the ordering scheme outlined in [112], the relation between the orders of v_i and its derivatives with respect to x_j is given as follows

$$O\left(\frac{\partial^t}{\partial x_1^t} \frac{\partial^s}{\partial x_2^s} \frac{\partial^r}{\partial x_3^r} v_i\right) \sim \left(\frac{1}{l}\right)^{(s+t)} \left(\frac{1}{h}\right)^r O(v_i)$$

$$r, s, t = 0, 1, 2, 3, \dots$$
(2.2)

Note that the 0^{th} order derivative represents no derivative, i.e., $\frac{\partial^0}{\partial x_i^0} O(v_i) = O(v_i)$. The supnorm (supremum norm) of strains $(||\underline{\underline{E}}||_{\infty})$ is defined below

$$||\underline{\underline{E}}||_{\infty} = \max_{1 \le i, j \le 3} \max_{x \in \Omega} |E_{ij}|$$
 (2.3)

The maximum value of $\frac{h}{l}$ and the supnorm is bounded by ξ and ε respectively as shown below mathematically

$$\frac{h}{l} \le \xi$$

$$||\underline{E}||_{\infty} \le \varepsilon$$

$$(2.4)$$

In the context of deformation with small strains, we consider bound on the supnorm of strains to be a very small parameter i.e. $\varepsilon \ll 1$. Also, for a plate-like structure bound on the maximum value of $\frac{h}{l}$ is small, i.e. $\xi < 1$. For the asymptotic expansion of the stains and strain energy, it is assumed that $\varepsilon = \xi^3$. It will be demonstrated later that the bound on the maximum value of the strains and $\frac{h}{l}$ with the ordering scheme given in Eq. (2.2) results in a unique estimation of the order of different quantities of interest.

2.3.2 Constitutive Relations and Strain Energy

Let $\sigma = \{\sigma_{11}, \sigma_{22}, \sigma_{33}, \tau_{23}, \tau_{13}, \tau_{12}\}^T$ be 2^{nd} Piola-Kirchhoff stress tensor which is energetically conjugate to the Green–St. Venant strain tensor [61], the constitutive relation

is given by

$$\sigma = CE, \tag{2.5}$$

where C represents the stiffness matrix and $E = \{E_{11}, E_{22}, E_{33}, 2E_{23}, 2E_{13}, 2E_{12}\}^T$. For materials exhibiting monoclinic symmetry, such as laminae in composite materials and crystalline solids like gypsum, borax, orthoclase, etc. [132], the stiffness matrix takes the following form [131]

$$C = \begin{bmatrix} C_{11} & C_{12} & C_{13} & 0 & 0 & C_{16} \\ C_{12} & C_{22} & C_{23} & 0 & 0 & C_{26} \\ C_{13} & C_{23} & C_{33} & 0 & 0 & C_{36} \\ 0 & 0 & 0 & C_{44} & C_{45} & 0 \\ 0 & 0 & 0 & C_{45} & C_{55} & 0 \\ C_{16} & C_{26} & C_{36} & 0 & 0 & C_{66} \end{bmatrix}$$

$$(2.6)$$

The order of all material constants, denoted by μ , is assumed to be the same [108]. The strain energy density is given by

$$U = \frac{1}{2}\sigma^T E \tag{2.7}$$

2.3.3 Dimensional Reduction

Let us consider tractions $\vec{q} = q \ \hat{e}_3$ and $\vec{t} = t_i \ \hat{e}_i$ on $\partial \Omega_{\rm tb}$ and $\partial \Omega_{\rm side}$ respectively. Application of the principle of virtual work yields

$$\int_{\Omega} \delta U dV - \int_{\partial \Omega_{\text{tb}}} \vec{q} \cdot \delta \vec{v} da_{\text{tb}} - \int_{\partial \Omega_{\text{side}}} \vec{t} \cdot \delta \vec{v} da_{\text{side}} = 0$$
 (2.8)

Eq. (2.8) describes a computationally intensive 3D elasticity problem. The major part of the literature solves this problem by reducing the 3D problem into a simpler 2D plate problem. Traditionally, this reduction involves $ad\ hoc$ and $a\ priori$ assumptions, which may not fully account for deformation energy considerations. The present work takes the energy aspects of the problem into consideration to develop a reduced order plate model.

The dimensional reduction procedure, which relies on VAM, aligns with that adopted by Harursampath et al. [126] to investigate non-linear behavior of long anisotropic tubes. To elucidate this procedure, we express U in Eq. (2.8) as a functional of the first-order derivatives of v_1 , v_2 , and v_3 with respect to x_1 , x_2 , and x_3 .

$$\int_{\Omega} \delta U \left(x_1, x_2, x_3, \frac{dv_1}{dx_1}, \frac{dv_1}{dx_2}, \frac{dv_1}{dx_3}, \frac{dv_2}{dx_1}, \frac{dv_2}{dx_2}, \frac{dv_2}{dx_3}, \frac{dv_3}{dx_1}, \frac{dv_3}{dx_2}, \frac{dv_3}{dx_3} \right) dV
- \int_{\partial \Omega_{\text{tb}}} \vec{q} \cdot \delta \vec{v} da_{\text{tb}} - \int_{\partial \Omega_{\text{side}}} \vec{t} \cdot \delta \vec{v} da_{\text{side}} = 0$$
(2.9)

Now, the order estimation scheme outlined in Section 2.3.1 is used to estimate the orders of v_1 , v_2 , and v_3 . Based on this order estimation, the most significant terms of U are selected, while less significant terms are neglected. This selection process simplifies Equation (2.9) into the following form:

$$\int_{\Omega} \delta U\left(x_1, x_2, x_3, \frac{dv_1}{dx_3}, \frac{dv_2}{dx_3}, \frac{dv_3}{dx_3}\right) dV - \int_{\partial \Omega_{\rm tb}} \vec{q} \cdot \delta \vec{v} da_{\rm tb} - \int_{\partial \Omega_{\rm side}} \vec{t} \cdot \delta \vec{v} da_{\rm side} = 0 \qquad (2.10)$$

Notably, in the above Eq. (2.10), U contains terms having derivatives of v_1 , v_2 and v_3 with respect to x_3 only. This makes the extremization done in the thickness direction independent of the boundary condition at the sides of the plate, thereby making it independent of the in-plane deformation of the plate. This naturally decomposes the 3D problem into two simpler subproblems: (a) a through-the-thickness 1D analysis and (b) an in-plane 2D analysis. The through-the-thickness 1D analysis gives the reduced-order model for the plates. This approach is repeatedly used to improve the reduced order model. The whole procedure is divided into different order solutions, each improves the solution obtained in the previous one. The details of each order solution are presented in the subsequent sections.

2.3.4 Zeroth Order Solutions (ZOS)

In this order solutions, the displacement field is assumed to be $v_i = v_i^0$, where $v_i^0(x_1, x_2, x_3)$ are zeroth order perturbation variables. The order estimation scheme presented in Section 2.3.1 is employed to evaluate the order of v_i^0 . The estimated order of $v_i^0(x_1, x_2, x_3)$ is determined to be $O(\xi^3 h)$. Based on this order estimation, the order of the different strain components is evaluated as shown below, with the orders indicated using underbraces.

$$E_{11} = O(\xi^{4}) \qquad 2E_{23} = \underbrace{\frac{\partial v_{2}^{0}}{\partial x_{3}}}_{O(\xi^{3})} + O(\xi^{4})$$

$$E_{22} = O(\xi^{4}) \qquad 2E_{13} = \underbrace{\frac{\partial v_{1}^{0}}{\partial x_{3}}}_{O(\xi^{3})} + O(\xi^{4})$$

$$E_{33} = \underbrace{\frac{\partial v_{3}^{0}}{\partial x_{3}}}_{O(\xi^{3})} \qquad 2E_{12} = O(\xi^{4})$$

$$(2.11)$$

It is noteworthy that the order of the perturbation variable v_i^0 determined in this section corresponds to the maximum permissible value that ensures the strains remain bounded by $\varepsilon = \xi^3$. This order is unique, as altering the order of v_i^0 would lead to a change in the upper bound of the strains, which is not allowable. This ordering of strains yields an ordered representation of U in terms of the small parameters ξ , as illustrated below.

$$U = \underbrace{U_{\text{sig}}}_{O(\xi^6 \mu)} + O\left(\xi^7 \mu\right)$$

$$U_{\text{sig}} = \frac{1}{2} \left[C_{55} \left(\frac{\partial v_1^0}{\partial x_3} \right)^2 + 2C_{45} \frac{\partial v_1^0}{\partial x_3} \frac{\partial v_2^0}{\partial x_3} + C_{44} \left(\frac{\partial v_2^0}{\partial x_3} \right)^2 + C_{33} \left(\frac{\partial v_3^0}{\partial x_3} \right)^2 \right]$$

$$(2.12)$$

The lowest order term, U_{sig} , in the above equation has the highest contribution to the energy functional. Therefore, this section targets the energy of this order only, neglecting the other higher order terms [137]. This reduces the virtual work Eq. (2.8) to the following form

$$\int_{\partial\Omega_{\rm sof}} \left[\int_{x_3} \delta U_{\rm sig} dx_3 \right] da_{\rm ref} - \int_{\partial\Omega_{\rm th}} \vec{q} \cdot \delta \vec{v} da_{\rm tb} - \int_{\partial\Omega_{\rm side}} \vec{t} \cdot \delta \vec{v} da_{\rm side} = 0 \tag{2.13}$$

Where $\partial\Omega_{\rm ref}$ is the reference plane of the plate. Due to historical precedence and ease of analysis, the midplane of the undeformed plate is taken as the reference plane. An interesting observation from Eq. (2.12) is that $U_{\rm sig}$ contains terms having derivatives of v_i^0 with respect to x_3 only. This allows to perform the minimization in two stages: (i) a 1D through the thickness analysis along x_3 only, and (ii) a 2D analysis in the x_1, x_2 plane, as expressed below.

$$\underbrace{\delta\Pi_{x_3} = 0}_{1D \text{ Analysis}} \underbrace{\delta\Pi = 0}_{2D \text{ Analysis}}$$

$$\Pi_{x_3} = \int_{x_3} U_{\text{sig}} dx_3$$

$$\Pi = \int_{\partial\Omega_{\text{ref}}} \Pi_{x_3} da_{\text{ref}} - \int_{\partial\Omega_{\text{tb}}} \vec{q} \cdot \vec{v} da_{\text{tb}} - \int_{\partial\Omega_{\text{side}}} \vec{t} \cdot \vec{v} da_{\text{side}}$$
(2.14)

This strategy naturally leads to a dimensional reduction of the problem.

Through the Thickness 1D Analysis

Extrimization of Π_{x_3} yields following Euler Lagrange governing equations

$$C_{55} \frac{\partial^2 v_1^0}{\partial x_3^2} + C_{45} \frac{\partial^2 v_2^0}{\partial x_3^2} = 0$$

$$C_{45} \frac{\partial^2 v_1^0}{\partial x_3^2} + C_{44} \frac{\partial^2 v_2^0}{\partial x_3^2} = 0$$

$$C_{33} \frac{\partial^2 v_3^0}{\partial x_2^2} = 0$$
(2.15)

and following associated boundary conditions

$$\begin{aligned}
&\mathcal{B}_{v_1^0}\big|_{x_3=-h/2} = \mathcal{B}_{v_1^0}\big|_{x_3=h/2} = 0 \\
&\mathcal{B}_{v_2^0}\big|_{x_3=-h/2} = \mathcal{B}_{v_2^0}\big|_{x_3=h/2} = 0 \\
&\mathcal{B}_{v_3^0}\big|_{x_3=-h/2} = \mathcal{B}_{v_3^0}\big|_{x_3=h/2} = 0 \\
&\mathcal{B}_{v_1^0} = C_{55} \frac{\partial v_1^0}{\partial x_3} + C_{45} \frac{\partial v_2^0}{\partial x_3} \\
&\mathcal{B}_{v_2^0} = C_{45} \frac{\partial v_1^0}{\partial x_3} + C_{44} \frac{\partial v_2^0}{\partial x_3} \\
&\mathcal{B}_{v_3^0} = C_{33} \frac{\partial v_3^0}{\partial x_3}
\end{aligned} \tag{2.16}$$

solving the Euler-Lagrange equations Eq. (2.15) with the boundary conditions Eq. (2.16) results in following solution

$$v_i^0 = u_i(x_1, x_2) (2.17)$$

This solution will be further refined for more accuracy in the upcoming sections. Note that this zeroth-order solution expresses the 3D displacement components v_i in terms of u_i , which are functions of x_1 and x_2 only and therefore are termed as 2D variables. In other words, u_i represent the rigid body like deformation A^0B^0 of a line segment AB lying along the thickness direction \hat{e}_3 , as shown in Fig. 2.3(b). Since this displacement is independent of x_3 , all points lying on AB have the same displacement. However, for convenience, u_i are expressed as the average through the thickness displacement components of the plate as shown below mathematically.

$$u_i = \frac{1}{h} \int_{-h/2}^{h/2} v_i \, dx_3 \tag{2.18}$$

2.3.5 First Order Solution (FOS)

In this section, The displacement field obtained in ZOS is perturbed to further improve it as follows¹.

$$v_i = v_i^0 + v_i^1 = u_i + v_i^1 (2.19)$$

Introduction of v_i^1 in Eq. (2.19) results in three additional degrees of freedom to the displacement field. To ensure the uniqueness of the solution, three constraints are essential. Eq. (2.18) result in the following three constraints on the n^{th} perturbation variables v_i^n

$$\int_{-h/2}^{h/2} v_i^n dx_3 = 0 (2.20)$$

It may be noted that the choice of the constraint is not unique. Several papers on the VAM-based analysis of plates [113, 111, 112, 108] uses the similar constraints as given in Eq. (2.20).

Following the procedure described in Section 2.3.1, we estimate the order of u_i and v_i^1 to be $O(\xi^3 l)$ and $O(\xi^3 h)$, respectively. Notably, the order of the perturbation variables v_i^0 and v_i^1 is the same, which seems to contradict the usual refinement procedure done through perturbations. However, we started with a conservative order of v_i , treating the plate as a 3D body and considering the maximum possible variation in v_i for all possible deformation modes with strains bounded by ε . As the refinement in the displacement field goes on, the plate reveals its true deformation pattern, relaxing the bound on v_i . This relaxation necessitates further refinement in the displacement field in the same order, justifying it.

Substituting v_i from Eq. (2.19) into Eq. (2.1) gives the following strains, along with their respective orders indicated in underbraces

¹Note that $v_i^n = v_i^n(x_1, x_2, x_3)$, termed as n^{th} order perturbation variable, will consistently be used in the upcoming work to improve the displacement field in the n^{th} order solution

$$E_{11} = \underbrace{\frac{\partial u_1}{\partial x_1}}_{O(\xi^3)} + O(\xi^4) \qquad 2E_{23} = \underbrace{\frac{\partial u_3}{\partial x_2} + \frac{\partial v_2^1}{\partial x_3}}_{O(\xi^3)} + O(\xi^4)$$

$$E_{22} = \underbrace{\frac{\partial u_2}{\partial x_2}}_{O(\xi^3)} + O(\xi^4) \qquad 2E_{13} = \underbrace{\frac{\partial u_3}{\partial x_1} + \frac{\partial v_1^1}{\partial x_3}}_{O(\xi^3)} + O(\xi^4)$$

$$E_{33} = \underbrace{\frac{\partial v_3^1}{\partial x_3}}_{O(\xi^3)} + O(\xi^4) \qquad 2E_{12} = \underbrace{\frac{\partial u_1}{\partial x_2} + \frac{\partial u_2}{\partial x_1}}_{O(\xi^3)} + O(\xi^4)$$

$$(2.21)$$

The revised strains given in Eq. (2.21) are used to recalculate U and U_{sig} . Similar to the ZOS, the perturbation variables v_i^1 present in U_{sig} have derivatives with respect to x_3 only allowing us to perform the 3D analysis in two stages (1D and 2D analyses).

Through the Thickness 1D Analysis

The functional Π_{x_3} is recalculated to accommodate the modifications in U_{sig} . Extremization of Π_{x_3} yields the following Euler Lagrange equations

$$C_{55} \frac{\partial^2 v_1^1}{\partial x_3^2} + C_{45} \frac{\partial^2 v_2^1}{\partial x_3^2} = 0$$

$$C_{45} \frac{\partial^2 v_1^1}{\partial x_3^2} + C_{44} \frac{\partial^2 v_2^1}{\partial x_3^2} = 0$$

$$C_{33} \frac{\partial^2 v_3^1}{\partial x_3^2} = 0$$
(2.22)

and following associated boundary conditions

$$\begin{split} & \mathcal{B}_{v_{1}^{1}}\big|_{x_{3}=-h/2} = \mathcal{B}_{v_{1}^{1}}\big|_{x_{3}=h/2} = 0 \\ & \mathcal{B}_{v_{2}^{1}}\big|_{x_{3}=-h/2} = \mathcal{B}_{v_{2}^{1}}\big|_{x_{3}=h/2} = 0 \\ & \mathcal{B}_{v_{3}^{1}}\big|_{x_{3}=-h/2} = \mathcal{B}_{v_{3}^{1}}\big|_{x_{3}=h/2} = 0 \\ & \mathcal{B}_{v_{1}^{1}} = C_{45}\frac{\partial u_{3}}{\partial x_{2}} + C_{55}\frac{\partial u_{3}}{\partial x_{1}} + C_{55}\frac{\partial v_{1}^{1}}{\partial x_{3}} + C_{45}\frac{\partial v_{2}^{1}}{\partial x_{3}} \\ & \mathcal{B}_{v_{1}^{1}} = C_{44}\frac{\partial u_{3}}{\partial x_{2}} + C_{45}\frac{\partial u_{3}}{\partial x_{1}} + C_{45}\frac{\partial v_{1}^{1}}{\partial x_{3}} + C_{44}\frac{\partial v_{2}^{1}}{\partial x_{3}} \\ & \mathcal{B}_{v_{3}^{1}} = C_{36}\frac{\partial u_{1}}{\partial x_{2}} + C_{23}\frac{\partial u_{2}}{\partial x_{2}} + C_{13}\frac{\partial u_{1}}{\partial x_{1}} + C_{36}\frac{\partial u_{2}}{\partial x_{1}} + C_{33}\frac{\partial v_{3}^{1}}{\partial x_{2}} \end{split}$$

$$(2.23)$$

Solving the Euler Lagrange equations in Eq. (2.22) with the boundary conditions in Eq. (2.23) and the constraints given in Eq. (2.20) yields

$$v_{1}^{1} = -x_{3} \frac{\partial u_{3}}{\partial x_{1}}$$

$$v_{2}^{1} = -x_{3} \frac{\partial u_{3}}{\partial x_{2}}$$

$$v_{3}^{1} = x_{3} f_{1}$$

$$f_{1} = \frac{-1}{C_{33}} \left[C_{36} \frac{\partial u_{1}}{\partial x_{2}} + C_{23} \frac{\partial u_{2}}{\partial x_{2}} + C_{13} \frac{\partial u_{1}}{\partial x_{1}} + C_{36} \frac{\partial u_{2}}{\partial x_{1}} \right]$$
(2.24)

2.3.6 Second Order Solution (SOS)

To improve the results of the FOS, the displacement field at this stage is further perturbed as follows.

$$v_{i} = v_{i}^{0} + v_{i}^{1} + v_{i}^{2}$$
 where
$$v_{1} = u_{1} - x_{3} \frac{\partial u_{3}}{\partial x_{1}} + v_{1}^{2}, \qquad v_{2} = u_{2} - x_{3} \frac{\partial u_{3}}{\partial x_{2}} + v_{2}^{2}$$

$$v_{3} = u_{3} + x_{3} f_{1} + v_{3}^{2}$$
 (2.25)

Following the procedure described in Section 2.3.1, the orders of u_{α} , u_{3} and v_{i}^{0} are estimated to be $O(\xi^{3}l)$, $O(\xi^{2}l)$ and $O(\xi^{3}h)$, respectively. Substituting v_{i} from Eq. (2.25) into Eq. (2.1) gives the following strains, along with their respective orders indicated using underbraces

$$E_{11} = \underbrace{\frac{\partial u_1}{\partial x_1} - x_3 \frac{\partial^2 u_3}{\partial x_1^2}}_{O(\xi^3)} + O\left(\xi^4\right) \quad 2E_{23} = \underbrace{\frac{\partial v_2^2}{\partial x_3}}_{O(\xi^3)} + O\left(\xi^4\right)$$

$$E_{22} = \underbrace{\frac{\partial u_2}{\partial x_2} - x_3 \frac{\partial^2 u_3}{\partial x_2^2}}_{O(\xi^3)} + O\left(\xi^4\right) \quad 2E_{13} = \underbrace{\frac{\partial v_1^2}{\partial x_3}}_{O(\xi^3)} + O\left(\xi^4\right)$$

$$E_{33} = \underbrace{f_1 + \frac{\partial v_3^2}{\partial x_3}}_{O(\xi^3)} + O\left(\xi^4\right)$$

$$2E_{12} = \underbrace{\frac{\partial u_1}{\partial x_2} + \frac{\partial u_2}{\partial x_1} - 2x_3 \frac{\partial^2 u_3}{\partial x_1 \partial x_2}}_{O(\xi^3)} + O\left(\xi^4\right)$$

The revised strains given in Eq. (2.26) are used to recalculate U and U_{sig} . Similar to the ZOS and FOS, the perturbation variables v_i^2 present in U_{sig} have derivatives with respect to x_3 only allowing us to perform the 3D analysis in two stages (1D and 2D analyses).

Through the Thickness 1D Analysis

The functional Π_{x_3} is recalculated to accommodate the modifications in U_{sig} . Extremization of Π_{x_3} yields the following Euler Lagrange equations

$$C_{55} \frac{\partial^{2} v_{1}^{2}}{\partial x_{3}^{2}} + C_{45} \frac{\partial^{2} v_{2}^{2}}{\partial x_{3}^{2}} = 0$$

$$C_{45} \frac{\partial^{2} v_{1}^{2}}{\partial x_{3}^{2}} + C_{44} \frac{\partial^{2} v_{2}^{2}}{\partial x_{3}^{2}} = 0$$

$$C_{23} \frac{\partial^{2} u_{3}}{\partial x_{2}^{2}} + 2C_{36} \frac{\partial^{2} u_{3}}{\partial x_{1} \partial x_{2}} + C_{13} \frac{\partial^{2} u_{3}}{\partial x_{1}^{2}} - C_{33} \frac{\partial^{2} v_{3}^{2}}{\partial x_{3}^{2}} = 0$$

$$(2.27)$$

and the following associated boundary conditions

$$\begin{aligned}
&\mathcal{B}_{v_1^2}\big|_{x_3=-h/2} = \mathcal{B}_{v_1^2}\big|_{x_3=h/2} = 0 \\
&\mathcal{B}_{v_2^2}\big|_{x_3=-h/2} = \mathcal{B}_{v_2^2}\big|_{x_3=h/2} = 0 \\
&\mathcal{B}_{v_3^2}\big|_{x_3=-h/2} = \mathcal{B}_{v_3^2}\big|_{x_3=h/2} = 0 \\
&\mathcal{B}_{v_1^2} = C_{55} \frac{\partial v_1^2}{\partial x_3} + C_{45} \frac{\partial v_2^2}{\partial x_3} \\
&\mathcal{B}_{v_2^2} = C_{45} \frac{\partial v_1^2}{\partial x_3} + C_{44} \frac{\partial v_2^2}{\partial x_3} \\
&\mathcal{B}_{v_3^2} = -x_3 \left(C_{23} \frac{\partial^2 u_3}{\partial x_2^2} + 2C_{36} \frac{\partial^2 u_3}{\partial x_1 \partial x_2} + C_{13} \frac{\partial^2 u_3}{\partial x_1^2} \right) + C_{33} \frac{\partial v_3^2}{\partial x_3}
\end{aligned}$$
(2.28)

Solving the Euler-Lagrange equations in Eq. (2.27) with the boundary conditions in Eq. (2.28) and the constraints given in Eq. (2.20) yields

$$v_{1}^{2} = 0$$

$$v_{2}^{2} = 0$$

$$v_{3}^{2} = -\frac{1}{12}(h^{2} - 12x_{3}^{2})g_{1}$$

$$g_{1} = \frac{1}{2C_{33}} \left[C_{23} \frac{\partial^{2} u_{3}}{\partial x_{2}^{2}} + 2C_{36} \frac{\partial^{2} u_{3}}{\partial x_{1} \partial x_{2}} + C_{13} \frac{\partial^{2} u_{3}}{\partial x_{1}^{2}} \right]$$

$$(2.29)$$

The zeroth-order solution to the second-order solution gives a CLPT like plate theory, which was the objective of Part A of this work. A summary of the approach followed and the key findings of the work done in Part A are presented in the following sections.

2.3.7 Summary of Part A

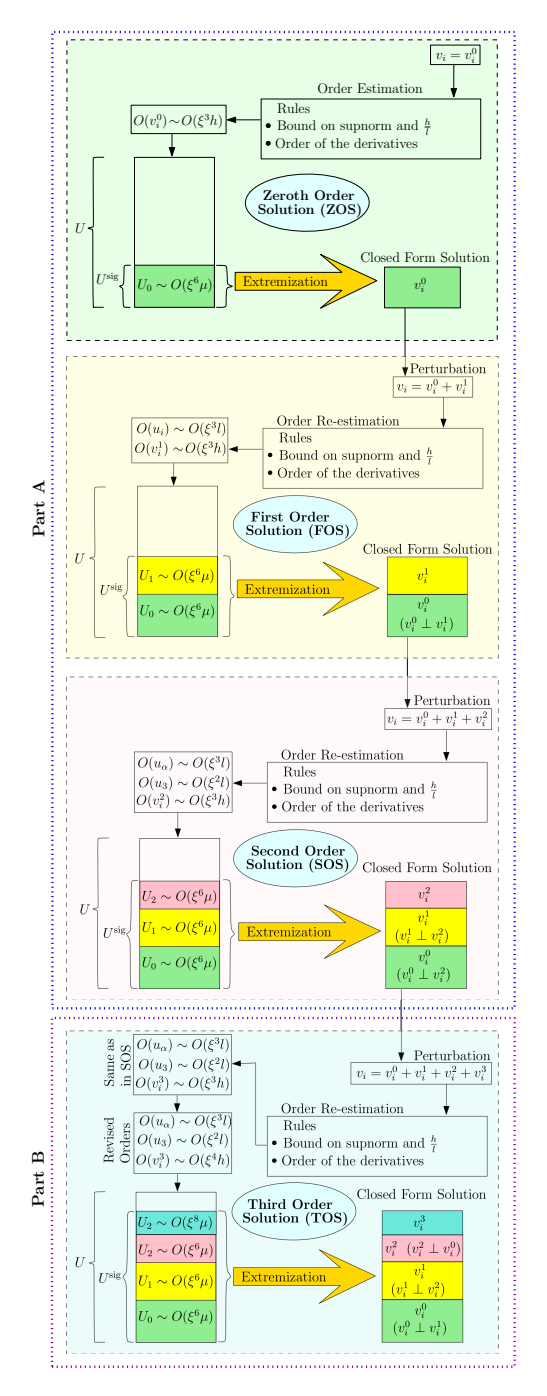


Figure 2.2: Systematic methodology adopted in deriving the reduced order model

Figure 2.2 presents a graphical representation of the adopted procedure. The procedure begins by calculating strains, considering the plate to be a 3D body. It uses an order estimation scheme based on the upper bound on the supnorm and $\frac{h}{l}$ given in Eq. (2.4) and a rule to calculate the order of derivatives of displacement components given in Eq. (2.2).

The zeroth order solution begins with order estimation of different quantities of interest, following the ordering strategy described in Section 2.3.1. This results in an ordered representation of the strain energy density U. The most significant portion of the strain energy density is isolated and termed U_{sig} . Extremization of U_{sig} yields a closed-form solution for the zeroth-order perturbation variables v_i^0 . In the first and second-order solutions, the entire procedure is repeated, including order re-estimation of different quantities of interest following the ordering scheme, selection of the most significant portion of the strain energy density, and its extremization to obtain a closed-form solution for the perturbation variables. A graphical representation of the above procedure has been presented in Fig. 2.2.

2.3.8 Displacement Field Obtained in Part A

The displacement field obtained in Part A of this work is given below

$$v_{1} = \underbrace{u_{1} - x_{3} \frac{\partial u_{3}}{\partial x_{1}}}_{O(\xi^{3}l)}$$

$$v_{2} = \underbrace{u_{2} - x_{3} \frac{\partial u_{3}}{\partial x_{2}}}_{O(\xi^{3}l)}$$

$$v_{3} = \underbrace{u_{3}}_{O(\xi^{2}l)} + \underbrace{x_{3}f_{1} - \frac{1}{12}(h^{2} - 12x_{3}^{2})g_{1}}_{O(\xi^{3}h)}$$

$$(2.30)$$

Let the inner product of the p^{th} and q^{th} order solution of v_i i.e. v_i^p and v_i^q be defined as follows

$$(v_i^p, v_i^q) = \int_{\Omega} v_i^p v_i^q dV = \int_{\Omega} \left(\int_{-h/2}^{h/2} v_i^p v_i^q dx_3 \right) da_{\text{ref}}$$
 (2.31)

For any values of p and q between 0 and 2, we have $(v_i^p, v_i^q) = 0$, which implies that v_i^p and v_i^q are orthogonal. The orthogonality between two solutions of different order ensures their independence and justifies splitting the displacement components into different orders of solutions at the same order of strain energy.

Notably, The displacement components v_1 and v_2 given in Eq. (2.30) are consistent with CLPT [100, 119, 130], validating Kirchhoff's assumption that a line segment perpendicular to the reference plane in the undeformed configuration remains straight and perpendicular to the deformed reference plane after deformation. However, displacement component v_3 given in Eq. (2.30) contradicts Kirchhoff's assumption that there is no change in the length of a transverse normal after deformation (i.e., the transverse normals are inextensible). Interestingly, as will be demonstrated in the next section, the assumption of the plane stress condition in CLPT makes it energetically equivalent to the asymptotically correct plate theory developed in Part A of this work.

2.3.9 Strains Obtained in Part A

Eq. (2.1) and (2.30) give the following strains corrected up to order ξ^3

$$E_{11} = \underbrace{\frac{\partial u_1}{\partial x_1} - x_3 \frac{\partial^2 u_3}{\partial x_1^2}}_{O(\xi^3)} \qquad E_{22} = \underbrace{\frac{\partial u_2}{\partial x_2} - x_3 \frac{\partial^2 u_3}{\partial x_2^2}}_{O(\xi^3)}$$

$$E_{33} = \underbrace{f_1 + 2x_3 g_1}_{O(\xi^3)} \qquad 2E_{23} = 0$$

$$2E_{13} = 0 \qquad 2E_{12} = \underbrace{\frac{\partial u_1}{\partial x_2} + \frac{\partial u_2}{\partial x_1} - 2x_3 \frac{\partial^2 u_3}{\partial x_1 \partial x_2}}_{O(\xi^3)}$$

$$(2.32)$$

It is interesting to note that substituting strains from Eq. (2.32) in Eq. (2.5) yields.

$$\sigma_{33} = C_{13} E_{11} + C_{23} E_{22} + C_{33} E_{33} + 2 C_{36} E_{12} = 0 (2.33)$$

Eq. (2.33) results in plane stress condition, which is valid up to the present level of accuracy in stresses. With $\sigma_{33} = 0$, the transverse normal strain E_{33} does not appear in the virtual work Eq. (2.8), although it is not identically zero. As a result, the transverse normal strain E_{33} is neglected. By omitting the transverse strain component, E_{33} , in Eq. (2.32), we obtain

$$E = \begin{cases} E_{11} \\ E_{22} \\ 2E_{23} \\ 2E_{13} \\ 2E_{12} \end{cases} = \begin{cases} \frac{\frac{\partial u_1}{\partial x_1} - x_3 \frac{\partial^2 u_3}{\partial x_1^2}}{\frac{\partial u_2}{\partial x_2} - x_3 \frac{\partial^2 u_3}{\partial x_2^2}} \\ 0 \\ 0 \\ \frac{\partial u_1}{\partial x_2} + \frac{\partial u_2}{\partial x_1} - 2x_3 \frac{\partial^2 u_3}{\partial x_1 \partial x_2} \end{cases}$$
(2.34)

Interestingly, despite the discrepancy in the displacement field shown in Section 3.8, the asymptotically correct strains E in Eq. (2.34) resemble the strains given by CLPT [100]. This indicates that CLPT plate theory is energetically equivalent to the asymptotically correct plate theory derived considering strain energy up to order ($\xi^6\mu$) and neglecting its higher order part.

The work done in Part A is further refined in Part B, considering the contribution of the higher-order Energy.

2.4 Part B: Refinement of Part A

Part B refines the plate theory obtained in Part A, while maintaining the consistency of the procedure. In addition to the work done in Part A, Part B includes the contribution of higher-order energy in the analysis. Part B is intentionally separated from Part A because the development done in Part B follows the usual procedure found in the literature on VAM-based development of plate theories, where the development begins with a presupposition-based kinematics similar to that developed in Part A, which is then refined by considering a warping vector. The refinement of Part A is presented in the following section.

2.4.1 Third Order Solution (TOS)

Perturbing the displacement field obtained in SOS results in as follows.

$$v_{i} = v_{i}^{0} + v_{i}^{1} + v_{i}^{2} + v_{i}^{3},$$
where
$$v_{1} = u_{1} - x_{3} \frac{\partial u_{3}}{\partial x_{1}} + v_{1}^{3}, \qquad v_{2} = u_{2} - x_{3} \frac{\partial u_{3}}{\partial x_{2}} + v_{2}^{3}$$

$$v_{3} = u_{3} + x_{3} f_{1} - \frac{1}{12} (h^{2} - 12x_{3}^{2}) g_{1} + v_{3}^{3}$$

$$(2.35)$$

It is essential to mention that, following the procedure outlined in section 2.3.1, the orders of u_{α} , u_3 , and v_i^3 are estimated to be $O(\xi^3 l)$, $O(\xi^2 l)$, and $O(\xi^3 h)$, respectively. The estimated orders of the variables are the same as in SOS. Therefore, if we perform extremization based on these variable orders, it will result in $v_i^3 = 0$, leading to no improvement in the displacement field. To improve the displacement field further, we must consider the contribution of higher-order strain energy at this stage. To account for the effect of strain energy of the order of $(\xi^8 \mu)$, we set the order of v_i^3 to $O(\xi^4 h)$ while keeping the orders of the other variables unchanged. Substituting v_i from Eq. (2.35) into Eq. (2.1) yields

$$E_{11} = \frac{\partial u_{1}}{\partial x_{1}} - x_{3} \frac{\partial^{2} u_{3}}{\partial x_{1}^{2}} + \frac{1}{2} \left(\frac{\partial u_{3}}{\partial x_{1}}\right)^{2} + \frac{\partial v_{1}^{3}}{\partial x_{1}} + O\left(\xi^{6}\right)$$

$$E_{22} = \frac{\partial u_{2}}{\partial x_{2}} - x_{3} \frac{\partial^{2} u_{3}}{\partial x_{2}^{2}} + \frac{1}{2} \left(\frac{\partial u_{3}}{\partial x_{2}}\right)^{2} + \frac{\partial^{2} v_{2}^{3}}{\partial x_{2}} + O\left(\xi^{6}\right)$$

$$E_{33} = \underbrace{f_{1} + 2x_{3}g_{1}}_{O(\xi^{3})} + \underbrace{\frac{1}{2} \left(\frac{\partial u_{3}}{\partial x_{1}}\right)^{2} + \frac{1}{2} \left(\frac{\partial u_{3}}{\partial x_{2}}\right)^{2} + \frac{\partial v_{3}^{3}}{\partial x_{3}}}_{O(\xi^{4})} + O\left(\xi^{6}\right)$$

$$2E_{23} = \underbrace{x_{3} \frac{\partial f_{1}}{\partial x_{2}} - \frac{1}{12} \left(h^{2} - 12x_{3}^{2}\right) \frac{\partial g_{1}}{\partial x_{2}} + \frac{\partial v_{3}^{3}}{\partial x_{3}}}_{O(\xi^{4})} + \underbrace{\frac{\partial u_{3}}{\partial x_{2}} \left(f_{1} + 2x_{3}g_{1} - \frac{\partial u_{2}}{\partial x_{2}} + x_{3} \frac{\partial^{2} u_{3}}{\partial x_{2}^{2}}\right)}_{O(\xi^{6})}$$

$$- \underbrace{\frac{\partial u_{1}}{\partial x_{2}} \frac{\partial u_{3}}{\partial x_{1}} + x_{3} \frac{\partial u_{3}}{\partial x_{1}} \frac{\partial^{2} u_{3}}{\partial x_{1} \partial x_{2}} + \frac{\partial v_{3}^{3}}{\partial x_{2}^{2}}}_{O(\xi^{6})} + \underbrace{\frac{\partial u_{3}}{\partial x_{1}} \left(f_{1} + 2x_{3}g_{1} - \frac{\partial u_{2}}{\partial x_{1}} + x_{3} \frac{\partial v_{3}}{\partial x_{2}}\right)}_{O(\xi^{6})}_{O(\xi^{6})} + \underbrace{\frac{\partial u_{3}}{\partial x_{1}} \left(f_{1} + 2x_{3}g_{1} - \frac{\partial u_{1}}{\partial x_{1}} + x_{3} \frac{\partial^{2} u_{3}}{\partial x_{2}}\right)}_{O(\xi^{6})}_{O(\xi^{6})} + \underbrace{\frac{\partial u_{3}}{\partial x_{1}} \left(f_{1} + 2x_{3}g_{1} - \frac{\partial u_{1}}{\partial x_{1}} + x_{3} \frac{\partial^{2} u_{3}}{\partial x_{2}}\right)}_{O(\xi^{6})}_{O(\xi^{6})} + \underbrace{\frac{\partial u_{3}}{\partial x_{1}} \left(f_{1} + 2x_{3}g_{1} - \frac{\partial u_{1}}{\partial x_{1}} + x_{3} \frac{\partial^{2} u_{3}}{\partial x_{2}}\right)}_{O(\xi^{6})}_{O(\xi^{6})} + \underbrace{\frac{\partial u_{3}}{\partial x_{1}} \frac{\partial^{2} u_{3}}{\partial x_{2}} + x_{3} \frac{\partial^{2} u_{3}}{\partial x_{1} \partial x_{2}} + \frac{\partial v_{3}^{3}}{\partial x_{1}} + O\left(\xi^{6}\right)}_{O(\xi^{6})}_{O(\xi^{6})} + \underbrace{\frac{\partial u_{3}}{\partial x_{1}} \frac{\partial^{2} u_{3}}{\partial x_{2}} + \frac{\partial v_{3}^{3}}{\partial x_{1} \partial x_{2}} + \frac{\partial v_{3}^{3}}{\partial x_{1}} + O\left(\xi^{6}\right)}_{O(\xi^{6})}_{O(\xi^{6})} + \underbrace{\frac{\partial u_{3}}{\partial x_{1}} \frac{\partial^{2} u_{3}}{\partial x_{2}} + \frac{\partial v_{3}^{3}}{\partial x_{1} \partial x_{2}} + \frac{\partial v_{3}^{3}}{\partial x_{1}} + O\left(\xi^{6}\right)}_{O(\xi^{6})}_{O(\xi^$$

The revised strains given in Eq. (2.36) are used to recalculate U which takes the following form

$$U = \underbrace{U_{\text{sig}}}_{O(\xi^{6}\mu)} + O(\xi^{9}\mu)$$
(2.37)

Where U_0 , U_1 , U_2 , and U_3 are the contributions of the strain energy density U in the zeroth, first, second, and third order solutions, respectively. To include the effect of higher order energy, the portion of U corrected up to $O(\xi^8\mu)$ is taken as U_{sig} . The functional Π_{x_3} is recalculated to incorporate the change in U_{sig} .

It is important to note that in the third order solution, unlike the zeroth, first, and second order solutions, the derivatives of the perturbation variables v_i^3 with respect to the x_{α} coordinates, i.e., $\left(\frac{\partial v_i^3}{\partial x_{\alpha}}\right)$, appear in the analysis. To eliminate these derivatives, integration by parts is performed, which results in boundary conditions defined at Ω_{side} . However, these boundary conditions are ignored in the present analysis, as the goal is to find the displacement field for the interior domain of the plate without considering edge effects.

Extremization of Π_{x_3} yields the following Euler Lagrange equations

$$2C_{55}f_2 + 6C_{55}x_3g_2 + 2C_{45}f_3 + 6C_{45}x_3g_3 = C_{55}\frac{\partial^2 v_1^3}{\partial x_3^2} + C_{45}\frac{\partial^2 v_2^3}{\partial x_3^2}$$

$$2C_{45}f_2 + 6C_{45}x_3g_2 + 2C_{44}f_3 + 6C_{44}x_3g_3 = C_{45}\frac{\partial^2 v_1^3}{\partial x_3^2} + C_{44}\frac{\partial^2 v_2^3}{\partial x_3^2}$$

$$C_{33}\frac{\partial^2 v_3^3}{\partial x_3^2} = 0$$

$$(2.38)$$

Where f_2 , f_3 , g_2 and g_3 are functions of x_1 and x_2 . The expressions for these functions in terms of derivatives of u_i w.r.t. x_j and the material constants are given in Appendix C. The associated boundary conditions are given below

$$\begin{aligned}
&\mathcal{B}_{v_{1}^{3}}\big|_{x_{3}=-h/2} = \mathcal{B}_{v_{1}^{3}}\big|_{x_{3}=h/2} = 0 \\
&\mathcal{B}_{v_{2}^{3}}\big|_{x_{3}=-h/2} = \mathcal{B}_{v_{2}^{3}}\big|_{x_{3}=h/2} = 0 \\
&\mathcal{B}_{v_{3}^{3}}\big|_{x_{3}=-h/2} = \mathcal{B}_{v_{3}^{3}}\big|_{x_{3}=h/2} = 0 \\
&\mathcal{B}_{v_{1}^{3}} = C_{45}x_{3}\frac{\partial f_{1}}{\partial x_{2}} + C_{45}\left(-\frac{h^{2}}{12} + x_{3}^{2}\right)\frac{\partial g_{1}}{\partial x_{2}} + C_{55}x_{3}\frac{\partial f_{1}}{\partial x_{1}} \\
&+ C_{55}\left(-\frac{h^{2}}{12} + x_{3}^{2}\right)\frac{\partial g_{1}}{\partial x_{1}} + C_{55}\frac{\partial v_{1}^{3}}{\partial x_{3}} + C_{45}\frac{\partial v_{2}^{3}}{\partial x_{3}} \\
&\mathcal{B}_{v_{2}^{3}} = C_{44}x_{3}\frac{\partial f_{1}}{\partial x_{2}} + C_{44}\left(-\frac{h^{2}}{12} + x_{3}^{2}\right)\frac{\partial g_{1}}{\partial x_{1}} + C_{45}\frac{\partial v_{1}^{3}}{\partial x_{3}} + C_{44}\frac{\partial v_{2}^{3}}{\partial x_{3}} \\
&+ C_{45}\left(-\frac{h^{2}}{12} + x_{3}^{2}\right)\frac{\partial g_{1}}{\partial x_{1}} + C_{45}\frac{\partial v_{1}^{3}}{\partial x_{3}} + C_{44}\frac{\partial v_{2}^{3}}{\partial x_{3}} \\
&\mathcal{B}_{v_{3}^{3}} = C_{33}\frac{\partial v_{3}^{3}}{\partial x_{3}}
\end{aligned} \tag{2.39}$$

solving the Euler Lagrange equations Eq. (2.38) with the boundary conditions Eq. (2.39) and the constraints given in Eq. (2.20) yields

$$f_{2} = -\frac{1}{2} \frac{\partial f_{1}}{\partial x_{1}}$$

$$f_{3} = -\frac{1}{2} \frac{\partial f_{1}}{\partial x_{2}}$$

$$v_{1}^{3} = \left(-\frac{3}{4}h^{2}x_{3} + x_{3}^{3}\right) g_{2} + \left(\frac{1}{24}h^{2} - \frac{1}{2}x_{3}^{2}\right) \frac{\partial f_{1}}{\partial x_{1}} - \frac{1}{6}h^{2}x_{3} \frac{\partial g_{1}}{\partial x_{1}}$$

$$v_{2}^{3} = \left(-\frac{3}{4}h^{2}x_{3} + x_{3}^{3}\right) g_{3} + \left(\frac{1}{24}h^{2} - \frac{1}{2}x_{3}^{2}\right) \frac{\partial f_{1}}{\partial x_{2}} - \frac{1}{6}h^{2}x_{3} \frac{\partial g_{1}}{\partial x_{2}}$$

$$v_{3}^{3} = -\frac{1}{2C_{33}}x_{3} \left[(C_{23} + C_{33}) \left(\frac{\partial u_{3}}{\partial x_{2}}\right)^{2} + 2C_{36} \frac{\partial u_{3}}{\partial x_{1}} \frac{\partial u_{3}}{\partial x_{2}} + (C_{13} + C_{33}) \left(\frac{\partial u_{3}}{\partial x_{1}}\right)^{2} \right]$$

$$(2.40)$$

A graphical representation of the adopted procedure for the development done in Part B is presented in Fig. 2.2.

2.4.2 A Discussion on the Displacement Field

The final displacement field obtained in Part A and B is given below.

$$v_{1} = \underbrace{u_{1} - x_{3} \frac{\partial u_{3}}{\partial x_{1}}}_{O(\xi^{3}l)} + \underbrace{\left(-\frac{3}{4}h^{2}x_{3} + x_{3}^{3}\right) g_{2} + \left(\frac{1}{24}h^{2} - \frac{1}{2}x_{3}^{2}\right) \frac{\partial f_{1}}{\partial x_{1}} - \frac{1}{6}h^{2}x_{3} \frac{\partial g_{1}}{\partial x_{1}}}_{O(\xi^{4}h)}$$

$$v_{2} = \underbrace{u_{2} - x_{3} \frac{\partial u_{3}}{\partial x_{2}}}_{O(\xi^{3}l)} + \underbrace{\left(-\frac{3}{4}h^{2}x_{3} + x_{3}^{3}\right) g_{3} + \left(\frac{1}{24}h^{2} - \frac{1}{2}x_{3}^{2}\right) \frac{\partial f_{1}}{\partial x_{2}} - \frac{1}{6}h^{2}x_{3} \frac{\partial g_{1}}{\partial x_{2}}}_{O(\xi^{4}h)}$$

$$v_{3} = \underbrace{u_{3}}_{O(\xi^{2}l)} + \underbrace{x_{3}f_{1} - \frac{1}{12}(h^{2} - 12x_{3}^{2})g_{1}}_{O(\xi^{3}h)}$$

$$- \underbrace{\frac{1}{2C_{33}}x_{3}\left[\left(C_{23} + C_{33}\right)\left(\frac{\partial u_{3}}{\partial x_{2}}\right)^{2} + 2C_{36}\frac{\partial u_{3}}{\partial x_{1}}\frac{\partial u_{3}}{\partial x_{2}} + \underbrace{\left(C_{13} + C_{33}\right)\left(\frac{\partial u_{3}}{\partial x_{1}}\right)^{2}\right]}_{O(\xi^{4}h)}$$

$$(2.41)$$

The evolution of this displacement field is influenced by each perturbation we go through. A graphical representation of the improvements made to the displacement field as we progress through each perturbation is depicted in Fig (2.3)

Fig. 2.3(a) displays a line segment CD in the reference plane, oriented along \hat{e}_1 , while line segment AB is oriented along \hat{e}_3 . The deformed configuration of line segment

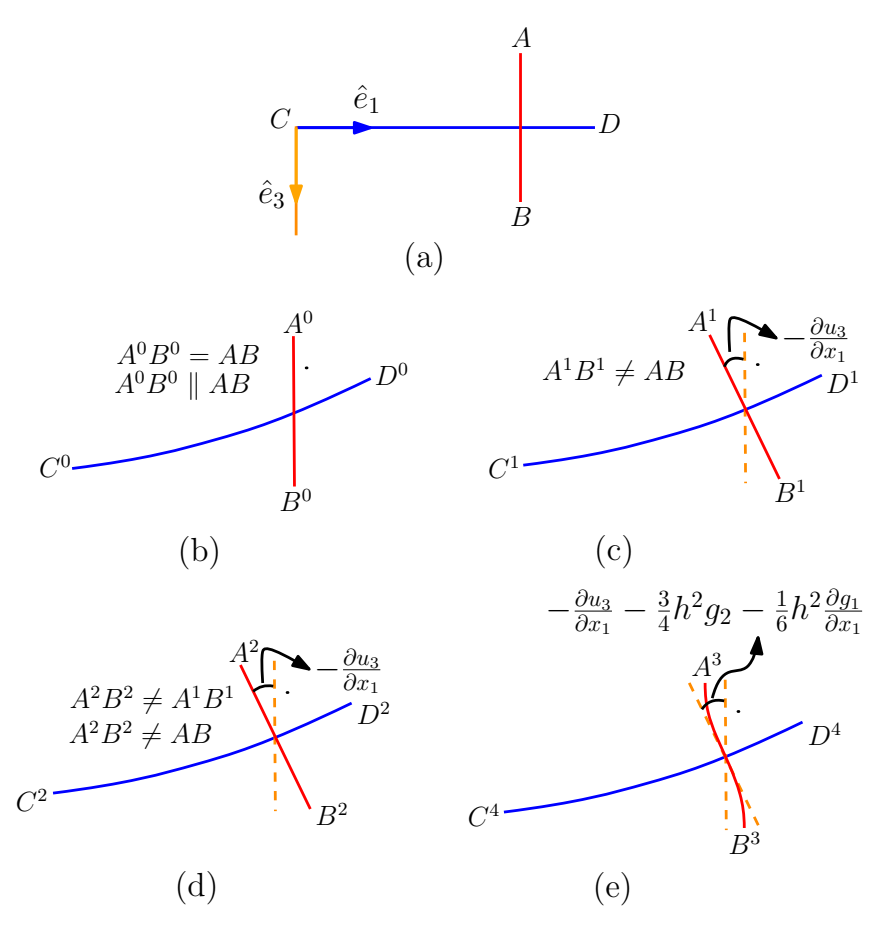


Figure 2.3: Deformation of lines AB and CD lying along direction \hat{e}_3 and \hat{e}_1 respectively. (a) Undeformed configuration (b) Configuration after zeroth perturbation (c) Configuration after first perturbation (d) Configuration after second perturbation (e) Configuration after third perturbation

AB in ZOS is depicted in Fig. 2.3(b) by line segment A^0B^0 . In the FOS and SOS, the displacement field undergoes refinements, incorporating a rotation of line AB and a change in its length, as shown in Fig. 2.3(c) and 2.3(d) by line segments A^1B^1 and A^2B^2 . In the third-order solutions, the line segment AB deforms to the curve line A^3B^3 as shown in Fig. 2.3(e).

2.4.3 A Discussion on the Strains, Stresses and Stiffness Matrix

Eq. (2.1) and (2.41) give the strains corrected up to order (ξ^4). These strains are given below:

$$E_{11} = \underbrace{\frac{\partial u_1}{\partial x_1} - x_3 \frac{\partial^2 u_3}{\partial x_1^2}}_{O(\xi^3)} + \underbrace{\frac{1}{2} \left(\frac{\partial u_3}{\partial x_1}\right)^2}_{O(\xi^4)}$$

$$E_{22} = \underbrace{\frac{\partial u_2}{\partial x_2} - x_3 \frac{\partial^2 u_3}{\partial x_2^2}}_{O(\xi^3)} + \underbrace{\frac{1}{2} \left(\frac{\partial u_3}{\partial x_1}\right)^2}_{O(\xi^4)}$$

$$E_{33} = \underbrace{-\frac{1}{2C_{33}} \left[-2C_{33}(f_1 + 2x_3g_1)\right]}_{O(\xi^4)}$$

$$+ \underbrace{\frac{1}{2C_{33}} \left[C_{23} \left(\frac{\partial u_3}{\partial x_2}\right)^2 + 2C_{36} \frac{\partial u_3}{\partial x_1} \frac{\partial u_3}{\partial x_2} + C_{13} \left(\frac{\partial u_3}{\partial x_1}\right)^2\right]}_{O(\xi^4)}$$

$$2E_{23} = \underbrace{-\frac{1}{4} (h^2 - 4x_3^2) \left(3g_3 + \frac{\partial g_1}{\partial x_2}\right)}_{O(\xi^4)}$$

$$2E_{13} = \underbrace{-\frac{1}{4} (h^2 - 4x_3^2) \left(3g_2 + \frac{\partial g_1}{\partial x_1}\right)}_{O(\xi^4)}$$

$$2E_{12} = \underbrace{\frac{\partial u_1}{\partial x_2} + \frac{\partial u_2}{\partial x_1} - 2x_3 \frac{\partial^2 u_3}{\partial x_1 \partial x_2}}_{O(\xi^4)} + \underbrace{\left(\frac{\partial u_3}{\partial x_1}\right) \left(\frac{\partial u_3}{\partial x_2}\right)}_{O(\xi^4)}$$

It is interesting to note that the plane stress condition, which was valid in Part A, is still valid. The plane stress condition can easily be verified by substituting strains from Eq. (2.42) in Eq. (2.5). This subtitution results in $\sigma_{33} = 0$. It is worth noting that the plane stress condition is a natural outcome of the adopted procedure without introducing it as an *ad hoc* or *a priori* assumption as done in many plate theories found in literature [119, 122, 68].

The plane stress condition, with its historical precedent, is often a popular choice for plate theories due to its simplicity, computational efficiency, and accuracy for many engineering applications. Following the same argument as in section 3.9, the transverse normal strain E_{33} is neglected. By omitting the transverse strain component, E_{33} , in Eq. (2.42), we obtain

$$E = \begin{cases} \frac{\partial u_1}{\partial x_1} - x_3 \frac{\partial^2 u_3}{\partial x_1^2} + \frac{1}{2} \left(\frac{\partial u_3}{\partial x_1} \right)^2 \\ \frac{\partial u_2}{\partial x_2} - x_3 \frac{\partial^2 u_3}{\partial x_2^2} + \frac{1}{2} \left(\frac{\partial u_3}{\partial x_2} \right)^2 \\ -\frac{1}{4} (h^2 - 4x_3^2) \left(3g_3 + \frac{\partial g_1}{\partial x_2} \right) \\ -\frac{1}{4} (h^2 - 4x_3^2) \left(3g_2 + \frac{\partial g_1}{\partial x_1} \right) \\ \frac{\partial u_1}{\partial x_2} + \frac{\partial u_2}{\partial x_1} - 2x_3 \frac{\partial^2 u_3}{\partial x_1 \partial x_2} + \left(\frac{\partial u_3}{\partial x_1} \right) \left(\frac{\partial u_3}{\partial x_2} \right) \end{cases}$$

$$(2.43)$$

Also, the stiffness matrix shown in Eq. (2.6) is modified according to the plane stress condition [119] as

$$D = \begin{bmatrix} D_{11} & D_{12} & 0 & 0 & D_{16} \\ D_{12} & D_{22} & 0 & 0 & D_{26} \\ 0 & 0 & D_{44} & D_{45} & 0 \\ 0 & 0 & D_{45} & D_{55} & 0 \\ D_{16} & D_{26} & 0 & 0 & D_{66} \end{bmatrix}$$

$$(2.44)$$

It is interesting to note that the strains accurate up to order (ξ^4) differ from those given by FSDT. This indicates that FSDT is not asymptotically correct, due to which it requires a shear correction factor and does not accurately represent the true behavior of transverse shear strains. Under plane stress conditions, stresses σ and strain energy density U take the following form

$$\sigma = \{\sigma_{11}, \ \sigma_{22}, \ \tau_{23}, \ \tau_{13}, \ \tau_{12}\}^T = DE,$$

$$U = \frac{1}{2}\sigma E = \frac{1}{2}(DE)E$$
(2.45)

2.5 Part C: Elimination of Higher Order Derivatives

It is important to note that though expressions $\left(3g_3 + \frac{\partial g_1}{\partial x_2}\right)$, and $\left(3g_2 + \frac{\partial g_1}{\partial x_1}\right)$ in Eq. (2.43) are asymptotically accurate but they depend on higher order derivatives of u_3 . This results in complexity in the 2D solution and thus limits its practical implementation. In contrast, FSDT, though asymptotically inaccurate, is very practical due to its simplicity and computational efficiency, thereby often preferred for the analysis of thin and moderately thick plates. Our goal is to derive a plate theory that is computationally efficient and simple, like FSDT, but more accurate and asymptotically correct.

FSDT plate theory accounts for the transverse shear deformation effects in the plate. In FSDT, it is assumed that a straight line normal to the undeformed reference plane $\partial\Omega_{\rm ref}$ remains straight but not perpendicular to the deformed reference plane $\partial\Omega_{\rm ref}$ and

has rotations ϕ_1 and ϕ_2 about the x_1 and x_2 axes. Thus, FSDT plate theory incorporates two additional degrees of freedom ϕ_1 and ϕ_2 . In the present work, a novel isoenergetic approach, which is illustrated in Fig. 2.4, has been developed. In this approach, the shear deformation energies obtained from the VAM-based asymptotically correct plate model are equated to that obtained from the FSDT plate model to calculate shear correction factors. Further, using these shear correction factors, the transverse shear force resultants Q_1 and Q_2 are calculated in terms of ϕ_1 and ϕ_2 . Now Q_1 and Q_2 are used to eliminate the inconvenient terms $\left(3g_3 + \frac{\partial g_1}{\partial x_2}\right)$ and $\left(3g_2 + \frac{\partial g_1}{\partial x_4}\right)$ from the VAM based asymptotically correct plate model. As a result of this, a modified asymptotically correct plate model is obtained, which is as simple and computationally efficient as the FSDT theory. In what follows, we present the above-mentioned procedure in detail.

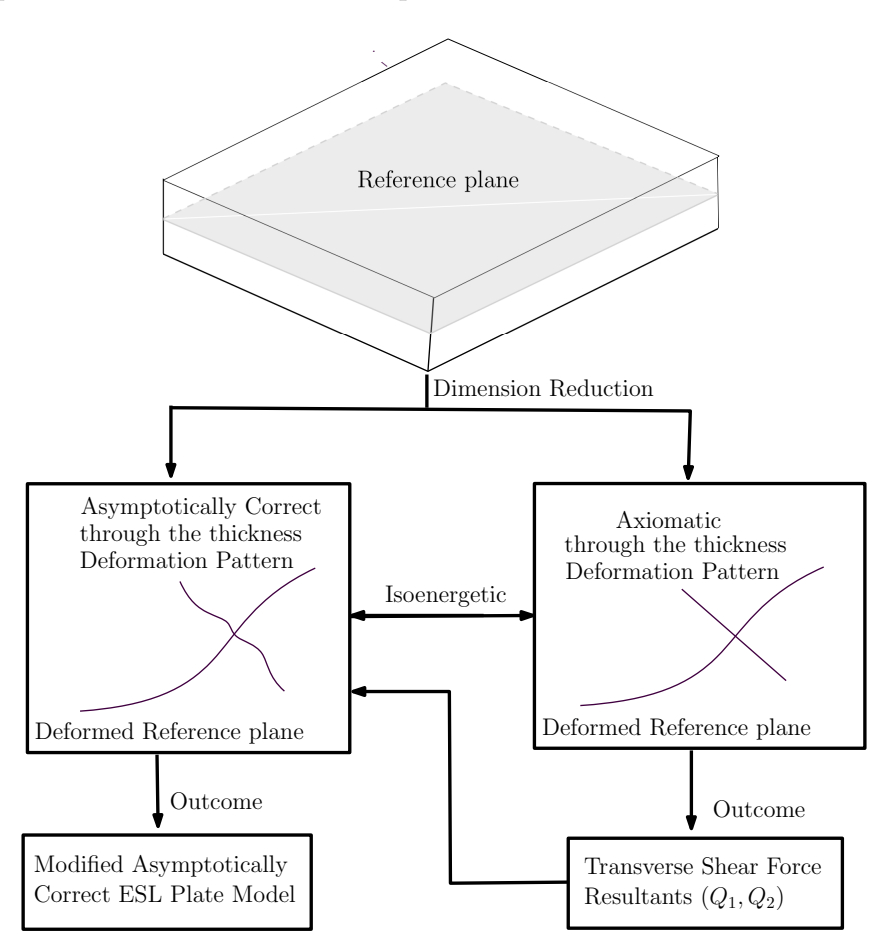


Figure 2.4: The isoenergetic approach

2.5.1 Simplified Model Based on Isoenergetics

The transverse shear force resultants Q_1 and Q_2 are given by

$$Q_1 = \int_{-h/2}^{h/2} \tau_{13} \, dx_3, \quad Q_2 = \int_{-h/2}^{h/2} \tau_{23} \, dx_3 \tag{2.46}$$

From Eqs. (2.45) and (2.46), we have

$$Q_{1} = \int_{-h/2}^{h/2} (2 D_{45} E_{23} + 2 D_{55} E_{13}) dx_{3}$$

$$Q_{2} = \int_{-h/2}^{h/2} (2 D_{44} E_{23} + 2 D_{45} E_{13}) dx_{3}$$
(2.47)

Eq. (2.47) gives,

$$\left(3g_3 + \frac{\partial g_1}{\partial x_2}\right) = -\frac{6\left(D_{45}Q_1 - D_{55}Q_2\right)}{\left(D_{45}^2 - D_{44}D_{55}\right)h^3}
\left(3g_2 + \frac{\partial g_1}{\partial x_1}\right) = -\frac{6\left(-D_{44}Q_1 + D_{45}Q_2\right)}{\left(D_{45}^2 - D_{44}D_{55}\right)h^3}$$
(2.48)

Substituting Eq. (2.48) in Eq. (2.43), we obtain

$$E = \begin{cases} \frac{\partial u_1}{\partial x_1} - x_3 \frac{\partial^2 u_3}{\partial x_1^2} + \frac{1}{2} \left(\frac{\partial u_3}{\partial x_1} \right)^2 \\ \frac{\partial u_2}{\partial x_2} - x_3 \frac{\partial^2 u_3}{\partial x_2^2} + \frac{1}{2} \left(\frac{\partial u_3}{\partial x_2} \right)^2 \\ \frac{3}{2} \left(h^2 - 4 x_3^2 \right) \frac{(D_{45}Q_1 - D_{55}Q_2)}{(D_{45}^2 - D_{44}D_{55})h^3} \\ \frac{3}{2} \left(h^2 - 4 x_3^2 \right) \frac{(-D_{44}Q_1 + D_{45}Q_2)}{(D_{45}^2 - D_{44}D_{55})h^3} \\ \frac{\partial u_1}{\partial x_2} + \frac{\partial u_2}{\partial x_1} - 2x_3 \frac{\partial^2 u_3}{\partial x_1 \partial x_2} + \left(\frac{\partial u_3}{\partial x_1} \right) \left(\frac{\partial u_3}{\partial x_2} \right) \end{cases}$$

$$(2.49)$$

In FSDT, the transverse shear strains E_{23}^{ϕ} and E_{13}^{ϕ} are given as

$$2E_{13}^{\phi} = \phi_1 + \frac{\partial u_3}{\partial x_1}, \quad 2E_{23}^{\phi} = \phi_2 + \frac{\partial u_3}{\partial x_2}$$
 (2.50)

and the transverse shear force resultants, Q_1 and Q_2 are given as

$$Q_{1} = K_{1} \int_{-h/2}^{h/2} \left[D_{45} \left(\phi_{2} + \frac{\partial u_{3}}{\partial x_{2}} \right) + D_{55} \left(\phi_{1} + \frac{\partial u_{3}}{\partial x_{1}} \right) \right] dx_{3}$$

$$Q_{2} = K_{2} \int_{-h/2}^{h/2} \left[D_{44} \left(\phi_{2} + \frac{\partial u_{3}}{\partial x_{2}} \right) + D_{45} \left(\phi_{1} + \frac{\partial u_{3}}{\partial x_{1}} \right) \right] dx_{3}$$
(2.51)

where K_1 and K_2 are shear correction factors [83]. Eq. (2.50) and (2.51) gives

$$2E_{13}^{\phi} = \phi_1 + \frac{\partial u_3}{\partial x_1} = -\frac{D_{44}K_2Q_1 - D_{45}K_1Q_2}{D_{45}^2hK_1K_2 - D_{44}D_{55}hK_1K_2}$$

$$2E_{23}^{\phi} = \phi_2 + \frac{\partial u_3}{\partial x_2} = \frac{D_{45}K_2Q_1 - D_{55}K_1Q_2}{D_{45}^2hK_1K_2 - D_{44}D_{55}hK_1K_2}$$
(2.52)

Now K_1 and K_2 are calculated by equating the transverse shear deformation energies [123, 117, 129, 145, 146] of the assumption based FSDT plate model and the present (ACI-ESL) plate model, as shown below:

$$\int_{-h/2}^{h/2} E_{13}^{\phi} \tau_{13} dx_3 = \int_{-h/2}^{h/2} E_{13} \left(D_{45} E_{23} + D_{55} E_{13} \right) dx_3
\int_{-h/2}^{h/2} E_{23}^{\phi} \tau_{23} dx_3 = \int_{-h/2}^{h/2} E_{23} \left(D_{44} E_{23} + D_{45} E_{13} \right) dx_3$$
(2.53)

Solving Eq. (2.53) for K_1 and K_2 we have

$$K_1 = K_2 = \frac{5}{6} \tag{2.54}$$

A key observation here is that the above-obtained values of the shear correction factors are a natural outcome of the present approach (without taking any assumptions). Furthermore, these values of shear correction factors are exactly the same as obtained for homogeneous materials in references [122, 123, 121]. Substituting Eq. (2.54) into Eq. (2.51) followed by Eq. (2.51) into Eq. (2.49), the following expressions for the transverse shear strains are established

$$2E_{\alpha 3} = \frac{5(h^2 - 4x_3^2)}{4h^2} \left(\phi_{\alpha} + \frac{\partial u_3}{\partial x_{\alpha}}\right) \tag{2.55}$$

Since the order of the transverse shear strains is $O(\xi^4)$, therefore we have

$$x_3 \frac{d}{dx_\alpha} \left(\phi_\beta + \frac{\partial u_3}{\partial x_\beta} \right) \sim O\left(\xi^5\right)$$
 (2.56)

Eqs. (2.56) results in as follows

$$-x_3 \frac{\partial^2 u_3}{\partial x_\alpha \partial x_\beta} = x_3 \frac{\partial \phi_\beta}{\partial x_\alpha} + O\left(\xi^5\right) \tag{2.57}$$

Eq. (2.49), (2.55) and (2.57) results is the following strains

$$E = \begin{cases} \frac{\partial u_1}{\partial x_1} + x_3 \frac{\partial \phi_1}{\partial x_1} + \frac{1}{2} \left(\frac{\partial u_3}{\partial x_1}\right)^2 \\ \frac{\partial u_2}{\partial x_2} + x_3 \frac{\partial \phi_2}{\partial x_2} + \frac{1}{2} \left(\frac{\partial u_3}{\partial x_2}\right)^2 \\ \frac{5(h^2 - 4x_3^2)}{4h^2} \left(\phi_2 + \frac{\partial u_3}{\partial x_2}\right) \\ \frac{5(h^2 - 4x_3^2)}{4h^2} \left(\phi_1 + \frac{\partial u_3}{\partial x_1}\right) \\ \frac{\partial u_1}{\partial x_2} + \frac{\partial u_2}{\partial x_1} + x_3 \left(\frac{\partial \phi_1}{\partial x_2} + \frac{\partial \phi_2}{\partial x_1}\right) + \left(\frac{\partial u_3}{\partial x_1}\right) \left(\frac{\partial u_3}{\partial x_2}\right) \end{cases}$$

$$(2.58)$$

Eq. (2.58) provides a simplified and computationally efficient reduced dimensional model of the plate. Although it is as simple as the FSDT, it is asymptotically accurate up to $O(\xi^4)$, which gives better results than the FSDT. Additionally, it does not require any shear correction factor.

2.6 Results and Discussion

This chapter introduces a new ACI-ESL plate theory, which is asymptotically correct up to $(O(\xi^4))$. To evaluate its accuracy, numerical examples dealing with different scenarios are presented. Six distinct examples (Examples 1-6) are detailed. All examples utilize the material properties outlined in Table 2.1. In this table, subscripts L and T denote the longitudinal (x) and transverse (y) directions, as illustrated in Figure 2.5. Furthermore, Figure 2.6 depicts the boundary conditions employed in the numerical examples and Table 2.2 presents the geometry, material properties, and boundary conditions used in different examples. In all examples, the plate edges are aligned with the x_1 and x_2 axes. In Example-1, Example-2 and Example-4, the plate is subjected to a uniform pressure P on the top face $(x_3 = -\frac{h}{2})$. In Example-3, a square plate [116] with length a and thickness a, subjected to a sinusoidally varying pressure a on its top face, is examined.

Table 2.1: Material properties used in different numerical examples

-	Material-1 [116]	Material-2 [153]	Material-3 [154]	Material-4 [144]
E_L (GPa)	172.369	40	227.53	206.843
E_T (GPa)	6.895	1	144.79	206.843
G_{LT} (GPa)	3.337	0.6	55.16	78.588
G_{TT} (GPa)	1.379	0.5	27.58	78.587
$ u_{LT}$	0.25	0.25	0.25	0.316
$ u_{TT}$	0.25	0.25	0.25	0.316

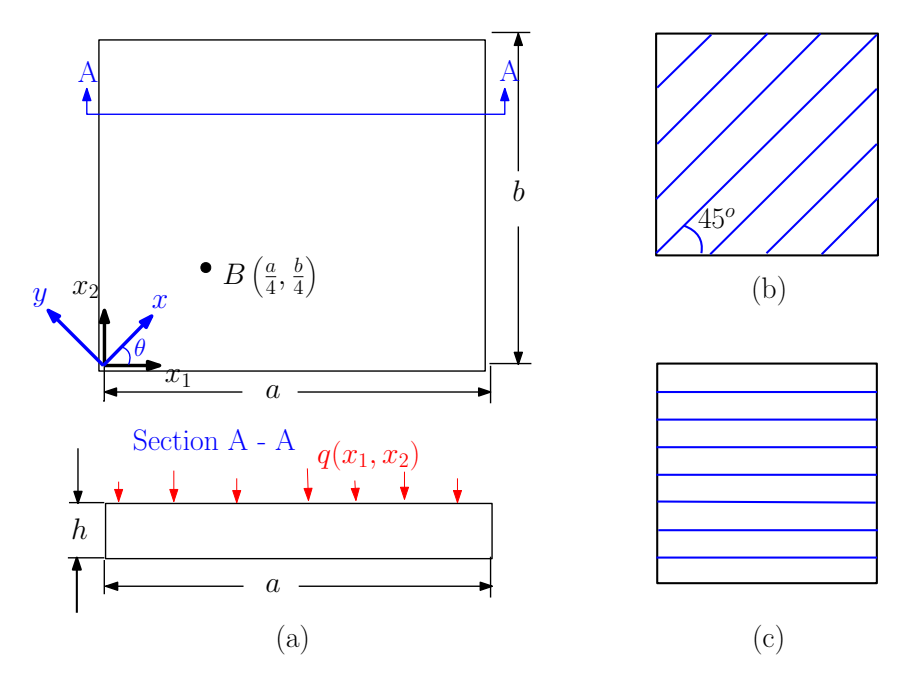


Figure 2.5: (a) Geometry, loading, and material orientation details for all numerical examples. (b) Specific material orientation used in Example-1 ($\theta = 45^{\circ}$). (c) Material orientation used in the remaining examples ($\theta = 0^{\circ}$).

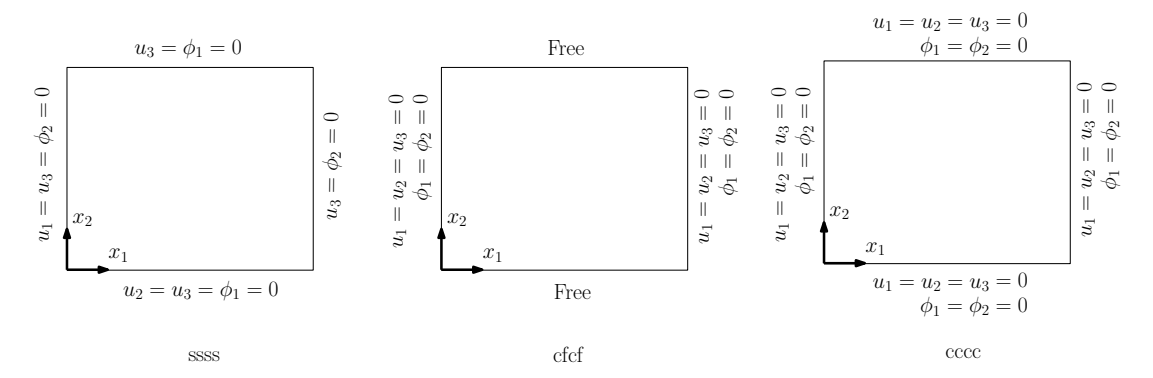


Figure 2.6: Boundary conditions used in different numerical examples

$$q = q_0 \sin\left(\frac{\pi \ x_1}{a}\right) \sin\left(\frac{\pi \ x_2}{a}\right) \tag{2.59}$$

In Example-1, as shown in Fig. 2.5(b), the longitudinal direction x of the material orientation makes an angle of 45° with the x_1 axis, resulting in the monoclinic symmetry about the mid-plane of the plate. In All other examples, as shown in Fig. 2.5(c), the longitudinal direction x of the material orientation aligns with the x_1 axis, leading to the orthotropic behavior of the material.

Numerical	Geometry				Material	Boundary
Example	(Fig. 2.5)				Properties	Conditions
	a (m)	b (m)	h (m)	$\frac{b}{h}$	(Table 2.1)	(Fig. 2.6)
Example-1	1	1	0.01	100	Material-1	SSSS
Example-2	0.5472	0.1824	0.001824	100	Material-2	cfcf
Example-3	a	a	h		Material-1	SSSS
Example-4	0.2	0.2	0.002667	75	Material-3	cccc

Table 2.2: Geometry, Material Properties and boundary conditions for the numerical examples

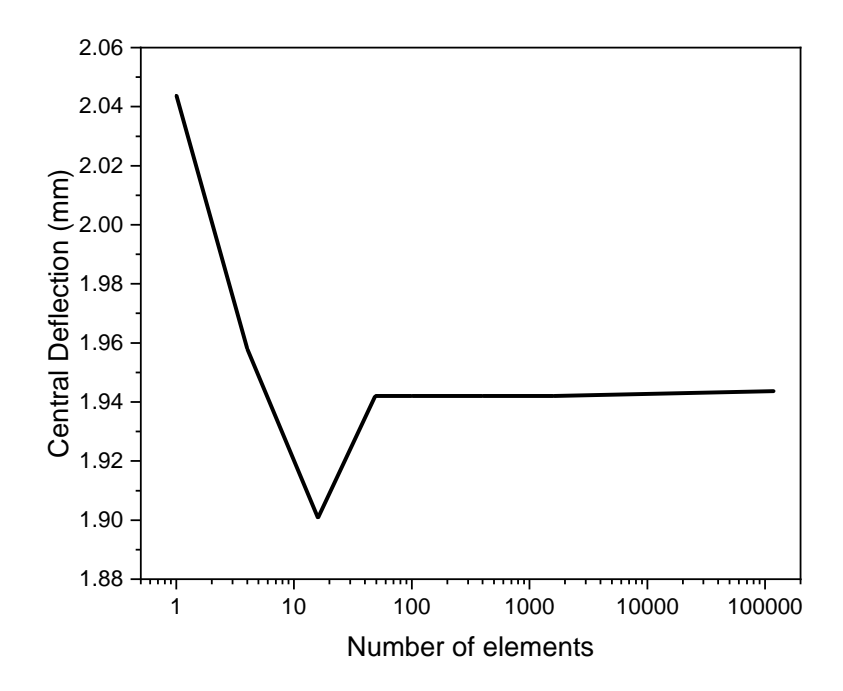


Figure 2.7: Convergence plot for the out of plane deflection u_3 for Example-1 under uniform Pressure of $P = 25 \text{ kN/m}^2$ applied at the top face.

For Example-1 and Example-2, the transverse displacement of the plate midpoint for different values of P is calculated [61, 138] utilizing the proposed plate model (ACI-ESL), FSDT, and 3D FEA approaches. Fig. 2.8 and 2.9 show that the transverse displacement computed by the proposed plate model for Example-1 and Example-2, respectively, is in excellent agreement with the 3D FEA. In this work, the 3D finite element analysis was performed using the Abaqus software. The chosen element type for the analysis was C3D20R, which corresponds to a 20-node quadratic brick element with reduced integra-

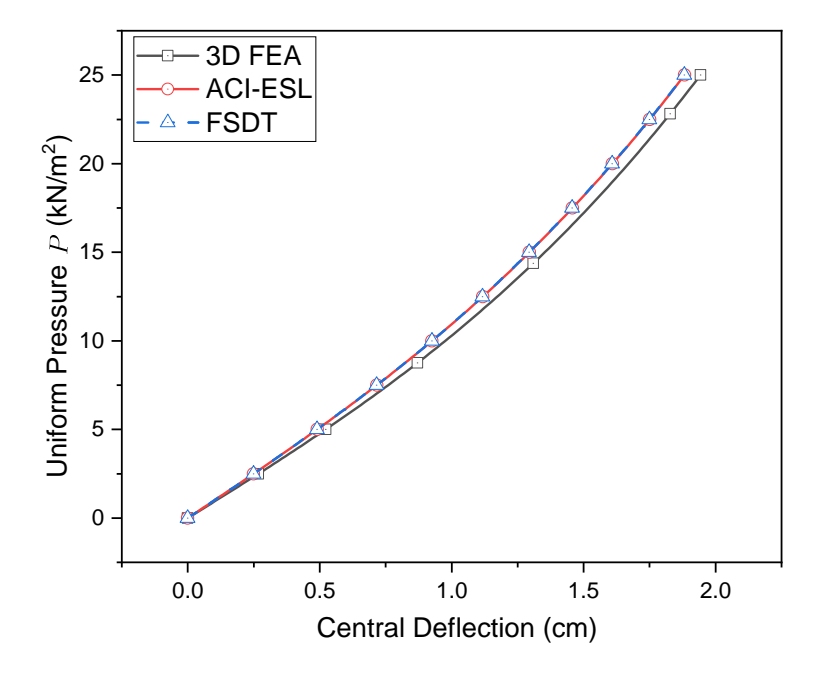


Figure 2.8: Load-deflection curves for the central point of the plate considered in Example-1 under uniform Pressure P applied at its top face

tion. A thorough convergence study was carried out to ensure the accuracy and reliability of the obtained results. This study involved systematically refining the mesh and monitoring the convergence behavior of relevant quantities such as displacements, strains, and stresses. For example, the convergence analysis for Example-1 done at $P = 25 \text{kN/m}^2$ is shown in Fig. 2.7. Nevertheless, for brevity, the convergence analysis is omitted for other examples. The analytical solutions were obtained using numerical methods or state-of-the-space methods (like Navier or Levy solution) [119].

For Example-1, the variation of the transverse deflection along the centerline parallel to x_1 axis predicted by the proposed plate model (ACI-ESL), FSDT, and 3D FEA for a pressure of $P = 25 \text{ kN/m}^2$ is compared in Fig. 2.10.

Fig. 2.11 displays the variation of the displacement component u_3 with respect to x_1 and x_2 for Example-1 under a uniform pressure of $P = 13 \text{ kN/m}^2$. Similar results are presented for Example-2 for $P = 400 \text{ N/m}^2$ in Figure 2.13. Fig. 2.11(a) and 2.13(a) were generated using the 3D FEA approach, while Fig. 2.11(b) and 2.13(b) were produced using the ACI-ESL plate theory. Fig. 2.12 and 2.14 illustrates the variation of the

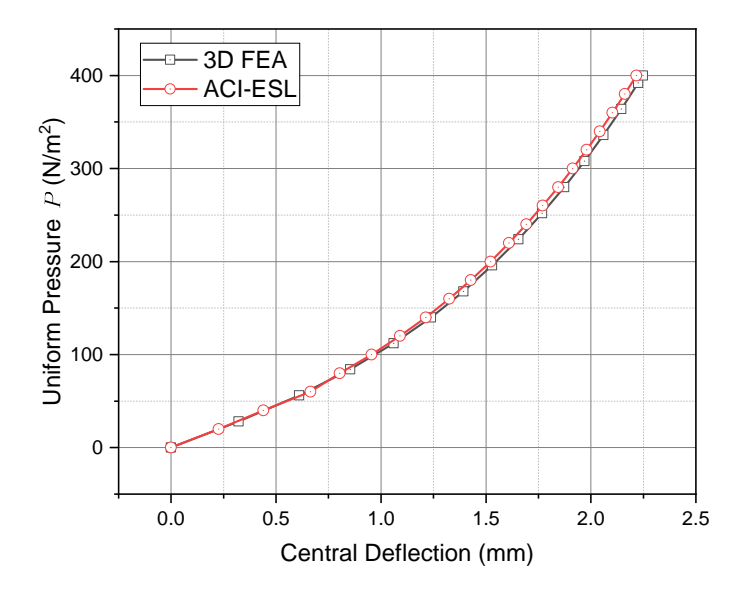


Figure 2.9: Load-deflection curves for the central point of the plate considered in Example-2 under uniform Pressure P applied at its top face

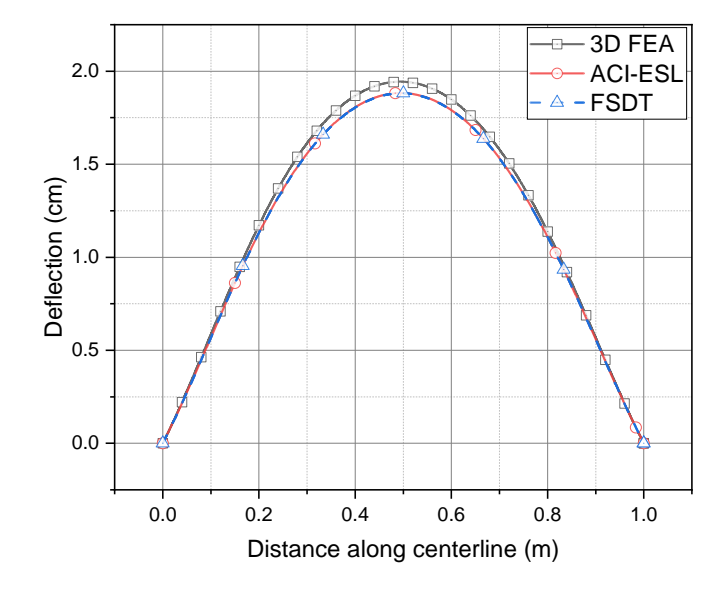


Figure 2.10: Out of plane deflection of the plate considered in Example-1 along centerline parallel to x_1 axis under uniform Pressure of $P=25\mathrm{kN/m^2}$ applied at its top face

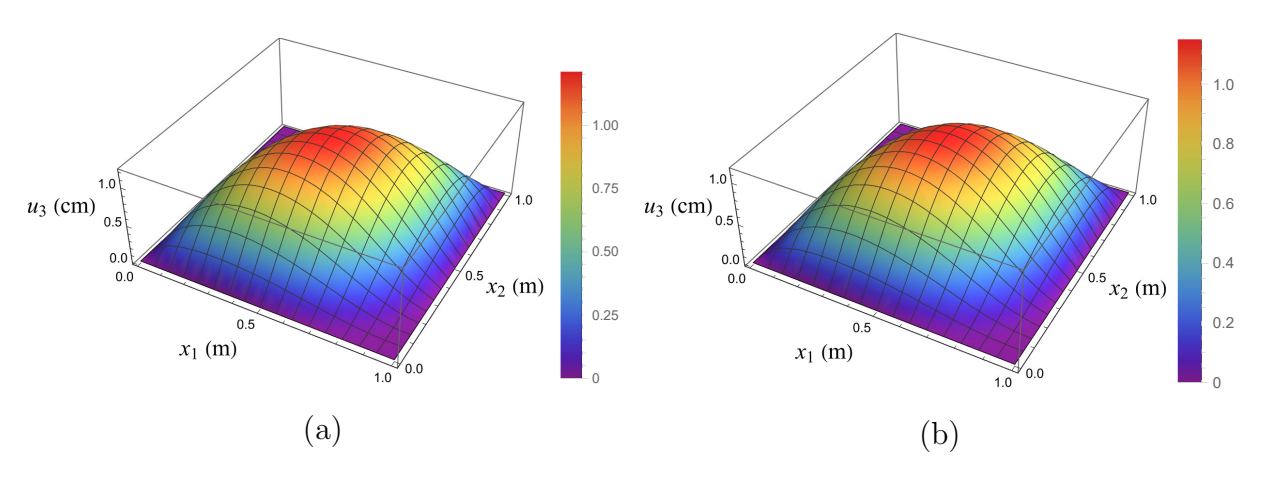


Figure 2.11: Out-of-plane deflection of the plate considered in Example-1 subjected to a uniform pressure of $P = 13 \text{ kN/m}^2$ applied on its top face. Deflections are obtained using: (a) 3D Finite Element Analysis (FEA) and (b) present ACI-ESL plate theory.

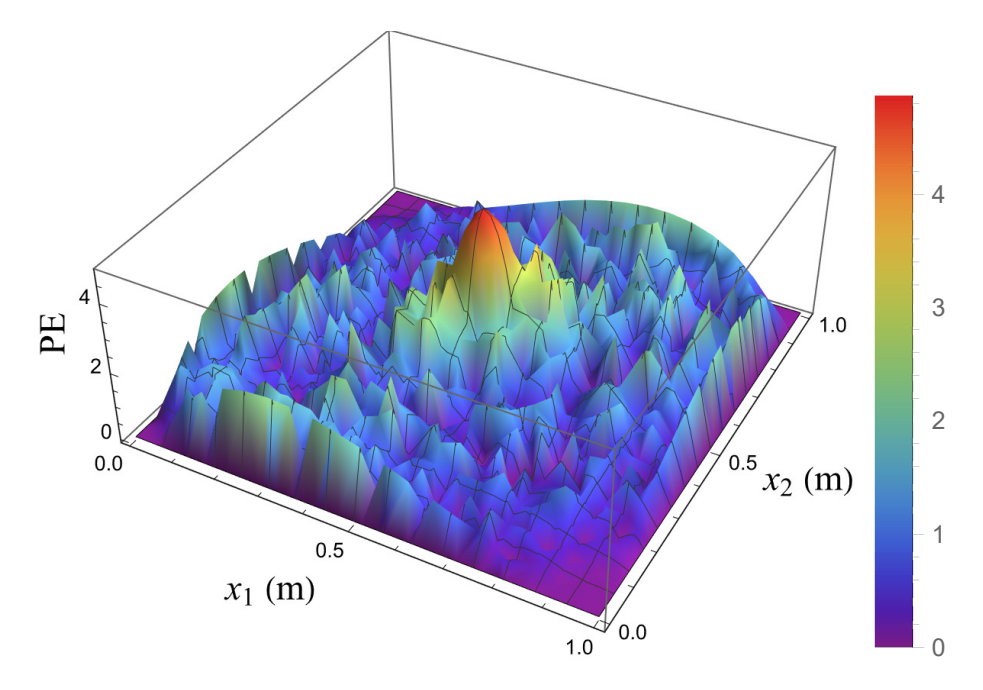


Figure 2.12: Percentage error in the out of plane deflection u_3 for Example-1 under uniform Pressure of $P = 13 \text{ kN/m}^2$ applied at the top face.

percentage error in the value of u_3 with respect to x_1 and x_2 , for Example-1 and Example-2, respectively. The percentage error (PE) for Figure 2.12 and 2.14 is defined in Eq. (2.60).

$$PE = 100 \left| \frac{u_{3,\text{FEA}} - u_{3,\text{ACI-ESL}}}{u_{3,\text{FEA}}^{max}} \right|$$
 (2.60)

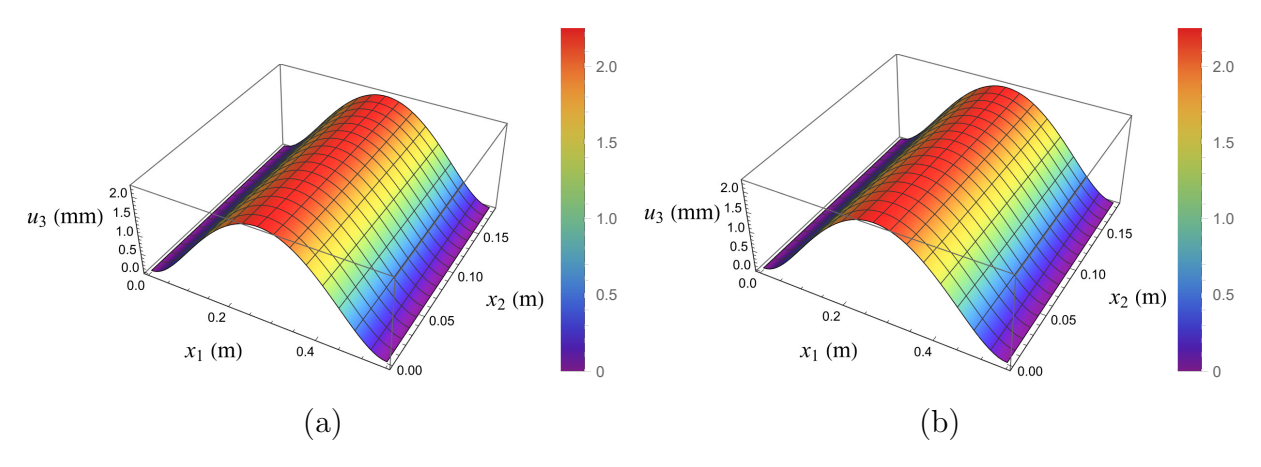


Figure 2.13: Out-of-plane deflection of the plate considered in Example-2 subjected to a uniform pressure of $P = 400 \text{ kN/m}^2$ applied on its top face. Deflections are obtained using: (a) 3D Finite Element Analysis (FEA) and (b) present ACI-ESL plate theory.

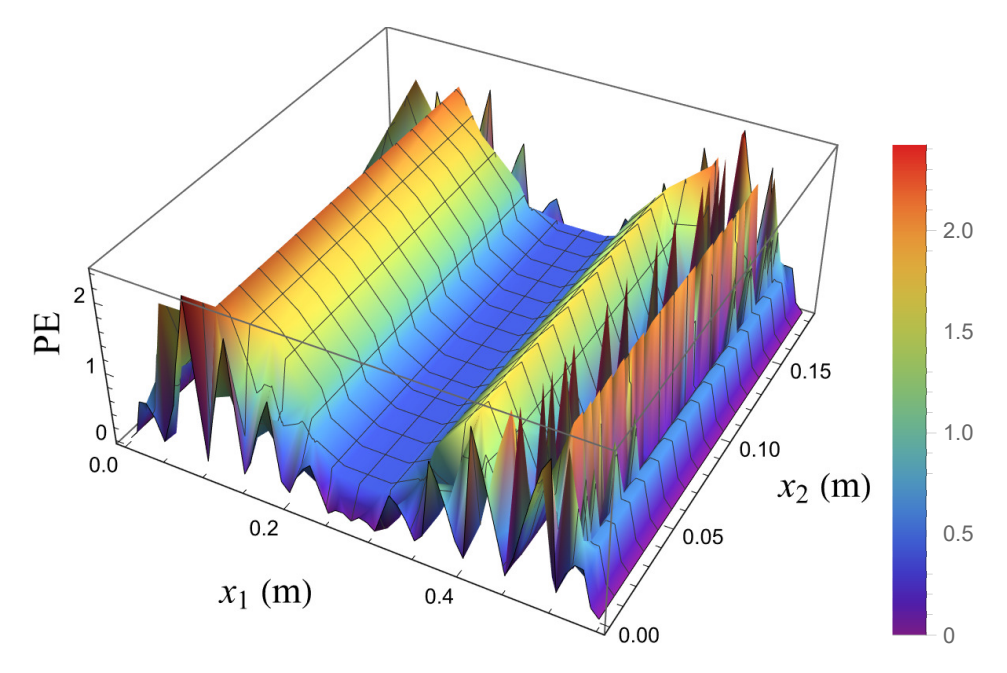


Figure 2.14: Percentage error in the out of plane deflection u_3 for Example-2 under uniform Pressure of $P = 400 \text{ N/m}^2$ applied at the top face.

Where $u_{3,\text{FEA}}$ and $u_{3,\text{ACI-ESL}}$ are values of u_3 obtained using the 3D FEA and ACI-ESL plate model approaches. $u_{3,\text{FEA}}^{max}$ is the maximum value of $u_{3,\text{FEA}}$. Figure 2.12 demonstrates that the results obtained by the 3D FEA and the present ACI-ESL model approach are in very good agreement.

To compare the results, the following non-dimensionalized quantities [122] are consid-

ered In Example-3

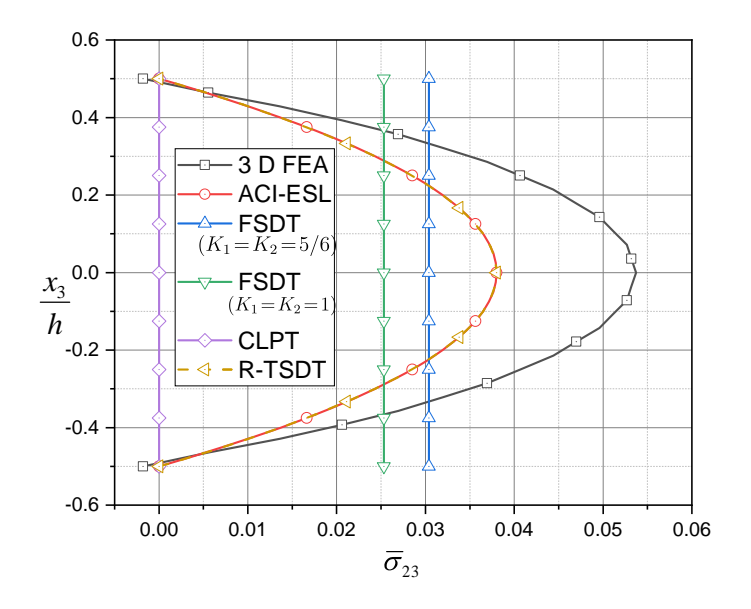
$$\overline{w} = 100 \left[\frac{u_3 \left(\frac{a}{2}, \frac{b}{2}, 0 \right) h^3 E_2}{q_0 a^4} \right], \quad \overline{\sigma}_{11} = \sigma_{11} \left(\frac{a}{2}, \frac{b}{2}, \frac{h}{2} \right) \frac{h^2}{q_0 a^2} \quad \overline{\sigma}_{23} = \sigma_{23} \left(\frac{a}{2}, 0, 0 \right) \frac{h}{q_0 a}$$

$$\overline{\sigma}_{22} = \sigma_{22} \left(\frac{a}{2}, \frac{b}{2}, \frac{h}{6} \right) \frac{h^2}{q_0 a^2} \quad \overline{\sigma}_{13} = \sigma_{13} \left(0, \frac{b}{2}, 0 \right) \frac{h}{q_0 a}$$
(2.61)

Fig. 2.15 illustrates the variation of the nondimensionalized transverse shear stresses along the thickness direction for the plate in Exaple-3. The proposed plate theory (ACI-ESL) provides a significantly better distribution of transverse shear stresses compared to FSDT and CLPT. The results are in very good agreement with Reddy's Third Order Shear Deformation Plate Theory (R-TSDT) [122]. The R-TSDT, being a higher-order theory, requires more computational cost than the present ACI-ESL plate model. To quantify the computational efficiency, the time taken by a processor to solve the differential equations of Example-3 obtained using the FSDT, Present ACI-ESL and R-TSDT theory were examined. All the parameters, such as system configuration and solution methodology (Navier solution approach), were kept the same. The results showed that the FSDT, ACI-ESL, and R-TSDT plate theories required 0.2469 seconds, 0.2595 seconds, and 0.4938 seconds, respectively. These calculations were performed using a single core of the Intel Xeon Gold 6248 CPU processor with a base speed of 2.50 GHz. The installed RAM in the system was 512GB with a speed of 2933 MHz. In contrast, the 3D Finite Element Analysis (FEA) approach using C3D20R elements in Abaqus required significantly more resources compared to the reduced-order plate theories. Solving the same problem with this method utilized 40 cores of the same processor and consumed 1 hour, 2 minutes, and 55 seconds.

For Example-3, Table 2.3 presents a comparison between the nondimensionalized stresses and transverse deflection as defined in Eq. (4.63) obtained using the proposed plate model (ACI-ESL) and that obtained using the CLPT, FSDT and 3D FEA approaches. The observations from the table indicate that as the $\frac{a}{h}$ ratio increases, the results converge towards the 3D FEA results. This trend is a consequence of the fact that the ordering of the strains has been carried out considering the smallness of the ratio $\frac{h}{a}$.

Fig. 2.16 illustrates transverse displacement u_3 along centerline parallel to x_1 axis and the stresses (σ_{11} , σ_{22} , σ_{23} , σ_{13} and σ_{12}) along the thickness in Example-4 for P = 50 N. The results are in good agreement with those obtained using 3D FEA.



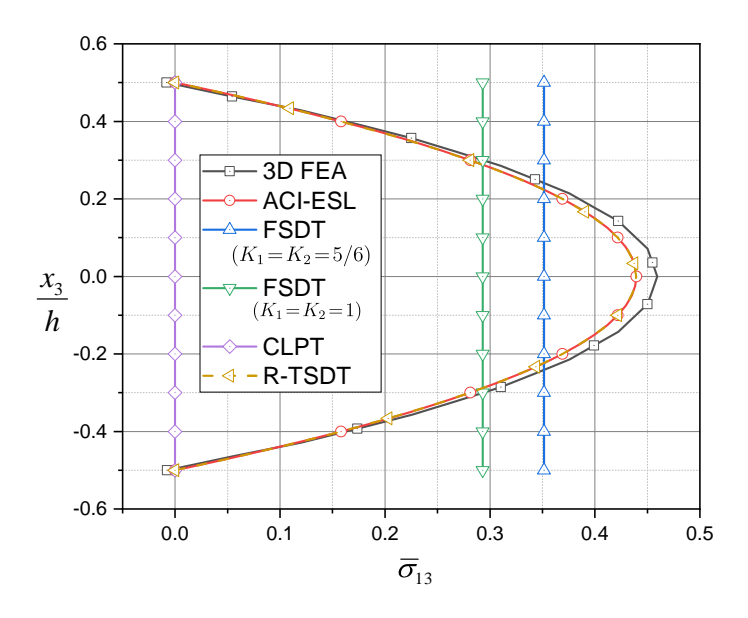


Figure 2.15: Through-thickness variation of the nondimensionalized transverse shear stress components in a thin orthotropic square plate ($\frac{a}{h} = 50$) considered in Example-3 based on 3D FEA, Present Work (ACI-SEL), FSDT, CLPT and Reddy's TSDT (R-TSDT).

Example-5 and Example-6 deal with circular and annular plates. Both the plates are made of Material-4 (see Table 2.1). The outer radius R of each plate is 1 m and the inner

Table 2.3: Nondimensionalized deflections and stresses in the plate considered in Example-3 under sinusoidal transverse loads[122]

$\frac{a}{h}$	Quant.	3D FEA	ACI-ESL	FSDT $K_1 = \frac{5}{6}$ $K_2 = \frac{5}{6}$	FSDT $K_1=1$ $K_2=1$	CLPT
	\overline{w}	0.6447	0.6383	0.6383	0.6042	0.4312
10	$\overline{\sigma}_{11}$	0.5727	0.5248	0.5248	0.5270	0.5387
	$\overline{\sigma}_{22}$	0.0124	0.0113	0.0113	0.0109	0.0089
	$\overline{\sigma}_{23}$	0.0552	0.0459	0.0368	0.0298	0
	$\overline{\sigma}_{13}$	0.4444	0.4315	0.3452	0.2885	0
	\overline{w}	0.4868	0.4836	0.4836	0.4749	0.4312
20	$\overline{\sigma}_{11}$	0.5492	0.5350	0.5350	0.5356	0.5387
	$\overline{\sigma}_{22}$	0.0097	0.0095	0.0095	0.0094	0.0089
	$\overline{\sigma}_{23}$	0.0532	0.0399	0.0319	0.0263	0
	$\overline{\sigma}_{13}$	0.4574	0.4376	0.3501	0.2920	0
	\overline{w}	0.4411	0.4396	0.4396	0.4382	0.4312
50	$\overline{\sigma}_{11}$	0.5411	0.5381	0.5381	0.5382	0.5387
	$\overline{\sigma}_{22}$	0.0090	0.0090	0.0090	0.0090	0.0089
	$\overline{\sigma}_{23}$	0.0528	0.0380	0.0304	0.0253	0
	$\overline{\sigma}_{13}$	0.4528	0.4394	0.3516	0.2930	0
	\overline{w}	0.4340	0.4333	0.4333	0.4330	0.4312
100	$\overline{\sigma}_{11}$	0.5396	0.5385	0.5385	0.5386	0.5387
	$\overline{\sigma}_{22}$	0.0071	0.0089	0.0089	0.0089	0.0089
	$\overline{\sigma}_{23}$	0.0524	0.0377	0.0302	0.0252	0
	$\overline{\sigma}_{13}$	0.4516	0.4397	0.3518	0.2932	0

radius r for the annular plate is 0.25 m as shown in Fig. 2.17. The thickness of both of the plates is 0.2 m (resulting in $\frac{2R}{h} = 10$). Both plates are rigidly clamped along their inner and outer boundaries. A uniformly distributed force P of 300 MPa is applied at the top surface of these plates. Figure 2.18 depicts the out-of-plane deflection u_3 along the centerline parallel to the x_1 axis for both the circular and annular plates. These results, along with others presented in this work, demonstrate the accuracy of the present work.

2.7 Conclusion

In this chapter, a novel VAM-based geometrically nonlinear plate model ACI-ESL has been developed by applying the first principles and the isoenergetic approach. Following are key highlights of the present work

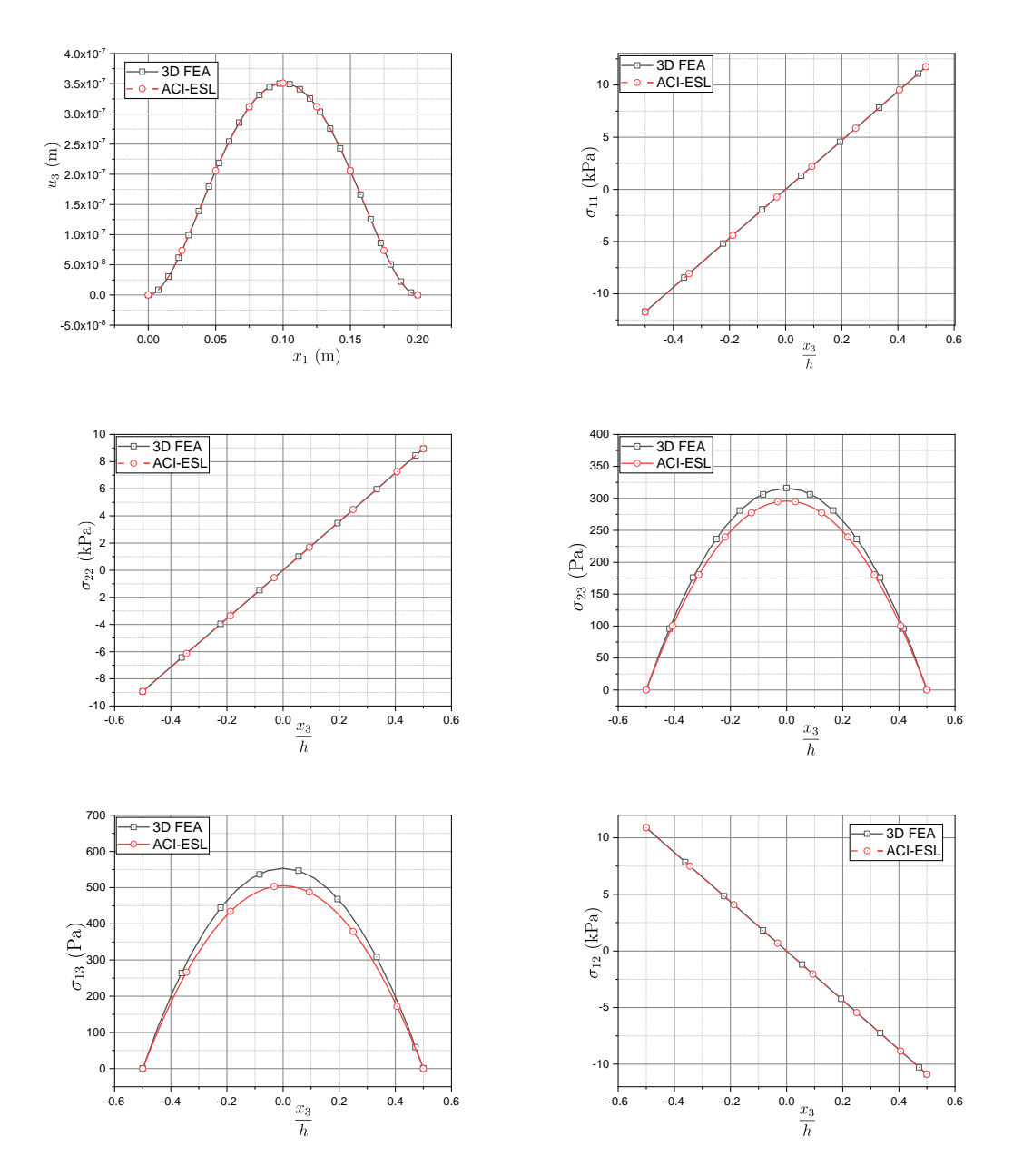


Figure 2.16: Comparison of out of plane deflection u_3 along the centerline parallel to x_1 and stress components at point B (shown in Fig. 2.5(a)) for an orthotropic square plate considered in Example-4.

1. A bound on thickness to length ratio $\left(\frac{h}{l}\right)$ and supnorm of strains has been used for the asymptotic expansion. In the energy functional this translates to asymptotic expansion in powers of (ξ) . The analysis with strain energy accurate up to the order of $(\xi^8\mu)$ results in analytic expressions for displacement vector and strains accurate

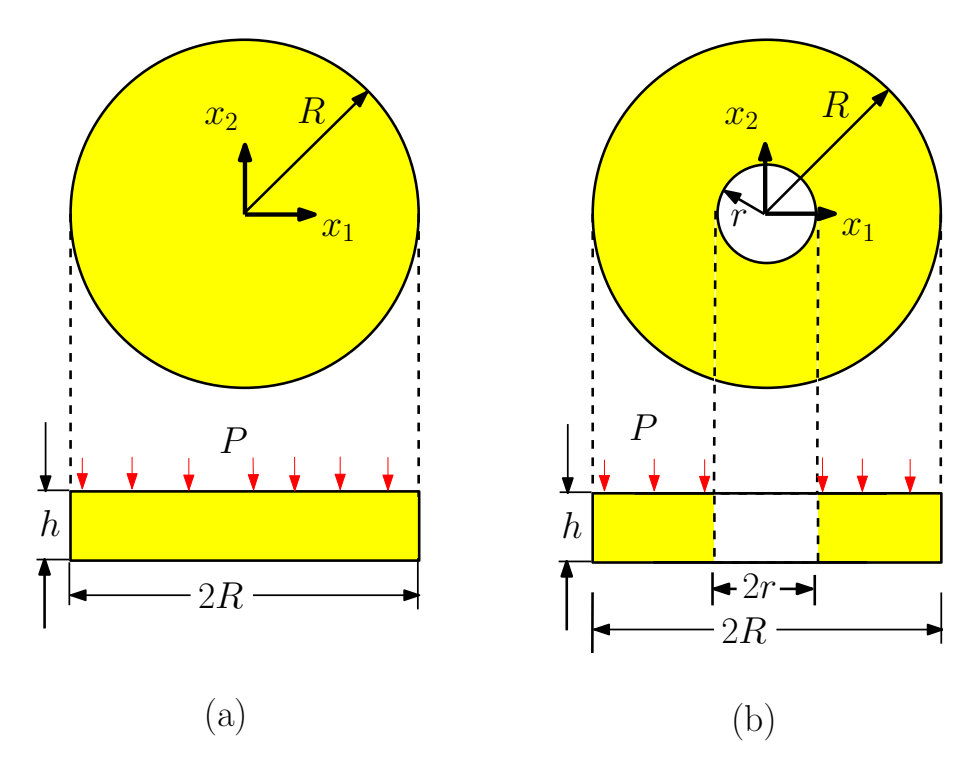


Figure 2.17: Geometric details and loading on (a) circular plate considered in Example-5 (b) annular plate considered in Example-6.

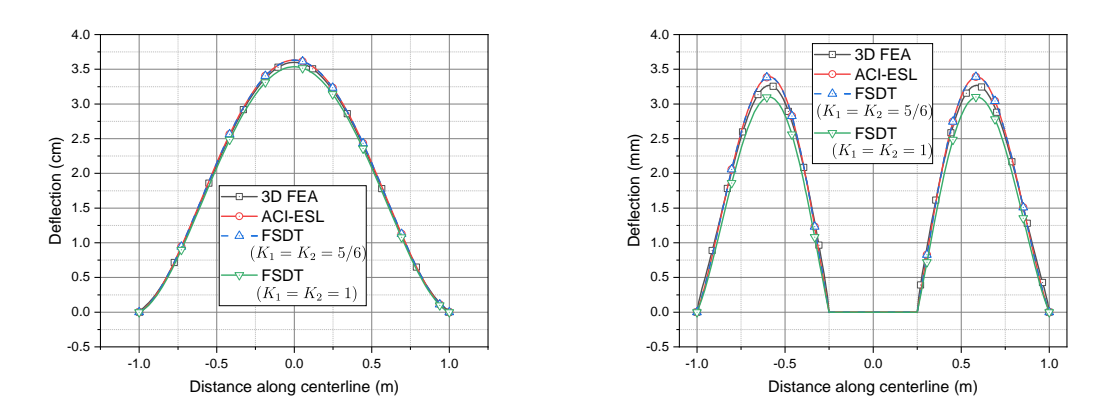


Figure 2.18: Comparison of out-of-plane deflection u_3 along the centerline parallel to x_1 axis for the circular and annular plates considered in Example-5 and Example-6, respectively.

up to the order of $(\xi^4 h)$ and (ξ^4) respectively. It is observed from the results that the diminishing value of small parameter $(\frac{h}{l})$ improves the accuracy, aligning them more closely with the results obtained from 3D FEA. Therefore, it becomes evident

- that the proposed model is asymptotically accurate and demonstrates satisfactory performance for thin and moderately thick plates.
- 2. It is interesting to observe that the zeroth order solution results in the estimation of 3D displacement field in terms of 2D variables $u_i(x_1, x_2)$. Essentially, this leads to the dimensional reduction of 3D problem to 2D, which is assumed a priori in classical plate theories.
- 3. The higher order 1D through the thickness analysis involves derivatives of $u_i(x_1, x_2)$ w.r.t x_{α} . The complexity involving these derivatives is eliminated through a novel isoenegetic approach, resulting in better estimation of the overall deformation.
- 4. It may be noted that most of the plate theories rely on the *ad hoc* assumption of plane stress condition as an integral part of their formulation. However, it is interesting to observe that the plane stress condition is a natural consequence of the mathematical procedure adopted in the present formulation.
- 5. The proposed model, as well as the FSDT, estimates strains up to the same order of accuracy, resulting in comparable levels of computational complexities and cost. However, due to its asymptotic correctness, the current model has the following advantages over FSDT model.
 - i. FSDT predicts a constant transverse shear stress and strain. In contrast, the present formulation provides an accurate quadratic variation of the same.
 - ii. The quadratic variation ensures the enforcement of zero tangential traction boundary conditions on the surface of the plate, ensuring excellent agreement with the expected physical behavior.
 - iii. Unlike FSDT, there is no need for a shear correction factor.
- 6. The quadratic variation of transverse shear strains predicted by the proposed plate model is in line with that given by higher-order plates models such as R-TSDT and G-TSDT (see Appendix C). However, the proposed plate model distinguishes itself from these higher-order plate models by excluding higher-order derivatives of the normal and in-plane shear strains. This isoenergetic and asymptotic correctness-based simplification effectively reduce computational complexities.

To summarize, this work provides a more refined, accurate, and computationally efficient ESL plate theory for thin and moderately thick plate structures. Comparison with established theories such as CLPT, FSDT, R-TSDT and 3D FEA demonstrates the accuracy of the present work.

Although the work done in this chapter is focused more on material anisotropy, it will be interesting to see the application of the proposed theory in plates/stiffened plates made up of inhomogeneous and composite materials, which will be done in the upcoming chapters.

Chapter 3

Asymptotically Accurate Geometrically Nonlinear Isoenergetic Analysis of Multilayered Composite plates

3.1 Introduction

Composite laminates are crafted through the strategic layering of thin sheets of composites, each characterized by distinctive fiber types (such as carbon, glass, aramid), matrix materials (including epoxy, polyester, and thermoplastic), and fiber orientations. These laminates typically have a width and length much larger than their thickness. As a result, they are commonly modeled as plate elements for engineering analysis. Due to their unique properties, composite laminates are often used in applications that require membrane and bending strength.

The present work develops an asymptotically correct reduced order pate theory utilizing the variational principles. This method for obtaining reduced-order models is referred to as the variational asymptotic method (VAM). VAM utilizes small geometric and material parameters to reduce the complexity of engineering problems elegantly. Applying it to plate analysis, VAM decomposes the 3D problem into a manageable 1D throughthe-thickness analysis and a 2D planar analysis. The development done in this Chapter is based on the mathematical foundation introduced in Chapter 2. However, to make the chapter self-contained, the important concepts introduced in Chapter 2 are repeated in this chapter whenever necessary.

Following the methodology similar to that used in Chapter 2 for anisotropic plates, this

chapter conducts a 1D through-the-thickness analysis for the multilayered composite plate problem. This first-principles-based derivation obtains a reduced-order 2D plate model from the energy of the 3D model. Unlike traditional methods that rely on pre-assumed plate kinematics and variable ordering, this work proposes a systematic ordering scheme. This scheme assigns orders to different quantities of interest and progressively refines them. The final order aligns perfectly with established literature, demonstrating its robustness. Furthermore, the present approach does not require an a priori reference plane. Instead, the analysis methodology naturally yields a reference plane as an outcome. Similarly, the position of this plane is not pre-assumed but determined logically to eliminate higher-order derivatives.

The 1D through the thickness analysis consider the continuity of the displacements and the transverse stresses at the interface of the layers of the multilayered composite laminate and gives close form solution for the displacement vector components in terms of 2D variables (functions of two independent variables) associated with the reference plane of the plate. Due to their dependence on the laminate's constructional details (material properties, layup sequence, fiber orientation), these closed-form solutions are unique to each problem. To facilitate analysis, a code has been developed in Mathematica. The 1D through the thickness analysis yields a reduced order 2D plate model. The 2D plate model obtained this way, though asymptotically correct, is computationally inefficient as it contain higher order derivatives of the 2D variables. Interestingly, for the accuracy in strains considerd in the present work, higher-order derivatives only appear in the transverse shear terms. This approach eliminates these higher order derivatives by selecting a reference plane suitable and using the concept of isoenergetics. The isoenergetics ensures that the strain energy of the VAM based reduced order model matches that of the FSDT plate theory for a given deformation pattern of the reference plane. Enforcement of this condition results in the determination of the shear correction factors and the transverse shear force resultants which are used to replace the The higher order derivatives present in the analysis by lower order derivatives. What follows present this work in a systematic way.

3.2 Analytical Development

A symmetric laminated composite plate is analyzed. The plate has length a, width b, and thickness h. A global coordinate system $x = (x_1, x_2, x_3)$ is defined. The origin O of this

system is located at a distance η from the midplane of the plate as shown in Fig 3.1(c).

The plate consists of n orthotropic layers. Each layer (termed as lamina) has its own principal material coordinate system, denoted by (x_1^r, x_2^r, x_3^r) for the r^{th} lamina (where r = 1, 2, 3, ..., n). The orientation of each lamina is specified by the angle θ^r relative to the global coordinate system x (see Fig. 3.1). The notation \hat{e}_i denotes the orthonormal basis vectors along the x_i axes.

In the undeformed configuration, the interior region of the $r^{\rm th}$ lamina is denoted by Ω^r and its boundaries comprise of the top surface $\partial \Omega^r_{\rm top}$, the bottom surface $\partial \Omega^r_{\rm bot}$ and the side surfaces $\partial \Omega^r_{\rm side}$ with $\partial \Omega^r_{\rm tb} = \partial \Omega^r_{\rm top} \cup \partial \Omega^r_{\rm bot}$. Similarly, in the undeformed configuration, the interior region of the entire plate is designated as Ω and its boundaries consists of the top surface $\partial \Omega_{\rm top}$, the bottom surface $\partial \Omega_{\rm bot}$ and the side surfaces $\partial \Omega_{\rm side}$ with $\partial \Omega_{\rm tb} = \partial \Omega_{\rm top} \cup \partial \Omega_{\rm bot}$. It is to be noted that $\partial \Omega_{\rm top} = \partial \Omega^1_{\rm top}$ and $\partial \Omega_{\rm bot} = \partial \Omega^n_{\rm bot}$.

The position vector of any arbitrary point P in this domain is given by $\vec{x} = x_i \hat{e}_i$. Throughout this work, Roman indices (i, j, k, ...) range from 1 to 3, while Greek indices $(\alpha, \beta, \gamma, ...)$ range from 1 to 2 unless their values are specified. A superscript indicates the number of a lamina, while parentheses () are used to distinguish mathematical exponents from these superscripts.

Consider the point P located within the r^{th} lamina. Due to deformation, P moves to a new position P'. This displacement is described by the vector $\vec{v}^r = v_i^r \hat{e}_i$, where v_i^r are the components of the displacement in the global coordinate directions. Assuming small strains and moderate rotations, Green–St. Venant strain tensor [128, 127, 119] for the r^{th} lamina can be expressed as follows.

$$\underline{\underline{E}}^{r} = \frac{1}{2} \left[\left(\vec{\nabla}_{x} \vec{v}^{r} \right) + \left(\vec{\nabla}_{x} \vec{v}^{r} \right)^{T} + \left(\vec{\nabla}_{x} \vec{v}^{r} \right)^{T} \left(\vec{\nabla}_{x} \vec{v}^{r} \right) \right]$$
(3.1)

where ∇_x is the gradient operator with respect to the global coordinates x. This work proposes a novel strategy for developing a reduced-order plate theory for multilayered composite materials. This theory builds upon the strain tensor defined in Eq. (3.1). Additionally, it leverages the geometrical dimensions of the plate and the maximum allowable strains to establish a mathematically rigorous reduced-order plate model. This approach avoids introducing any arbitrary and/or pre-assumed simplifications.

Interestingly, it will be shown that successive refinements of this reduced-order model lead to progressively more accurate plate theories, ultimately encompassing CLPT and even higher-order plate theories.

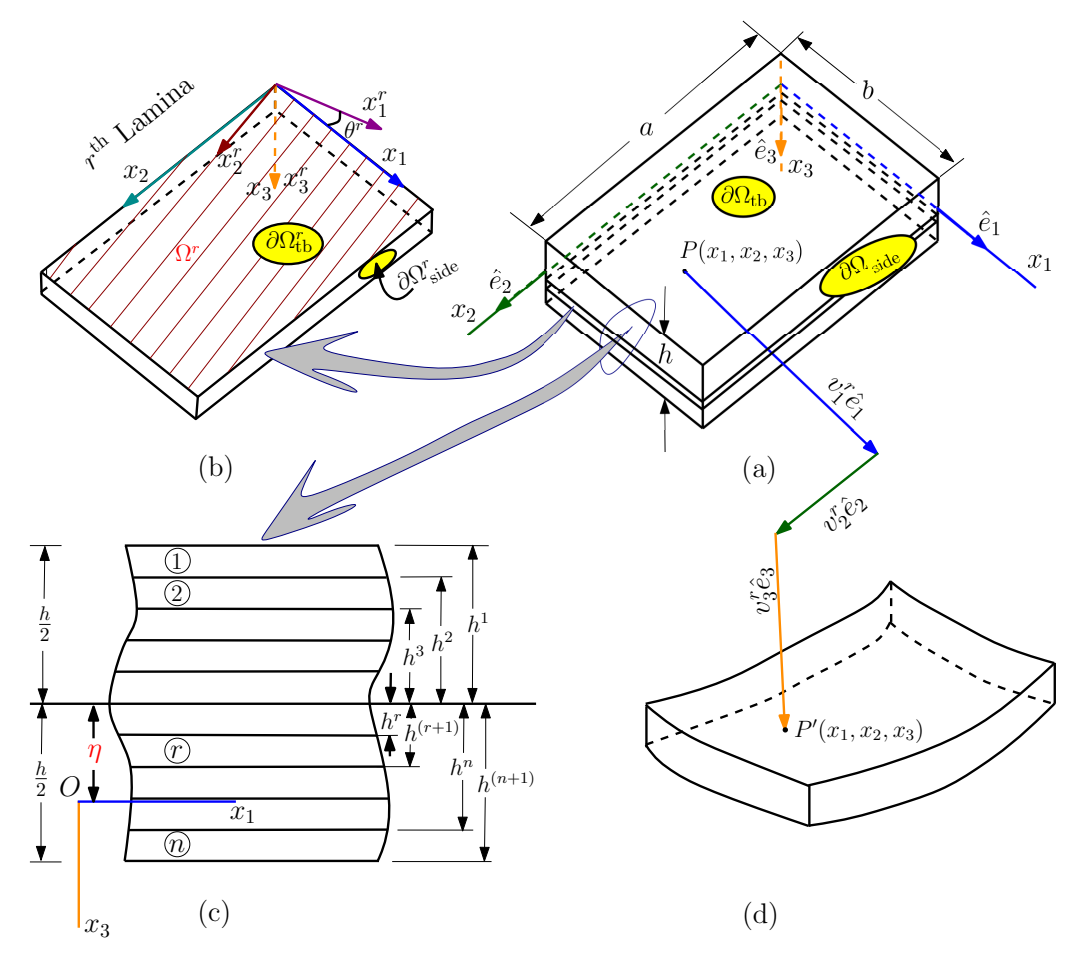


Figure 3.1: Schematic of the plate (a) Undeformed state of the plate (b) r^{th} lamina of the plate (c) through-the-thickness lay-up sequence (d) Deformed state of the plate

The development is divided into three parts:

- Part A: Establishes a reduced-order model for the plate, aligning with CLPT.
- Part B: Refines the model from Part A by incorporating the contribution of higher-order energy terms.
- Part C: Introduces the concept of isoenergetics to eliminate higher-order derivatives from the analysis, improving computational efficiency.

3.3 Part A: Development of a reduced order model

This section leverages the geometry of the plate and a bound on the maximum strain value to estimate the order of various quantities of interest. The estimation scheme follows the approach outlined in [57]. The ordering scheme is presented in the next subsection.

3.3.1 Order Estimation Scheme

Following the ordering scheme from [112], The relationship between the orders of displacement components, v_i^r , and their derivatives with respect to the spatial coordinates, x_j can be expressed as follows.

$$O\left[\left(\frac{\partial}{\partial x_1}\right)^m \left(\frac{\partial}{\partial x_2}\right)^n \left(\frac{\partial}{\partial x_3}\right)^p v_i^r\right] \sim \left(\frac{1}{l}\right)^{(m+n)} \left(\frac{1}{h}\right)^p v_i^r$$

$$m, n, p = 0, 1, 2, 3, \dots$$
(3.2)

Here, the 0th order derivative signifies no differentiation, i.e., $O\left[\left(\frac{\partial}{\partial x_i}\right)^0 v_i^r\right] = O(v_i^r)$.

The support (supremum norm) of strains for the r^{th} lamina, denoted by $||\underline{\underline{E}^r}||_{\infty}$, is defined as follows.

$$||\underline{\underline{E}^r}||_{\infty} = \max_{1 \le i, j \le 3} \max_{x \in \Omega^r} |E_{ij}^r|$$
 (3.3)

The maximum aspect ratio $(\frac{h}{l})$ and the supnorm of strains are bounded by ξ and ε respectively.

$$\frac{h}{l} \le \xi$$
 and $||\underline{\underline{E}}^r||_{\infty} \le \varepsilon$ (3.4)

In the context of small strains, the supnorm of strains is considered a very small parameter, i.e., $\varepsilon \ll 1$. Similarly, for plate-like structures, the maximum aspect ratio is also bound to be small, i.e., $\xi < 1$. For the asymptotic expansion of strains and strain energy, we will assume $\varepsilon = \xi^3$.

It will be demonstrated later that the order estimation scheme introduced in this section provides a unique estimation of the order of various relevant quantities.

3.3.2 Constitutive Relations and Strain Energy

The relationship between stress and strain for the r^{th} lamina is governed by the following equation [61]

$$\sigma^r = C^r E^r \tag{3.5}$$

Where $E^r = \{E_{11}^r, E_{22}^r, E_{33}^r, 2E_{23}^r, 2E_{13}^r, 2E_{12}^r\}^T$, $\sigma^r = \{\sigma_{11}^r, \sigma_{22}^r, \sigma_{33}^r, \sigma_{23}^r, \sigma_{13}^r, \sigma_{12}^r\}^T$ and C^r are Green-Lagrange strain tensor, Second Piola-Kirchhoff stress tensor and Stiffness matrix for the r^{th} lamina respectively.

Here, C^r captures the elastic properties of the r^{th} lamina in the global coordinate system x. The components of C^r depend on the specific material properties of the lamina. Each lamina in the laminate exhibits monoclinic symmetry with respect to the global coordinate system x. Therefore the stiffness matrix C^r for the r^{th} lamina takes the following structure

$$C^{r} = \begin{bmatrix} C_{11}^{r} & C_{12}^{r} & C_{13}^{r} & 0 & 0 & C_{16}^{r} \\ C_{12}^{r} & C_{22}^{r} & C_{23}^{r} & 0 & 0 & C_{26}^{r} \\ C_{13}^{r} & C_{23}^{r} & C_{33}^{r} & 0 & 0 & C_{36}^{r} \\ 0 & 0 & 0 & C_{44}^{r} & C_{45}^{r} & 0 \\ 0 & 0 & 0 & C_{45}^{r} & C_{55}^{r} & 0 \\ C_{16}^{r} & C_{26}^{r} & C_{36}^{r} & 0 & 0 & C_{66}^{r} \end{bmatrix}$$

$$(3.6)$$

It is assumed that all the material constants are of the same order μ . The strain energy density for each lamina is given by.

$$U^r = \frac{1}{2} (\sigma^r)^T E^r \tag{3.7}$$

3.3.3 Dimensional Reduction

Let $\vec{q} = q \ \hat{e}_3$ and $\vec{t} = t_i \ \hat{e}_i$ be traction forces on $\partial \Omega_{\rm tb}$ and $\partial \Omega_{\rm side}$ respectively. The principle of virtual work results in

$$\sum_{r=1}^{n} \int_{\Omega^{r}} \delta U^{r} dV - \int_{\partial \Omega_{\text{tb}}} \vec{q} \cdot \delta \vec{v} da_{\text{tb}} - \int_{\partial \Omega_{\text{side}}} \vec{t} \cdot \delta \vec{v} da_{\text{side}} = 0$$
 (3.8)

Where $\vec{v} = \vec{v}^r$ for all values of r between 1 to n (n = total number of laminae). Eq. (3.8) presents a computationally expensive 3D elasticity problem. This problem is typically addressed by simplifying it to a 2D plate problem. However, traditional approaches to this simplification rely on assumptions that may not fully account for the energy involved in deforming the material. This work considers the energy aspects of the problem while creating the reduced-order 2D plate model. The details of the present approach are explained in the sections that follow.

3.3.4 Zeroth Order Solutions (ZOS)

ZOS assumes v_i^r , the displacement field of the r^{th} lamina, to be ${}^0v_i^r$. Here ${}^0v_i^r(x_1, x_2, x_3)$ represent zeroth order perturbation variables. Throughout this work, the following notation is consistently used

$$\binom{m \bullet_i^r}{\operatorname{top/bot}}^p$$

Interpretation

• : Represents the quantity of interest (e.g., displacement, stress, strain).

m: Denotes the $m^{\rm th}$ order solution/contribution of \bullet .

r: Indicates the rth lamina.

i: indicates the ith component

p: Exponent of the quantity within the parentheses

top/bot: Denotes the top/bottom surface of r^{th} lamina

The approach outlined in Section 3.3.1 is utilized to estimate the order of ${}^{0}v_{i}^{r}$. The estimated order of ${}^{0}v_{i}^{r}$ is found to be $O(\xi^{3}h)$. Subsequently, the order of various strain components is evaluated. The various strain components with their respective orders denoted using underbraces are given below.

$$E_{11}^{r} = O(\xi^{4}) \qquad 2E_{23}^{r} = \underbrace{\frac{\partial^{0}v_{2}^{r}}{\partial x_{3}}}_{O(\xi^{3})} + O(\xi^{4})$$

$$E_{22}^{r} = O(\xi^{4}) \qquad 2E_{13}^{r} = \underbrace{\frac{\partial^{0}v_{1}^{r}}{\partial x_{3}}}_{O(\xi^{3})} + O(\xi^{4})$$

$$E_{33}^{r} = \underbrace{\frac{\partial^{0}v_{3}^{r}}{\partial x_{3}}}_{O(\xi^{3})} \qquad 2E_{12}^{r} = O(\xi^{4})$$
(3.9)

It is important to highlight that the order estimated for the perturbation variable ${}^{0}v_{i}^{r}$ represents its maximum acceptable value. This order is crucial because it ensures that the strains stay within their maximum allowable value, denoted by $\varepsilon = \xi^{3}$. Importantly, there is only one valid order for ${}^{0}v_{i}^{r}$. Choosing a different order would affect the maximum allowed strain, which is unacceptable. By following this specific ordering of strains, we

can represent the strain energy density, U^r , as an ordered series in terms of the small parameter ξ , as shown below.

$$U^{r} = \underbrace{U_{\text{sig}}^{r}}_{O(\xi^{6}\mu)} + O\left(\xi^{7}\mu\right)$$

$$U_{\text{sig}}^{r} = \frac{1}{2} \left[C_{55}^{r} \left(\frac{\partial^{0}v_{1}^{r}}{\partial x_{3}}\right)^{2} + 2C_{45}^{r} \frac{\partial^{0}v_{1}^{r}}{\partial x_{3}} \frac{\partial^{0}v_{2}^{r}}{\partial x_{3}} + C_{44}^{r} \left(\frac{\partial^{0}v_{2}^{r}}{\partial x_{3}}\right)^{2} + C_{33}^{r} \left(\frac{\partial^{0}v_{3}^{r}}{\partial x_{3}}\right)^{2} \right]$$

$$(3.10)$$

The term with the lowest order, U_{sig}^r , in the equation above makes the most significant contribution to the energy functional. By concentrating solely on this contribution, the virtual work Eq. (3.8) simplifies to the following form

$$\int_{\partial\Omega_{\text{ref}}} \left[\sum_{r=1}^{n} \int_{x_3} \delta U_{\text{sig}}^r dx_3 \right] da_{\text{ref}} - \int_{\partial\Omega_{\text{tb}}} \vec{q} \cdot \delta \vec{v} da_{\text{tb}} - \int_{\partial\Omega_{\text{side}}} \vec{t} \cdot \delta \vec{v} da_{\text{side}} = 0$$
 (3.11)

The reference plane of the plate, denoted by $\partial\Omega_{\rm ref}$, is defined as a plane parallel to the midplane but located at a distance η away, as shown in Fig. 3.1. The magnitude of η will be determined later on logical grounds. Interestingly, Equation (3.10) shows that $U_{\rm sig}^r$ contains terms with derivatives of ${}^0v_i^r$ with respect to x_3 alone. This allows us to perform the minimization process in two stages:(i) A through the thickness 1D analysis along the x_3 direction. (ii) A 2D in-plane analysis in the x_1x_2 plane, as expressed below.

$$\underbrace{\delta\Pi_{x_3} = 0}_{1D \text{ Analysis}} \underbrace{\delta\Pi = 0}_{2D \text{ Analysis}}$$

$$\Pi_{x_3} = \sum_{r=1}^{n} \Pi_{x_3}^{r} \qquad \Pi_{x_3}^{r} = \int_{x_3} U_{\text{sig}}^{r} dx_3$$

$$\Pi = \int_{\partial\Omega_{\text{ref}}} \Pi_{x_3} da_{\text{ref}} - \int_{\partial\Omega_{\text{tb}}} \vec{q} \cdot \vec{v} da_{\text{tb}} - \int_{\partial\Omega_{\text{side}}} \vec{t} \cdot \vec{v} da_{\text{side}}$$
(3.12)

This approach inherently reduces the dimensionality of the problem. During the 1D analysis, we can neglect the external loads for now. These external loads will be considered later in the 2D in-plane analysis, as described in references [111, 124]. Minimizing the potential energy functional Π_{x_3} leads to the minimization of $\Pi_{x_3}^r$ while ensuring continuity of displacements and transverse stresses (σ_{i3}) at the interface between adjacent laminas [92, 111, 56]. This is illustrated in the figure below.

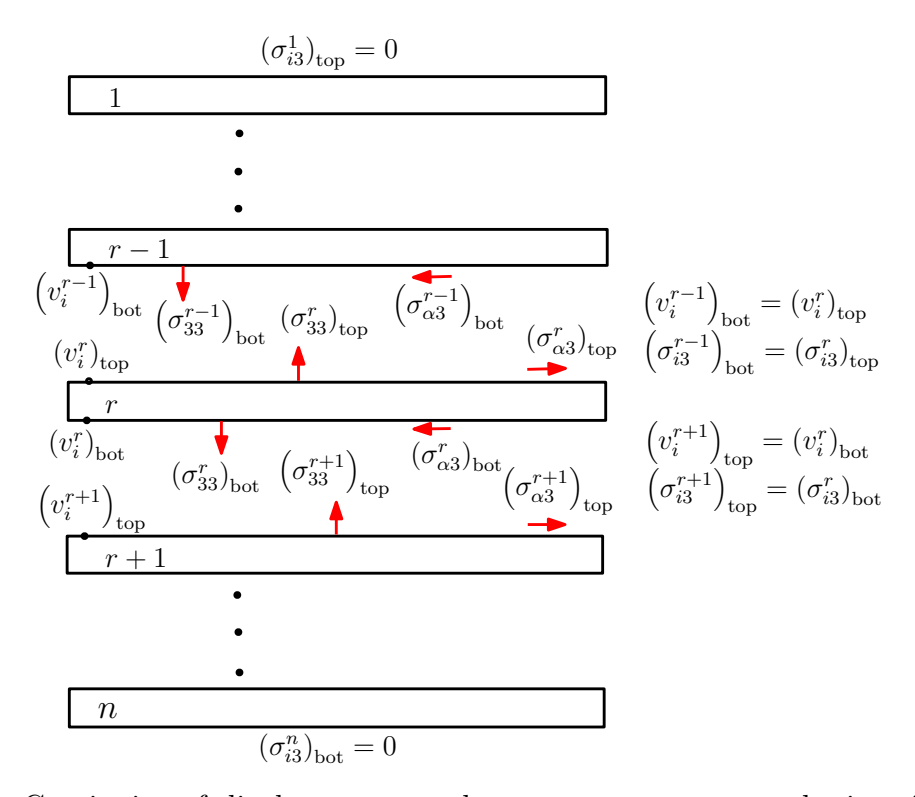


Figure 3.2: Continuity of displacements and transverse stresses at the interface of two consecutive laminae

Through the Thickness 1D Analysis

Extrimization of $\Pi^r_{x_3}$ yields following Euler-Lagrange governing equations for $r^{\rm th}$ lamina

$$C_{55}^{r} \left(\frac{\partial}{\partial x_{3}}\right)^{2} {}^{0}v_{1}^{r} + C_{45}^{r} \left(\frac{\partial}{\partial x_{3}}\right)^{2} {}^{0}v_{2}^{r} = 0$$

$$C_{45}^{r} \left(\frac{\partial}{\partial x_{3}}\right)^{2} {}^{0}v_{1}^{r} + C_{44}^{r} \left(\frac{\partial}{\partial x_{3}}\right)^{2} {}^{0}v_{2}^{r} = 0$$

$$C_{33}^{r} \left(\frac{\partial}{\partial x_{3}}\right)^{2} {}^{0}v_{3}^{r} = 0$$

$$(3.13)$$

The associated boundary conditions are as follows

$$\mathcal{B}_{0v_{1}^{r}}\big|_{x_{3}=h^{r}-\eta} = (\sigma_{13}^{r})_{\text{top}} \qquad \mathcal{B}_{0v_{1}^{r}}\big|_{x_{3}=h^{(r+1)}-\eta} = (\sigma_{13}^{r})_{\text{bot}}
\mathcal{B}_{0v_{2}^{r}}\big|_{x_{3}=h^{r}-\eta} = (\sigma_{23}^{r})_{\text{top}} \qquad \mathcal{B}_{0v_{2}^{r}}\big|_{x_{3}=h^{(r+1)}-\eta} = (\sigma_{13}^{r})_{\text{bot}}
\mathcal{B}_{0v_{3}^{r}}\big|_{x_{3}=h^{r}-\eta} = (\sigma_{33}^{r})_{\text{top}} \qquad \mathcal{B}_{0v_{3}^{r}}\big|_{x_{3}=h^{(r+1)}-\eta} = (\sigma_{33}^{r})_{\text{bot}}
\mathcal{B}_{0v_{1}^{r}} = C_{55}^{r} \frac{\partial^{0}v_{1}^{r}}{\partial x_{3}} + C_{45}^{r} \frac{\partial^{0}v_{2}^{r}}{\partial x_{3}}
\mathcal{B}_{0v_{2}^{r}} = C_{45}^{r} \frac{\partial^{0}v_{1}^{r}}{\partial x_{3}} + C_{44}^{r} \frac{\partial^{0}v_{2}^{r}}{\partial x_{3}}
\mathcal{B}_{0v_{3}^{r}} = C_{33}^{r} \frac{\partial^{0}v_{3}^{r}}{\partial x_{3}}$$

$$(3.14)$$

with $(\sigma_{13}^1)_{\text{top}} = (\sigma_{13}^n)_{\text{bot}} = (\sigma_{23}^1)_{\text{top}} = (\sigma_{23}^n)_{\text{bot}} = (\sigma_{33}^n)_{\text{top}} = (\sigma_{33}^n)_{\text{bot}} = 0$, for traction free top and bottom surfaces of the plate. Solving the Euler-Lagrange equations Eq. (3.13) with the boundary conditions Eq. (3.14) and imposing the continuity of displacements and transverse stresses at the boundaries of each lamina results in following solution

$${}^{0}v_{i}^{r} = u_{i}(x_{1}, x_{2}) (3.15)$$

This solution will undergo further refinement for increased accuracy in subsequent sections. It's important to note that this zeroth-order solution expresses the 3D displacement components v_i in terms of u_i , which are functions solely of x_1 and x_2 , hence referred to as 2D variables. Essentially, u_i depict the rigid body-like deformation of a line segment AB, denoted as ${}^0A{}^0B$, along the thickness direction \hat{e}_3 , as illustrated in Fig. 3.4(b). Since this displacement remains independent of x_3 , all points along AB exhibit the same displacement. However, for convenience, u_i are expressed as the displacement components associated with the x_1, x_2 plane of the global coordinate system, which is referred to as the reference plane of the plate.

$$u_i = v_i \Big|_{x_2 = 0} \tag{3.16}$$

3.3.5 First Order Solution (FOS)

The displacement field obtained in ZOS is perturbed to improve it further as follows

$$v_i^r = {}^{0}v_i^r + {}^{1}v_i^r = u_i + {}^{1}v_i^r \tag{3.17}$$

Including the term v_i^r in Equation (3.17) introduces three additional degrees of freedom to the displacement field. However, to guarantee a unique solution, we need three

constraints. Equation (3.16) provides these three constraints for the n^{th} order perturbation variables, denoted by ${}^{n}v_{i}$.

$${}^{n}v_{i}\big|_{x_{3}=0} = 0$$
 (3.18)

It may be noted that the choice of the constraint is not unique. Several papers on the VAM based analysis of plates [113, 111, 112] assume that the through-thickness average value of warping components is zero i.e. $\int_{-h/2}^{h/2} {}^{n}v_{i}dx_{3} = 0$. However, constraints defined in Eq.(3.18) are simpler and straight forward to use from the point of view of numerical implementation, further same constraint have been adapted for analysis of beam sections in [114].

Following the procedure outlined in Section 3.3.1, we determine the order of u_i and ${}^1v_i^r$ to be $O(\xi^3 l)$ and $O(\xi^3 h)$, respectively. However, this might seem counter-intuitive as both ${}^0v_i^r$ and ${}^1v_i^r$ have the same order, which deviates from the usual refinement process. The key here is that we initially assumed a conservative order for v_i^r , treating the plate as a 3D object and considering the most extreme possible deformation within the strain limit of ε . As the refinement process progresses and the displacement field becomes more accurate, the actual deformation pattern of the plate emerges. This allows for a relaxation of the bound on v_i^r . Consequently, further refinement of the displacement field in the same order is necessary, justifying the order for the perturbation variables.

By substituting v_i^r from Equation (3.17) into Equation (3.1), The following strains are obtained.

$$E_{11}^{r} = \underbrace{\frac{\partial u_{1}}{\partial x_{1}}}_{O(\xi^{3})} + O(\xi^{4}) \qquad 2E_{23}^{r} = \underbrace{\frac{\partial u_{3}}{\partial x_{2}}}_{O(\xi^{3})} + O(\xi^{4})$$

$$E_{22}^{r} = \underbrace{\frac{\partial u_{2}}{\partial x_{2}}}_{O(\xi^{3})} + O(\xi^{4}) \qquad 2E_{13}^{r} = \underbrace{\frac{\partial u_{3}}{\partial x_{1}}}_{O(\xi^{3})} + O(\xi^{4})$$

$$E_{33}^{r} = \underbrace{\frac{\partial^{1} v_{3}^{r}}{\partial x_{3}}}_{O(\xi^{3})} + O(\xi^{4}) \qquad 2E_{12}^{r} = \underbrace{\frac{\partial u_{1}}{\partial x_{2}}}_{O(\xi^{3})} + O(\xi^{4})$$

$$(3.19)$$

The revised strains from Equation (3.19) are employed to re-evaluate the strain energy density, U^r , and its significant part, U^r_{sig} . Similar to the ZOS, the perturbation variables ${}^{1}v^{r}_{i}$ appearing in U^{r}_{sig} only have derivatives with respect to x_3 . This allows us to divide

the minimization process into two stages: a through-the-thickness 1D analysis and an in-plane 2D analysis.

Through the Thickness 1D Analysis

The functional $\Pi_{x_3}^r$ is updated to account for the changes made to U_{sig}^r . Minimizing $\Pi_{x_3}^r$ leads to the following Euler-Lagrange equations for the r^{th} lamina.

$$C_{55}^{r} \left(\frac{\partial}{\partial x_3}\right)^2 {}^{1}v_1^r + C_{45}^{r} \left(\frac{\partial}{\partial x_3}\right)^2 {}^{1}v_2^r = 0$$

$$C_{45}^{r} \left(\frac{\partial}{\partial x_3}\right)^2 {}^{1}v_1^r + C_{44}^{r} \left(\frac{\partial}{\partial x_3}\right)^2 {}^{1}v_2^r = 0$$

$$C_{33}^{r} \left(\frac{\partial}{\partial x_3}\right)^2 {}^{1}v_3^r = 0$$

$$(3.20)$$

The associated boundary conditions are as follows

$$\mathcal{B}_{0v_{1}^{r}}\big|_{x_{3}=h^{r}-\eta} = (\sigma_{13}^{r})_{\text{top}} \qquad \mathcal{B}_{0v_{1}^{r}}\big|_{x_{3}=h^{(r+1)}-\eta} = (\sigma_{13}^{r})_{\text{bot}}
\mathcal{B}_{0v_{2}^{r}}\big|_{x_{3}=h^{r}-\eta} = (\sigma_{23}^{r})_{\text{top}} \qquad \mathcal{B}_{0v_{2}^{r}}\big|_{x_{3}=h^{(r+1)}-\eta} = (\sigma_{13}^{r})_{\text{bot}}
\mathcal{B}_{0v_{3}^{r}}\big|_{x_{3}=h^{r}-\eta} = (\sigma_{33}^{r})_{\text{top}} \qquad \mathcal{B}_{0v_{3}^{r}}\big|_{x_{3}=h^{(r+1)}-\eta} = (\sigma_{33}^{r})_{\text{bot}}
\mathcal{B}_{1v_{1}^{r}} = C_{45}^{r} \frac{\partial u_{3}}{\partial x_{2}} + C_{55}^{r} \frac{\partial u_{3}}{\partial x_{1}} + C_{55}^{r} \frac{\partial^{1}v_{1}^{r}}{\partial x_{3}} + C_{45}^{r} \frac{\partial^{1}v_{2}^{r}}{\partial x_{3}}
\mathcal{B}_{1v_{2}^{r}} = C_{44}^{r} \frac{\partial u_{3}}{\partial x_{2}} + C_{45}^{r} \frac{\partial u_{3}}{\partial x_{1}} + C_{45}^{r} \frac{\partial^{1}v_{1}^{r}}{\partial x_{3}} + C_{44}^{r} \frac{\partial^{1}v_{2}^{r}}{\partial x_{3}}
\mathcal{B}_{1v_{3}^{r}} = C_{36}^{r} \frac{\partial u_{1}}{\partial x_{2}} + C_{23}^{r} \frac{\partial u_{2}}{\partial x_{2}} + C_{13}^{r} \frac{\partial u_{1}}{\partial x_{1}} + C_{36}^{r} \frac{\partial u_{2}}{\partial x_{1}} + C_{33}^{r} \frac{\partial^{1}v_{3}^{r}}{\partial x_{3}}$$

$$(3.21)$$

The Euler-Lagrange equations given in Equation (3.20) are solved, subject to the boundary conditions from Equation (3.21) and the constraints in Equation (3.18). Additionally, the continuity of displacements and transverse stresses at the interfaces between each lamina is ensured. This yields

Where the expression for $c_1^r = c_1^r(x_1, x_2)$ is obtained in terms of f_1^r by considering continuity of displacements at the interface of each lamina and the constraint given in Eq (3.18), leading in estimation of order of c_1^r as $h O(f_1^r)$. It is intersting to note that for homogeneous monoclinic materials $c_1^r = 0$.

3.3.6 Second Order Solution (SOS)

To achieve higher accuracy in the solution, we further refine the displacement field at this stage using the following perturbation

$$v_i^r = {}^0v_i^r + {}^1v_i^r + {}^2v_i^r$$
 where
$$v_1^r = u_1 - x_3 \frac{\partial u_3}{\partial x_1} + {}^2v_1^r, \qquad v_2^r = u_2 - x_3 \frac{\partial u_3}{\partial x_2} + {}^2v_2^r$$

$$v_3^r = u_3 + x_3 f_1^r + {}^2v_3^r$$
 (3.23)

Following the scheme outlined in Section 3.3.1, the orders of u_{α} , u_{3} and ${}^{0}v_{i}^{r}$ are determined. The estimated orders for these quantities are $O(\xi^{3}l)$, $O(\xi^{2}l)$, and $O(\xi^{3}h)$, respectively. Notably, by substituting v_{i} from Equation (3.23) into Equation (3.1), the corresponding strains are obtained. These strains are presented below, along with their respective orders indicated using underbraces.

$$E_{11}^{r} = \underbrace{\frac{\partial u_{1}}{\partial x_{1}} - x_{3} \left(\frac{\partial}{\partial x_{1}}\right)^{2} u_{3} + O(\xi^{4})}_{O(\xi^{3})} \quad 2E_{23}^{r} = \underbrace{\frac{\partial^{2} v_{2}^{r}}{\partial x_{3}}}_{O(\xi^{3})} + O\left(\xi^{4}\right)$$

$$E_{22}^{r} = \underbrace{\frac{\partial u_{2}}{\partial x_{2}} - x_{3} \left(\frac{\partial}{\partial x_{2}}\right)^{2} u_{3} + O(\xi^{4})}_{O(\xi^{3})} \quad 2E_{13}^{r} = \underbrace{\frac{\partial^{2} v_{1}^{r}}{\partial x_{3}}}_{O(\xi^{3})} + O\left(\xi^{4}\right)$$

$$E_{33}^{r} = \underbrace{f_{1}^{r} + \frac{\partial^{2} v_{3}^{r}}{\partial x_{3}}}_{O(\xi^{3})} + O\left(\xi^{4}\right)$$

$$2E_{12}^{r} = \underbrace{\frac{\partial u_{1}}{\partial x_{2}} + \frac{\partial u_{2}}{\partial x_{1}} - 2x_{3} \left(\frac{\partial}{\partial x_{1}}\right) \left(\frac{\partial}{\partial x_{2}}\right) u_{3}}_{O(\xi^{3})} + O(\xi^{4})$$

$$2E_{12}^{r} = \underbrace{\frac{\partial u_{1}}{\partial x_{2}} + \frac{\partial u_{2}}{\partial x_{1}} - 2x_{3} \left(\frac{\partial}{\partial x_{1}}\right) \left(\frac{\partial}{\partial x_{2}}\right) u_{3}}_{O(\xi^{3})} + O(\xi^{4})$$

The revised strains obtained in Equation (3.24) are utilized to re-evaluate the strain energy density U^r and its significant component U^r_{sig} . Similar to the ZOS and FOS, the

perturbation variables ${}^2v_i^r$ appearing in U_{sig}^r have derivatives with respect to x_3 alone. This splits the 3D analysis into two stages (1D and 2D analyses).

Through the Thickness 1D Analysis

We update the functional $\Pi_{x_3}^r$ to account for the changes made to U_{sig}^r . Minimizing $\Pi_{x_3}^r$ leads to the following Euler-Lagrange equations for the r^{th} lamina.

$$C_{55}^{r} \left(\frac{\partial}{\partial x_{3}}\right)^{2} v_{1}^{r} + C_{45}^{r} \left(\frac{\partial}{\partial x_{3}}\right)^{2} v_{2}^{r} = 0$$

$$C_{45}^{r} \left(\frac{\partial}{\partial x_{3}}\right)^{2} v_{1}^{r} + C_{44}^{r} \left(\frac{\partial}{\partial x_{3}}\right)^{2} v_{2}^{r} = 0$$

$$C_{23}^{r} \left(\frac{\partial}{\partial x_{2}}\right)^{2} u_{3} + 2C_{36}^{r} \left(\frac{\partial}{\partial x_{1}}\right) \left(\frac{\partial}{\partial x_{2}}\right) u_{3}$$

$$+ C_{13}^{r} \left(\frac{\partial}{\partial x_{1}}\right)^{2} u_{3} - C_{33}^{r} \left(\frac{\partial}{\partial x_{3}}\right)^{2} v_{3}^{r} = 0$$

$$(3.25)$$

The associated boundary conditions are as follows

$$\mathcal{B}_{0v_{1}^{r}}\big|_{x_{3}=h^{r}-\eta} = (\sigma_{13}^{r})_{\text{top}} \qquad \mathcal{B}_{0v_{1}^{r}}\big|_{x_{3}=h^{(r+1)}-\eta} = (\sigma_{13}^{r})_{\text{bot}}
\mathcal{B}_{0v_{2}^{r}}\big|_{x_{3}=h^{r}-\eta} = (\sigma_{23}^{r})_{\text{top}} \qquad \mathcal{B}_{0v_{2}^{r}}\big|_{x_{3}=h^{(r+1)}-\eta} = (\sigma_{13}^{r})_{\text{bot}}
\mathcal{B}_{0v_{3}^{r}}\big|_{x_{3}=h^{r}-\eta} = (\sigma_{33}^{r})_{\text{top}} \qquad \mathcal{B}_{0v_{3}^{r}}\big|_{x_{3}=h^{(r+1)}-\eta} = (\sigma_{33}^{r})_{\text{bot}}
\mathcal{B}_{2v_{1}^{r}} = C_{55}^{r} \frac{\partial^{2} v_{1}^{r}}{\partial x_{3}} + C_{45}^{r} \frac{\partial^{2} v_{2}^{r}}{\partial x_{3}}
\mathcal{B}_{2v_{2}^{r}} = C_{45}^{r} \frac{\partial^{2} v_{1}^{r}}{\partial x_{3}} + C_{44}^{r} \frac{\partial^{2} v_{2}^{r}}{\partial x_{3}}
\mathcal{B}_{2v_{3}^{r}} = -x_{3} \left\{ C_{23}^{r} \left(\frac{\partial}{\partial x_{2}} \right)^{2} u_{3} + 2C_{36}^{r} \left(\frac{\partial}{\partial x_{1}} \right) \left(\frac{\partial}{\partial x_{2}} \right) u_{3} \right.
\left. + C_{13}^{r} \left(\frac{\partial}{\partial x_{1}} \right)^{2} u_{3} \right\} + C_{33}^{r} \frac{\partial^{2} v_{3}^{r}}{\partial x_{3}}$$

Euler-Lagrange equations in Eq. (3.25) are solved considering the boundary conditions in Eq. (3.26) and the constraints given in Eq. (3.18) with addition to the continuity of displacements and transverse stresses at the boundaries of each lamina. The solution to the Euler-Lagrange equations is as follows

Where the expression for $c_2^r = c_2^r(x_1, x_2)$ is obtained in terms of g_1^r by considering continuity of displacements at the interface of each lamina and the constraint given in Eq (3.18), leading in estimation of order of c_2^r as $h^2 O(g_1^r)$. For homogeneous monoclinic materials $c_2^r = -\frac{1}{12}h^2g_1^r$.

Part A of this work aimed to develop a plate theory similar to CLPT. The solution approach employed in this work achieves this objective by starting with a zeroth-order solution and iteratively refining it to reach a second-order solution. The following sections provide a concise summary of the methodology used and the key findings from Part A.

3.3.7 Summary of Part A

Figure 3.3 visually depicts the systematic methodology employed to derive the reducedorder model. The procedure commences by calculating strains, assuming the plate as a 3D object. An order estimation scheme is used, based on the upper bound on the supnorm and $\frac{h}{l}$ as given in Equation (3.4). Additionally, a rule for calculating the order of displacement component derivatives, provided in Equation (3.2), is employed.

The zeroth-order solution starts with order estimation of various quantities of interest, following the ordering strategy outlined in Section 3.3.1. This leads to an ordered representation of the strain energy density, U^r . The most significant portion of U^r , denoted as U^r_{sig} , is isolated. Minimizing U^r_{sig} yields a closed-form solution for the zeroth-order perturbation variables, ${}^0v^r_i$. The first and second-order solutions follow an identical procedure, including order re-estimation of relevant quantities based on the ordering scheme, selection of the most significant part of the strain energy density, and its minimization to obtain closed-form solutions for the perturbation variables.

3.3.8 Displcement Field Obtained in Part A

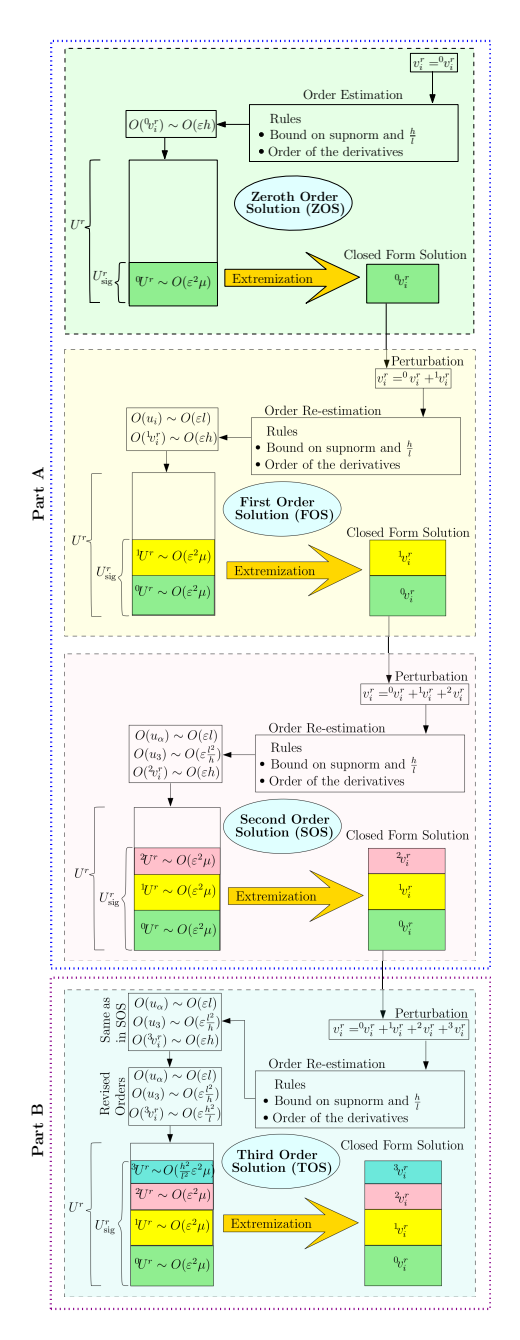


Figure 3.3: Systematic methodology adopted in deriving the reduced order model

The Part A of this work gives the following displacement field

$$v_{1}^{r} = \underbrace{u_{1} - x_{3} \frac{\partial u_{3}}{\partial x_{1}}}_{O(\xi^{3}l)}$$

$$v_{2}^{r} = \underbrace{u_{2} - x_{3} \frac{\partial u_{3}}{\partial x_{2}}}_{O(\xi^{3}l)}$$

$$v_{3}^{r} = \underbrace{u_{3} + \underbrace{x_{3} f_{1}^{r} + (x_{3})^{2} g_{1}^{r} + c^{r}(x_{1}, x_{2})}_{O(\xi^{3}h)}}_{O(\xi^{3}h)}$$
(3.28)

Where $c^r = c_1^r + c_2^r$. The displacement components v_1 and v_2 in Equation (3.28) align with those found in CLPT [100, 119, 130]. This is consistent with Kirchhoff's assumption: a line segment normal to the undeformed reference plane remains straight and perpendicular to the deformed reference plane after deformation. However, the displacement component v_3 in Equation (3.28) deviates from Kirchhoff's assumption of no change in length for transverse normals after deformation (i.e., they are inextensible). Interestingly, the next section will demonstrate that despite this difference, the plane stress assumption in CLPT makes it energetically equivalent to the asymptotically correct plate theory evolved in Part A of this work.

3.3.9 Strains Obtained in Part A

The strains, as shown below, corrected up to order ξ^3 are calculated by Eq. (3.1) and (3.28).

$$E_{11}^{r} = \underbrace{\frac{\partial u_{1}}{\partial x_{1}} - x_{3} \left(\frac{\partial}{\partial x_{1}}\right)^{2} u_{3}}_{O(\xi^{3})} \qquad E_{22}^{r} = \underbrace{\frac{\partial u_{2}}{\partial x_{2}} - x_{3} \left(\frac{\partial}{\partial x_{2}}\right)^{2} u_{3}}_{O(\xi^{3})}$$

$$E_{33}^{r} = \underbrace{f_{1}^{r} + 2x_{3}g_{1}^{r}}_{O(\xi^{3})} \qquad 2E_{23}^{r} = 0$$

$$2E_{13}^{r} = 0 \qquad 2E_{12}^{r} = \underbrace{\frac{\partial u_{1}}{\partial x_{2}} + \frac{\partial u_{2}}{\partial x_{1}} - 2x_{3} \left(\frac{\partial}{\partial x_{1}}\right) \left(\frac{\partial}{\partial x_{2}}\right) u_{3}}_{O(\xi^{3})} \qquad (3.29)$$

It is interesting to note that substituting strains from Eq. (3.29) in Eq. (3.5) yields

$$\sigma_{33}^r = C_{13}^r E_{11}^r + C_{23}^r E_{22}^r + C_{33}^r E_{33}^r + 2 C_{36}^r E_{12}^r = 0$$
(3.30)

Equation (3.30) leads to a plane stress condition that holds true with the current level of accuracy achieved for stresses. Consequently, since $\sigma_{33}^r = 0$, the virtual work equation Eq. (3.8) does not include the transverse normal strain E_{33}^r even though it is not zero. Therefore, we neglect the transverse normal strain E_{33}^r and by omitting this term from Equation (3.29), we obtain

$$E_{ps} = \begin{cases} E_{11}^r \\ E_{22}^r \\ 2E_{13}^r \\ 2E_{12}^r \end{cases} = \begin{cases} \frac{\partial u_1}{\partial x_1} - x_3 \left(\frac{\partial}{\partial x_1}\right)^2 u_3 \\ \frac{\partial u_2}{\partial x_2} - x_3 \left(\frac{\partial}{\partial x_2}\right)^2 u_3 \\ 0 \\ 0 \\ \frac{\partial u_1}{\partial x_2} + \frac{\partial u_2}{\partial x_1} - 2x_3 \left(\frac{\partial}{\partial x_1}\right) \left(\frac{\partial}{\partial x_2}\right) u_3 \end{cases}$$
(3.31)

An intriguing observation emerges despite the difference in the displacement field discussed in Section 3.3.8. The asymptotically correct strains, $E_{\rm ps}$, obtained in Equation (3.31) become similar to the strains predicted by CLPT [100]. This implies that CLPT is energetically equivalent to the asymptotically correct plate theory we formulated. Part B of this work improves the results from Part A by incorporating the effects of the higher-order energy terms.

3.4 Part B: Refinement of Part A

Building upon the foundation established in Part A, Part B refines the plate theory while preserving the overall methodological consistency. Notably, Part B incorporates the effects of higher-order energy terms within the analysis, improving the accuracy of Part A. Part B aligns with the conventional VAM-based approach for plate theory development found in the literature. The details of this refinement process are presented in the following section.

3.4.1 Third Order Solution (TOS)

The displacement components obtained in the SOS are further refined through perturbation as follows:

$$v_i^r = {}^0v_i^r + {}^1v_i^r + {}^2v_i^r + {}^3v_i^r,$$
 where
$$v_1^r = u_1 - x_3 \frac{\partial u_3}{\partial x_1} + {}^3v_1^r, \qquad v_2^r = u_2 - x_3 \frac{\partial u_3}{\partial x_2} + {}^3v_2^r$$

$$v_3^r = u_3 + x_3 f_1^r + (x_3)^2 g_1^r + c^r(x_1, x_2) + {}^3v_2^r$$
 (3.32)

Following the order estimation scheme outlined in Section 3.3.1, we estimate the order of the displacement components u_{α} , u_3 , and the perturbation variable ${}^3v_i^r$. These are determined to be $O(\xi^3 l)$, $O(\xi^2 l)$, and $O(\xi^3 h)$, respectively. Interestingly, these estimates are identical to those obtained in the SOS. Consequently, minimizing the potential energy based on these orders would lead to ${}^3v_i^r = 0$, resulting in no further improvement to the displacement field.

To overcome this limitation and achieve further refinement, we must consider the contribution of higher-order strain energy terms at this stage. Specifically, to account for the effects of strain energy of order $(\xi^8\mu)$, we elevate the order of ${}^3v_i^r$ to $O(\xi^4h)$ while maintaining the orders of the other variables. By substituting v_i from Equation (3.32) into Equation (3.1), we obtain

$$E_{11}^{r} = \underbrace{\frac{\partial u_{1}}{\partial x_{1}} - x_{3} \left(\frac{\partial}{\partial x_{1}}\right)^{2} u_{3}}_{O(\xi^{4})} + \underbrace{\frac{1}{2} \left(\frac{\partial u_{3}}{\partial x_{1}}\right)^{2}}_{O(\xi^{4})} + \underbrace{\frac{\partial^{3} v_{1}^{r}}{\partial x_{1}}}_{O(\xi^{5})} + O\left(\xi^{6}\right)$$

$$E_{22}^{r} = \underbrace{\frac{\partial u_{2}}{\partial x_{2}} - x_{3} \left(\frac{\partial}{\partial x_{2}}\right)^{2} u_{3} + \frac{1}{2} \left(\frac{\partial u_{3}}{\partial x_{2}}\right)^{2}}_{O(\xi^{4})} + \underbrace{\frac{\partial^{3} v_{1}^{r}}{\partial x_{2}}}_{O(\xi^{5})} + O\left(\xi^{6}\right)$$

$$E_{33}^{r} = \underbrace{\frac{f_{1}^{r} + 2x_{3}g_{1}^{r}}_{O(\xi^{3})} + \frac{1}{2} \left(\frac{\partial u_{3}}{\partial x_{1}}\right)^{2} + \frac{1}{2} \left(\frac{\partial u_{3}}{\partial x_{2}}\right)^{2} + \frac{\partial^{3} v_{2}^{r}}{\partial x_{3}}}_{O(\xi^{4})} + O\left(\xi^{6}\right)$$

$$2E_{23}^{r} = \underbrace{x_{3}}_{O(\xi^{3})} \underbrace{\frac{\partial f_{1}^{r}}{\partial x_{2}} + (x_{3})^{2} \frac{\partial g_{1}^{r}}{\partial x_{2}} + \frac{\partial c^{r}}{\partial x_{2}}}_{O(\xi^{4})} + \underbrace{\frac{\partial v_{3}^{2}}{\partial x_{3}}}_{O(\xi^{4})}_{O(\xi^{4})} + \underbrace{\frac{\partial u_{3}}{\partial x_{2}} \frac{\partial u_{3}}{\partial x_{1}} + x_{3}}_{O(\xi^{4})}_{O(\xi^{5})} + \underbrace{\frac{\partial u_{3}}{\partial x_{2}} \frac{\partial u_{3}}{\partial x_{1}} + x_{3}}_{O(\xi^{4})}_{O(\xi^{5})} + O\left(\xi^{6}\right)$$

$$2E_{13}^{r} = \underbrace{x_{3}}_{O(\xi^{4})} \underbrace{\frac{\partial f_{1}^{r}}{\partial x_{1}} + (x_{3})^{2} \frac{\partial g_{1}^{r}}{\partial x_{1}} + \frac{\partial c^{r}}{\partial x_{1}} + \frac{\partial v_{1}^{3}}{\partial x_{3}}}_{O(\xi^{4})} + \underbrace{\frac{\partial v_{1}^{3}}{\partial x_{3}} \frac{\partial u_{3}}{\partial x_{2}} + x_{3}}_{O(\xi^{5})}_{O(\xi^{5})} + \underbrace{\frac{\partial v_{1}^{3}}{\partial x_{3}} \frac{\partial u_{3}}{\partial x_{1}} + x_{3}}_{O(\xi^{5})}_{O(\xi^{5})} + O\left(\xi^{6}\right)}_{O(\xi^{5})}$$

$$2E_{12}^{r} = \underbrace{\frac{\partial u_{1}}{\partial x_{2}} + \frac{\partial u_{2}}{\partial x_{1}} - \frac{\partial u_{1}}{\partial x_{1}} + x_{3}}_{O(\xi^{5})} + \underbrace{\frac{\partial v_{1}^{3}}{\partial x_{1}} \frac{\partial u_{3}}{\partial x_{2}} + x_{3}}_{O(\xi^{5})}_{O(\xi^{5})} + \underbrace{\frac{\partial v_{1}^{3}}{\partial x_{1}} \frac{\partial v_{1}^{3}}{\partial x_{2}} + O\left(\xi^{6}\right)}_{O(\xi^{5})}_{O(\xi^{5})} + \underbrace{\frac{\partial u_{3}}{\partial x_{1}} \frac{\partial v_{1}^{3}}{\partial x_{1}} + O\left(\xi^{6}\right)}_{O(\xi^{5})}_{O(\xi^{5})}$$

$$2E_{12}^{r} = \underbrace{\frac{\partial u_{1}}{\partial x_{2}} + \frac{\partial u_{2}}{\partial x_{1}} - 2x_{3} \left(\frac{\partial}{\partial x_{1}}\right) \left(\frac{\partial}{\partial x_{2}}\right) u_{3} + \underbrace{\frac{\partial^{3} v_{1}^{3}}{\partial x_{1}} + \frac{\partial^{3} v_{1}^{3}}{\partial x_{1}} + O\left(\xi^{6}\right)}_{O(\xi^{5})$$

The revised strains given in Eq. (3.33) are utilized to recalculate U^r which takes the following form

$$U^{r} = \underbrace{0 U^{r} + U^{r} + 2U^{r} + 0 (\xi^{9} \mu)}^{U_{\text{sig}}^{r}} + O(\xi^{9} \mu)$$
(3.34)

where ${}^pU^r$ is the portion of the strain energy density U^r considered in p^{th} order solution. To account for higher-order energy effects, we define U^r_{sig} as the portion of U^r corrected up to $O(\xi^8\mu)$. The functional $\Pi^r_{x_3}$ is then recalculated based on this refined expression for U^r_{sig} .

A key distinction between the third-order solution and the zeroth, first, and secondorder solutions lies in the appearance of derivatives of the perturbation variables ${}^3v_i^r$ with respect to the x_{α} coordinates (i.e., $\frac{\partial^3v_i^r}{\partial x_{\alpha}}$). To eliminate these derivatives, integration by parts is employed, leading to boundary conditions defined at the edges of the plate domain, Ω_{side} . However, for the present analysis, we focus on the interior domain of the plate and disregard these edge effects, aiming to determine the displacement field within the plate interior without considering the influence of its boundaries [108, 112].

Finally, extremization of the modified functional $\Pi_{x_3}^r$ leads to the following Euler-Lagrange equations for the r^{th} lamina

$$C_{55}^{r} \left(\frac{\partial}{\partial x_{3}}\right)^{2} {}_{3}v_{1}^{r} + C_{45}^{r} \left(\frac{\partial}{\partial x_{3}}\right)^{2} {}_{3}v_{2}^{r} = 2C_{55}^{r} f_{2}^{r} + 6C_{55}^{r} x_{3} g_{2}^{r} + 2C_{45}^{r} f_{3}^{r} + 6C_{45}^{r} x_{3} g_{3}^{r}$$

$$C_{45}^{r} \left(\frac{\partial}{\partial x_{3}}\right)^{2} {}_{3}v_{1}^{r} + C_{44}^{r} \left(\frac{\partial}{\partial x_{3}}\right)^{2} {}_{3}v_{2}^{r} = 2C_{45}^{r} f_{2}^{r} + 6C_{45}^{r} x_{3} g_{2}^{r} + 2C_{44}^{r} f_{3}^{r} + 6C_{44}^{r} x_{3} g_{3}^{r}$$

$$C_{33}^{r} \left(\frac{\partial}{\partial x_{3}}\right)^{2} {}_{3}v_{2}^{r} = 0$$

$$(3.35)$$

The functions f_2^r , f_3^r , g_2^r , and g_3^r depend on the in-plane coordinates x_1 and x_2 . Detailed expressions for these functions in terms of the material constants and derivatives of u_i w.r.t. x_j are provided in Appendix D. The associated boundary conditions are presented below.

$$\mathcal{B}_{0_{v_{1}^{r}}}|_{x_{3}=h^{r}-\eta} = (\sigma_{13}^{r})_{\text{top}} \qquad \mathcal{B}_{0_{v_{1}^{r}}}|_{x_{3}=h^{(r+1)}-\eta} = (\sigma_{13}^{r})_{\text{bot}}
\mathcal{B}_{0_{v_{2}^{r}}}|_{x_{3}=h^{r}-\eta} = (\sigma_{23}^{r})_{\text{top}} \qquad \mathcal{B}_{0_{v_{2}^{r}}}|_{x_{3}=h^{(r+1)}-\eta} = (\sigma_{13}^{r})_{\text{bot}}
\mathcal{B}_{0_{v_{3}^{r}}}|_{x_{3}=h^{r}-\eta} = (\sigma_{33}^{r})_{\text{top}} \qquad \mathcal{B}_{0_{v_{3}^{r}}}|_{x_{3}=h^{(r+1)}-\eta} = (\sigma_{33}^{r})_{\text{bot}}
\mathcal{B}_{3_{v_{1}^{r}}} = C_{45}^{r}x_{3}\frac{\partial f_{1}^{r}}{\partial x_{2}} + C_{45}^{r}x_{3}^{2}\frac{\partial g_{1}^{r}}{\partial x_{2}} + C_{45}^{r}\frac{\partial c^{r}}{\partial x_{2}} + C_{55}^{r}x_{3}\frac{\partial f_{1}^{r}}{\partial x_{1}}
+ C_{55}^{r}x_{3}^{2}\frac{\partial g_{1}^{r}}{\partial x_{1}} + C_{55}^{r}\frac{\partial c^{r}}{\partial x_{1}} + C_{55}^{r}\frac{\partial^{3}v_{1}^{r}}{\partial x_{3}} + C_{45}^{r}\frac{\partial^{3}v_{2}^{r}}{\partial x_{3}}
\mathcal{B}_{3_{v_{2}^{r}}} = C_{44}^{r}x_{3}\frac{\partial f_{1}^{r}}{\partial x_{2}} + C_{45}^{r}\frac{\partial c^{r}}{\partial x_{1}} + C_{45}^{r}\frac{\partial^{3}v_{1}^{r}}{\partial x_{2}} + C_{45}^{r}\frac{\partial^{3}v_{1}^{r}}{\partial x_{1}}
+ C_{45}^{r}x_{3}^{2}\frac{\partial g_{1}^{r}}{\partial x_{1}} + C_{45}^{r}\frac{\partial c^{r}}{\partial x_{1}} + C_{45}^{r}\frac{\partial^{3}v_{1}^{r}}{\partial x_{3}} + C_{44}^{r}\frac{\partial^{3}v_{2}^{r}}{\partial x_{3}}
\mathcal{B}_{3_{v_{3}^{r}}} = C_{33}^{r}\frac{\partial^{3}v_{3}^{r}}{\partial x_{2}}$$

$$(3.36)$$

solution to the Euler-Lagrange equations Eq. (3.35) is given by

$${}^{3}v_{1}^{r} = a_{1}^{r} + x_{3}a_{2}^{r} + (x_{3})^{2}f_{2}^{r} + (x_{3})^{3}g_{2}^{r}$$

$${}^{3}v_{2}^{r} = a_{3}^{r} + x_{3}a_{4}^{r} + (x_{3})^{2}f_{3}^{r} + (x_{3})^{3}g_{3}^{r}$$

$${}^{3}v_{3}^{r} = a_{5}^{r} + x_{3}a_{6}^{r}$$

$$(3.37)$$

Where a_1^r , a_2^r , a_3^r , a_4^r , a_5^r , and a_6^r are constants of integration. These are determined by considering the boundary conditions in Eq. (3.36), the constraints in Eq. (3.18) and the continuity of the displacement components and transverse stresses at the interface of two consecutive laminae. A Mathematica code is developed to determine these quantities for a given laminate. However, the expression for a_6^r is straightforward and is given below.

$$a_{6}^{r} = -\frac{1}{2C_{33}^{r}} \left[\left(C_{23}^{r} + C_{33}^{r} \right) \left(\frac{\partial u_{3}}{\partial x_{2}} \right)^{2} + 2C_{36}^{r} \frac{\partial u_{3}}{\partial x_{1}} \frac{\partial u_{3}}{\partial x_{2}} \right. \\ \left. + \left(C_{13}^{r} + C_{33}^{r} \right) \left(\frac{\partial u_{3}}{\partial x_{1}} \right)^{2} \right]$$
(3.38)

Also, applying the boundary conditions in Eq. (3.36) for a symmetric plate with shear traction-free top and bottom surfaces leads to

$$\left(2f_2^r + \frac{\partial f_1^r}{\partial x_1}\right) - 2\eta \left(3g_2^r + \frac{\partial g_1^r}{\partial x_1}\right) = 0$$

$$\left(2f_3^r + \frac{\partial f_1^r}{\partial x_2}\right) - 2\eta \left(3g_3^r + \frac{\partial g_1^r}{\partial x_2}\right) = 0$$
(3.39)

Eq. (3.39) will be utilized later to find η and to eliminate higher-order derivatives from the strains. A graphical representation of the adopted procedure for the development done in Part B is presented in Fig. 3.3.

3.4.2 A Discussion on the Displacement Field

The final displacement field obtained in Part A and B is given below

$$v_{1}^{r} = \underbrace{u_{1} - x_{3} \frac{\partial u_{3}}{\partial x_{1}}}_{O(\xi^{3}l)} + \underbrace{a_{1}^{r} + x_{3}a_{2}^{r} + (x_{3})^{2}f_{2}^{r} + (x_{3})^{3}g_{2}^{r}}_{O(\xi^{4}h)}$$

$$v_{2}^{r} = \underbrace{u_{2} - x_{3} \frac{\partial u_{3}}{\partial x_{2}}}_{O(\xi^{3}l)} + \underbrace{a_{3}^{r} + x_{3}a_{4}^{r} + (x_{3})^{2}f_{3}^{r} + (x_{3})^{3}g_{3}^{r}}_{O(\xi^{4}h)}$$

$$v_{3}^{r} = \underbrace{u_{3}}_{O(\xi^{2}l)} + \underbrace{x_{3}f_{1}^{r} + (x_{3})^{2}g_{1}^{r} + c^{r}(x_{1}, x_{2})}_{O(\xi^{3}h)} + \underbrace{a_{5}^{r} + x_{3}a_{6}^{r}}_{O(\xi^{4}h)}$$

$$(3.40)$$

Each successive perturbation refines the displacement field. Figure 3.4 visually depicts the progressive improvements achieved in the displacement field with the introduction of each perturbation.

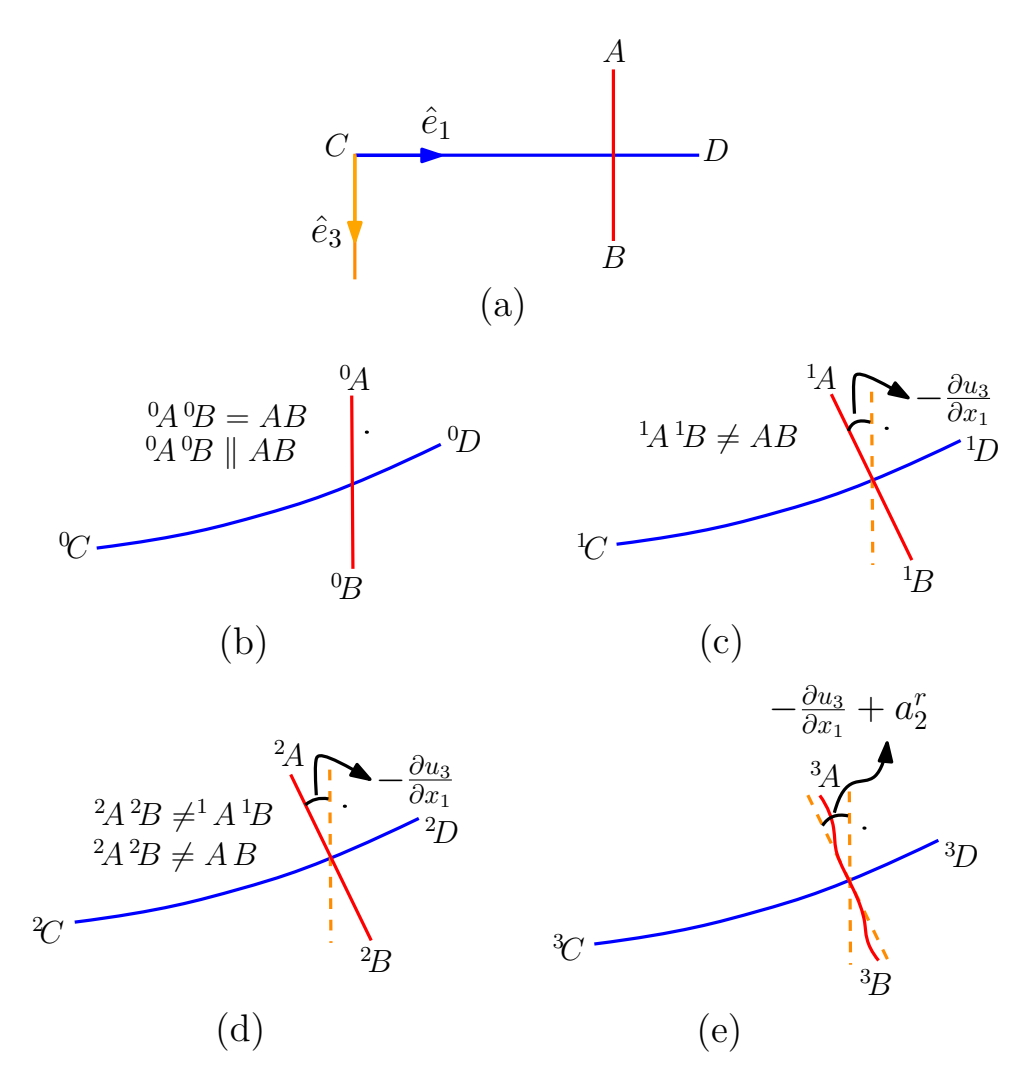


Figure 3.4: Progression of Deformation in lines AB and CD: (a) Undeformed configuration. (b) Configuration after zeroth-order perturbation. (c) Configuration after first-order perturbation. (d) Configuration after second-order perturbation. (e) Configuration after third-order perturbation.

Figure 3.4(a) depicts the undeformed configuration. Line segment CD lies in the reference plane oriented along direction \hat{e}_1 , while line segment AB is oriented along \hat{e}_3 .

Figure 3.4(b) illustrates the deformed configuration of line segment AB in the ZOS, represented by line segment ${}^{0}A{}^{0}B$. In the FOS and SOS (Figures 3.4(c) and 3.4(d) respectively), the displacement field is refined to include a rotation and a change in length

of line segment AB, as shown by line segments ${}^{1}A{}^{1}B$ and ${}^{2}A{}^{2}B$.

Finally, in the Third Order Solution, line segment AB deforms into the curved line segment ${}^{3}A$ ${}^{3}B$ as depicted in Figure 3.4(e).

3.4.3 A Discussion on the Strains, Stresses and Stiffness Matrix

Eq. (3.1) and (3.40) provide the expressions for the strains accurate up to order (ξ^4). These refined strains are presented below:

$$E_{11}^{r} = \underbrace{\frac{\partial u_{1}}{\partial x_{1}} - x_{3} \left(\frac{\partial}{\partial x_{1}}\right)^{2} u_{3} + \frac{1}{2} \left(\frac{\partial u_{3}}{\partial x_{1}}\right)^{2}}_{O(\xi^{4})}$$

$$E_{22}^{r} = \underbrace{\frac{\partial u_{2}}{\partial x_{2}} - x_{3} \left(\frac{\partial}{\partial x_{2}}\right)^{2} u_{3} + \frac{1}{2} \left(\frac{\partial u_{3}}{\partial x_{1}}\right)^{2}}_{O(\xi^{4})}$$

$$E_{33}^{r} = \underbrace{-\frac{1}{2C_{33}} \left[-2C_{33}(f_{1}^{r} + 2x_{3}g_{1}^{r})\right]}_{O(\xi^{3})} + \underbrace{\frac{1}{2C_{33}} \left[C_{23} \left(\frac{\partial u_{3}}{\partial x_{2}}\right)^{2} + 2C_{36} \frac{\partial u_{3}}{\partial x_{1}} \frac{\partial u_{3}}{\partial x_{2}} + C_{13} \left(\frac{\partial u_{3}}{\partial x_{1}}\right)^{2}\right]}_{O(\xi^{4})}$$

$$2E_{23}^{r} = \underbrace{a_{4}^{r} + \frac{\partial c^{r}}{\partial x_{2}} + x_{3} \left(2f_{3}^{r} + \frac{\partial f_{1}^{r}}{\partial x_{2}}\right) + (x_{3})^{2} \left(3g_{3}^{r} + \frac{\partial g_{1}^{r}}{\partial x_{2}}\right)}_{O(\xi^{4})}$$

$$2E_{13}^{r} = \underbrace{a_{2}^{r} + \frac{\partial c^{r}}{\partial x_{1}} + x_{3} \left(2f_{2}^{r} + \frac{\partial f_{1}^{r}}{\partial x_{1}}\right) + (x_{3})^{2} \left(3g_{2}^{r} + \frac{\partial g_{1}^{r}}{\partial x_{1}}\right)}_{O(\xi^{4})}$$

$$2E_{12}^{r} = \underbrace{\frac{\partial u_{1}}{\partial x_{2}} + \frac{\partial u_{2}}{\partial x_{1}} - 2x_{3} \left(\frac{\partial}{\partial x_{1}}\right) \left(\frac{\partial}{\partial x_{2}}\right) u_{3} + \left(\frac{\partial u_{3}}{\partial x_{1}}\right) \left(\frac{\partial u_{3}}{\partial x_{2}}\right)}_{O(\xi^{4})}}_{O(\xi^{4})}$$

$$(3.41)$$

The transverse shear strains, $2E_{13}$ and $2E_{23}$, depend on the derivatives of the in-plane displacement, u_{α} . Specifically, they involve terms like $\left(2f_3^r + \frac{\partial f_1^r}{\partial x_2}\right)$ and $\left(2f_2^r + \frac{\partial f_1^r}{\partial x_1}\right)$, which include higher-order derivatives of u_{α} . As shown in Eq. (3.39), setting the reference plane distance η to zero, eliminates these terms. This simplification justifies choosing the mid-plane of the plate (where $\eta=0$) as the reference plane for further analysis.

An interesting observation is that the plane stress condition, established in Part A, remains valid even with the higher-order strain terms incorporated here. This can be read-

ily verified by substituting the strains from Eq. (3.41) into Eq. (3.5). This substitution confirms that $\sigma_{33}^r = 0$, signifying the plane stress condition.

It is noteworthy that the plane stress condition arises naturally from the adopted procedure, eliminating the need for an *ad hoc* or *a priori* assumption as commonly encountered in various plate theories from the literature [119, 122, 68]. The historical precedent and simplicity of the plane stress condition, make it a popular choice for plate theories.

Following the reasoning presented in Section 3.3.9, the transverse normal strain E_{33}^r can be neglected. Omitting this term from Eq. (3.41) and selecting the mid-plane of the plate as the reference plane, we obtain

$$E^{r} = \begin{cases} \frac{\partial u_{1}}{\partial x_{1}} - x_{3} \left(\frac{\partial}{\partial x_{1}}\right)^{2} u_{3} + \frac{1}{2} \left(\frac{\partial u_{3}}{\partial x_{1}}\right)^{2} \\ \frac{\partial u_{2}}{\partial x_{2}} - x_{3} \left(\frac{\partial}{\partial x_{2}}\right)^{2} u_{3} + \frac{1}{2} \left(\frac{\partial u_{3}}{\partial x_{2}}\right)^{2} \\ a_{4}^{r} + \frac{\partial c^{r}}{\partial x_{2}} + (x_{3})^{2} \left(3g_{3}^{r} + \frac{\partial g_{1}^{r}}{\partial x_{2}}\right) \\ a_{2}^{r} + \frac{\partial c^{r}}{\partial x_{1}} + (x_{3})^{2} \left(3g_{2}^{r} + \frac{\partial g_{1}^{r}}{\partial x_{1}}\right) \\ \frac{\partial u_{1}}{\partial x_{2}} + \frac{\partial u_{2}}{\partial x_{1}} - 2x_{3} \left(\frac{\partial}{\partial x_{1}}\right) \left(\frac{\partial}{\partial x_{2}}\right) u_{3} + \left(\frac{\partial u_{3}}{\partial x_{1}}\right) \left(\frac{\partial u_{3}}{\partial x_{2}}\right) \end{cases}$$

$$(3.42)$$

Also, the stiffness matrix for r^{th} lamina is modified according to the plane stress condition [119] as

$$D^{r} = \begin{bmatrix} D_{11}^{r} & D_{12}^{r} & 0 & 0 & D_{16}^{r} \\ D_{12}^{r} & D_{22}^{r} & 0 & 0 & D_{26}^{r} \\ 0 & 0 & D_{44}^{r} & D_{45}^{r} & 0 \\ 0 & 0 & D_{45}^{r} & D_{55}^{r} & 0 \\ D_{16}^{r} & D_{26}^{r} & 0 & 0 & D_{66}^{r} \end{bmatrix}$$

$$(3.43)$$

Under plane stress conditions, stresses σ^r and strain energy density U^r for the $r^{\rm th}$ lamina are given as follows

$$\sigma^{r} = \left\{ \sigma_{11}^{r}, \ \sigma_{22}^{r}, \ \sigma_{23}^{r}, \ \sigma_{13}^{r}, \ \sigma_{12}^{r} \right\}^{T} = D^{r} E^{r},$$

$$U^{r} = \frac{1}{2} (\sigma^{r})^{T} E^{r} = \frac{1}{2} (D^{r} E^{r})^{T} E^{r}$$
(3.44)

The transverse shear force resultants Q_{α} , strain energy per unit area \overline{U} and transverse shear strain energy per unit area $\overline{U}_{\rm shear}$ are given by

$$Q_{2} = \sum_{r=1}^{n} \int_{h^{r}}^{h^{(r+1)}} \sigma_{23}^{r} dx_{3}$$

$$Q_{1} = \sum_{r=1}^{n} \int_{h^{r}}^{h^{(r+1)}} \sigma_{13}^{r} dx_{3}$$

$$\overline{U} = \sum_{r=1}^{n} \int_{h^{r}}^{h^{(r+1)}} U^{r} dx_{3}$$

$$\overline{U}_{\text{shear}} = \frac{1}{2} \sum_{r=1}^{n} \int_{h^{r}}^{h^{(r+1)}} (\sigma_{23}^{r} E_{23}^{r} + \sigma_{13}^{r} E_{13}^{r}) dx_{3}$$
(3.45)

Substitution of the strain energy from Eq. (3.45) in the virtual work Eq. (3.8) reduces it in the following form

$$\int_{\partial\Omega^{r}} \left(\delta \overline{U}_{\text{rest}} + \delta \overline{U}_{\text{shear}} \right) da_{\text{ref}} - \int_{\partial\Omega_{\text{tb}}} \vec{q} \cdot \delta \vec{v} da_{\text{tb}} - \int_{\partial\Omega_{\text{side}}} \vec{t} \cdot \delta \vec{v} da_{\text{side}} = 0$$
Where $\overline{U}_{\text{rest}} = \overline{U} - \overline{U}_{\text{shear}}$ (3.46)

The Virtual work Eq. (3.46) can used for the 2D in plane analysis considering u_i as the independent variables of the problem resulting in the solution to the 2D variables. However, Due to dependency of \overline{U} on the higher order derivatives of u_3 , This Equation involve computational complexities and becomes computationally inefficient. To circumvent the computational complexities by eliminating these higher order derivatives FSDT plate theory and the concept of isoenergetics [57] are used. The following section presents the details of this procedure.

3.5 Part C: Elimination of Higher Order Derivatives

FSDT plate theory, though asymptotically inaccurate, is very practical due to its simplicity and computational efficiency thereby often preferred for the analysis of thin and moderately thick plates. This theory accounts for the transverse shear deformation effects in the plate. In This theory, it is assumed that a straight line normal to the undeformed reference plane $\partial\Omega_{\rm ref}$ remains straight but not perpendicular to the deformed reference plane $\partial\Omega_{\rm ref}$ and has rotations ϕ_1 and ϕ_2 about the x_1 and x_2 axes. Thus FSDT plate theory incorporates two additional degrees of freedom ϕ_1 and ϕ_2 . The strains for FSDT plate theory [100, 101] are given below

$$E^{\text{FSDT}} = \begin{cases} E_{11}^{\text{FSDT}} \\ E_{22}^{\text{FSDT}} \\ 2E_{23}^{\text{FSDT}} \\ 2E_{13}^{\text{FSDT}} \\ 2E_{12}^{\text{FSDT}} \end{cases} = \begin{cases} \frac{\partial u_1}{\partial x_1} + x_3 \frac{\partial \phi_1}{\partial x_1} + \frac{1}{2} \left(\frac{\partial u_3}{\partial x_1} \right)^2 \\ \frac{\partial u_2}{\partial x_2} + x_3 \frac{\partial \phi_2}{\partial x_2} + \frac{1}{2} \left(\frac{\partial u_3}{\partial x_2} \right)^2 \\ \phi_2 + \frac{\partial u_3}{\partial x_2} \\ \phi_1 + \frac{\partial u_3}{\partial x_1} \\ \frac{\partial u_1}{\partial x_2} + \frac{\partial u_2}{\partial x_1} + x_3 \left(\frac{\partial \phi_1}{\partial x_2} + \frac{\partial \phi_2}{\partial x_1} \right) + \left(\frac{\partial u_3}{\partial x_1} \right) \left(\frac{\partial u_3}{\partial x_2} \right) \end{cases}$$
(3.47)

The through the thickness constant value of the transverse strains $(2E_{\alpha 3}^{\rm FSDT})$ in FSDT results in an inaccurate calculation of transverse shear strain energies [54, 53, 52, 51]. To remove this shortcoming of the FSDT plate theory, SCFs are emplyed. Following references [50, 49], The expressions for the transverse shear force resultants $Q_{\alpha}^{\rm FSDT}$ and transverse shear strain energy per unit area $\overline{U}_{\rm shear}^{\rm FSDT}$ for FSDT Plate theory with SCfs are given by

$$Q_{2}^{\text{FSDT}} = \sum_{r=1}^{n} \int_{h^{r}}^{h^{(r+1)}} \left(2D_{44}^{r} E_{23}^{\text{FSDT}} + 2D_{45}^{r} E_{13}^{\text{FSDT}} \right) dx_{3}$$

$$Q_{1}^{\text{FSDT}} = \sum_{r=1}^{n} \int_{h^{r}}^{h^{(r+1)}} \left(2D_{45}^{r} E_{23}^{\text{FSDT}} + 2D_{55}^{r} E_{13}^{\text{FSDT}} \right) dx_{3}$$

$$\overline{U}_{\text{shear}}^{\text{FSDT}} = \sum_{r=1}^{n} \int_{h^{r}}^{h^{(r+1)}} \left[2D_{44}^{r} (E_{23}^{\text{FSDT}})^{2} + 4D_{45}^{r} E_{13}^{\text{FSDT}} E_{23}^{\text{FSDT}} + 2D_{55}^{r} (E_{13}^{\text{FSDT}})^{2} \right] dx_{3}$$

$$(3.48)$$

Where $(k_{\alpha})^2 = K_{\alpha}$ are SCFs. The FSDT plate theory is made isoenergetic to the asymptotically correct plate theory by finding suitable shear correction factors (SCFs) in such a way that the asymptotically correct plate theory and the FSDT plate theory result in the same strain energy per unit area for same deformation pattern of the reference plane. To calculate SCFs, the equality of the relevant quantities in Eq. (3.45) and (3.48) is employed as shown below

$$Q_2^{\text{FSDT}} = Q_2 \qquad Q_1^{\text{FSDT}} = Q_1 \qquad \overline{U}_{\text{shear}}^{\text{FSDT}} = \overline{U}_{\text{shear}}$$
 (3.49)

To find K_{α} using Eq. (3.49), the cylindrical bending about the x_1 and x_2 axes is considered [50, 123]. First cylindrical bending about x_2 axis resulting in $u_3(x_1, x_2) = u_3(x_1)$ is investigated. Eq. (3.49) is used to establish a relation between k_1 and k_2 which is independent of the quantities associated with the deformation pattern (viz. $\gamma_{\alpha 3}$ and

derivatives of u_3 with respect to x_1). Following a similar approach, another relation between k_1 and k_2 is set by considering cylindrical bending about x_1 axis. The two relations in k_1 and k_2 are used to find the SCFs.

As determined in the present work, the order of transverse shear strains is $O(\xi^4)$. Thearfore, Eq. (3.47) and the order estimation scheme in article 3.3.1 gives

$$-x_3 \frac{\partial^2 u_3}{\partial x_\alpha \partial x_\beta} = x_3 \frac{\partial \phi_\beta}{\partial x_\alpha} + O\left(\xi^5\right) \tag{3.50}$$

Considering strains accurate up to the order of $O(\xi^4)$, Eq. (3.50) is utilized to replace second and higher-order derivatives of u_3 with derivatives of ϕ_{α} from Eq. (3.42), neglecting quantities of order $O(\xi^5)$ and higher. This replacement modifies Eqs. (3.42), (3.44), (3.45), and (3.46), rendering $E_{\alpha\beta} = E_{\alpha\beta}^{\rm FSDT}$. Additionally, Eq. (3.49) enables the replacement of \overline{U} shear with $\overline{U}_{\rm shear}^{\rm FSDT}$ in the virtual work equation (3.46). This makes the FSDT plate theory with SCFs Isoenergetic to the asymptotically correct plate theory developed in this work. Hence, the present work employs Isoenergetic FSDT plate theory to calculate in-plane displacement variables u_i and ϕ_i . Once these variables are determined, the actual through-the-thickness variation of strains is recovered using the following strains, obtained by replacing higher-order derivatives of u_3 with lower-order derivatives of ϕ_{α} using Eq. (3.50) in Eq. (3.42).

$$E = \begin{cases} \frac{\partial u_1}{\partial x_1} + x_3 \frac{\partial \phi_1}{\partial x_1} + \frac{1}{2} \left(\frac{\partial u_3}{\partial x_1} \right)^2 \\ \frac{\partial u_2}{\partial x_2} + x_3 \frac{\partial \phi_2}{\partial x_2} + \frac{1}{2} \left(\frac{\partial u_3}{\partial x_2} \right)^2 \\ a_4^r + \frac{\partial c^r}{\partial x_2} + (x_3)^2 \left(3g_3^r + \frac{\partial g_1^r}{\partial x_2} \right) \\ a_2^r + \frac{\partial c^r}{\partial x_1} + (x_3)^2 \left(3g_2^r + \frac{\partial g_1^r}{\partial x_1} \right) \\ \frac{\partial u_1}{\partial x_2} + \frac{\partial u_2}{\partial x_1} + x_3 \left(\frac{\partial \phi_1}{\partial x_2} + \frac{\partial \phi_2}{\partial x_1} \right) + \left(\frac{\partial u_3}{\partial x_1} \right) \left(\frac{\partial u_3}{\partial x_2} \right) \end{cases}$$

$$(3.51)$$

3.6 Results and Discussion

In this work, a novel approach is introduced for analyzing multilayered composite structures. To assess its accuracy, numerical examples involving various scenarios are provided. The material properties listed in Table 3.1 are utilized in these numerical illustrations. In this table, subscripts L and T represent the longitudinal (along the fiber orientation) and transverse (perpendicular to the fiber orientation) directions, respectively. For systematic presentation, the Validation is divided into two subsections: the first subsection validates

the SCFs obtained using the present approach, while the second subsection validates the deformation of plates obtained using the present approach.

	Material-1 [48]	Material-2 [116]	Material-3 [47]	Material-4 [144]	Material-5 [144]
E_L (GPa)	139.3	172.369	103.421	12.605	227.53
E_T (GPa)	9.72	6.895	6.895	12.628	144.79
G_{LT} (GPa)	5.58	3.337	3.447	2.155	55.16
G_{TT} (GPa)	3.45	1.379	2.413	2.155	27.58
$ u_{LT}$	0.29	0.25	0.3	0.2395	0.25
$ u_{TT}$	0.4	0.25	0.49	0.2395	0.25

Table 3.1: Material properties used in different numerical examples

3.6.1 Validation of the SCFs

A number of examples are presented to find SCFs. The results are compared with those found in literature. In all the examples, different symmetric layer sequences with equal layer thickness within a total thickness h are investigated.

First a laminate with n laminae is examined [123]. The laminate is constructed of alternate plies of 0° and 90° orientations relative to the x_1 axis of the plate with the two centre layers oriented at 90° to provide symmetry. All plies have the same thickness $\frac{h}{n}$. Each ply is composed of Material-2, whose properties are given in Table 3.1.

The SCFs K_1 and K_2 have been plotted versus the number of plies, n, in Fig. 3.5. It is clear that the SCFs calculated using the present approach are in excellent match with given in the the work done by Vlachoutsis et al. [123]. Also the values of K_{α} ($K_1 = 0.6808$, $K_2 = 0.6794$) for n = 120 matched exactly with those given in his work. The SCF versus the $\frac{G_{13}}{G_{23}}$ are plotted in Fig. (3.6), for n = 120, when only G_{23} changes while the other values remain unchanged.

Next SCFs are calculated for different symmetric lay-up sequences. The results are compared with those found in literature in Table 3.2. the results obtained using the present appoach are found in good agreement with those given in literature.

Finally the SCFs are calculated for the homogeneous Isotropic/orthotropic/monoclinic materials. the SCFs $(K_1 = K_2 = \frac{5}{6})$ are found to be in agreement with literature [47, 123].

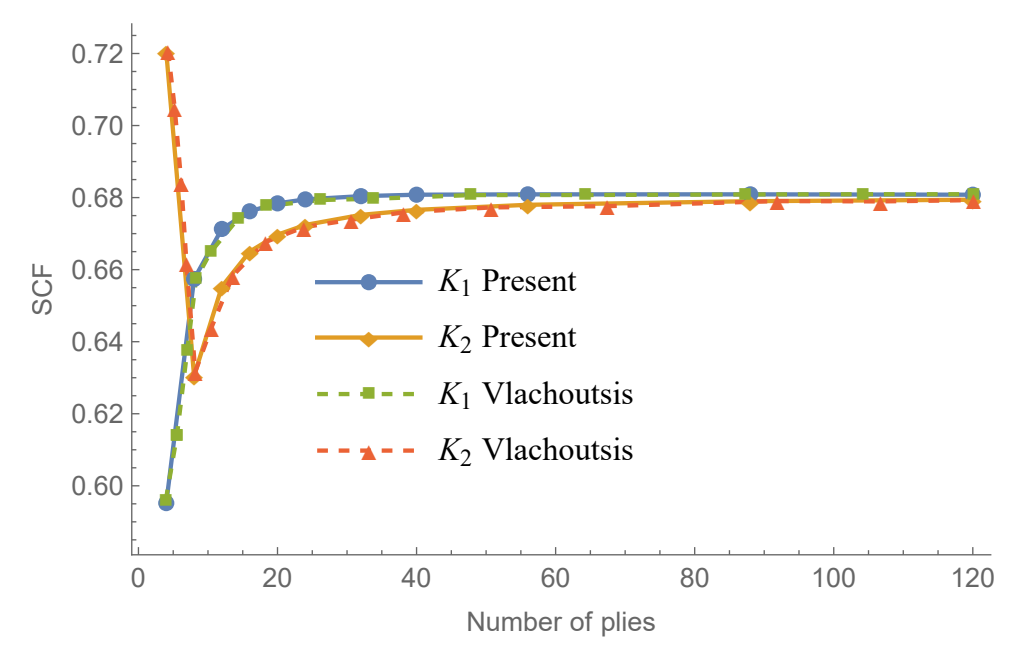


Figure 3.5: Variation of SCFs with number of plies

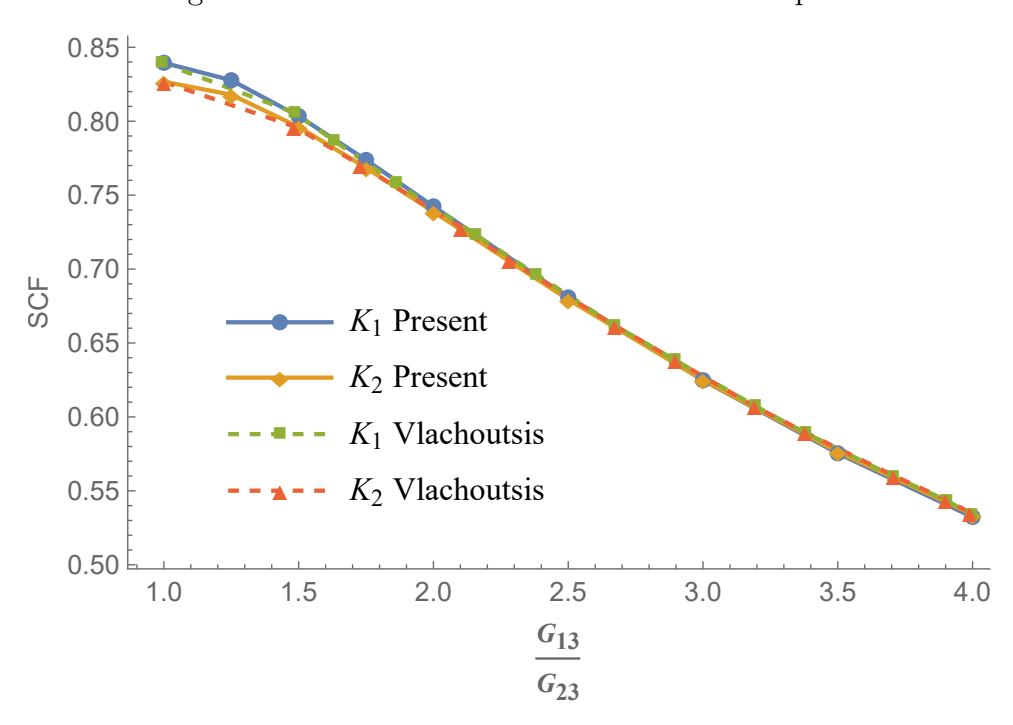


Figure 3.6: Variation of SCFs with $\frac{G_{13}}{G_{23}}$

3.6.2 Validation of the Deformation of Plates

In this section displacements and stresses are calculated for different Numerical examples. Fig. 3.7 and 3.8 depict the dimensions of the plats, the lay-up sequences and the boundary

Lay-up $(^{\circ})$	Material (Table 3.1)	Theory	K_1	K_2
[0,90,0]	Material-2	[47]	0.7031	0.8676
		Present	0.5828	0.8028
$[0, 90]_S$	Material-2	[46]	0.5952	0.7205
		[45]	0.5936	0.7788
		Present	0.5952	0.7205
	Materia-4	Present	0.8332	0.8334
$[30/-30]_S$	Material-2	[50]	0.7549	0.6730
		[45]	0.6773	0.6722
		Present	0.6472	0.6361
10/5/0/5/10	Material-3	[47]	0.8313	0.8298
		Present	0.8303	0.8309
1 - 14.80/75.20/ - 75.20/	Material-1	Present	0.8029	0.3926
$14.80/-22.87/67.13]_S$				
$[0/90/0/90]_S$	Material-2	Present	0.6574	0.6305
$[45/-45]_S$	Material-5	Present	0.7237	0.7237

Table 3.2: SCFs for different symmetric lay-up sequences

conditions for different numeric examples. The values of length of the plate a, width of the plate b and thickness of the plate h along with material properties and boundary conditions used in different examples are given in Table 3.3.

Table 3.3: Geometry, Material Properties and boundary conditions for the numerical examples

Numerical	Geometry				Material	Boundary
Example		(Fig. 3.7)				Conditions
	a (m)	b (m)	h (m)	$\frac{b}{h}$	(Table 3.1)	(Fig. 3.8)
Example-1	0.5472	0.1824	0.001824	100	Material-1	cfcf
Example-2	0.3048	0.3048	0.002438	125	Material-4	cccc
Example-3	a	a	h	20	Material-2	SSSS
Example-4	a	a	h		Material-2	SSSS
Example-5	5	1	0.02	50	Material-5	cccc

Result for the center point deflection of the plate considered in Example-2 is plotted in Fig. 3.12. it is compared with that obtained using 3D FEA, MXFEM [144], Experimental [43] and Linear [144] approaches. The results obtained using present, 3D FEA and MXFEM approachs are in good aggreement. However, there is a small difference in experimental results. This difference might be due to limitations in modeling the experiment's actual support conditions and material properties within the simulations.

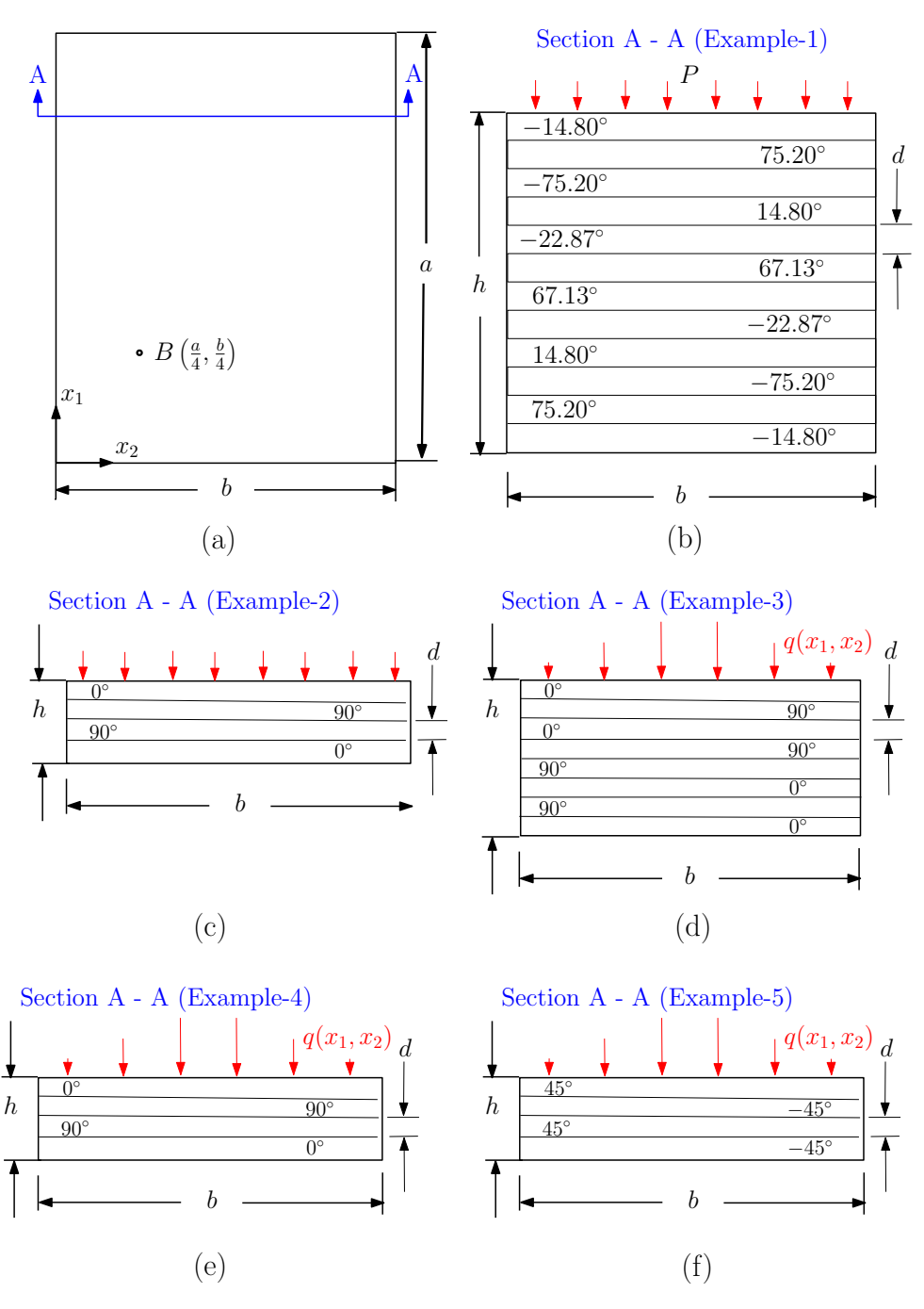


Figure 3.7: Geometry of the plate examined in the numerical examples (a) in-plane dimensions of the plate (b) through the thickness structure of the plate in Example-1 (c) through the thickness structure of the plate in Example-2 (d) through the thickness structure of the plate in Example-3 (e) through the thickness structure of the plate in Example-4, (f) through the thickness structure of the plate in Example-5.

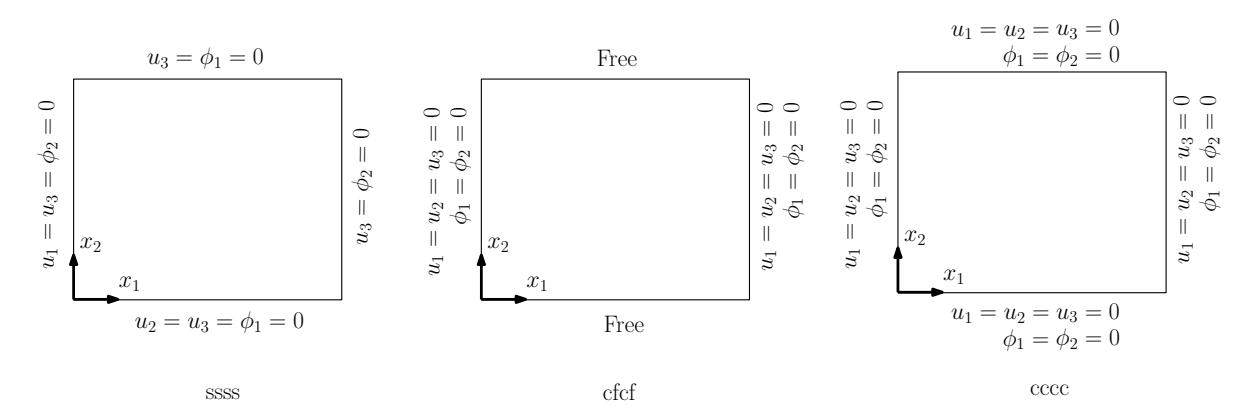


Figure 3.8: Boundary conditions used in different numerical examples

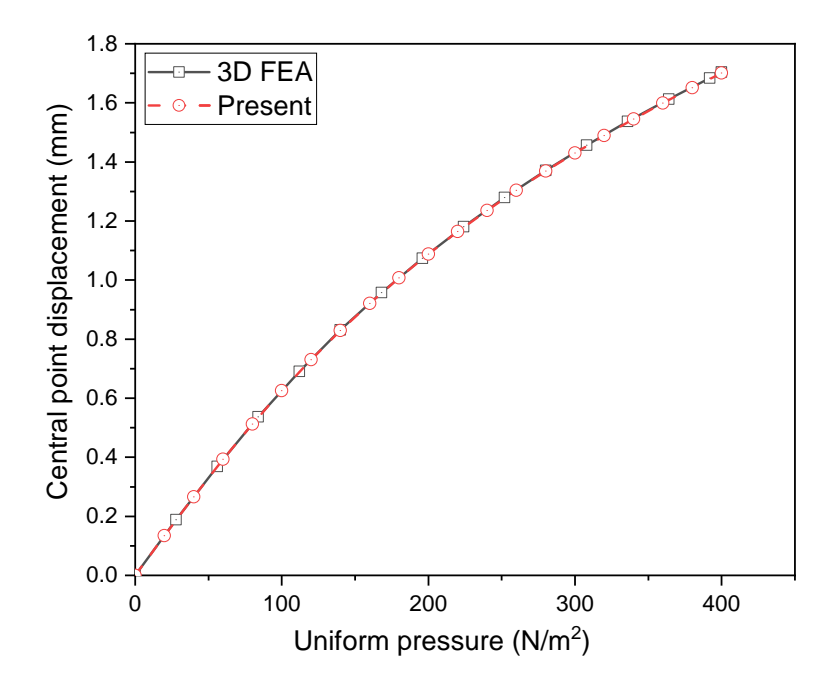


Figure 3.9: Load-deflection curves for the central point of the plate considered in Example-1 under uniform Pressure P applied at its top face

In Example-1 and Example-2 the plate is subjected to a uniform pressure P on the top face $(x_3 = -\frac{h}{2})$. In rest of the numerical examples (Example-3, Example-4 and Example-5), plates subjected to a sinusoidally varying pressure q on its top face is examined.

$$q = q_0 \sin\left(\frac{\pi \ x_1}{a}\right) \sin\left(\frac{\pi \ x_2}{b}\right) \tag{3.52}$$

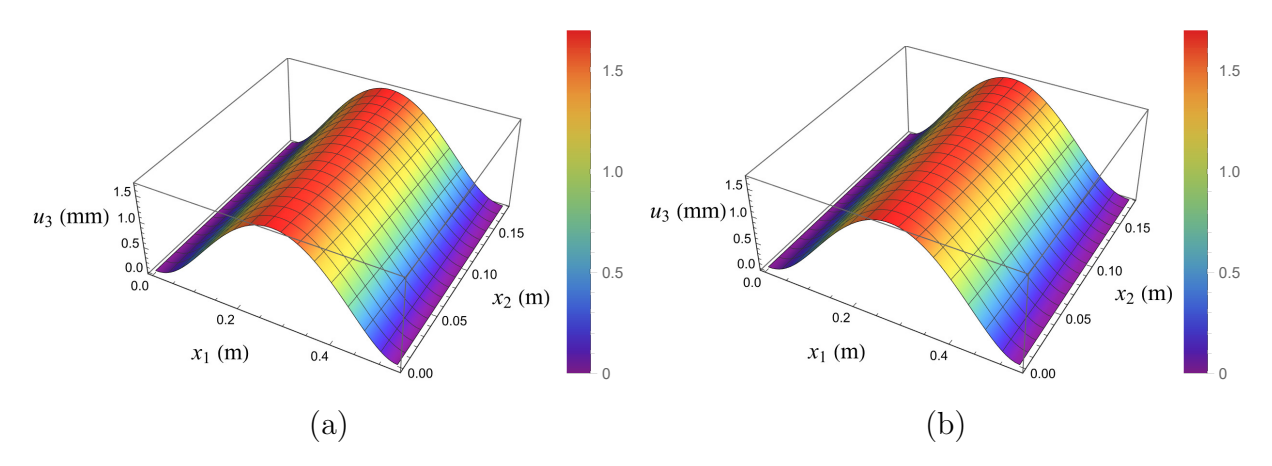


Figure 3.10: Out-of-plane deflection of the plate considered in Example-1 subjected to a uniform pressure of $P = 400 \text{ N/m}^2$ applied on its top face. Deflections are obtained using: (a) 3D Finite Element Analysis (FEA) and (b) present ACI-ESL plate theory.

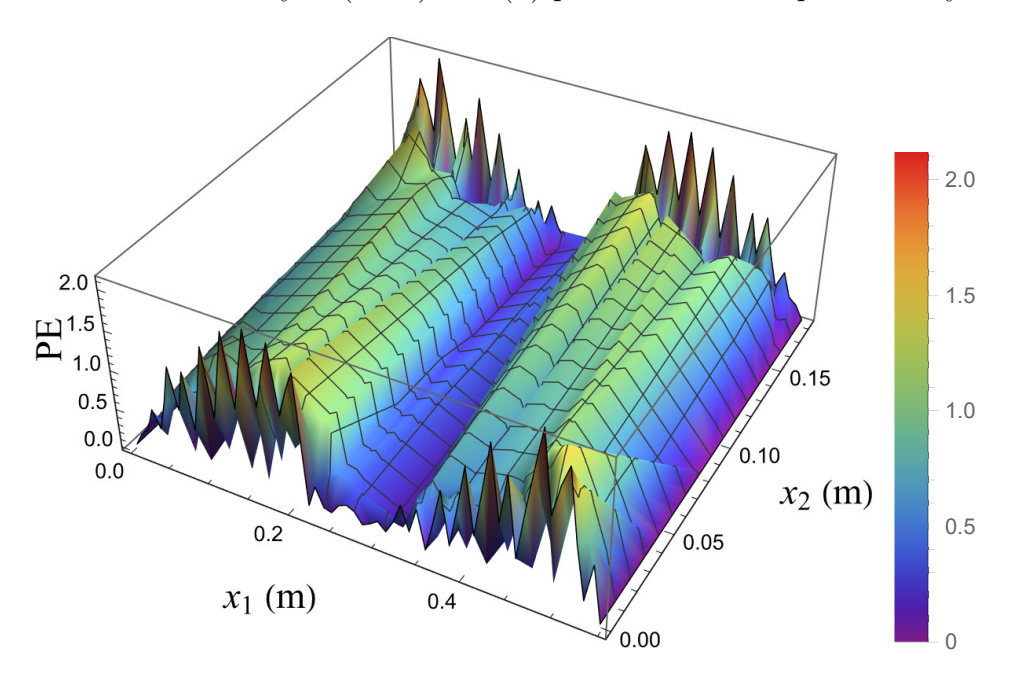


Figure 3.11: Percentage error in the out of plane deflection u_3 obtained using 3D FEA and present approach under uniform Pressure of $P = 400 \text{N/m}^2$ applied at the top face

The lay-up sequence for the laminate in Example-1, Example-3 and Example-5 are $[-14.80^{\circ}/75.20^{\circ}/-75.20^{\circ}/14.80^{\circ}/-22.87^{\circ}/67.13^{\circ}]_S$, $[0^{\circ}/90^{\circ}/0^{\circ}/90^{\circ}]_S$, $[45^{\circ}/-45^{\circ}]_S$ respectively. The first example has a hygrothermally stable lay-up sequence [44]. The lay-up sequence for Example-2 and Example-4 is $[0^{\circ}/90^{\circ}]_S$. The SCFs corresponding to the all numerical examples are calculated following the present approach. These SCFs are listed

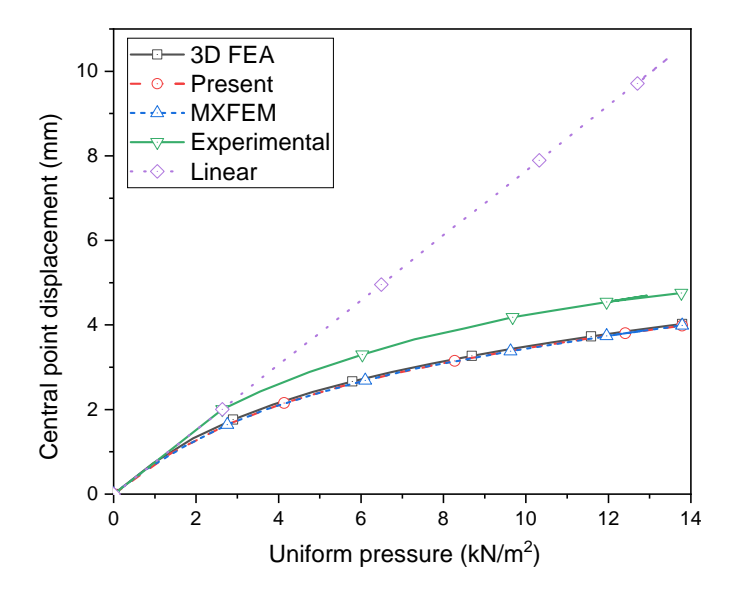


Figure 3.12: Load-deflection curves for the central point of the plate considered in Example-2 under uniform Pressure P applied at its top face

in Table 3.2.

For Example-1, the transverse displacement (u_3) of the plate midpoint $\left(x_1 = \frac{a}{2}, x_2 = \frac{b}{2}\right)$ for different values of constant pressures P is calculated [61] utilizing the present approach, and 3D FEA. Fig. 3.9 shows that the transverse displacement computed by the proposed plate model is in excellent agreement with the 3D FEA. In this work, the 3D finite element analysis was performed using the Abaqus software. The element type chosen for the analysis was C3D20R, which corresponds to a 20-node quadratic brick element with reduced integration. A thorough convergence study was carried out to ensure the accuracy and reliability of the obtained results. This study involved systematically refining the mesh and monitoring the convergence behavior of relevant quantities such as displacements, strains, and stresses. Nevertheless, for brevity, the convergence analysis is omitted from this presentation. Analytical solutions were obtained using numerical methods or state-of-the-space methods (such as the Navier or Levy solution) [119].

Figures 3.10 shows the variation of the displacement component u_3 with respect to x_1 and x_2 for Example-1 with a uniform pressure of $P = 400 \text{ N/m}^2$. Figure 3.10(a) was generated using the 3D FEA approach, while Figure 3.10(b) was produced using the present approach. Figure 3.11 illustrates the variation of the percentage error in the value

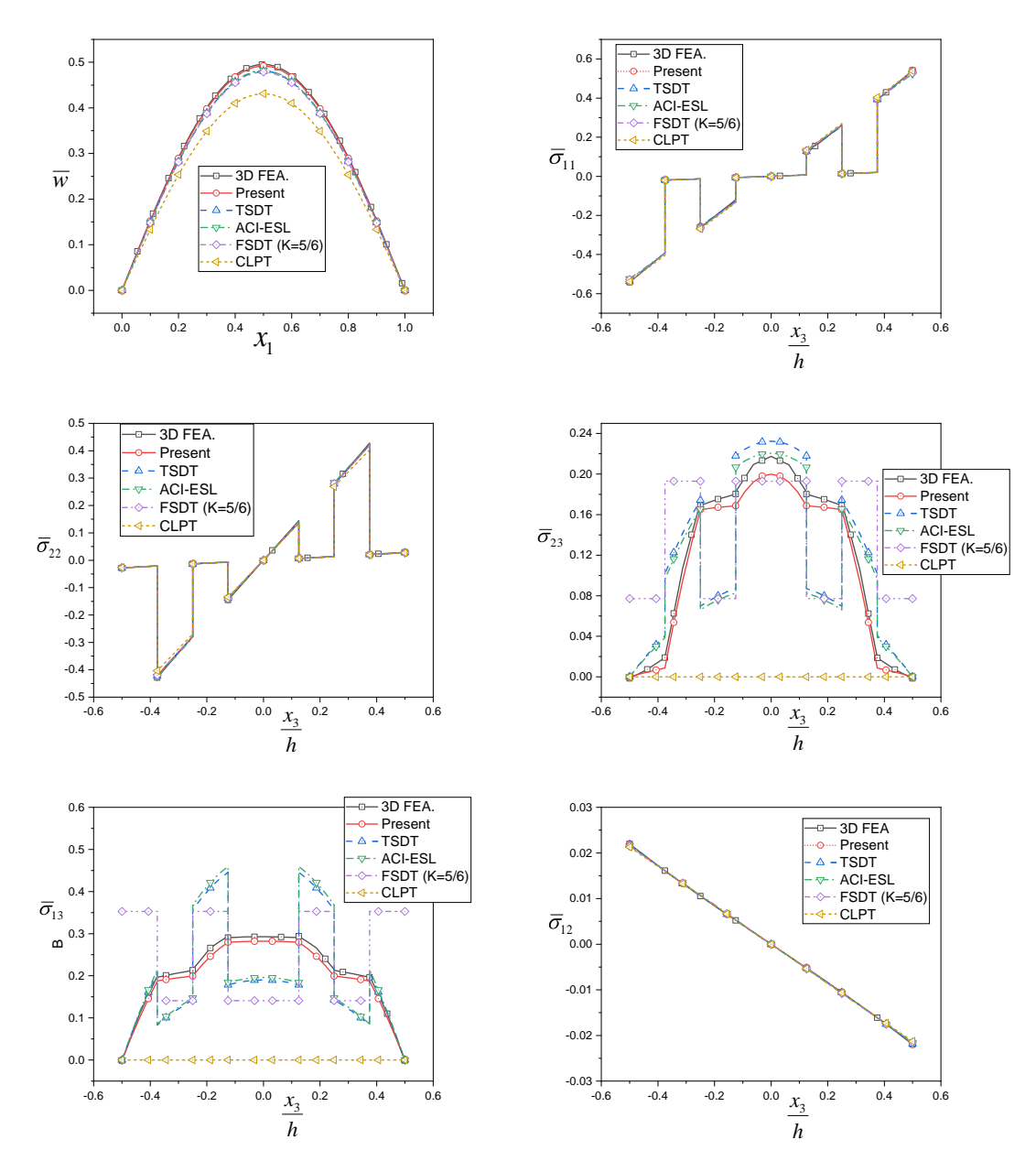


Figure 3.13: Variation of out of plane non-dimensionalized deflection \overline{w} along the centerline parallel to x_1 and non-dimensionalized stress components $\overline{\sigma}_{ij}$ along the thickness of the plate considered in Example-3

of u_3 with respect to x_1 and x_2 between the results obtained by the two approaches. The percentage error (PE) for Figure 3.11 is defined as follows

Table 3.4: Comparison of the dimensionless quantities (Max Value) computed in Example-4

$\frac{a}{h}$	Quant. (Max. Value)	3D FEA	3 <i>D</i> Elasticity [122]	Present	TSDT [122]	$ \begin{array}{c} \text{FSDT} \\ (K = \frac{5}{6}) \\ [122] \end{array} $
	\overline{w}	0.7469	0.743	0.7447	0.7147	0.6628
10	$\overline{\sigma}_{11}$	0.5652	0.559	0.4827	0.5456	0.4989
	$\overline{\sigma}_{22}$	0.4056	0.401	0.3988	0.3888	0.3615
	$\overline{\sigma}_{23}$	0.2124	0.196	0.1992	0.1531	0.1292
	$\overline{\sigma}_{13}$	0.3147	0.301	0.3082	0.2640	0.1667
	$\overline{\sigma}_{12}$	0.0235	0.0275	0.0253	0.0268	0.0241
	\overline{w}	0.5164	0.517	0.5138	0.5060	0.4912
20	$\overline{\sigma}_{11}$	0.5464	0.543	0.5222	0.5393	0.5273
	$\overline{\sigma}_{22}$	0.3113	0.308	0.3076	0.3043	0.2957
	$\overline{\sigma}_{23}$	0.1664	0.156	0.1562	0.1234	0.1087
	$\overline{\sigma}_{13}$	0.3384	0.328	0.3301	0.2825	0.1749
	$\overline{\sigma}_{12}$	0.0216	0.0230	0.0225	0.0228	0.0221
	\overline{w}	0.4354	0.4385	0.4346	0.4343	0.4337
100	$\overline{\sigma}_{11}$	0.5398	0.539	0.5380	0.5387	0.5382
	$\overline{\sigma}_{22}$	0.2711	0.276	0.2710	0.2708	0.2705
	$\overline{\sigma}_{23}$	0.1492	0.141	0.1382	0.1117	0.1009
	$\overline{\sigma}_{13}$	0.3492	0.337	0.3385	0.2897	0.1780
	$\overline{\sigma}_{12}$	0.0212	0.0216	0.0213	0.0213	0.0213

$$PE = 100 \left| \frac{u_{3,\text{FEA}} - u_{3,\text{Present}}}{u_{3,\text{FEA}}^{max}} \right|$$
 (3.53)

Where $u_{3,\text{FEA}}$ and $u_{3,\text{Present}}$ are values of u_3 obtained using the 3D FEA and the present approaches. $u_{3,\text{FEA}}^{max}$ is the maximum value of $u_{3,\text{FEA}}$. Figure 3.11 demonstrates that the results obtained by the 3D FEA and the present approach are in very good agreement.

To compare the results, following dimensionless quantities [116] are considered in Example-3, Example-4 and Example-5.

CHAPTER 3 3.7. CONCLUSION

$$\overline{w} = 100 \ u_3 \left(x_1, \frac{b}{2} \right) \frac{h^3 E_2}{q_0 b^4} \quad \overline{\sigma}_{23} = \sigma_{23} \left(\frac{a}{2}, 0, x_3 \right) \frac{h}{q_0 b}$$

$$\overline{\sigma}_{11} = \sigma_{11} \left(\frac{a}{2}, \frac{b}{2}, x_3 \right) \frac{h^2}{q_0 b^2} \quad \overline{\sigma}_{13} = \sigma_{13} \left(0, \frac{b}{2}, x_3 \right) \frac{h}{q_0 b}$$

$$\overline{\sigma}_{22} = \sigma_{22} \left(\frac{a}{2}, \frac{b}{2}, x_3 \right) \frac{h^2}{q_0 b^2} \quad \overline{\sigma}_{12} = \sigma_{12} \left(0, 0, x_3 \right) \frac{h^2}{q_0 b^2}$$
(3.54)

Fig. 3.13 illustrates the variation of the dimensionless transverse displacement \overline{w} along the centerline parallel to the x_1 axis and the variation of the dimensionless stresses $(\overline{\sigma}_{11}, \overline{\sigma}_{22}, \overline{\sigma}_{23}, \overline{\sigma}_{13} \text{ and } \overline{\sigma}_{12})$ along the thickness direction of the plate considered in Example-3. The results were compared with those obtained using 3D FEA, TSDT [122], ACI-ESL [57], FSDT [119] and CLPT [119].

Table 3.4 presents a comparison of the maximum values of the dimensionless quantities in Example-4. The observations from the table indicate that as the $\frac{a}{h}$ ratio increases, the results converge towards the 3D FEA results. This trend is a consequence of the fact that the ordering of the strains has been carried out considering the smallness of the ratio $\frac{h}{a}$. The results of the present approach aligns well with results from 3D FEA and 3D elasticity. Notably, a significant improvement in the displacement field and transverse shear stresses is observed compared to the TSDT and FSDT plate theories.

Fig. 3.14 shows the variation of \overline{w} along the center-line parallel to x_1 axis, It also presents the variation of $\overline{\sigma}11$, $\overline{\sigma}22$, $\overline{\sigma}23$, $\overline{\sigma}13$ and $\overline{\sigma}_{12}$ along the thickness in Example-4. Notably, these quantities are calculates for pint B having in-plane coordinates $(\frac{a}{4}, \frac{b}{4})$ as shown in Fig. 3.7 insted of the locations defined in Eq. (3.54). The results obtained using the present approach are compared with 3D FEA.

3.7 Conclusion

In this chapter, a computationally efficient framework is presented to analyze multilayered symmetric composite plates. This framework makes the FSDT plate theory isoenergetic to the asymptotically correct plate theory by finding suitable SCFs. the isoenergetic FSDT plate theory is used to find the 2D displacement components. The through the thickness variation of the displacement field, strains and stresses is recovered by substituting these 2D variables in the asymptotically correct displacement, strains and stresses. Following are key highlights of the present work

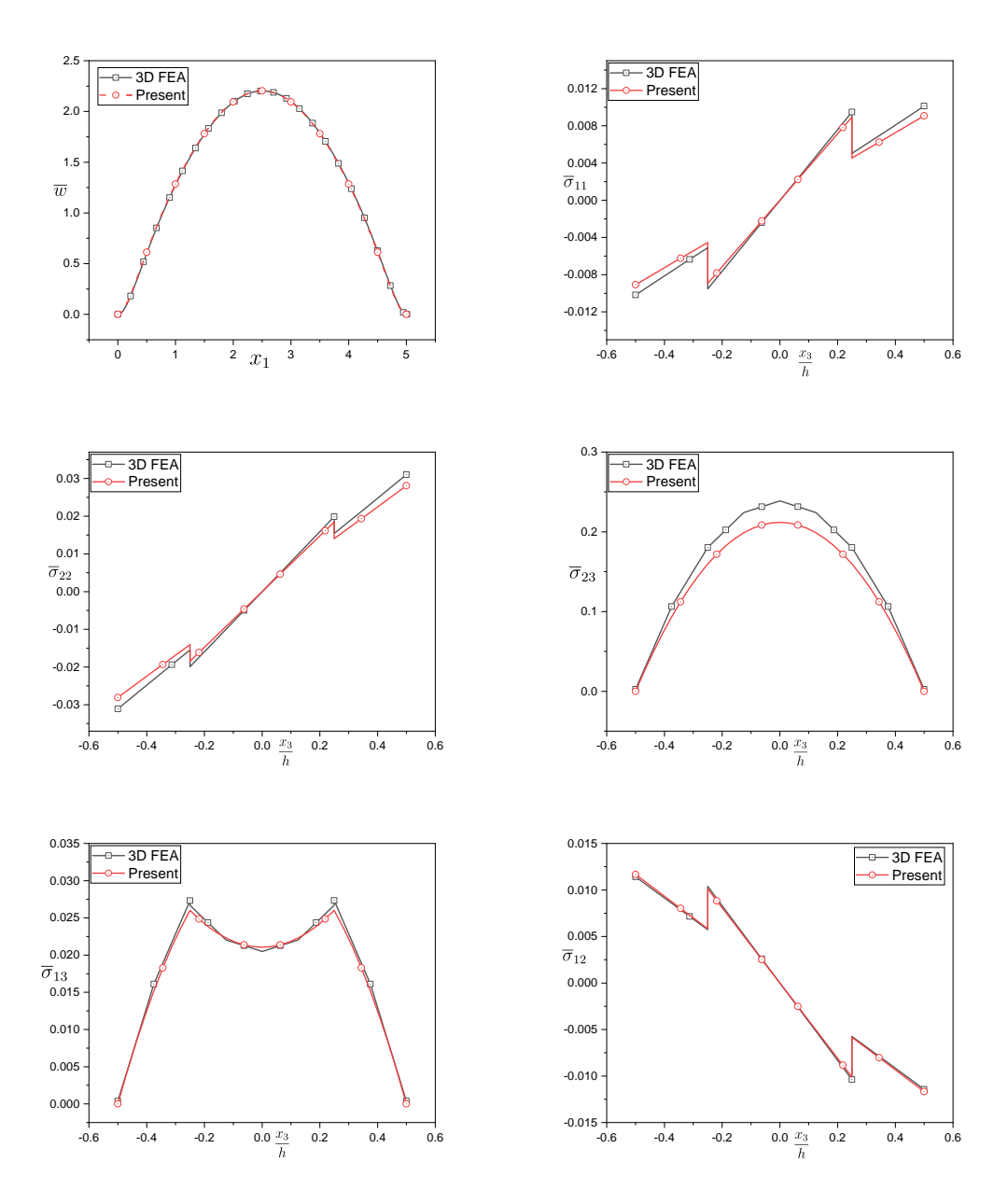


Figure 3.14: Variation of out of plane non-dimensionalized deflection \overline{w} along the centerline parallel to x_1 and non-dimensionalized stress components $\overline{\sigma}_{ij}$ along the thickness of the plate considered in Example-5

- 1. The utilization of isoenergetic FSDT plate theory in this work results in a low computational cost similar to FSDT plate theory.
- 2. The dimensional reduction using VAM is based on first principles, avoiding reliance

- on pre-assumed kinematics of the plate and assumptions regarding the order of different quantities of interest.
- 3. The zeroth order solution yields the estimation of the 3D displacement field in terms of 2D variables $u_i(x_1, x_2)$, leading to the dimensional reduction of the 3D problem to 2D, which is traditionally assumed in classical plate theories.
- 4. The reference plane of the plate emerges naturally as a consequence of the systematic approach adopted in this work, and its position is determined on logical grounds rather than being set *a priori*.
- 5. A mathematically sound ordering scheme is employed, utilizing the plate's geometry and a bound on the maximum value of the strains to determine the orders of different quantities of interest. The final order of these quantities matches exactly with those found in the literature, demonstrating the robustness of the ordering scheme.
- 6. The higher order 1D through the thickness analysis involves derivatives of $u_i(x_1, x_2)$ w.r.t x_{α} . The complexity involving these derivatives is eliminated through a novel isoenegetic approach resulting in better estimation of the overall deformation.
- 7. The plane stress condition emerges naturally from the mathematical procedure adopted in this formulation, rather than being an *ad hoc* assumption as in many other plate theories.
- 8. Numerical examples demonstrate the asymptotic correctness of the present work, with improved results observed as the small parameter $(\frac{h}{l})$ decreases. Satisfactory performance is achieved for thin and moderately thick plates.
- 9. The present framework outperforms FSDT and higher-order (TSDT) ESL plate theories, particularly in the displacement field and transverse shear strains and stresses.

In summary, this work presents a more refined, accurate, and computationally efficient framework for analyzing thin and moderately thick plate structures. Comparison with established theories such as CLPT, FSDT, R-TSDT, and 3D FEA demonstrates the accuracy of the proposed approach.

Chapter 4

Analysis of Functionally Graded Plates Using Novel Isoenergetic Formulation

4.1 Introduction

Functionally Graded Materials (FGMs), inspired by the structure of bamboo, represent a cutting-edge advancement. Composed of two or more materials with a gradual compositional change in desired direction [20], FGMs were pioneered by Japanese scientists for rocket nozzle applications to withstand extreme thermal and mechanical loads [19]. Looking at the exceptional results/properties offered by these materials, they are now widely employed in many applications such as in artificial hip joints, in transducers for filtering out the noise, piezoelectric, aircraft structures, biomedical devices, dental implant, various kind of sensors etc. [82, 18, 17]

This chapter presents an asymptotically correct isoenergetic formulation for the functionally graded plates. Some of the literature studies on analytical approaches for studying FGM plate-type structures are as follows: Kumar et al. [13] conducted a study on the bending behavior of FGM plates. In this work a higher order shear displacement model approach has been adopted where the displacement variables are assumed as a series solution. For finding out the solution use of Navier's empirical equations has been made. However, no analytical expressions have been provided in the study and just the results are plotted. It is suspected that the solutions obtained might be quite complex which can not be represented in mathematical expression form. Nguyen et al. [12] proposed a first-order shear deformation model for the FGM plates using the stress based formula-

tion. For obtaining correct results, use of Shear Correction Factor (SCF) has been made which is calculated using the shear deformation energy. Numerical results for deflection and stresses have been presented in tabular and graphical form without any evidence to the mathematical expressions for the results. The approach has ad-hoc assumptions associated to it and also the calculations involved are quite combersome. Singha et al. [11] conducted a non linear finite element analysis of functionally graded plates under transverse loads. The material properties are assumed to follow a power law variation along the thickness of the plate. Use of FSDT theory has been made to formulate the problem. The position of neutral plane of the plate is found out by using the literature results. Since, they are finite element based results thus don't give sufficient insight into the mechanics of the problem and also involves ad-hoc assumtions. Le [124] presented first order shear deformation theory for functionally graded plates. A linear strain tensor has been used which restricts the effects of geometric non-linearity to be included in the analysis. Also, the mid-plane is selected as the reference plane without any justification. The use of VAM technique leads to complicated expressions. Silvia et al. [10] presented a finite element based displacement calculus of functionally graded plate. The analysis has been done by assuming homogeneous layers which limit the scope of the formulation. Vidal et al. [9] analyzed FGM plates using a variable seperation method. A computationally intensive layer-wise approach has been used. The displacement field has been approximated as a sum of seperated functions of in-plane coordinate and out of plane/transverse coordinate. The fourth order expansion for transverse coordinate leads to correct solutions for the problem while the in-plane coordinates have been solved using FEA approach. The computational cost for this fourth order expansion is not in par with the improvement in the results.

From the literature above, it is clear that all the models have certain assumptions associated to them or the solutions provided are quite cumbersome which require higher computational cost. Thus, a simpler and assumptions free analysis with lesser computational cost is still required. Further, It has also been observed that the displacement based formulation offers a simpler analysis which makes this approach a wise choice to use. In this work we proceed with the reduced order model formulation by adopting displacement based formulation. To make this formulation more robust and fundamental we have adopted Variational Asymptotic Method (VAM) [107] where the 3D problem is split up into a 1D through the thickness analysis and 2D cross-sectional analysis with the help of small parameters inherent to the problem. This small parameter assists in systematic

derivation and asymptotic expansion of the strain energy for a refined solution. To obtain the solution, use of first principle has been made. Further, as already highlighted about the limitation of various reduced order models regarding higher order derivatives, this issue has been resolved by the use of novel isoenergetic principle where the strain energy of this model is equated to the strain energy of the FSDT model thus resulting in the considerable savings of computational cost without compromising on the accuracy of the solution [57]. The obtained results have been verified with the help of 3D FEA results and few prominent literature results. A good agreement with a considerable savings in computational cost justifies the requirement of the presented formulation. Since this approach is asymptotically correct and use the novel concept of isoenergetic so we name it as Asymptotically Correct Isoenergetic Formulation (ACIF). The detailed derivation and verfication of the proposed ACIF is presented in the next section.

4.2 Analytical Formulation

An FGM plate with length a, width b, and thickness h, has been shown in Fig. 4.1. A right handed orthogonal cartesian coordinate system x_i with unit vectors \hat{e}_i has been adopted, where, x_3 -axis is oriented along the thickness of the plate while x_1, x_2 represents the in-plane coordinates. The reference plane is taken at a distance η from the mid-plane of the plate as shown in Fig 4.1(b). For a plate-like structure, usually, the thickness h is much smaller than the other two dimensions i.e. a and b. Thus, exploiting this feature to define a and b to be of the order l, so the ratio $\frac{h}{l}$ becomes a small parameter i.e. $\frac{h}{l} < 1$. For making the analysis simpler, the interior region of the plate has been denoted by Ω while the boundary which comprises of the top surface is denoted by $\partial\Omega_{\text{top}}$, the bottom surface boundary is denoted by $\partial\Omega_{\rm bot}$ and the side surfaces are denoted by $\partial\Omega_{\rm side}$ with $\partial\Omega_{\rm tb} = \partial\Omega_{\rm top} \cup \partial\Omega_{\rm bot}$. Now, the position vector of an arbitrary point P in this domain can be represented by $\vec{x} = x_i \hat{e}_i$. It is to be noted that the Roman indices (i, j, k, ...)range from 1 to 3, while Greek indices $(\alpha, \beta, \gamma, ...)$ range from 1 to 2 unless their values are specified. Now, after deformation the point P shifts to a new location represented by P'. The displacement vector for this shift is given by $\vec{v} = v_i \hat{e}_i$. For the present study, we consider Green-St. Venant strain tensor [128, 127, 119, 139] which accounts for deformation having small strains and moderate rotations

$$\underline{\underline{E}} = \frac{1}{2} \left[\left(\vec{\nabla}_x \vec{v} \right) + \left(\vec{\nabla}_x \vec{v} \right)^T + \left(\vec{\nabla}_x \vec{v} \right)^T \left(\vec{\nabla}_x \vec{v} \right) \right] \tag{4.1}$$

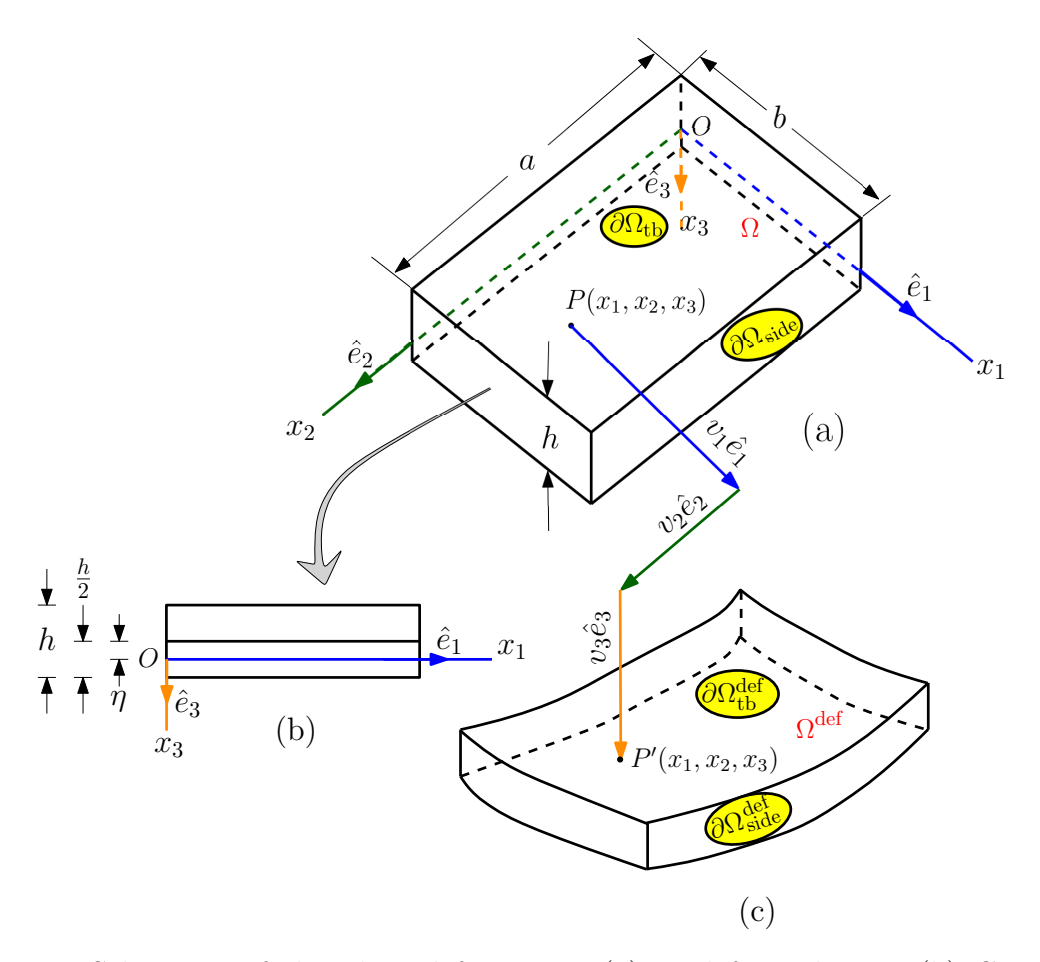


Figure 4.1: Schematic of the plate deformation (a) Undeformed state (b) Coordinate system (c) Deformed state

Using the information discussed up to now, we formulate the problem in the subsequent sections, where a novel strategy for developing a reduced order plate theory has been presented. This analytical development is categorized into three parts: Part A presents the development a Classical Laminated Plate Theory (CLPT) type theory, Part B discusses the refinement in the model presented in Part A considering the contribution of higher-order energy, and Part C presents a novel iso-energetic concept that eliminates higher-order derivatives and thus reduces the computational cost without compromising the accuracy of the approach.

4.3 Part A: CLPT-type plate theory

For efficient and accurate modeling, the use of small parameter has been made along with imposing a limit on the maximum value of strain. Various quantities that are of interest in the present analysis are ordered using this small parameter. The detailed discussion on this ordering is as follows:

4.3.1 Ordering Scheme

The idea of ordering comes from the work of Hodges et al. [112], Using this idea the relation between the orders of v_i and its derivatives with respect to x_j can be written as

$$O\left(\frac{\partial^t}{\partial x_1^t} \frac{\partial^s}{\partial x_2^s} \frac{\partial^r}{\partial x_3^r} v_i\right) \sim \left(\frac{1}{l}\right)^{(s+t)} \left(\frac{1}{h}\right)^r O(v_i)$$

$$r, s, t = 0, 1, 2, 3, \dots$$

$$(4.2)$$

It is to be noted that these derivatives follow the simple differential calculus laws where $O\left(\frac{\partial^0}{\partial x_i^0} v_i\right) = O(v_i)$. The supnorm (supremum norm) of strains $(||\underline{\underline{E}}||_{\infty})$ is defined below

$$||\underline{\underline{E}}||_{\infty} = \max_{1 \le i,j \le 3} \max_{x \in \Omega} |E_{ij}|$$
 (4.3)

The maximum value of $\frac{h}{l}$ and the support is bounded by ξ and ε respectively as shown below mathematically

$$\frac{h}{l} \le \xi \tag{4.4}$$

$$||\underline{E}||_{\infty} \le \varepsilon$$

Now, as per the small deformation and moderate rotations discussed in the analytical development section, we consider bound on the supnorm of strains to be a very small parameter i.e. $\varepsilon \ll 1$. For a plate-like structure bound on the maximum value of $\frac{h}{l}$ is small i.e. $\xi < 1$. For the asymptotic expansion of the stains and strain energy, it is assumed that $\varepsilon = \xi^3$. The bound on the maximum value of the strains and $\frac{h}{l}$ with the ordering scheme given in Eq. (4.2) results in a unique estimation of the order of different quantities of interest which will be evident in the coming sections.

4.3.2 Constitutive Relations and Strain Energy

Second Piola-Kirchhoff stress tensor is given by $\sigma = \{\sigma_{11}, \sigma_{22}, \sigma_{33}, \tau_{23}, \tau_{13}, \tau_{12}\}^T$ and the constitutive relation is given by

$$\sigma = CE, \tag{4.5}$$

where C represents the stiffness matrix and $E = \{E_{11}, E_{22}, E_{33}, 2E_{23}, 2E_{13}, 2E_{12}\}^T$. For FGM plates with material gradation in x_3 direction, the stiffness matrix takes the following form [82]

$$C = \frac{Y}{(1+\nu)(1-2\nu)} \begin{bmatrix} (1-\nu) & \nu & \nu & 0 & 0 & 0 \\ \nu & (1-\nu) & \nu & 0 & 0 & 0 \\ \nu & \nu & (1-\nu) & 0 & 0 & 0 \\ 0 & 0 & 0 & \frac{1}{2}(1-2\nu) & 0 & 0 \\ 0 & 0 & 0 & 0 & \frac{1}{2}(1-2\nu) & 0 \\ 0 & 0 & 0 & 0 & 0 & \frac{1}{2}(1-2\nu) \end{bmatrix}$$

$$(4.6)$$

Where $Y = Y(x_3)$ is youngs modulus of elasticity which changes in the thickness direction following different material gradation laws (viz. exponential, power law and reciprocal gradation) and ν is Poisson's ratio. The order of Y is taken μ . The strain energy density is given by

$$U = \frac{1}{2}\sigma^T E \tag{4.7}$$

4.3.3 Dimensional Reduction

For this, let us start with the application of the principle of virtual work

$$\int_{\Omega} \delta U dV - \int_{\partial \Omega_{\text{th}}} \vec{q} \cdot \delta \vec{v} da_{\text{tb}} - \int_{\partial \Omega_{\text{side}}} \vec{t} \cdot \delta \vec{v} da_{\text{side}} = 0$$
(4.8)

where $\vec{q} = q \ \hat{e}_3$ and $\vec{t} = t_i \ \hat{e}_i$ are traction vectors on $\partial \Omega_{\rm tb}$ and $\partial \Omega_{\rm side}$ respectively. It has been observed that the use of Eq. (4.8) results in a computationally intensive 3D elasticity problem. Thus, to save the cost a lot of literature work uses the concept where 3D problem is reduced into 2D, and then the energy is calculated, but this reduction involves $ad\ hoc$ and $a\ priori$ assumptions, which may not fully account for deformation energy considerations. In the present work we consider the energy aspects of the problem to develop a reduced order plate model. The dimensional reduction process is divided into different order solutions. The details of each order solution are presented in the subsequent sections.

4.3.4 Zeroth Order Solutions (ZOS)

Here the order of displacement field is assumed to be 0 so that $v_i = v_i^0$. The discussion regarding the ordering scheme has been done in section 3.1. Using this scheme the estimated order of $v_i^0(x_1, x_2, x_3)$ is determined to be $O(\xi^3 h)$. Now using this order estimation,

the order of the different strain components is evaluated which is shown as

$$E_{11} = O(\xi^{4}) \qquad 2E_{23} = \underbrace{\frac{\partial v_{2}^{0}}{\partial x_{3}}}_{O(\xi^{3})} + O(\xi^{4})$$

$$E_{22} = O(\xi^{4}) \qquad 2E_{13} = \underbrace{\frac{\partial v_{1}^{0}}{\partial x_{3}}}_{O(\xi^{3})} + O(\xi^{4})$$

$$E_{33} = \underbrace{\frac{\partial v_{3}^{0}}{\partial x_{3}}}_{O(\xi^{3})} \qquad 2E_{12} = O(\xi^{4})$$

$$(4.9)$$

It is to be noted that the quantities with under-braces represents the orders. Further, it is important to highlight that the order of v_i^0 here, corresponds to the maximum permissible value that ensures the strains remain bounded by $\varepsilon = \xi^3$. The order of v_i in this section is unique in itself, as altering the order of v_i^0 would lead to a change in the upper bound of the strains, which is not allowable. This ordering of strains yields an ordered representation of U in terms of the small parameters ξ as illustrated below.

$$U = \underbrace{U_{\text{sig}}}_{O(\xi^6 \mu)} + O\left(\xi^7 \mu\right)$$

$$U_{\text{sig}} = \frac{Y}{4(1+\nu)} \left[\left(\frac{\partial v_1^0}{\partial x_3}\right)^2 + \left(\frac{\partial v_2^0}{\partial x_3}\right)^2 + \frac{2(1-\nu)}{(1-2\nu)} \left(\frac{\partial v_3^0}{\partial x_3}\right)^2 \right]$$

$$(4.10)$$

As per the ordering, term, U_{sig} , will have the highest contribution to the energy functional. Therefore, for zeroth order contribution only this energy becomes important [137]. This reduces the virtual work Eq. (4.8) to the following form

$$\int_{\partial\Omega_{\text{ref}}} \left[\int_{x_3} \delta U_{\text{sig}} dx_3 \right] da_{\text{ref}} - \int_{\partial\Omega_{\text{tb}}} \vec{q} \cdot \delta \vec{v} da_{\text{tb}}
- \int_{\partial\Omega_{\text{side}}} \vec{t} \cdot \delta \vec{v} da_{\text{side}} = 0$$
(4.11)

where $\partial\Omega_{\rm ref}$ is the reference plane of the plate. For functionally graded materials, neutral plane do not coincide with the geometrical central plane of the plate thus, x_1, x_2 plane which is η distance away from the geometrical central plane, is taken as its reference plane. It is worth noting that the Eq. (4.10) contains terms having derivatives of v_i^0 with respect to x_3 only. Thus, the minimization problem can be split into two stages: (i) a 1D

through the thickness analysis along x_3 only, and (ii) a 2D analysis in the x_1, x_2 plane, as expressed below

$$\frac{\delta \Pi_{x_3} = 0}{1D \text{ Analysis}} \qquad \underbrace{\delta \Pi = 0}_{2D \text{ Analysis}}$$

$$\Pi_{x_3} = \int_{x_3} U_{\text{sig}} dx_3 \qquad (4.12)$$

$$\Pi = \int_{\partial \Omega_{\text{ref}}} \Pi_{x_3} da_{\text{ref}} - \int_{\partial \Omega_{\text{tb}}} \vec{q} \cdot \vec{v} da_{\text{tb}} - \int_{\partial \Omega_{\text{side}}} \vec{t} \cdot \vec{v} da_{\text{side}}$$

It can be observed that the dimensional reduction of the problem is a natural outcome of this strategy.

Through the Thickness 1D Analysis

Extremization of Π_{x_3} yields following Euler Lagrange governing equations

$$\frac{\partial Y}{\partial x_3} \frac{\partial v_1^0}{\partial x_3} + Y \frac{\partial^2 v_1^0}{\partial x_3^2} = 0$$

$$\frac{\partial Y}{\partial x_3} \frac{\partial v_2^0}{\partial x_3} + Y \frac{\partial^2 v_2^0}{\partial x_3^2} = 0$$

$$\frac{\partial Y}{\partial x_3} \frac{\partial v_3^0}{\partial x_3} + Y \frac{\partial^2 v_3^0}{\partial x_3^2} = 0$$

$$(4.13)$$

and following associated boundary conditions

$$\mathcal{B}_{v_1^0} \Big|_{x_3 = -(h/2) - \eta} = \mathcal{B}_{v_1^0} \Big|_{x_3 = (h/2) - \eta} = 0$$

$$\mathcal{B}_{v_2^0} \Big|_{x_3 = -(h/2) - \eta} = \mathcal{B}_{v_2^0} \Big|_{x_3 = (h/2) - \eta} = 0$$

$$\mathcal{B}_{v_3^0} \Big|_{x_3 = -(h/2) - \eta} = \mathcal{B}_{v_3^0} \Big|_{x_3 = (h/2) - \eta} = 0$$

$$\mathcal{B}_{v_1^0} = \frac{Y}{2(1 + \nu)} \frac{\partial v_1^0}{\partial x_3}$$

$$\mathcal{B}_{v_2^0} = \frac{Y}{2(1 + \nu)} \frac{\partial v_2^0}{\partial x_3}$$

$$\mathcal{B}_{v_3^0} = \frac{Y(1 - \nu)}{(1 - 2\nu)(1 + \nu)} \frac{\partial v_3^0}{\partial x_3}$$
(4.14)

solving Eq. (4.13) with the boundary conditions Eq. (4.14) results in following solution

$$v_i^0 = u_i(x_1, x_2) (4.15)$$

It can be observed that the zeroth-order solution manifest the 3D displacement components v_i , in terms of u_i . Here, u_i are functions of only the in-plane coordinates x_1 and

 x_2 , making them 2D variables which means, at this stage the displacements are constant along the thickness of the plate. Further, refinement in the solutions will be carried out in the higher order solutions. For convenience, these 2D variables, u_i , are chosen to represent the in-plane displacements of the reference plane (the x_1 - x_2 plane) of the plate. This is achieved through the following equation.

$$u_i = v_i \Big|_{x_2 = 0}$$
 (4.16)

4.3.5 First Order Solution (FOS)

The solution obtained in zeroth-order is perturbed to obtain first order solution¹.

$$v_i = v_i^0 + v_i^1 = u_i + v_i^1 (4.17)$$

It is important to note that the term v_i^1 in Eq. (4.17) leads to three additional degrees of freedom to the displacement field. Thus, to remove this redundancy and to ensure the uniqueness of the solution, three constraints are essential. These constraints are

$$v_i^n \Big|_{x_2=0} = 0 (4.18)$$

Now using the procedure described in Section 4.3.1, the order of quantities u_i and v_i^1 is found to be $O(\xi^3 l)$ and $O(\xi^3 h)$, respectively. One may note that the order of the perturbation variables v_i^0 and v_i^1 is the same, which essentially contradict the usual refinement procedure done through perturbations. However, the analysis starts with a conservative order of v_i , treating the plate as a 3D body and considering the maximum possible variation in v_i for all possible deformation modes with strains bounded by ε . As the refinement is carried out in the displacement field, the plate reveals its true deformation pattern, relaxing the bound on v_i . This relaxation necessitates further refinement in the displacement field in the same order, justifying it. Substituting v_i from Eq. (4.17) into Eq. (4.1) gives

¹Note that $v_i^n = v_i^n(x_1, x_2, x_3)$, termed as n^{th} order perturbation variable, will consistently be used in the upcoming work to improve the displacement field in the n^{th} order solution

the following strains, along with their respective orders indicated in underbraces

$$E_{11} = \underbrace{\frac{\partial u_1}{\partial x_1}}_{O(\xi^3)} + O(\xi^4) \qquad 2E_{23} = \underbrace{\frac{\partial u_3}{\partial x_2} + \frac{\partial v_2^1}{\partial x_3}}_{O(\xi^3)} + O(\xi^4)$$

$$E_{22} = \underbrace{\frac{\partial u_2}{\partial x_2}}_{O(\xi^3)} + O(\xi^4) \qquad 2E_{13} = \underbrace{\frac{\partial u_3}{\partial x_1} + \frac{\partial v_1^1}{\partial x_3}}_{O(\xi^3)} + O(\xi^4)$$

$$E_{33} = \underbrace{\frac{\partial v_3^1}{\partial x_3}}_{O(\xi^3)} + O(\xi^4) \qquad 2E_{12} = \underbrace{\frac{\partial u_1}{\partial x_2} + \frac{\partial u_2}{\partial x_1}}_{O(\xi^3)} + O(\xi^4)$$

$$(4.19)$$

Using these strains Eq. (4.19) strain energy terms U and U_{sig} are recalculated. Just like the Zeroth order solution, the perturbation variables v_i^1 in U_{sig} contain derivatives with respect to x_3 only thus allowing us to perform the 3D analysis in two stages (1D and 2D analyses).

Through the Thickness 1D Analysis

The functional Π_{x_3} is calculated agarin to accommodate the changes in U_{sig} . Extremizing Π_{x_3} yields the following Euler Lagrange equations

$$\frac{\partial Y}{\partial x_3} \left(\frac{\partial u_3}{\partial x_1} + \frac{\partial v_1^1}{\partial x_3} \right) + Y \left(\frac{\partial^2 v_1^1}{\partial x_3^2} \right) = 0$$

$$\frac{\partial Y}{\partial x_3} \left(\frac{\partial u_3}{\partial x_2} + \frac{\partial v_2^1}{\partial x_3} \right) + Y \left(\frac{\partial^2 v_2^1}{\partial x_3^2} \right) = 0$$

$$\nu \frac{\partial Y}{\partial x_3} \frac{\partial u_2}{\partial x_2} + \nu \frac{\partial Y}{\partial x_3} \frac{\partial u_1}{\partial x_1} + (1 - \nu) \frac{\partial Y}{\partial x_3} \frac{\partial v_3^1}{\partial x_3} + (1 - \nu) Y \frac{\partial^2 v_3^1}{\partial x_3^2} = 0$$

$$(4.20)$$

and associated boundary conditions

$$\begin{aligned}
&\mathcal{B}_{v_{1}^{1}}\big|_{x_{3}=-(h/2)-\eta} = \mathcal{B}_{v_{1}^{1}}\big|_{x_{3}=(h/2)-\eta} = 0 \\
&\mathcal{B}_{v_{2}^{1}}\big|_{x_{3}=-(h/2)-\eta} = \mathcal{B}_{v_{2}^{1}}\big|_{x_{3}=(h/2)-\eta} = 0 \\
&\mathcal{B}_{v_{3}^{1}}\big|_{x_{3}=-(h/2)-\eta} = \mathcal{B}_{v_{3}^{1}}\big|_{x_{3}=(h/2)-\eta} = 0 \\
&\mathcal{B}_{v_{1}^{1}} = \frac{Y}{2(1+\nu)} \left(\frac{\partial u_{3}}{\partial x_{1}} + \frac{\partial v_{1}^{1}}{\partial x_{3}}\right) \\
&\mathcal{B}_{v_{2}^{1}} = \frac{Y}{2(1+\nu)} \left(\frac{\partial u_{3}}{\partial x_{2}} + \frac{\partial v_{2}^{1}}{\partial x_{3}}\right) \\
&\mathcal{B}_{v_{3}^{1}} = \frac{\nu Y}{(1-2\nu)(1+\nu)} \left(\frac{\partial u_{1}}{\partial x_{1}} + \frac{\partial u_{2}}{\partial x_{2}}\right) + \frac{Y(1-\nu)}{(1-2\nu)(1+\nu)} \frac{\partial v_{3}^{1}}{\partial x_{3}}
\end{aligned} \tag{4.21}$$

Solving the Euler Lagrange equations in Eq. (4.20) with the boundary conditions in Eq. (4.21) and the constraints given in Eq. (4.18) results in

$$v_1^1 = -x_3 \frac{\partial u_3}{\partial x_1}$$

$$v_2^1 = -x_3 \frac{\partial u_3}{\partial x_2}$$

$$v_3^1 = \frac{-x_3 \nu}{1 - \nu} \left(\frac{\partial u_1}{\partial x_1} + \frac{\partial u_2}{\partial x_2} \right)$$

$$(4.22)$$

4.3.6 Second Order Solution (SOS)

Further perturbation in the displacement field leads to

$$v_i = v_i^0 + v_i^1 + v_i^2$$

where

$$v_1 = u_1 - x_3 \frac{\partial u_3}{\partial x_1} + v_1^2, \qquad v_2 = u_2 - x_3 \frac{\partial u_3}{\partial x_2} + v_2^2,$$

$$v_3 = u_3 + x_3 f_1 + v_3^2$$
(4.23)

Using the similar procedure as explained earlier, the orders of u_{α} , u_{3} and v_{i}^{2} are estimated to be $O(\xi^{3}l)$, $O(\xi^{2}l)$ and $O(\xi^{3}h)$, respectively. Substituting v_{i} from Eq. (4.23) into Eq. (4.1) leads to

$$E_{11} = \underbrace{\frac{\partial u_1}{\partial x_1} - x_3 \frac{\partial^2 u_3}{\partial x_1^2}}_{O(\xi^3)} + O\left(\xi^4\right) \qquad 2E_{23} = \underbrace{\frac{\partial v_2^2}{\partial x_3}}_{O(\xi^3)} + O\left(\xi^4\right)$$

$$E_{22} = \underbrace{\frac{\partial u_2}{\partial x_2} - x_3 \frac{\partial^2 u_3}{\partial x_2^2}}_{O(\xi^3)} + O\left(\xi^4\right) \qquad 2E_{13} = \underbrace{\frac{\partial v_1^2}{\partial x_3}}_{O(\xi^3)} + O\left(\xi^4\right)$$

$$E_{33} = \underbrace{f_1 + \frac{\partial v_3^2}{\partial x_3}}_{O(\xi^3)} + O\left(\xi^4\right)$$

$$2E_{12} = \underbrace{\frac{\partial u_1}{\partial x_2} + \frac{\partial u_2}{\partial x_1} - 2x_3 \frac{\partial^2 u_3}{\partial x_1 \partial x_2}}_{O(\xi^3)} + O\left(\xi^4\right)$$

$$(4.24)$$

Using the strains from Eq. (4.24) the strain energy U and U_{sig} is calculated again. Similar observations are noted regarding the splitting of problem into two separate stages i.e. 1D and 2D analysis.

Through the Thickness 1D Analysis

Extremization of Π_{x_3} results in following Euler Lagrange equations

$$\frac{\partial Y}{\partial x_3} \frac{\partial v_1^2}{\partial x_3} + Y \frac{\partial^2 v_1^2}{\partial x_3^2} = 0$$

$$\frac{\partial Y}{\partial x_3} \frac{\partial v_2^2}{\partial x_3} + Y \frac{\partial^2 v_2^2}{\partial x_3^2} = 0$$

$$\nu Y \frac{\partial^2 u_3}{\partial x_1^2} - \nu \frac{\partial Y}{\partial x_3} \left(\frac{\partial u_1}{\partial x_1} - x_3 \frac{\partial^2 u_3}{\partial x_1^2} \right) + \nu Y \frac{\partial^2 u_3}{\partial x_2^2} - \nu \frac{\partial Y}{\partial x_3} \left(\frac{\partial u_2}{\partial x_2} - x_3 \frac{\partial^2 u_3}{\partial x_2^2} \right)$$

$$-(1 - \nu) \frac{\partial Y}{\partial x_3} \left(\frac{-\nu}{1 - \nu} \frac{\partial u_2}{\partial x_2} + \frac{-\nu}{1 - \nu} \frac{\partial u_1}{\partial x_1} + \frac{\partial v_3^2}{\partial x_3} \right) - (1 - \nu) Y \frac{\partial^2 v_3^2}{\partial x_3^2} = 0$$

$$(4.25)$$

and associated boundary conditions

$$\begin{aligned}
&\mathcal{B}_{v_1^2}\big|_{x_3=-(h/2)-\eta} = \mathcal{B}_{v_1^2}\big|_{x_3=(h/2)-\eta} = 0\\
&\mathcal{B}_{v_2^2}\big|_{x_3=-(h/2)-\eta} = \mathcal{B}_{v_2^2}\big|_{x_3=(h/2)-\eta} = 0\\
&\mathcal{B}_{v_3^2}\big|_{x_3=-(h/2)-\eta} = \mathcal{B}_{v_3^2}\big|_{x_3=(h/2)-\eta} = 0\\
&\mathcal{B}_{v_1^2} = \frac{Y}{2(1+\nu)} \frac{\partial v_1^2}{\partial x_3} \\
&\mathcal{B}_{v_2^2} = \frac{Y}{2(1+\nu)} \frac{\partial v_2^2}{\partial x_3} \\
&\mathcal{B}_{v_3^2} = \frac{-Y}{(1-2\nu)(1+\nu)} \left(x_3\nu \frac{\partial^2 u_3}{\partial x_1^2} + x_3\nu \frac{\partial^2 u_3}{\partial x_2^2} - (1-\nu)\frac{\partial v_3^2}{\partial x_3}\right)
\end{aligned} \tag{4.26}$$

Solution to these equations along with the constraints given in Eq. (4.18) leads to following solution

$$v_1^2 = 0$$

$$v_2^2 = 0$$

$$v_3^2 = \frac{x_3^2 \nu}{2(1 - \nu)} \left(\frac{\partial^2 u_3}{\partial x_1^2} + \frac{\partial^2 u_3}{\partial x_2^2} \right)$$
(4.27)

It is hereby emphasized that the solution obtained up to this stage i.e.second order solution gives a CLPT like plate theory, which was the objective of Part A of this work. Summary and key findings of the work done so fat is briefed in the following section

4.3.7 Summary of Part A

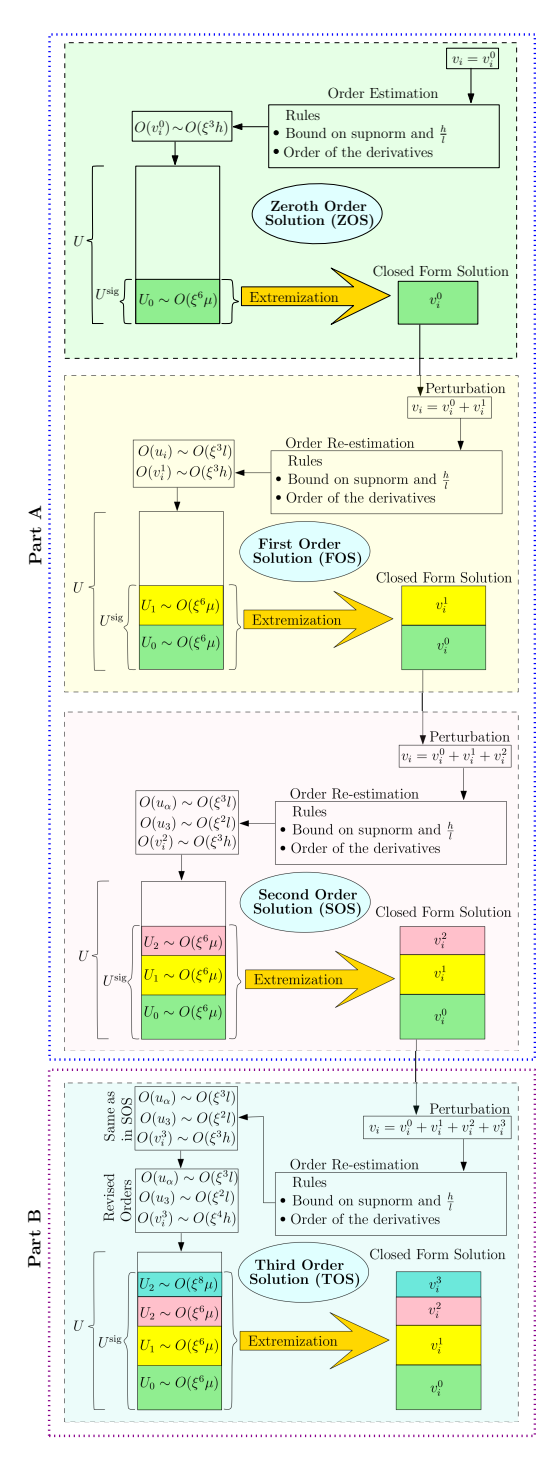


Figure 4.2: Systematic methodology adopted in deriving the reduced order model

A graphical representation of the adopted procedure is shown in Figure 4.2. The analysis starts with the calculation of strains where the plate is considered to be a 3D body. Then an order estimation scheme is adopted which based on the upper bound on the support and $\frac{h}{l}$ which is then followed by a rule to calculate the order of derivatives of displacement components given in Eq. (4.2). The zeroth order solution starts with order estimation for the quantities of interest which follows the ordering strategy described in Section 3.1. The result obtained is an ordered representation of the strain energy density U. The most significant portion of this strain energy density is separated and termed as U_{sig} . This U_{sig} is extremized to yield Euler-Lagrange equations and associated boundary conditions. The solutions to these equations results in a closed form solution. In the first and second order solutions, the entire procedure is repeated, by perturbing the solution obtained in the preceeding order i.e. zeroth order perturbation for first order solution and perturbation in first order for finding the second order solution.

4.3.8 Displcement Field of Part A

The displacement field derived in Part A of this work is shown as

$$v_{1} = \underbrace{u_{1} - x_{3} \frac{\partial u_{3}}{\partial x_{1}}}_{O(\xi^{3}l)}$$

$$v_{2} = \underbrace{u_{2} - x_{3} \frac{\partial u_{3}}{\partial x_{2}}}_{O(\xi^{3}l)}$$

$$v_{3} = \underbrace{u_{3}}_{O(\xi^{2}l)} - \underbrace{\frac{x_{3}\nu}{1 - \nu} \left(\frac{\partial u_{1}}{\partial x_{1}} + \frac{\partial u_{2}}{\partial x_{2}}\right) + \frac{x_{3}^{2}\nu}{2(1 - \nu)} \left(\frac{\partial^{2}u_{3}}{\partial x_{1}^{2}} + \frac{\partial^{2}u_{3}}{\partial x_{2}^{2}}\right)}_{O(\xi^{3}h)}$$

$$(4.28)$$

It can be observed that the displacement components v_1 and v_2 given in Eq. (4.28) are in line with the results of CLPT theory [100, 119, 130], thus validating the Kirchhoff's assumption that a line segment perpendicular to the reference plane in the undeformed configuration remains straight and perpendicular to the deformed reference plane after deformation. But the displacement component v_3 seems to contradict Kirchhoff's assumption that there is no change in the length of a transverse normal after deformation (i.e., the transverse normals are inextensible). Interestingly, the plane stress condition in CLPT makes it energetically equivalent to the asymptotically correct plate theory developed in Part A of this work the detailed discussion is followed in the next section.

4.3.9 Strains of Part A

Eq. (4.1) and (4.28) give the following strains corrected up to order ξ^3

$$E_{11} = \underbrace{\frac{\partial u_1}{\partial x_1} - x_3 \frac{\partial^2 u_3}{\partial x_1^2}}_{O(\xi^3)} \qquad E_{22} = \underbrace{\frac{\partial u_2}{\partial x_2} - x_3 \frac{\partial^2 u_3}{\partial x_2^2}}_{O(\xi^3)}$$

$$E_{33} = \underbrace{f_1 + 2x_3 g_1}_{O(\xi^3)} \qquad 2E_{23} = 0$$

$$2E_{13} = 0 \qquad 2E_{12} = \underbrace{\frac{\partial u_1}{\partial x_2} + \frac{\partial u_2}{\partial x_1} - 2x_3 \frac{\partial^2 u_3}{\partial x_1 \partial x_2}}_{O(\xi^3)}$$

$$(4.29)$$

Using strains from Eq. (4.29) in Eq. (4.5) leads to

$$\sigma_{33} = C_{13} E_{11} + C_{23} E_{22} + C_{33} E_{33} + 2 C_{36} E_{12} = 0$$

$$(4.30)$$

This justifies the plane stress condition which is valid up to the present level of accuracy. With $\sigma_{33} = 0$, the transverse normal strain E_{33} does not appear in the virtual work Eq. (4.8), although it is not identically zero. As a result, the transverse normal strain E_{33} is neglected. By omitting the transverse strain component, E_{33} , in Eq. (4.29), one can write

$$E_{ps} = \begin{cases} E_{11} \\ E_{22} \\ 2E_{23} \\ 2E_{13} \\ 2E_{12} \end{cases} = \begin{cases} \frac{\partial u_1}{\partial x_1} - x_3 \frac{\partial^2 u_3}{\partial x_1^2} \\ \frac{\partial u_2}{\partial x_2} - x_3 \frac{\partial^2 u_3}{\partial x_2^2} \\ 0 \\ 0 \\ \frac{\partial u_1}{\partial x_2} + \frac{\partial u_2}{\partial x_1} - 2x_3 \frac{\partial^2 u_3}{\partial x_1 \partial x_2} \end{cases}$$
(4.31)

It is worth noting that despite the discrepancy in the displacement field shown in Section 3.8, the asymptotically correct strains E_{ps} in Eq. (4.31) resemble the strains given by CLPT [100]. This indicates that the CLPT plate theory is energetically equivalent to the asymptotically correct plate theory derived considering strain energy up to order $(\xi^6 \mu)$ and neglecting its higher order part. The work done in Part A is further refined in Part B considering the contribution of the higher order Energy

4.4 Part B: Refinement of Part A

This section refines the plate theory by including higher-order energy terms which facilitate for a more comprehensive analysis by capturing the influence of material property variations through the thickness direction. Notably, Part A derives strains independent of such variations, while Part B extracts this information.

4.4.1 Third Order Solution (TOS)

Perturbing the displacement field obtained in second order solution as

$$v_i = v_i^0 + v_i^1 + v_i^2 + v_i^3$$

where

$$v_{1} = u_{1} - x_{3} \frac{\partial u_{3}}{\partial x_{1}} + v_{1}^{3}, \qquad v_{2} = u_{2} - x_{3} \frac{\partial u_{3}}{\partial x_{2}} + v_{2}^{3}$$

$$v_{3} = u_{3} - \frac{x_{3}\nu}{1 - \nu} \left(\frac{\partial u_{1}}{\partial x_{1}} + \frac{\partial u_{2}}{\partial x_{2}} \right) + \frac{x_{3}^{2}\nu}{2(1 - \nu)} \left(\frac{\partial^{2}u_{3}}{\partial x_{1}^{2}} + \frac{\partial^{2}u_{3}}{\partial x_{2}^{2}} \right) + v_{3}^{3}$$

$$(4.32)$$

Now using the procedure discussed in section 3.1, the orders of u_{α} , u_3 , and v_i^3 are estimated to be $O(\xi^3 l)$, $O(\xi^2 l)$, and $O(\xi^3 h)$, respectively which is identical to the second order

solution, So the extremization on these quantities will lead to $v_i^3 = 0$ meaning that the solution has no improvement. Thus we need to consider the contribution of higher-order strain energy at this stage. To account for the effect of higher order strain energy i.e. of the order of $(\xi^8 \mu)$, we set the order of v_i^3 to $O(\xi^4 h)$ while keeping the orders of the other variables unchanged. Substituting v_i from Eq. (4.32) into Eq. (4.1) yields

$$E_{11} = \frac{\partial u_1}{\partial x_1} - x_3 \frac{\partial^2 u_3}{\partial x_1^2} + \frac{1}{2} \left(\frac{\partial u_3}{\partial x_1} \right)^2 + \frac{\partial v_1^3}{\partial x_1} + O\left(\xi^6\right)$$

$$E_{22} = \frac{\partial u_2}{\partial x_2} - x_3 \frac{\partial^2 u_3}{\partial x_2^2} + \frac{1}{2} \left(\frac{\partial u_3}{\partial x_2} \right)^2 + \frac{\partial^2 v_2^3}{\partial x_2} + O\left(\xi^6\right)$$

$$E_{33} = \frac{-\nu}{1 - \nu} \left[\frac{\partial u_2}{\partial x_2} + \frac{\partial u_1}{\partial x_1} - x_3 \left(\frac{\partial^2 u_3}{\partial x_1^2} + \frac{\partial^2 u_3}{\partial x_2^2} \right) \right] + \frac{1}{2} \left(\frac{\partial u_3}{\partial x_1} \right)^2 + \frac{1}{2} \left(\frac{\partial u_3}{\partial x_2} \right)^2 + \frac{\partial v_3^3}{\partial x_3} + O\left(\xi^6\right)$$

$$2E_{23} = \frac{x_3 \nu}{2(1 - \nu)} \left[-2 \frac{\partial^2 u_2}{\partial x_2^2} - 2 \frac{\partial^2 u_1}{\partial x_1 \partial x_2} + x_3 \left(\frac{\partial^3 u_3}{\partial x_2^3} + \frac{\partial^3 u_3}{\partial x_1^2 \partial x_2} \right) \right] + \frac{\partial v_2^3}{\partial x_3}$$

$$+ \frac{\partial u_3}{\partial x_1} \left(-\frac{\partial u_1}{\partial x_2} + x_3 \frac{\partial u_3}{\partial x_1 \partial x_2} \right) - \frac{1}{1 - \nu} \frac{\partial u_3}{\partial x_2} \left[\nu \frac{\partial u_1}{\partial x_1} + \frac{\partial u_2}{\partial x_2} - x_3 \left(\nu \frac{\partial^2 u_3}{\partial x_1^2} + \frac{\partial^2 u_3}{\partial x_2^2} \right) \right] + \frac{\partial v_3^3}{\partial x_2} + O\left(\xi^6\right)$$

$$2E_{13} = \underbrace{\frac{x_3 \nu}{2(1 - \nu)} \left[-2 \frac{\partial^2 u_1}{\partial x_1^2} - 2 \frac{\partial^2 u_2}{\partial x_1 \partial x_2} + x_3 \left(\frac{\partial^3 u_3}{\partial x_1 \partial x_2} + \frac{\partial^3 u_3}{\partial x_1 \partial x_2^2} \right) \right] + \frac{\partial v_1^3}{\partial x_3}$$

$$+ \underbrace{\frac{\partial u_3}{\partial x_1} \left(-\frac{\partial u_2}{\partial x_1} + x_3 \frac{\partial u_3}{\partial x_1 \partial x_2} \right) - \frac{1}{1 - \nu} \frac{\partial u_3}{\partial x_1} \left[\nu \frac{\partial u_2}{\partial x_2} + \frac{\partial u_1}{\partial x_1} - x_3 \left(\nu \frac{\partial^2 u_3}{\partial x_1^2} + \frac{\partial^2 u_3}{\partial x_1^2} \right) \right] + \frac{\partial v_3^3}{\partial x_1}} + O\left(\xi^6\right)$$

$$2E_{12} = \underbrace{\frac{\partial u_1}{\partial x_2} + \frac{\partial u_2}{\partial x_1} - 2x_3 \frac{\partial^2 u_3}{\partial x_1 \partial x_2}} + \underbrace{\frac{\partial u_3}{\partial x_1 \partial x_2} \left(\frac{\partial u_3}{\partial x_1} \right) \left(\frac{\partial u_3}{\partial x_2} \right) + \frac{\partial u_2}{\partial x_2} + \frac{\partial u_3}{\partial x_1} \right) + \underbrace{\frac{\partial v_3^3}{\partial x_1^2 \partial x_2} + \frac{\partial v_3^3}{\partial x_1^2 \partial x_2}} + \underbrace{\frac{\partial v_3^3}{\partial x_1^2 \partial x_2} + \frac{\partial v_3^3}{\partial x_1^2 \partial x_2} + \underbrace{\frac{\partial v_3}{\partial x_1^2} + \frac{\partial v_3^3}{\partial x_1^2 \partial x_2} + \underbrace{\frac{\partial v_3}{\partial x_1^2} + \frac{\partial v_3^3}{\partial x_1^2 \partial x_2} + \underbrace{\frac{\partial v_3}{\partial x_1^2 \partial x_2} + \frac{\partial v_3^3}{\partial x_1^3 \partial x_1^2} + \underbrace{\frac{\partial v_3}{\partial x_1^3} + \frac{\partial v_3^3}{\partial x_1^3 \partial x_1^3} + \underbrace{\frac{\partial v_3}{\partial x_1^3} + \frac{\partial v_3^3}{\partial x_1^3} + \underbrace{\frac{\partial v_3}{\partial x_1^3} + \frac{\partial v_3^3}{\partial x_1^3} + \underbrace{\frac{\partial v_3}{\partial x_1^3} + \frac{\partial v_3^3}{\partial x_1^3} + \frac{\partial v_3^3}{\partial x_1^3} + \underbrace{\frac{\partial v_3}{\partial x_1^3} + \frac{\partial v_3^3}{\partial x_1^3} + \underbrace{\frac{\partial v_3}{\partial x_1^3} + \frac{\partial v_3^3}{\partial x_1^3} + \underbrace{\frac{\partial v_3}{\partial x_1^3} + \frac{\partial$$

Using the strains from Eq. (4.33) strain energy U is calculated again, which takes the following form

$$U = \underbrace{U_{\text{sig}}}_{O(\xi^6 \mu)} + \underbrace{U_3}_{O(\xi^8 \mu)} + O(\xi^9 \mu)$$
(4.34)

where U_0 , U_1 , U_2 , and U_3 represents the energy contributions corresponding to zeroth, first, second, and third order solutions, respectively. To include the effect of higher order energy, the portion of U corrected up to $O\left(\xi^8\mu\right)$ is taken as $U_{\rm sig}$. Now the functional Π_{x_3} is recalculated to incorporate the change in $U_{\rm sig}$. It has been observed that in the third order solution the derivatives of the perturbation variables v_i^3 with respect to the x_α coordinates, i.e., $\left(\frac{\partial v_i^3}{\partial x_\alpha}\right)$, appears which create difficulty in the analysis. To eliminate these derivatives, integration by parts is performed, which results in boundary conditions defined at $\Omega_{\rm side}$. However, these boundary conditions are ignored in the present analysis, as the aim is to find the displacement field for the interior domain of the plate without considering the edge effects. Extremization of Π_{x_3} yields the following Euler Lagrange equations

$$-\frac{\partial Y}{\partial x_{3}} \left[-2x_{3}\nu \frac{\partial^{2}u_{2}}{\partial x_{1}\partial x_{2}} + x_{3}^{2}\nu \frac{\partial^{3}u_{3}}{\partial x_{1}\partial x_{2}^{2}} - 2x_{3}\nu \frac{\partial^{2}u_{1}}{\partial x_{1}^{2}} + x_{3}^{2}\nu \frac{\partial^{3}u_{3}}{\partial x_{1}^{3}} + 2(1-\nu) \frac{\partial^{2}v_{1}^{3}}{\partial x_{3}} \right]$$

$$+2Y \left[(-1+\nu) \frac{\partial^{2}u_{1}}{\partial x_{2}^{2}} - \frac{\partial^{2}u_{2}}{\partial x_{1}\partial x_{2}} + x_{3}(2-\nu) \frac{\partial^{3}u_{3}}{\partial x_{1}\partial x_{2}^{2}} - (2-\nu) \frac{\partial^{2}u_{1}}{\partial x_{1}^{2}} \right]$$

$$+x_{3}(2-\nu) \frac{\partial^{3}u_{3}}{\partial x_{1}^{3}} - (1-\nu) \frac{\partial^{2}v_{1}^{3}}{\partial x_{3}^{2}} \right] = 0$$

$$-\frac{\partial Y}{\partial x_{3}} \left[-2x_{3}\nu \frac{\partial^{2}u_{1}}{\partial x_{1}\partial x_{2}} + x_{3}^{2}\nu \frac{\partial^{3}u_{3}}{\partial x_{1}^{2}\partial x_{2}} - 2x_{3}\nu \frac{\partial^{2}u_{2}}{\partial x_{2}^{2}} + x_{3}^{2}\nu \frac{\partial^{3}u_{3}}{\partial x_{2}^{3}} + 2(1-\nu) \frac{\partial^{2}v_{2}^{3}}{\partial x_{3}} \right]$$

$$+2Y \left[(-1+\nu) \frac{\partial^{2}u_{2}}{\partial x_{1}^{2}} - \frac{\partial^{2}u_{1}}{\partial x_{1}\partial x_{2}} + x_{3}(2-\nu) \frac{\partial^{3}u_{3}}{\partial x_{1}^{2}\partial x_{2}} - (2-\nu) \frac{\partial^{2}u_{2}}{\partial x_{2}^{2}} \right]$$

$$+x_{3}(2-\nu) \frac{\partial^{3}u_{3}}{\partial x_{2}^{3}} - (1-\nu) \frac{\partial^{2}v_{2}^{3}}{\partial x_{3}^{2}} \right] = 0$$

$$-\frac{\partial Y}{\partial x_{3}} \left[\left(\frac{\partial u_{3}}{\partial x_{1}} \right)^{2} + \left(\frac{\partial u_{3}}{\partial x_{2}} \right)^{2} + 2(1-\nu) \frac{\partial^{2}v_{3}^{3}}{\partial x_{3}} \right] - 2(1-\nu)Y \frac{\partial^{2}v_{3}^{3}}{\partial x_{3}^{2}} = 0$$

where f_2 , f_3 , g_2 and g_3 are functions of x_1 and x_2 . The details for this is given in Appendix A. The associated boundary conditions are given below

$$\begin{aligned}
&\mathcal{B}_{v_{1}^{3}}\big|_{x_{3}=-(h/2)-\eta} = \mathcal{B}_{v_{1}^{3}}\big|_{x_{3}=(h/2)-\eta} = 0 \\
&\mathcal{B}_{v_{2}^{3}}\big|_{x_{3}=-(h/2)-\eta} = \mathcal{B}_{v_{2}^{3}}\big|_{x_{3}=(h/2)-\eta} = 0 \\
&\mathcal{B}_{v_{3}^{3}}\big|_{x_{3}=-(h/2)-\eta} = \mathcal{B}_{v_{3}^{3}}\big|_{x_{3}=(h/2)-\eta} = 0 \\
&\mathcal{B}_{v_{3}^{3}}\big|_{x_{3}=-(h/2)-\eta} = \mathcal{B}_{v_{3}^{3}}\big|_{x_{3}=(h/2)-\eta} = 0 \\
&\mathcal{B}_{v_{1}^{3}} = \frac{1}{4(1-\nu^{2})}Y\left[-2x_{3}\nu\frac{\partial^{2}u_{2}}{\partial x_{1}\partial x_{2}} + x_{3}^{2}\nu\frac{\partial^{3}u_{3}}{\partial x_{1}\partial x_{2}^{2}} - 2x_{3}\nu\frac{\partial^{2}u_{1}}{\partial x_{1}^{2}} + x_{3}^{2}\nu\frac{\partial^{3}u_{3}}{\partial x_{1}^{3}} + 2(1-\nu)\frac{\partial^{2}v_{1}^{3}}{\partial x_{3}}\right] \\
&\mathcal{B}_{v_{2}^{3}} = \frac{1}{4(1-\nu^{2})}Y\left[-2x_{3}\nu\frac{\partial^{2}u_{1}}{\partial x_{1}\partial x_{2}} + x_{3}^{2}\nu\frac{\partial^{3}u_{3}}{\partial x_{1}^{2}\partial x_{2}} - 2x_{3}\nu\frac{\partial^{2}u_{2}}{\partial x_{2}^{2}} + x_{3}^{2}\nu\frac{\partial^{3}u_{3}}{\partial x_{3}^{3}} + 2(1-\nu)\frac{\partial^{2}v_{2}^{3}}{\partial x_{3}}\right] \\
&\mathcal{B}_{v_{3}^{3}} = -\frac{Y}{2(-1+\nu+2\nu^{2})}\left(\left(\frac{\partial u_{3}}{\partial x_{1}}\right)^{2} + \left(\frac{\partial u_{3}}{\partial x_{2}}\right)^{2} - 2(-1+\nu)\frac{\partial v_{3}^{3}}{\partial x_{3}}\right) \\
\end{aligned} \tag{4.36}$$

The Euler-Lagrange equations, Eq. (4.35), can be solved for different gradation models, making the procedure versatile. Here, we are specifically considering the exponential gradation model for further analysis. However, it's important to note that the same procedure can be applied to other gradation models as well. The mathematical form for the exponential model is given by [82]

$$Y = Y_0 \ e^{\left\{\frac{\lambda(x_3 - \eta)}{h}\right\}} \tag{4.37}$$

where λ is gradation index. Solving Eq. (4.35) and (4.36) for this gradation model leads to

$$\eta = \frac{1}{2} \left(h \coth\left(\frac{\lambda}{2}\right) - \frac{2h + \frac{f_1}{g_1}}{\lambda} \right)
\eta = \frac{1}{2} \left(h \coth\left(\frac{\lambda}{2}\right) - \frac{2h + \frac{f_2}{g_2}}{\lambda} \right)
f_1 = \lambda (1 - \nu) \frac{\partial^2 u_1}{\partial x_2^2} + \lambda (1 + \nu) \frac{\partial^2 u_2}{\partial x_1 \partial x_2} + 2\lambda \frac{\partial^2 u_1}{\partial x_1^2}
f_2 = \lambda (1 - \nu) \frac{\partial^2 u_2}{\partial x_1^2} + \lambda (1 + \nu) \frac{\partial^2 u_1}{\partial x_1 \partial x_2} + 2\lambda \frac{\partial^2 u_2}{\partial x_2^2}
g_1 = \frac{\partial^3 u_3}{\partial x_1 \partial x_2^2} + \frac{\partial^3 u_3}{\partial x_1^3}
g_2 = \frac{\partial^3 u_3}{\partial x_1^2 \partial x_2} + \frac{\partial^3 u_3}{\partial x_2^3}$$
(4.38)

It can be observed that the quantities f_1 and f_2 contain second order derivatives of u_{α} w.r.t. x_1 and x_2 so to eliminate them position of the reference plane of the plate is selected

by taking η as given below [82]

$$\eta = \frac{h}{2} \left(\coth\left(\frac{\lambda}{2}\right) - \frac{2}{\lambda} \right) \tag{4.39}$$

Solving Eq. (4.18), (4.35), (4.36), (4.37) and (4.39) results in the following solution

$$v_{1}^{3} = \frac{e^{-\frac{x_{3}\lambda}{h} - \frac{1}{2}\lambda \coth\frac{\lambda}{2}}}{6\lambda^{2}(-1+\nu)} \left[e^{\frac{x_{3}\lambda}{h} + \frac{1}{2}\lambda \coth\frac{\lambda}{2}} x_{3} \left(12h^{2} - 6hx_{3}\lambda + x_{3}^{2}\lambda^{2}\nu \right) - 6e \left(-1 + e^{\frac{x_{3}\lambda}{h}} \right) h^{3} \operatorname{csch} \frac{\lambda}{2} \right] g_{1}$$

$$v_{2}^{3} = \frac{e^{-\frac{x_{3}\lambda}{h} - \frac{1}{2}\lambda \coth\frac{\lambda}{2}}}{6\lambda^{2}(-1+\nu)} \left[e^{\frac{x_{3}\lambda}{h} + \frac{1}{2}\lambda \coth\frac{\lambda}{2}} x_{3} \left(12h^{2} - 6hx_{3}\lambda + x_{3}^{2}\lambda^{2}\nu \right) - 6e \left(-1 + e^{\frac{x_{3}\lambda}{h}} \right) h^{3} \operatorname{csch} \frac{\lambda}{2} \right] g_{2}$$

$$v_{3}^{3} = \frac{x_{3}}{2(-1+\nu)} \left[\left(\frac{\partial u_{3}}{\partial x_{1}} \right)^{2} + \left(\frac{\partial u_{3}}{\partial x_{2}} \right)^{2} \right]$$

$$(4.40)$$

A graphical representation of the adopted procedure for the development done in Part B has been shown in Fig. 4.2.

4.4.2 A Discussion on the Displacement Field

The final displacement field obtained in Part A and B is given below

$$v_{1} = \underbrace{u_{1} - x_{3} \frac{\partial u_{3}}{\partial x_{1}}}_{O(\xi^{3}l)} + \underbrace{\frac{e^{-\frac{x_{3}\lambda}{h} - \frac{1}{2}\lambda \coth \frac{\lambda}{2}}}{6\lambda^{2}(-1 + \nu)}}_{(2} \left[e^{\frac{x_{3}\lambda}{h} + \frac{1}{2}\lambda \coth \frac{\lambda}{2}} x_{3} \left(12h^{2} - 6hx_{3}\lambda + x_{3}^{2}\lambda^{2}\nu \right) - 6e \left(-1 + e^{\frac{x_{3}\lambda}{h}} \right) h^{3} \operatorname{csch} \frac{\lambda}{2} \right] g_{1}}_{O(\xi^{4}h)}$$

$$v_{2} = \underbrace{u_{2} - x_{3} \frac{\partial u_{3}}{\partial x_{2}}}_{O(\xi^{3}l)} + \underbrace{\frac{e^{-\frac{x_{3}\lambda}{h} - \frac{1}{2}\lambda \coth \frac{\lambda}{2}}}{6\lambda^{2}(-1 + \nu)}}_{O(\xi^{4}h)} \left[e^{\frac{x_{3}\lambda}{h} + \frac{1}{2}\lambda \coth \frac{\lambda}{2}} x_{3} \left(12h^{2} - 6hx_{3}\lambda + x_{3}^{2}\lambda^{2}\nu \right) - 6e \left(-1 + e^{\frac{x_{3}\lambda}{h}} \right) h^{3} \operatorname{csch} \frac{\lambda}{2} \right] g_{2}}_{O(\xi^{4}h)}$$

$$v_{3} = \underbrace{u_{3}}_{O(\xi^{2}l)} + \underbrace{\frac{-x_{3}\nu}{1 - \nu}}_{O(\xi^{4}h)} \left(\frac{\partial u_{1}}{\partial x_{1}} + \frac{\partial u_{2}}{\partial x_{2}} \right) + \underbrace{\frac{x_{3}\nu}{2(1 - \nu)}}_{O(\xi^{3}h)} \left(\frac{\partial^{2}u_{3}}{\partial x_{1}^{2}} + \frac{\partial^{2}u_{3}}{\partial x_{2}^{2}} \right) + \underbrace{\frac{x_{3}}{2(-1 + \nu)}}_{O(\xi^{4}h)} \left[\left(\frac{\partial u_{3}}{\partial x_{1}} \right)^{2} + \left(\frac{\partial u_{3}}{\partial x_{2}} \right)^{2} \right]}_{O(\xi^{4}h)}$$

$$- \frac{\partial^{2}u_{3}}{\partial x_{1}^{2}} + \frac{e^{-\frac{1}{2}\lambda \coth \frac{\lambda}{2}}}{\lambda^{2}(-1 + \nu)} h^{2} \left(2e^{\frac{1}{2}\lambda \coth \frac{\lambda}{2}} - e\lambda \operatorname{csch} \frac{\lambda}{2} \right) \left(\frac{\partial^{3}u_{3}}{\partial x_{1}^{3}} + \frac{\partial^{3}u_{3}}{\partial x_{1}\partial x_{2}^{2}} \right)$$

$$(4.41)$$

The improvement in solution of this displacement field is influenced by each perturbation we go through. This has been explained graphically in Fig (4.3) Fig. 4.3(a) shows a line

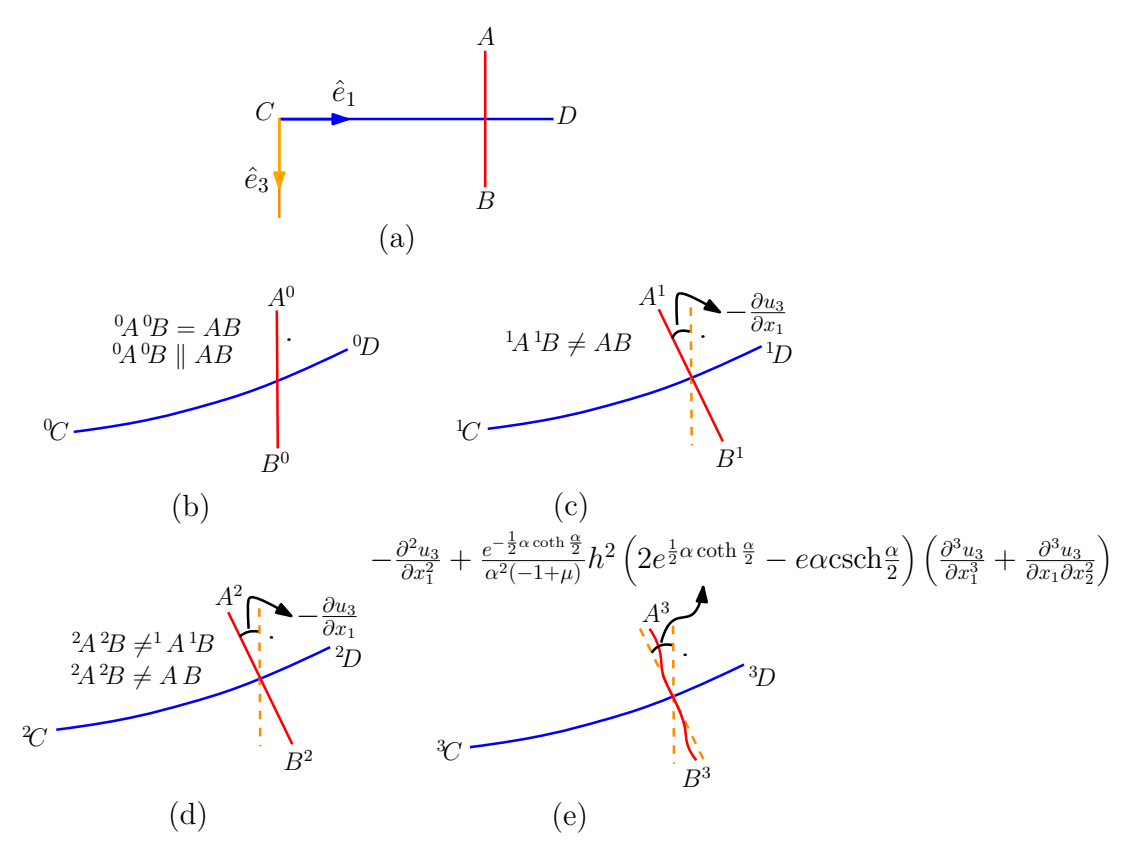


Figure 4.3: Deformation of lines AB and CD lying along direction \hat{e}_3 and \hat{e}_1 respectively. (a) Undeformed configuration (b) Configuration after zeroth perturbation (c) Configuration after first perturbation (d) Configuration after second perturbation (e) Configuration after third perturbation

segment CD in the reference plane which is oriented along \hat{e}_1 and another line segment AB that oriented along \hat{e}_3 . Now as per the zeroth order contribution to the solution there is no change in the length or direction of the line segment AB thus, it is represented by A^0B^0 in Fig. 4.3(b). In the first and second order contributions the displacement field incorporates the effect of rotation and change in length of line AB which is shown in Fig. 4.3(c) and 4.3(d) respectively. In the third order solutions, the line segment AB deforms to the curve line A^3B^3 as shown in Fig. 4.3(e).

4.4.3 A Discussion on the Strains, Stresses and Stiffness Matrix

Eq. (4.1) and (4.41) give the strains corrected up to order (ξ^4). These strains are given below:

$$E_{11} = \underbrace{\frac{\partial u_1}{\partial x_1} - x_3 \frac{\partial^2 u_3}{\partial x_1^2}}_{O(\xi^3)} + \underbrace{\frac{1}{2} \left(\frac{\partial u_3}{\partial x_1} \right)^2}_{O(\xi^4)}$$

$$E_{22} = \underbrace{\frac{\partial u_2}{\partial x_2} - x_3 \frac{\partial^2 u_3}{\partial x_2^2}}_{O(\xi^3)} + \underbrace{\frac{1}{2} \left(\frac{\partial u_3}{\partial x_1} \right)^2}_{O(\xi^4)}$$

$$E_{33} = \underbrace{\frac{\nu}{2(-1+\nu)} \left(2 \frac{\partial u_2}{\partial x_2} + \left(\frac{\partial u_3}{\partial x_2} \right)^2 + 2 \frac{\partial u_1}{\partial x_1} + \left(\frac{\partial u_3}{\partial x_1} \right)^2 - 2x_3 \left(\frac{\partial^2 u_3}{\partial x_1^2} + \frac{\partial^2 u_3}{\partial x_2^2} \right) \right)}_{O(\xi^4)}$$

$$2E_{23} = \underbrace{\frac{1}{\lambda^2(-1+\nu)} e^{-\frac{x_3\lambda}{h} - \frac{1}{2}\lambda \coth\left(\frac{\lambda}{2}\right)} h\left(2e^{\frac{x_3\lambda}{h} + \frac{1}{2}\lambda \coth\left(\frac{\lambda}{2}\right)} (h - x_3\lambda) - eh\lambda \operatorname{csch}\left(\frac{\lambda}{2}\right) \right) \left(\frac{\partial^3 u_3}{\partial x_1^3} + \frac{\partial^2 u_3}{\partial x_1^2 \partial x_2} \right)}_{O(\xi^4)}$$

$$2E_{13} = \underbrace{\frac{1}{\lambda^2(-1+\nu)} e^{-\frac{x_3\lambda}{h} - \frac{1}{2}\lambda \coth\left(\frac{\lambda}{2}\right)} h\left(2e^{\frac{x_3\lambda}{h} + \frac{1}{2}\lambda \coth\left(\frac{\lambda}{2}\right)} (h - x_3\lambda) - eh\lambda \operatorname{csch}\left(\frac{\lambda}{2}\right) \right) \left(\frac{\partial^3 u_3}{\partial x_1^3} + \frac{\partial^2 u_3}{\partial x_1 \partial x_2^2} \right)}_{O(\xi^4)}$$

$$2E_{12} = \underbrace{\frac{\partial u_1}{\partial x_2} + \frac{\partial u_2}{\partial x_1} - 2x_3 \frac{\partial^2 u_3}{\partial x_1 \partial x_2}}_{O(\xi^3)} + \underbrace{\left(\frac{\partial u_3}{\partial x_1} \right) \left(\frac{\partial u_3}{\partial x_2} \right)}_{O(\xi^4)}$$

It is important to note that the plane stress condition which was valid in Part A, is still valid. This can be verified by substituting strains from Eq. (4.42) in Eq. (4.5). This is a natural outcome of the formulation without considering any ad-hoc and apriori assumptions. This plane stress condition facilitate the analysis by introducing simplicity, computational efficiency and accuracy for many engineering applications. Following the same argument as in section 3.9, the transverse normal strain E_{33} is neglected. By omitting

the transverse strain component, E_{33} , in Eq. (4.42), we obtain

$$E = \begin{cases} \frac{\partial u_1}{\partial x_1} - x_3 \frac{\partial^2 u_3}{\partial x_1^2} + \frac{1}{2} \left(\frac{\partial u_3}{\partial x_1} \right)^2 \\ \frac{\partial u_2}{\partial x_2} - x_3 \frac{\partial^2 u_3}{\partial x_2^2} + \frac{1}{2} \left(\frac{\partial u_3}{\partial x_2} \right)^2 \\ \frac{1}{\lambda^2 (-1+\nu)} e^{-\frac{x_3\lambda}{h} - \frac{1}{2}\lambda \coth\left(\frac{\lambda}{2}\right)} h \left(2e^{\frac{x_3\lambda}{h} + \frac{1}{2}\lambda \coth\left(\frac{\lambda}{2}\right)} (h - x_3\lambda) - eh\lambda \operatorname{csch}\left(\frac{\lambda}{2}\right) \right) \left(\frac{\partial^3 u_3}{\partial x_2^3} + \frac{\partial^2 u_3}{\partial x_1^2 \partial x_2} \right) \\ \frac{1}{\lambda^2 (-1+\nu)} e^{-\frac{x_3\lambda}{h} - \frac{1}{2}\lambda \coth\left(\frac{\lambda}{2}\right)} h \left(2e^{\frac{x_3\lambda}{h} + \frac{1}{2}\lambda \coth\left(\frac{\lambda}{2}\right)} (h - x_3\lambda) - eh\lambda \operatorname{csch}\left(\frac{\lambda}{2}\right) \right) \left(\frac{\partial^3 u_3}{\partial x_1^3} + \frac{\partial^2 u_3}{\partial x_1 \partial x_2^2} \right) \\ \frac{\partial u_1}{\partial x_2} + \frac{\partial u_2}{\partial x_1} - 2x_3 \frac{\partial^2 u_3}{\partial x_1 \partial x_2} + \left(\frac{\partial u_3}{\partial x_1} \right) \left(\frac{\partial u_3}{\partial x_2} \right) \end{cases}$$

$$(4.43)$$

The simplified stiffness matrix considering the plane stress claim can be written as

$$D = \frac{Y_0 e^{\frac{\lambda(x_3 - \eta)}{h}}}{1 - \nu^2} \begin{bmatrix} 1 & \nu & 0 & 0 & 0\\ \nu & 1 & 0 & 0 & 0\\ 0 & 0 & \frac{1 - \nu}{2} & 0 & 0\\ 0 & 0 & 0 & \frac{1 - \nu}{2} & 0\\ 0 & 0 & 0 & 0 & \frac{1 - \nu}{2} \end{bmatrix}$$
(4.44)

If we compare the strains (accurate up to order (ξ^4)) with the strains of FSDT, it can be observed that they don't match. This indicates that FSDT is not asymptotically correct and do not represent the actual behavior. That is why the need to introduce a shear correction factor arises in FSDT. Under plane stress conditions, stresses σ and strain energy density U take the following form

$$\sigma = \{\sigma_{11}, \ \sigma_{22}, \ \tau_{23}, \ \tau_{13}, \ \tau_{12}\}^T = DE,$$

$$U = \frac{1}{2}\sigma E = \frac{1}{2}(DE)E$$
(4.45)

4.5 Part C: Elimination of the Higher Order Derivatives

It is important to note that though strains given in Eq. (4.43) are asymptotically accurate but they depend on higher order derivatives of u_3 . This higher order derivative introduces complexities in the 2D solution and thus limits its practical implementation whereas FSDT which is although asymptotically inaccurate but is very practical due to its simplicity and computational efficiency. The aim of the present work is to derive a plate theory that is computationally efficient and simple like FSDT but more accurate and asymptotically correct.

FSDT accounts for the transverse shear effects in the plate where it is assumed that a straight line normal to the undeformed reference plane $\partial\Omega_{\rm ref}$ remains straight but rotates by angle ϕ_1 and ϕ_2 about the x_1 and x_2 axes respectively, which introduces two additional degrees of freedom. In the present work a novel isoenergetics approach, which is illustrated in Fig. 4.4, has been developed where the shear deformation energies obtained from the VAM based asymptotically correct plate model are equated to that obtained from the FSDT plate model to calculate shear correction factors. Use of this shear correction factors results in the calculation of transverse shear force resultants Q_1 and Q_2 in terms of ϕ_1 and ϕ_2 . Now these Q_1 and Q_2 are utilized to eliminate the inconvenient terms $\left(3g_3 + \frac{\partial g_1}{\partial x_2}\right)$ and $\left(3g_2 + \frac{\partial g_1}{\partial x_4}\right)$ from the VAM based asymptotically correct plate model. This process results in a modified asymptotically correct plate model which is as simple and computationally efficient as the FSDT theory. In what follows we present the above mentioned procedure in detail.

4.5.1 Simplified Model Based on Isoenergetics

The transverse shear force resultants Q_1 and Q_2 are given by

$$Q_1 = \int_{-h/2-\eta}^{h/2-\eta} \tau_{13} \ dx_3, \quad Q_2 = \int_{-h/2-\eta}^{h/2-\eta} \tau_{23} \ dx_3 \tag{4.46}$$

From Eqs. (4.45) and (4.46), we have

$$Q_{1} = \frac{1}{2\lambda^{3}(-1+\nu^{2})}e^{2-\lambda\coth\frac{\lambda}{2}}h^{3}Y_{0}(2+\lambda^{2}-2\cosh\lambda)\operatorname{csch}\frac{\lambda}{2}\left(\frac{\partial^{3}u_{3}}{\partial x_{1}\partial x_{2}^{2}}+\frac{\partial^{3}u_{3}}{\partial x_{1}^{3}}\right)$$

$$Q_{2} = \frac{1}{2\lambda^{3}(-1+\nu^{2})}e^{2-\lambda\coth\frac{\lambda}{2}}h^{3}Y_{0}(2+\lambda^{2}-2\cosh\lambda)\operatorname{csch}\frac{\lambda}{2}\left(\frac{\partial^{3}u_{3}}{\partial x_{1}^{2}\partial x_{2}}+\frac{\partial^{3}u_{3}}{\partial x_{1}^{3}}\right)$$

$$(4.47)$$

Eq. (4.47) gives,

$$\frac{\partial^3 u_3}{\partial x_1 \partial x_2^2} + \frac{\partial^3 u_3}{\partial x_1^3} = -\frac{2e^{-2+\lambda \coth(\frac{\lambda}{2})}\lambda^3(-1+\nu^2)Q_1\sinh(\frac{\lambda}{2})}{h^3 Y_0(2+\lambda^2-2\cosh(\lambda))}$$

$$\frac{\partial^3 u_3}{\partial x_1^2 \partial x_2} + \frac{\partial^3 u_3}{\partial x_2^3} = -\frac{2e^{-2+\lambda \coth(\frac{\lambda}{2})}\lambda^3(-1+\nu^2)Q_2\sinh(\frac{\lambda}{2})}{h^3 Y_0(2+\lambda^2-2\cosh(\lambda))}$$
(4.48)

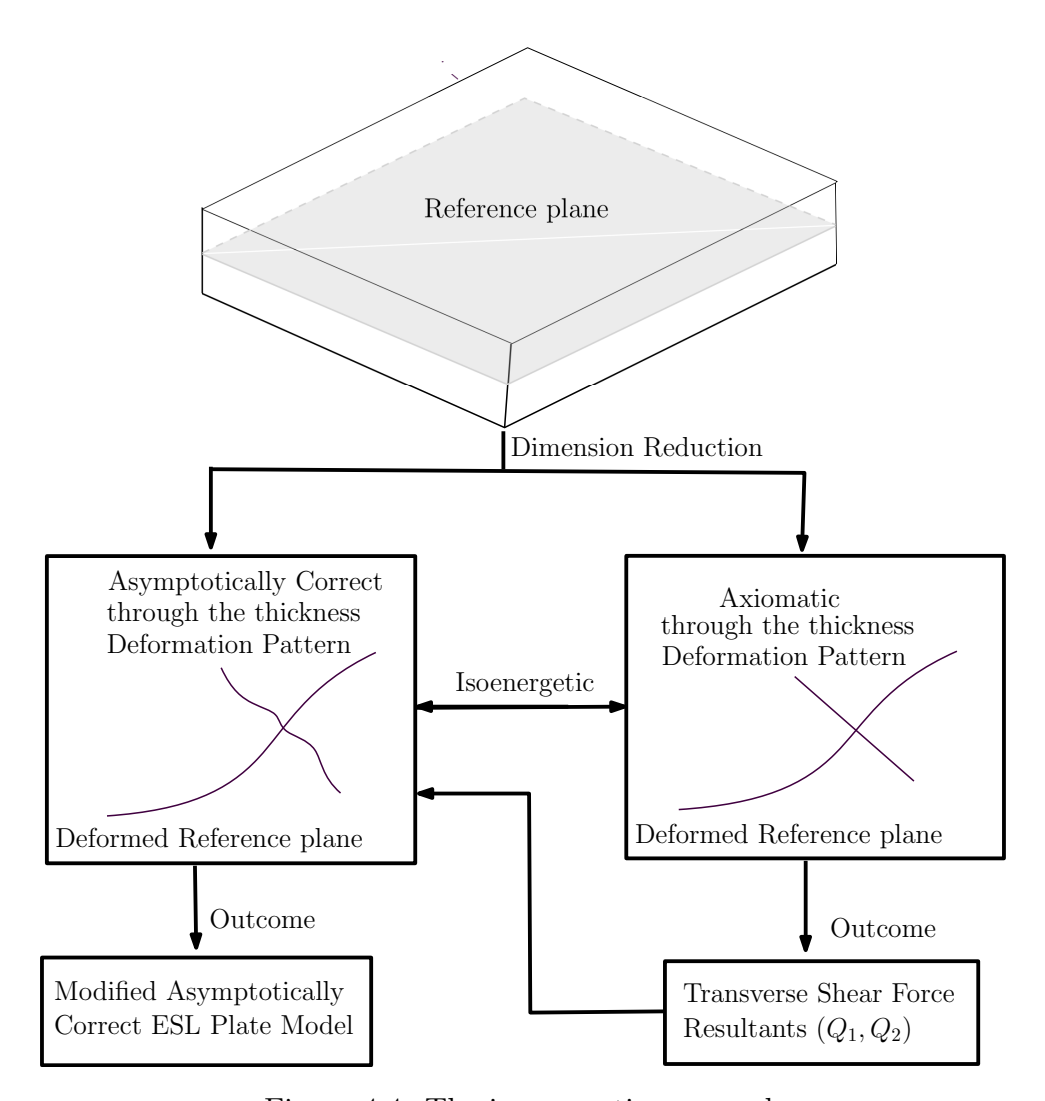


Figure 4.4: The isoenergetic approach

Substituting Eq. (4.48) in Eq. (4.43), we obtain

$$E = \begin{cases} \frac{\partial u_1}{\partial x_1} - x_3 \frac{\partial^2 u_3}{\partial x_1^2} + \frac{1}{2} \left(\frac{\partial u_3}{\partial x_1}\right)^2 \\ \frac{\partial u_2}{\partial x_2} - x_3 \frac{\partial^2 u_3}{\partial x_2^2} + \frac{1}{2} \left(\frac{\partial u_3}{\partial x_2}\right)^2 \\ \frac{2e^{-2 - \frac{x_3\lambda}{h} + \frac{1}{2}\lambda \coth(\frac{\lambda}{2})} \lambda(1 + \nu) Q_2(eh\lambda - 2e^{\frac{x_3\lambda}{h} + \frac{1}{2}\lambda \coth(\frac{\lambda}{2})} (h - x_3\lambda) \sinh(\frac{\lambda}{2}))}{h^2 Y_0(2 + \lambda^2 - 2\cosh(\lambda))} \\ \frac{2e^{-2 - \frac{x_3\lambda}{h} + \frac{1}{2}\lambda \coth(\frac{\lambda}{2})} \lambda(1 + \nu) Q_1(eh\lambda - 2e^{\frac{x_3\lambda}{h} + \frac{1}{2}\lambda \coth(\frac{\lambda}{2})} (h - x_3\lambda) \sinh(\frac{\lambda}{2}))}{h^2 Y_0(2 + \lambda^2 - 2\cosh(\lambda))} \\ \frac{\partial u_1}{\partial x_2} + \frac{\partial u_2}{\partial x_1} - 2x_3 \frac{\partial^2 u_3}{\partial x_1 \partial x_2} + \left(\frac{\partial u_3}{\partial x_1}\right) \left(\frac{\partial u_3}{\partial x_2}\right) \end{cases}$$

In FSDT, the transverse shear strains E_{23}^{ϕ} and E_{13}^{ϕ} are given as

$$2E_{13}^{\phi} = \phi_1 + \frac{\partial u_3}{\partial x_1}, \quad 2E_{23}^{\phi} = \phi_2 + \frac{\partial u_3}{\partial x_2}$$
 (4.50)

and the transverse shear force resultants, Q_1 and Q_2 are given as

$$Q_{1} = K_{1} \frac{e^{2-\lambda \coth \frac{\lambda}{2}} h Y_{0} \sinh \frac{\lambda}{2} \left(\phi_{1} + \frac{\partial u_{3}}{\partial x_{1}}\right)}{\lambda (1+\nu)}$$

$$Q_{2} = K_{2} \frac{e^{2-\lambda \coth \frac{\lambda}{2}} h Y_{0} \sinh \frac{\lambda}{2} \left(\phi_{2} + \frac{\partial u_{3}}{\partial x_{2}}\right)}{\lambda (1+\nu)}$$

$$(4.51)$$

where K_1 and K_2 are shear correction factors [83]. Eq. (4.50) and (4.51) gives

$$2E_{13}^{\phi} = \phi_1 + \frac{\partial u_3}{\partial x_1} = \frac{e^{-2+\lambda \coth\left(\frac{\lambda}{2}\right)}\lambda(1+\nu)\operatorname{csch}\left(\frac{\lambda}{2}\right)Q_1}{hK_1Y_0}$$

$$2E_{23}^{\phi} = \phi_2 + \frac{\partial u_3}{\partial x_2} = \frac{e^{-2+\lambda \coth\left(\frac{\lambda}{2}\right)}\lambda(1+\nu)\operatorname{csch}\left(\frac{\lambda}{2}\right)Q_2}{hK_2Y_0}$$

$$(4.52)$$

Now K_1 and K_2 are calculated by equating the transverse shear deformation energies [123, 117, 129, 145, 146] of the assumption based FSDT plate model and the present (ACI-ESL) plate model. This equality results in as follows

$$e^{\lambda \coth(\lambda/2)} \lambda (1+\nu) \operatorname{csch}(\lambda/2) Q_1 \left[6 - 12K_1 + 4\lambda^2 + \lambda^4 + 4(-2 + 4K_1 - \lambda^2) \operatorname{cosh}(\lambda) + (2 - 4K_1) \operatorname{cosh}(2\lambda) + 2K_1\lambda^3 \operatorname{sinh}(\lambda) \right] = 0$$

$$e^{\lambda \coth(\lambda/2)} \lambda (1+\nu) \operatorname{csch}(\lambda/2) Q_2 \left[6 - 12K_2 + 4\lambda^2 + \lambda^4 + 4(-2 + 4K_2 - \lambda^2) \operatorname{cosh}(\lambda) + (2 - 4K_2) \operatorname{cosh}(2\lambda) + 2K_2\lambda^3 \operatorname{sinh}(\lambda) \right] = 0$$
(4.53)

Solving Eq. (4.53) for K_1 and K_2 we have

$$K_1 = K_2 = -\frac{\left[2 + \lambda^2 - 2\cosh(\lambda)\right]^2 \operatorname{csch}^4\left(\frac{\lambda}{2}\right)}{-32 + 2\lambda^3 \operatorname{csch}^4\left(\frac{\lambda}{2}\right) \sinh(\lambda)}$$
(4.54)

It is important to note that the shear correction factors are a natural outcome of the present approach (without taking any assumptions). Substituting Eq. (4.54) into Eq. (4.51) followed by Eq. (4.51) into Eq. (4.49), the following expressions for the transverse shear strains are established

$$2E_{\alpha 3} = -\frac{\lambda \left[2 + \lambda^2 - 2\cosh(\lambda)\right] \operatorname{csch}^4\left(\frac{\lambda}{2}\right) \left[eh\lambda - 2e^{\frac{x_3\lambda}{h} + \frac{1}{2}\lambda \coth(\frac{\lambda}{2})}(h - x_3\lambda)\sinh(\frac{\lambda}{2})\right]}{2eh\left[-16 + \lambda^3 \operatorname{csch}^4\left(\frac{\lambda}{2}\right)\sinh(\lambda)\right]} \left(\phi_{\alpha} + \frac{\partial u_3}{\partial x_{\alpha}}\right)$$

$$(4.55)$$

Since the order of the transverse shear strains is $O(\xi^4)$, therefore we have

$$x_3 \frac{d}{dx_\alpha} \left(\phi_\beta + \frac{\partial u_3}{\partial x_\beta} \right) \sim O\left(\xi^5\right)$$
 (4.56)

Eqs. (4.56) results in as follows

$$-x_3 \frac{\partial^2 u_3}{\partial x_\alpha \partial x_\beta} = x_3 \frac{\partial \phi_\beta}{\partial x_\alpha} + O\left(\xi^5\right) \tag{4.57}$$

Eq. (4.49), (4.55) and (4.57) results is the following strains

$$E = \begin{cases} \frac{\partial u_1}{\partial x_1} + x_3 \frac{\partial \phi_1}{\partial x_1} + \frac{1}{2} \left(\frac{\partial u_3}{\partial x_1} \right)^2 \\ \frac{\partial u_2}{\partial x_2} + x_3 \frac{\partial \phi_2}{\partial x_2} + \frac{1}{2} \left(\frac{\partial u_3}{\partial x_2} \right)^2 \\ -\frac{\lambda \left[2 + \lambda^2 - 2\cosh(\lambda) \right] \operatorname{csch}^4\left(\frac{\lambda}{2}\right) \left[eh\lambda - 2e^{\frac{x_3\lambda}{h} + \frac{1}{2}\lambda \coth(\frac{\lambda}{2})} (h - x_3\lambda) \sinh(\frac{\lambda}{2}) \right]}{2eh \left[-16 + \lambda^3 \operatorname{csch}^4\left(\frac{\lambda}{2}\right) \sinh(\lambda) \right]} \left(\phi_2 + \frac{\partial u_3}{\partial x_2} \right) \\ -\frac{\lambda \left[2 + \lambda^2 - 2\cosh(\lambda) \right] \operatorname{csch}^4\left(\frac{\lambda}{2}\right) \left[eh\lambda - 2e^{\frac{x_3\lambda}{h} + \frac{1}{2}\lambda \coth(\frac{\lambda}{2})} (h - x_3\lambda) \sinh(\frac{\lambda}{2}) \right]}{2eh \left[-16 + \lambda^3 \operatorname{csch}^4\left(\frac{\lambda}{2}\right) \sinh(\lambda) \right]} \left(\phi_1 + \frac{\partial u_3}{\partial x_1} \right) \\ -\frac{\partial u_1}{\partial x_2} + \frac{\partial u_2}{\partial x_1} + x_3 \left(\frac{\partial \phi_1}{\partial x_2} + \frac{\partial \phi_2}{\partial x_1} \right) + \left(\frac{\partial u_3}{\partial x_1} \right) \left(\frac{\partial u_3}{\partial x_2} \right) \end{cases}$$

Eq. (4.58) provides an asymptotically accurate, simplified and computationally efficient reduced dimensional model of the plate.

4.6 Results and Discussion

This Capter introduces a new ESL plate theory for functionally graded Materials. The presented theory is asymptotically correct up to $(O(\xi^4))$. To evaluate its accuracy, numerical examples dealing with different scenarios are presented. Two different material gradations are examined. Details of each gradation are given in section 4.6.1 and 4.6.2.

In this work, the in-plane 2D analysis was done using non-linear (Example-1 and Example-2) and linear (Example-3, Example-4) finite element analysis code written in Mathematica based on the present formulation. To assess the accuracy of cases where data from literature is not available the 3D finite element analysis was performed using Abaqus software. The USDFLD subroutine written in FORTRAN [3] was used to mimic the gradation in Abaqus. The chosen element type for the analysis was C3D20R, which corresponds to a 20-node quadratic brick element with reduced integration. A thorough convergence study was carried out to ensure the accuracy and reliability of the obtained results. This study involved systematically refining the mesh and monitoring the convergence behavior of relevant quantities such as displacements, strains, and stresses. Nevertheless, for brevity, the convergence analysis is omitted from this presentation.

4.6.1 Material Gradation-1

An exponential variation of Young's modulus Y with the mathematical form [4] given in Eq. (4.64) is considered.

$$Y = Y_t \exp\left[-\delta \left(1 - \frac{2y_3}{h}\right)\right]$$

$$\delta = \frac{1}{2} \log\left(\frac{Y_t}{Y_b}\right)$$

$$y_3 = x_3 + \eta$$

$$(4.59)$$

Where Y_t and Y_b are Young's modulus of the top and bottom surfaces of the plate respectively. For this gradation, the reference plane shift relative to the mid-plane of the plate η and the shear correction factor K are determined as follows.

$$\begin{split} \eta &= -\frac{(Y_b + Y_t)h}{2(Y_b - Y_t)} - \frac{h}{\log\left(\frac{Y_t}{Y_b}\right)} \\ K &= -\frac{\left(\frac{Y_t}{Y_b}\right)^{\frac{Y_t}{Y_b - Y_t}} \left\{\log(Y_b) - \log(Y_t)\right\} \left\{(Y_b - Y_t)^2 - Y_b Y_t \log\left(\frac{Y_t}{Y_b}\right)^2\right\}^2}{\text{Denominator}} \\ \text{Denominator} &= (Y_b - Y_t) \log\left(\frac{Y_t}{Y_b}\right) \left[Y_b^2 \left(\frac{Y_t}{Y_b}\right)^{\frac{Y_b}{Y_b - Y_t}} \log\left(\frac{Y_t}{Y_b}\right)^2 \left\{Y_b - Y_t\right\} + (Y_b + Y_t) \log\left(\frac{Y_t}{Y_b}\right)^2\right\} + (Y_b - Y_t) \left(\frac{Y_t}{Y_b}\right)^{\frac{Y_t}{Y_b - Y_t}} \left\{2(Y_b - Y_t)^2 - Y_b Y_t \log\left(\frac{Y_t}{Y_b}\right)^2\right\} \right] \end{split}$$

$$(4.60)$$

A plate made of ceramic-metal combination is examined in the first and second examples. The bottom and top surfaces of the plate are composed of aluminum metal and alumina ceramic, respectively [4]. Young's modulus is taken to be $Y_b = 70$ GPa for aluminum and $Y_t = 380$ GPa for alumina. Poisson's ratio μ for both of the materials is 0.3. The variation of Young's Modulus Y of the plat along the thickness of the plate is plotted in Fig. 4.5. For varied values of Y_t , keeping the other parameters constant, η and K are plotted in Fig. 4.6. Notably, for homogeneous materials (when $Y_t = Y_b$), $\eta = 0$ and K = 0.8333. The values of η and K match exactly with those found in the literature for homogeneous materials [122, 123, 121].

For this material gradation, the strains are given as follows

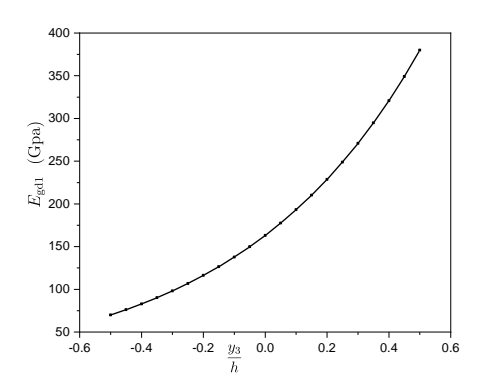
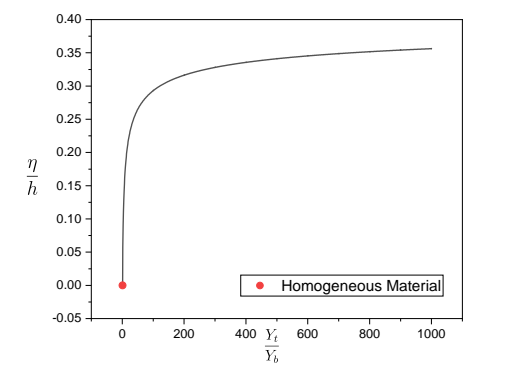


Figure 4.5: Variation of the Young's modulus along the thickness of the plate for the first and second examples



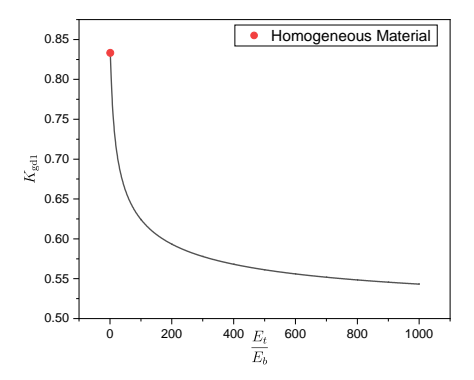


Figure 4.6: Variation of the shift of the reference plane η and shear correction factor K with $\frac{Y_t}{Y_h}$ for the first and second examples

$$E_{gd1} = \begin{cases} \frac{\partial u_1}{\partial x_1} + x_3 \frac{\partial \phi_1}{\partial x_1} + \frac{1}{2} \left(\frac{\partial u_3}{\partial x_1}\right)^2 \\ \frac{\partial u_2}{\partial x_2} + x_3 \frac{\partial \phi_2}{\partial x_2} + \frac{1}{2} \left(\frac{\partial u_3}{\partial x_2}\right)^2 \\ \frac{\left(\frac{Y_t}{Y_b}\right)^{\frac{Y_t}{Y_b - Y_t} - \frac{x_3}{h}} \left[(Y_b - Y_t)^2 - Y_b Y_t \log\left(\frac{Y_t}{Y_b}\right)^2 \right] \left[e Y_b \left(\frac{Y_t}{Y_b}\right)^{\frac{Y_b}{Y_b - Y_t}} h \log\left(\frac{Y_t}{Y_b}\right) + (Y_b - Y_t) \left(\frac{Y_t}{Y_b}\right)^{\frac{x_3}{h}} \left(h - x_3 \log\left(\frac{Y_t}{Y_b}\right)\right) \right] \left(\phi_2 + \frac{\partial u_3}{\partial x_2}\right)}{h \left[Y_b^2 \left(\frac{Y_t}{Y_b}\right)^{\frac{Y_b}{Y_b - Y_t}} \log\left(\frac{Y_t}{Y_b}\right)^2 \left\{ Y_b - Y_t + (Y_b + Y_t) \log\left(\frac{Y_t}{Y_b}\right) \right\} + (Y_b - Y_t) \left(\frac{Y_t}{Y_b}\right)^{\frac{Y_t}{Y_b - Y_t}} \left\{ 2(Y_b - Y_t)^2 - Y_b Y_t \log\left(\frac{Y_t}{Y_b}\right)^2 \right\} \right]} \\ \frac{\left(\frac{Y_t}{Y_b}\right)^{\frac{Y_b}{Y_b - Y_t}} - \frac{x_3}{h}}{h} \left[(Y_b - Y_t)^2 - Y_b Y_t \log\left(\frac{Y_t}{Y_b}\right)^2 \right] \left[e Y_b \left(\frac{Y_t}{Y_b}\right)^{\frac{Y_b}{Y_b - Y_t}} h \log\left(\frac{Y_t}{Y_b}\right) + (Y_b - Y_t) \left(\frac{Y_t}{Y_b}\right)^{\frac{x_3}{h}} \left(h - x_3 \log\left(\frac{Y_t}{Y_b}\right)\right) \right] \left(\phi_1 + \frac{\partial u_3}{\partial x_1}\right)}{h \left[Y_b^2 \left(\frac{Y_t}{Y_b}\right)^{\frac{Y_b}{Y_b - Y_t}} \log\left(\frac{Y_t}{Y_b}\right)^2 \left\{ Y_b - Y_t + (Y_b + Y_t) \log\left(\frac{Y_t}{Y_b}\right) \right\} + (Y_b - Y_t) \left(\frac{Y_t}{Y_b}\right)^{\frac{Y_t}{Y_b - Y_t}} \left\{ 2(Y_b - Y_t)^2 - Y_b Y_t \log\left(\frac{Y_t}{Y_b}\right)^2 \right\} \right]}{h \left[\frac{\partial u_1}{\partial x_2} + \frac{\partial u_2}{\partial x_1} + x_3 \left(\frac{\partial \phi_1}{\partial x_2} + \frac{\partial \phi_2}{\partial x_1}\right) + \left(\frac{\partial u_3}{\partial x_1}\right) \left(\frac{\partial u_3}{\partial x_2}\right)}{h \left[\frac{\partial u_3}{\partial x_2} + \frac{\partial u_2}{\partial x_1} + x_3 \left(\frac{\partial \phi_1}{\partial x_2} + \frac{\partial \phi_2}{\partial x_1}\right) + \left(\frac{\partial u_3}{\partial x_1}\right) \left(\frac{\partial u_3}{\partial x_2}\right)}{h \left[\frac{\partial u_1}{\partial x_2} + \frac{\partial u_2}{\partial x_1} + x_3 \left(\frac{\partial \phi_1}{\partial x_2} + \frac{\partial \phi_2}{\partial x_1}\right) + \left(\frac{\partial u_3}{\partial x_1}\right) \left(\frac{\partial u_3}{\partial x_2}\right)}{h \left[\frac{\partial u_1}{\partial x_2} + \frac{\partial u_2}{\partial x_1} + x_3 \left(\frac{\partial \phi_1}{\partial x_2} + \frac{\partial \phi_2}{\partial x_1}\right) + \left(\frac{\partial u_3}{\partial x_2}\right) \left(\frac{\partial u_3}{\partial x_2}\right)}{h \left[\frac{\partial u_1}{\partial x_2} + \frac{\partial u_2}{\partial x_1} + x_3 \left(\frac{\partial \phi_1}{\partial x_2} + \frac{\partial \phi_2}{\partial x_1}\right) + \left(\frac{\partial u_3}{\partial x_2}\right) \left(\frac{\partial u_3}{\partial x_2}\right)}{h \left[\frac{\partial u_1}{\partial x_2} + \frac{\partial u_2}{\partial x_1} + \frac{\partial u_2}{\partial x_2} \right)}{h \left[\frac{\partial u_1}{\partial x_2} + \frac{\partial u_2}{\partial x_2} + \frac{\partial u_2}$$

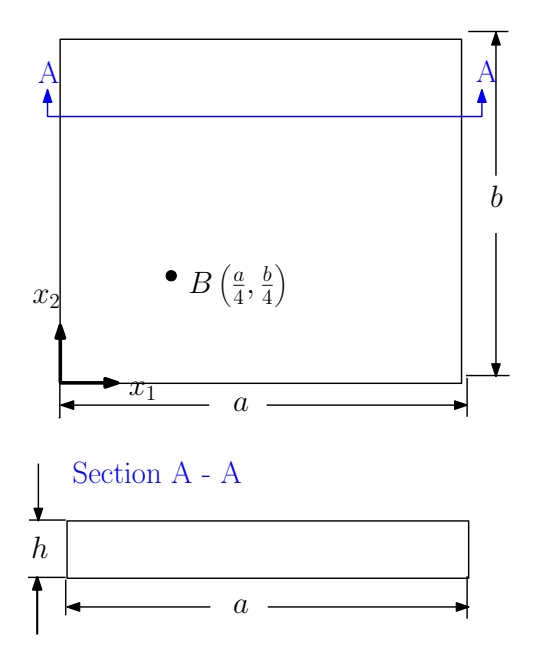


Figure 4.7: Geometry of the plate

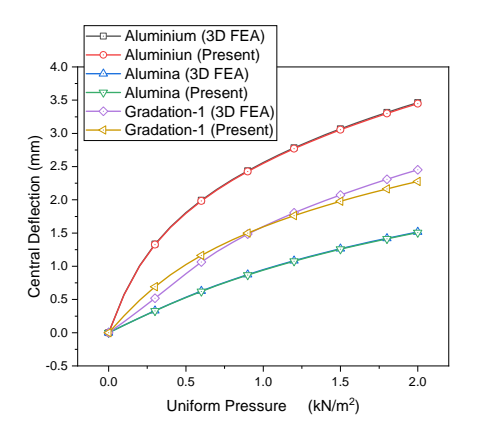


Figure 4.8: Load-deflection curves for the central point of the plate considered in the first example under uniform Pressure P applied at its top face

Also for this case, the stiffness matrix takes the following form

$$D = \frac{Y_t \exp\left[-\delta\left(1 - \frac{2y_3}{h}\right)\right]}{1 - \mu^2} \begin{bmatrix} 1 & \mu & 0 & 0 & 0\\ \mu & 1 & 0 & 0 & 0\\ 0 & 0 & \frac{1-\mu}{2} & 0 & 0\\ 0 & 0 & 0 & \frac{1-\mu}{2} & 0\\ 0 & 0 & 0 & 0 & \frac{1-\mu}{2} \end{bmatrix}$$
(4.62)

In first example, a rectangular plate with sides a = 0.5472 m, b = 0.1824 m and height

h = 1.824 mm as shown in Fig.4.7 is considered. Two opposite boundaries (at $x_1 = 0$ and $x_1 = a$) of the plate are clamped and the rest two are free. A uniform pressure load P is applied to the bottom surface $(x_3 = -\frac{h}{2})$ of the plate.

The displacement of the midpoint of the plate is plotted in Fig. 4.8 for three different cases: (a) plate is composed of Aluminum (b) plate is composed of Alumina and (c) plate is composed of functionally graded material. The results obtained using the present approach agree with the 3D FEA results.

In the second example, a square plate with side a and thickness h is considered. The side to length ratio $\frac{a}{h}$ is taken 20. The plate is simply supported at all its edges. The following non-dimensionalized quantities [122] are considered to compare the results.

$$\overline{w} = \frac{100 \ h^3 \ Y_t}{q_0 \ a^4} u_3 \left(x_1, \frac{b}{2}, 0 \right) \qquad \overline{\sigma}_{11} = \frac{h^2}{q_0 \ a^2} \sigma_{11} \left(x_1, x_2, x_3 \right)
\overline{\sigma}_{22} = \frac{h^2}{q_0 \ a^2} \sigma_{22} \left(x_1, x_2, x_3 \right) \qquad \overline{\sigma}_{23} = \frac{h}{q_0 \ a} \sigma_{23} \left(x_1, x_2, x_3 \right)
\overline{\sigma}_{12} = \frac{h^2}{q_0 \ a^2} \sigma_{12} \left(x_1, x_2, x_3 \right) \qquad \overline{\sigma}_{13} = \frac{h}{q_0 \ a} \sigma_{13} \left(x_1, x_2, x_3 \right)$$
(4.63)

Fig. 4.9 illustrates non-dimensionalized displacement u_3 along the centerline parallel to x_1 axis and it also plots non-dimensionalized stresses σ_{11} , σ_{23} and σ_{23} at point B (shown in Fig. 4.7) along the thickness of the plate in the second example.

4.6.2 Material Gradation-2

A power law variation of Young's modulus Y with the mathematical form [1] given in Eq. (4.64) is considered.

$$Y = Y_b + (Y_t - Y_b) V$$

$$V = \left(\frac{y_3}{h} + \frac{1}{2}\right)^n$$

$$y_3 = x_3 + \eta$$

$$(4.64)$$

Where Y_t and Y_b are Young's modulus of the top and bottom surfaces of the plate respectively. V and n are the volume fraction and volume fraction index respectively. For this gradation, the shift of the reference plane relative to the mid-plane of the plate η and the shear correction factor K are determined as follows.

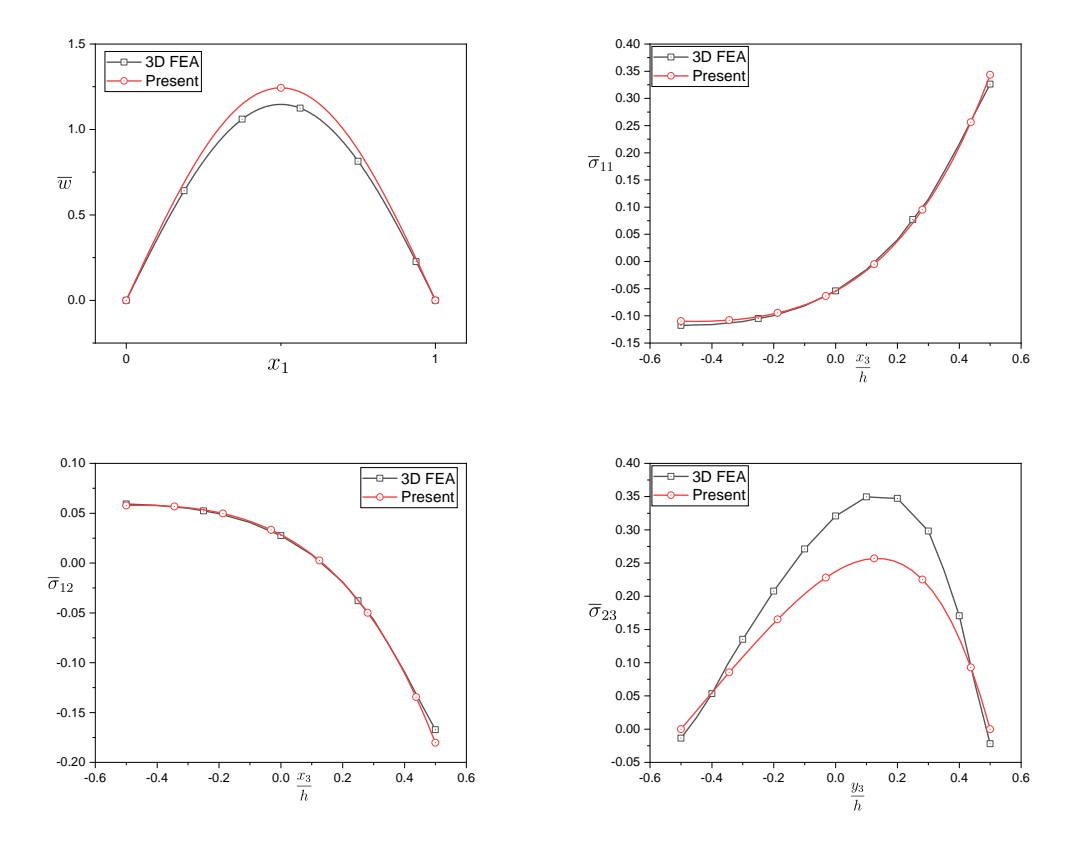


Figure 4.9: Variation of the non-dimensionalized displacement \overline{w} along the centerline of the plate and through-the-thickness variation of the different non-dimensionalized stress components $\overline{\sigma}_{ij}$ evaluated at point B (shown in Fig. 4.7) for an orthotropic square plate considered in the second example.

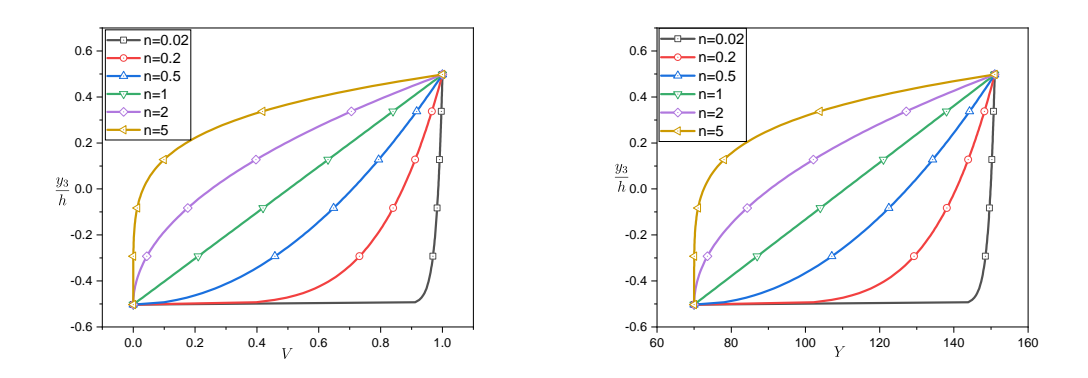
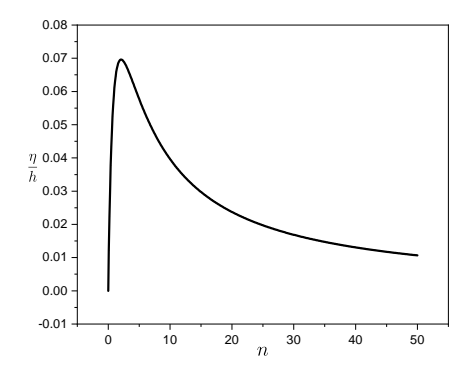


Figure 4.10: Through-the-thickness variation of the volume fraction V and Young's modulus Y of the plate considered in the third example.



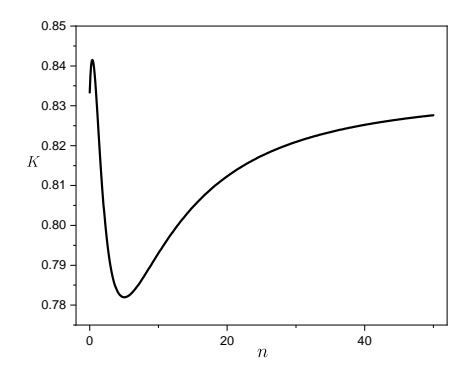


Figure 4.11: Variation of the shift of the reference plane η and shear correction factor K with volume fraction index n

$$\begin{split} \eta &= \frac{hn(Y_t - Y_b)}{2(2+n)(nY_b + Y_t)} \\ K &= \frac{(1+n)(1+\mu)}{h(nY_b + Y_t) \int_{-\frac{h}{2} - \eta}^{\frac{h}{2} - \eta} g \ dx_3} \\ g &= \frac{2^{-2-n} \left[2^n Y_b + (Y_t - Y_b) \left(1 + \frac{2x_3}{h} + \frac{n(Y_t - Y_b)}{(2+n)(nY_b + Y_t)} \right)^n \right] f^2}{1+\mu} \\ f &= -\frac{Numerator}{h^3 (2+n)(nY_b + Y_t) \left[n^2 (7 + 4n + n^2) Y_b^2 + 4n (7 + 4n + n^2) Y_b Y_t + 12 Y_t^2 \right] \left[2^n Y_b + (-Y_b + Y_t) \left(1 + \frac{2x_3}{h} + \frac{n(-Y_b + Y_t)}{(2+n)(nY_b + Y_t)} \right)^n \right]} \\ Numerator &= 3(3+n) \left[2(2+n)x_3(nY_b + Y_t) + h(1+n)(nY_b + 2Y_t) \right] \left[2(Y_b - Y_t) \left(1 + \frac{2x_3}{h} + \frac{n(-Y_b + Y_t)}{(2+n)(nY_b + Y_t)} \right)^n \right] \\ (-2(2+n)x_3(nY_b + Y_t) + h(nY_b + 2Y_t)) - 2^n (2+n)Y_b \left(-2(2+n)x_3(nY_b + Y_t) + h(1+n)(nY_b + 2Y_t) \right) \right] (1+\mu) \end{split}$$

Notably, for homogeneous materials where $Y_t = Y_b$, we have $\eta = 0$, $K = \frac{5}{6}$. These values of η and K are in agreement with literature [122, 123, 121].

For this material gradation, the strains are given as follows

$$E = \begin{cases} \frac{\partial u_1}{\partial x_1} + x_3 \frac{\partial \phi_1}{\partial x_1} + \frac{1}{2} \left(\frac{\partial u_3}{\partial x_1} \right)^2 \\ \frac{\partial u_2}{\partial x_2} + x_3 \frac{\partial \phi_2}{\partial x_2} + \frac{1}{2} \left(\frac{\partial u_3}{\partial x_2} \right)^2 \\ \frac{f\left(\phi_2 + \frac{\partial u_3}{\partial x_2}\right)}{2\int_{-\frac{h}{2} - \eta}^{\frac{h}{2} - \eta} g dx_3} \\ \frac{f\left(\phi_1 + \frac{\partial u_3}{\partial x_1}\right)}{2\int_{-\frac{h}{2} - \eta}^{\frac{h}{2} - \eta} g dx_3} \\ \frac{\partial u_1}{\partial x_2} + \frac{\partial u_2}{\partial x_1} + x_3 \left(\frac{\partial \phi_1}{\partial x_2} + \frac{\partial \phi_2}{\partial x_1} \right) + \left(\frac{\partial u_3}{\partial x_1} \right) \left(\frac{\partial u_3}{\partial x_2} \right) \end{cases}$$

$$(4.66)$$

Also for this case the stiffness matrix takes the following form

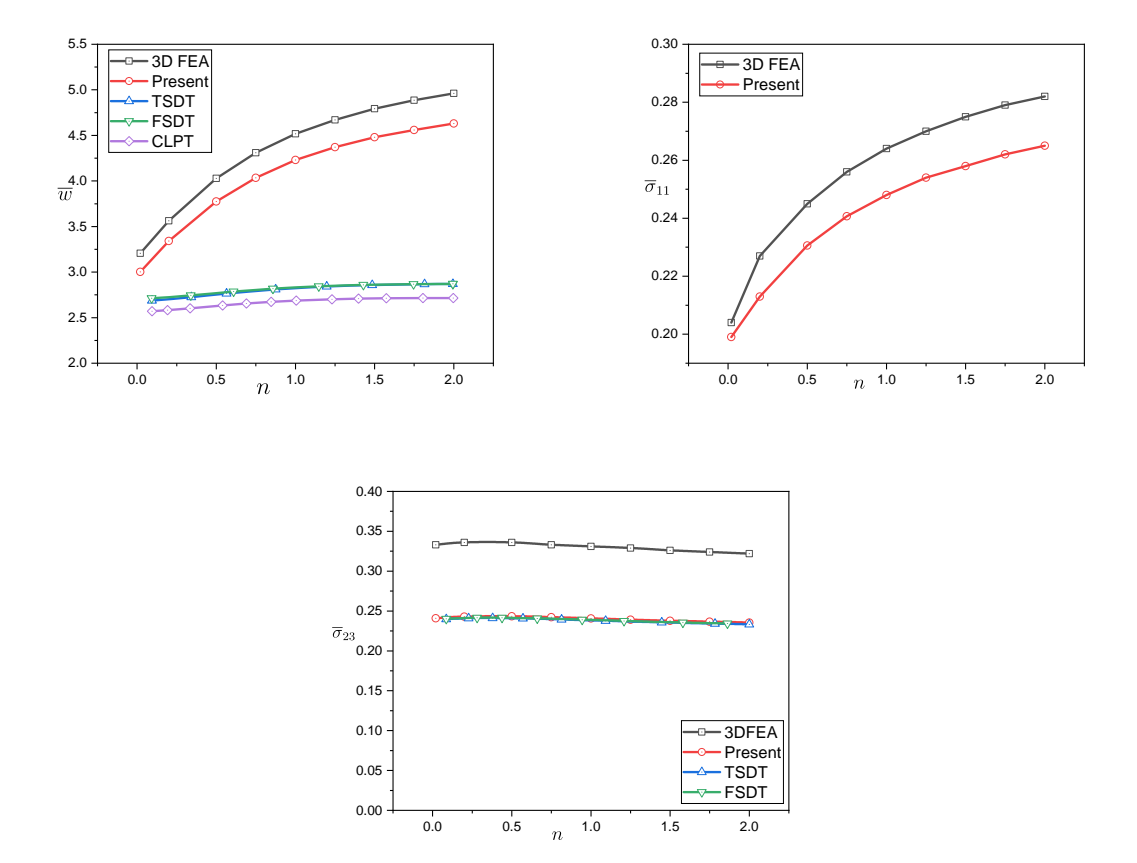
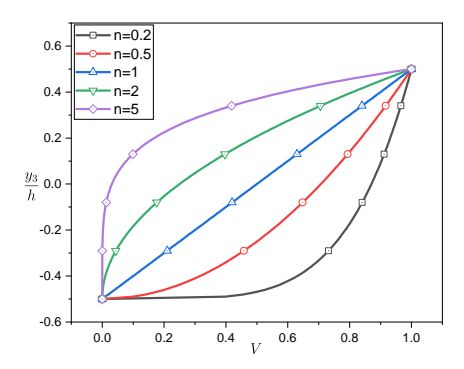


Figure 4.12: Variation of the non-dimensionalized quantities with volume fraction index for the third example. The non-denationalized displacement \overline{w} , normal stress $\overline{\sigma}_{11}$ and transverse shear stress $\overline{\sigma}_{23}$ are calculated at points $(x_1 = \frac{a}{2}, x_2 = \frac{b}{2}, y_3 = 0)$, $(x_1 = \frac{a}{2}, x_2 = \frac{b}{2}, y_3 = \frac{b}{2})$ and $(x_1 = \frac{a}{2}, x_2 = 0, y_3 = 0)$ respectively.

$$D = \frac{Y_b + (Y_t - Y_b)V}{1 - \mu^2} \begin{bmatrix} 1 & \mu & 0 & 0 & 0\\ \mu & 1 & 0 & 0 & 0\\ 0 & 0 & \frac{1-\mu}{2} & 0 & 0\\ 0 & 0 & 0 & \frac{1-\mu}{2} & 0\\ 0 & 0 & 0 & 0 & \frac{1-\mu}{2} \end{bmatrix}$$
(4.67)

A simply supported square functionally graded plate with side a=b=1 m and height h=0.1 m (i.e. $\frac{a}{h}=10$) is examined in the third example. The schematic of the plate is given in Fig. 4.7. The plate is subjected by a sinusoidally distributed load q of intensity q_0 (i.e. $q=q_0\sin\left(\frac{\pi x_1}{a}\right)\sin\left(\frac{\pi x_2}{a}\right)$). Young's modulus for the bottom and top surfaces of the plate are taken to be $Y_b=70$ GPa and $Y_t=151$ GPa respectively. Poisson's ratio for both of the materials is taken to be 0.3 [1]. The variation of the volume fraction V



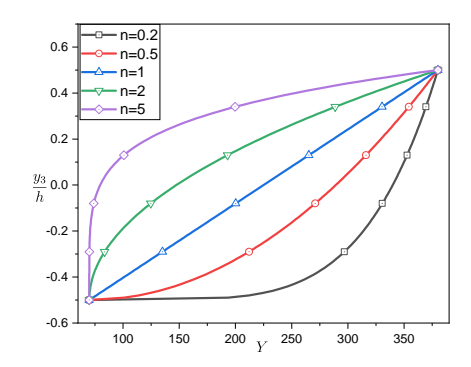
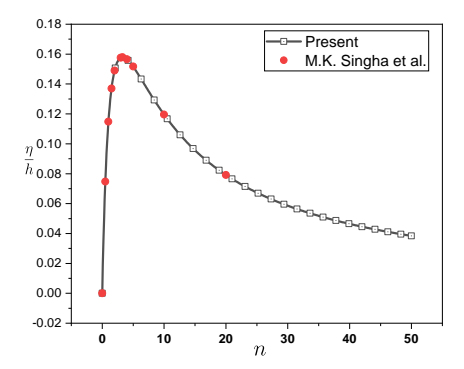


Figure 4.13: Through-the-thickness variation of the volume fraction V and Young's modulus Y of the plate considered in the second example



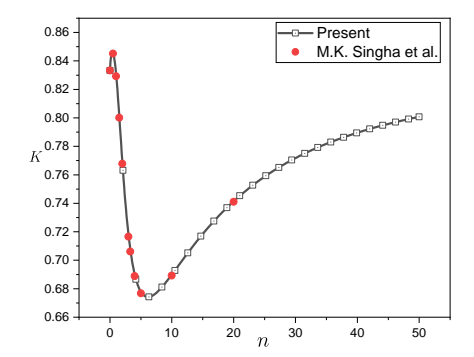


Figure 4.14: Variation of $\frac{\eta}{h}$ and K with volume fraction index n

and Young's Modulus Y of the plat along its thickness is plotted in Fig. 4.10. For varied values of volume fraction index n, keeping the other parameters constant, $\frac{\eta}{h}$ and K are plotted in Fig. 4.11.

The non-dimensionalized quantities defined in Eq. (4.63) are calculated and compared against the results given by Reddy [1] and obtained using 3D FEA approach. This comparision is presented in Fig. 4.12. The non-denationalized displacement \overline{w} , normal stress $\overline{\sigma}_{11}$ and transverse shear stress $\overline{\sigma}_{23}$ are calculated at points $(x_1 = \frac{a}{2}, x_2 = \frac{b}{2}, y_3 = 0)$, $(x_1 = \frac{a}{2}, x_2 = \frac{b}{2}, y_3 = \frac{h}{2})$ and $(x_1 = \frac{a}{2}, x_2 = 0, y_3 = 0)$ respectively.

A square simply supported functionally graded plate with side a=b=1 m and height h=0.01 m (i.e., $\frac{a}{h}=100$) is examined in the fourth example. The schematic of the plate is given in Fig. 4.7. The plate is subjected to a uniformly distributed load P acting on

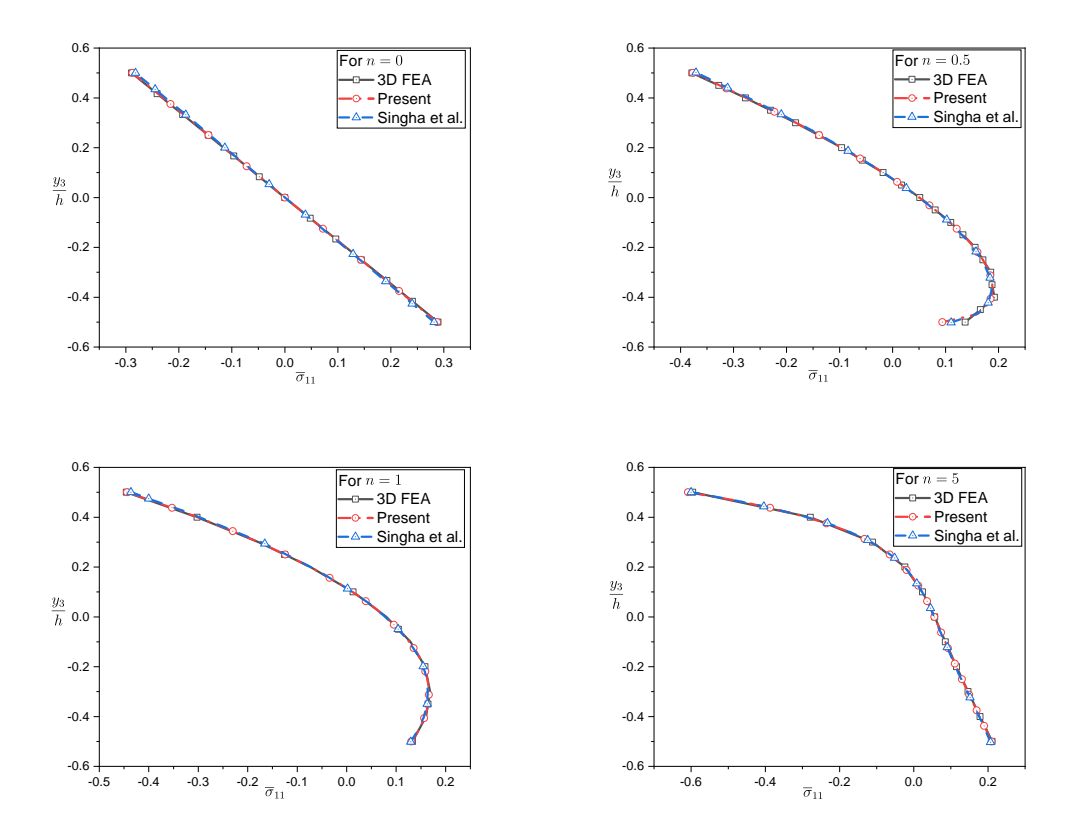


Figure 4.15: Variation of the non-dimensionalized normal stresses $\overline{\sigma}_{11}$ along the thickness of the plate for the different values of the volume fraction index n. $\overline{\sigma}_{11}$ is calculated at the middle point of the plate in the fourth example.

its bottom surface. Young's modulus for the bottom and top surfaces of the plate are taken to be $Y_b = 70$ GPa and $Y_t = 380$ GPa respectively. Poisson's ratio μ for both of the materials is taken to be 0.3 [11]. The variation of the volume fraction V and Young's Modulus Y of the plat along its thickness is plotted in Fig. 4.13. For varied values of volume fraction index n, keeping the other parameters constant, $\frac{\eta}{h}$ and K are plotted in Fig. 4.14.

The non-dimensionalized quantities defined in Eq. (4.63) are calculated and compared with the results given by Singha et al. [11] and 3D FEA. Fig. 4.15 illustrates through-the-thickness variation of the non-dimensionalized normal stress $\overline{\sigma}_{11}$ at the middle point of the plate and Fig. 4.16 presents through-the-thickness variation of the non-dimensionalized shear stress $\overline{\sigma}_{13}$ at $x_1 = a$, and $x_2 = 0$

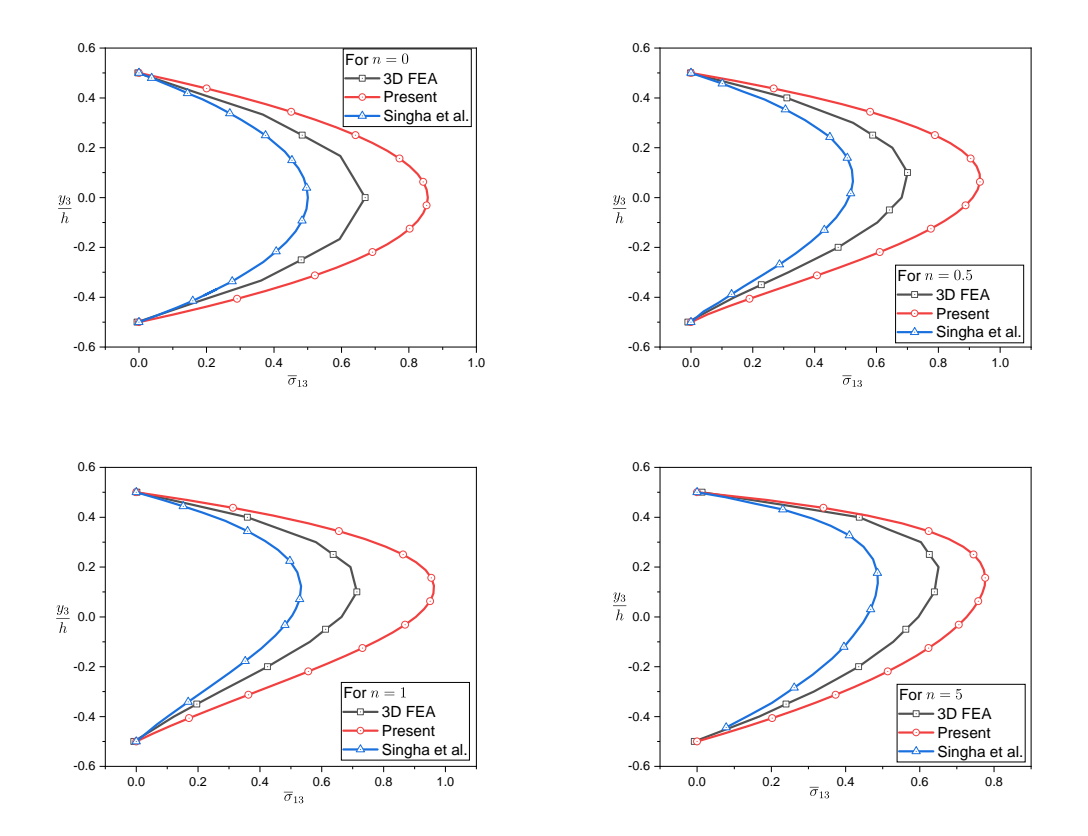


Figure 4.16: Variation of the non-dimensionalized normal stresses $\overline{\sigma}_{13}$ along the thickness of the plate for the different values of the volume fraction index n. $\overline{\sigma}_{13}$ is calculated at $x_1 = a$, and $x_2 = 0$

4.7 Conclusion

In this chapter, a novel VAM based geometrically nonlinear ESL plate theory for functionally graded plates has been developed by applying the first principles and the isoenergetic approach. Following are key highlights of the present work

- 1. This work formulates an asymptotically accurate ESL plate theory by expanding the energy function in terms of a small parameter related to the geometry of the plate and state of strain.
- 2. present work uses the first principles-based approach to reduce the 3D problem to a 2D analysis by estimating the 3D displacement field in terms of 2D variables.
- 3. The higher order 1D through the thickness analysis involves derivatives of $u_i(x_1, x_2)$

w.r.t x_{α} . The complexity involving these derivatives is eliminated by (a) slectin the reference plane suitably and (b) using the concept of isoenegetics.

- 4. Unlike most existing plate theories that assume plane stress condition, this model derives it naturally through its mathematical formulation.
- 5. It predicts an accurate quadratic variation of transverse shear stress and strain, compared to FSDT's constant value.
- 6. The quadratic variation of transverse shear stresses enforces zero tangential traction on the boundaries of the plate, reflecting realistic physical behavior.

To summarize, this work provides a more refined, accurate, and computationally efficient ESL plate theory for thin and moderately thick functionally graded plate structures.

Chapter 5

Analysis of Stiffened Plates

5.1 Introduction

Stiffened plates are a fundamental building block in many engineering applications. They consist of a thin plate reinforced with elements called stiffeners, which can be bars, ribs, or other shapes. Depending on the positioning of the stiffeners, the stiffened plates are classified as: (a) symmetric stiffened plates (b) assymetric stiffened plates. Symmetric stiffened plates have stiffeners arranged in a mirrored pattern on either side of the plate, creating a symmetrical structure. Asymmetric stiffened plates have an uneven distribution of stiffeners. This asymmetry can result from design considerations, loading conditions, or specific structural requirements. Stiffened plates find application in various engineering fields where structural efficiency, high load capacity, and the ability to tailor performance to specific needs are crucial. Some common applications include

- 1. **Aerospace:** Stiffened plates are used in aircraft fuselages, wings, and structural components to provide strength, rigidity, and aerodynamic performance.
- 2. **Automotive:** They find application in vehicle chassis, frames, and body panels to enhance structural integrity, crashworthiness, and weight efficiency.
- 3. Marine: Stiffened plates are employed in ship hulls, decks, and superstructures to withstand hydrodynamic forces, wave loads, and structural stresses.
- 4. **Civil Engineering:** They are used in bridges, buildings, and infrastructure projects to support heavy loads, resist seismic forces, and ensure long-term durability.

Researchers employ diverse formulations to consider the impact of stiffeners, leading to significant variations between different approaches. Some of these formulations encompass the orthotropic plate approximation, the grillage approximation, and the plate beam idealization. Initially, earlier investigators approximated the effects of stiffeners by distributing them across the plate and treating the structure as an orthotropic system. This method produced satisfactory outcomes when the spacing between stiffeners was minimal [42, 36]. In the grillage approximation, the plate's effects are incorporated into the stiffener by increasing the beam's second moment of area [41, 40]. However, determining the effective width, which serves as a hypothetical flange representing the plate in the beam, poses a challenge in this approximation. In the most general scenario, the plate and stiffener are separately analyzed [39, 38, 37]. Then, by ensuring equilibrium and continuity along the attachment line, the plate and beam are made compatible.

Deb et al. [36] proposed an approximate shear deformation theory for stiffened plates based on the Reissner-Mindlin plate theory and Timoshenko beam theory, utilizing the smeared-out idealization. Mukherjee et al. [35], Sadek et al. [34], Biswal et al. [33], and Ghosh et al. [32] presented finite element methods based on a higher-order shear deformation theory (HSDT) for static and vibrational analysis of laminated stiffened plates. Bhar et al. [31] compared the finite element results of composite stiffened plates using the firstorder shear deformation theory (FSDT) and HSDT. They strongly recommended the use of HSDT over the Classical Plate Theory and even FSDT, particularly for thick panels. Sapountzakis et al. [30] introduced an optimized model based on the classical approach that considers the in-plane forces and displacements at the interface of the plate and the beam. By comparing their results with various finite element models, they emphasized the significance of considering in-plane shear forces for a more accurate description of the stiffened plate's behavior. Qing et al. [29] developed a three-dimensional solution for the free vibrations of stiffened plates using the variational approach, employing finite elements to solve state vector equations. The model automatically incorporates transverse shear deformations and rotary inertia. Kamineni et al. [28] used VAM for the analysis of laminated composite flat stiffened panels. In their approach, they modeled the stiffened plate using VAM, and then they attached a stiffener with the plate. The integration of skin and the stiffener technique was used by introducing a constraint matrix. Chen Jiaqi et al. [27] did a static and dynamic analysis of Isogrid Stiffened Composite Plates (ISCP) using an equivalent model based on VAM.

The present approach considers the stiffener reinforced plate as one continuous struc-

ture with varying material properties in the thickness direction instead of a combination of two structures (stiffener and plate). VAM is used to systematically reduce the dimension of the stiffener reinforced structure up to a desired level of accuracy by taking advantage of the smallness of the thickness of the structure as compared to the other two dimensions. The framework developed in chapter-2, chapter-3, and chapter-4 forms the basis for obtaining a reduced order model for the stiffened plates. In what follows, this approach is elucidated.

5.2 Methodology Used

The present work treats the stiffened plate as a single structure with a position-dependent through-the-thickness configuration. This captures the effect of the stiffeners in a natural way by performing through-the-thickness 1D analysis for each distinct section of the plate by leveraging the framework established in Chapters 2, 3, and 4. Consequently, a reduced-order two-dimensional (2D) model is obtained for stiffened plates. Figure 5.1 illustrates this approach for the symmetric stiffened plates where the mid-plane of the plate is taken as its reference plane due to the symmetry of the structure about this plane.

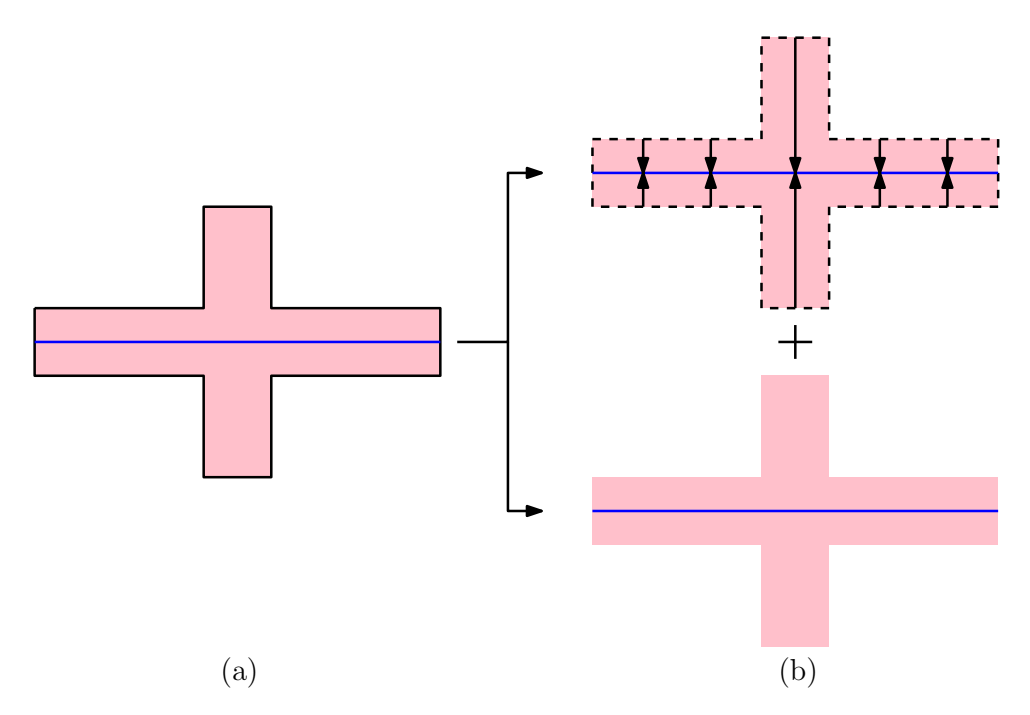


Figure 5.1: Approach used for the analysis of the symmetric stiffened plates (a) symmetric stiffened plate (b) splitting of the analysis in through-the-thickness 1D analysis and inplane 2D analysis

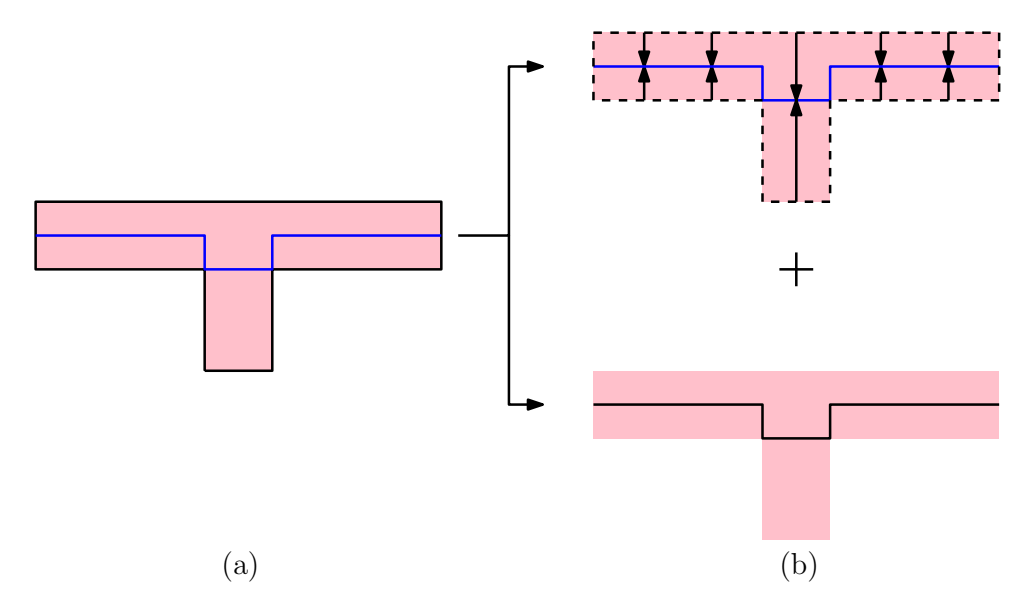


Figure 5.2: Approach used for the analysis of the asymmetric stiffened plates (a) asymmetric stiffened plate with its reference plane (b) splitting of the analysis in through-the-thickness 1D analysis and in-plane 2D analysis

In the case of assymetrically stiffened plates, the geometric discontinuity caused by the stiffeners results in a localized shift in the reference plane at the attachment region of the plate and the stiffeners. To handle this, in this work, we assume that the interface of the plate and stiffeners becomes the reference plane at the locations where they are attached, and for the rest of the plate, the mid-plane of the plate is the reference plane (as shown in Fig. 5.2).

It is important to note that the present approach leads to inaccurate normal and shear stresses within the width of the stiffeners. This inaccuracy arises because, during 1D through-the-thickness analysis, the zero traction boundary conditions were not imposed at the surfaces of the stiffeners perpendicular to the width direction of the stiffeners. To address this issue, consider a representative section of a stiffener as shown in Fig. 5.3. We define a local coordinate system (y_1, y_2, y_3) with axes lying along the length, width, and height directions of the stiffener respectively. The displacement components along these directions are denoted as w_1 , w_2 , and w_3 . To eliminate the inaccurate stresses, it is assumed that the displacement components w_1 and w_3 are constant across the width $(y_2$ direction) of the stiffener section. Additionally, The displacement component w_2 is assumed to be zero. These assumptions, taken from the classical beam theories [26], simplify the analysis by focusing on the primary stiffening effect and eliminate the introduction of overvalued stresses in the width direction.

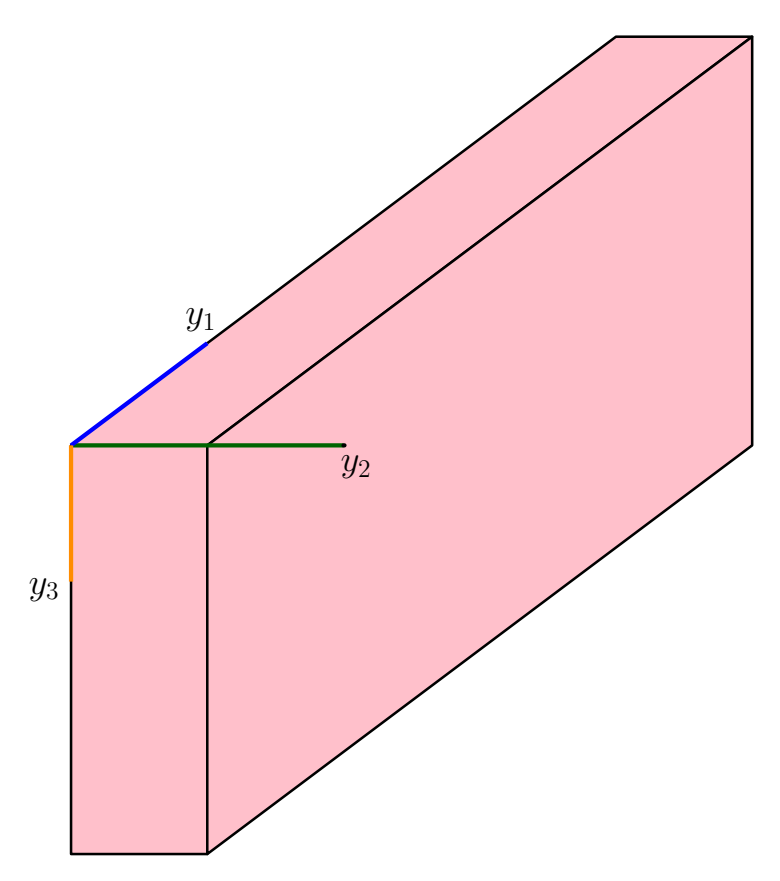


Figure 5.3: Approach used for the analysis of the symmetric stiffened plates (a) symmetric stiffened plate (b) splitting of the analysis in through-the-thickness 1D analysis and inplane 2D analysis

5.3 Results and discussion

In the first example, a square plate with two symmetric stiffeners (one along the x_1 axis and the other along the x_2 axis) is analysed. the geometry of the stiffened plate is given in Fig. 5.4 where a=1.016 m, t=2.54 cm, h=5.08 mm and H=5.08 mm. The plate is mate of homogeneous isotropic material with young modulus E=206.843GPa and poisions ratio $\nu=0.3$. The plate is simply supported. Due to symmetry only one quarter of the plate is modeled. the boundary conditions are taken as given below

$$u_1 = u_2 = u_3 = \phi_2 = 0$$
 at $x_1 = \frac{a}{2}$
 $u_1 = u_2 = u_3 = \phi_1 = 0$ at $x_2 = \frac{a}{2}$
 $u_1 = \phi_1 = 0$ at $x_1 = 0$
 $u_2 = \phi_2 = 0$ at $x_2 = 0$ (5.1)

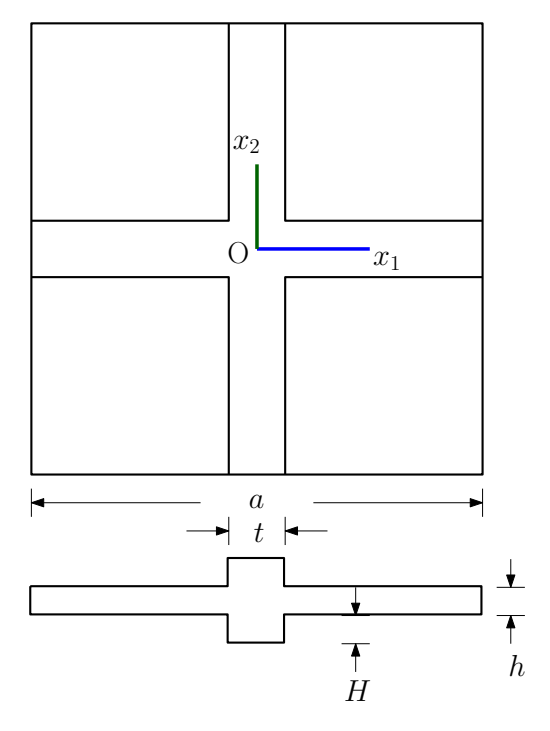


Figure 5.4: Geometry of the plate with symmetric stiffeners considered in the first example

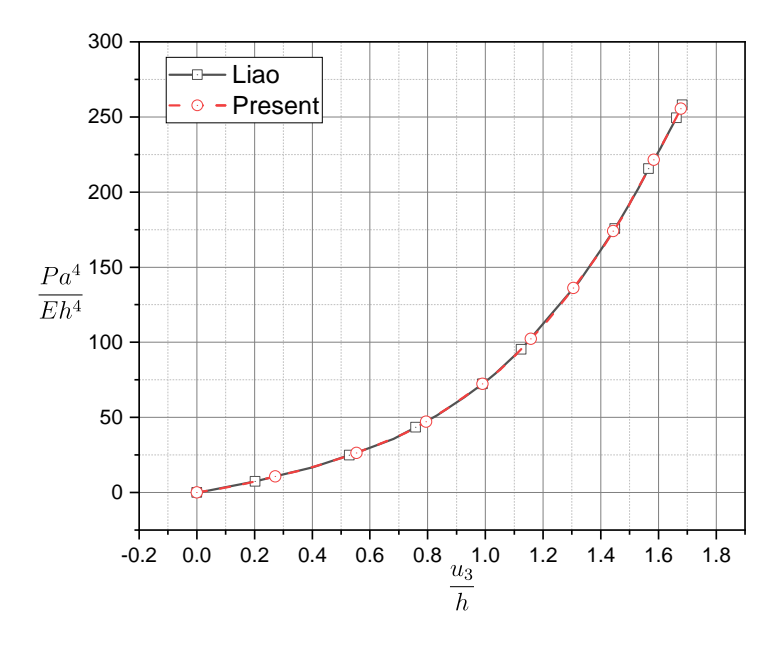


Figure 5.5: Load deflection curve for the mid point of the plate with symmetric stiffeners considered in the first example

Fig. 5.5 shows the deflection of the mid point O of the plate. the results obtained using the present approach are in good aggreement with those given by Liao et al. [61].

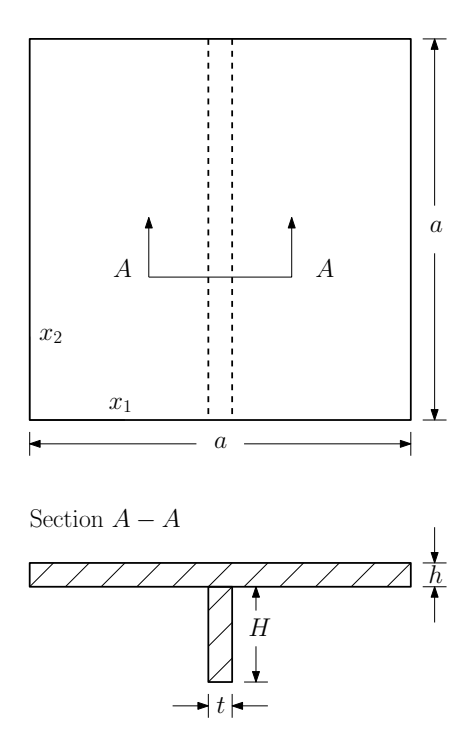


Figure 5.6: Geometry of the plate with an asymmetric stiffener considered in the second example

In the second example, a square plate with an asymmetric stiffener oriented along the x_2 axis and passing through the center of the plate is analyzed. the geometry of the stiffened plate is given in Fig. 5.6 where a=2.54 cm, t=0.254 mm, h=0.254 mm and H=2.54 mm. The plate is made of homogeneous isotropic material with young modulus E=117.2109 GPa and positions ratio $\nu=0.3$. The plate is simply supported at all its edges.

Fig. 5.7 shows the deflection of the asymmetric stiffened plate considered in the second example along its centerlines parallel to the x_1 and x_2 axes. the results obtained using the present approach are in good agreement with those given by A Islam et al. [61] and Chattopadhyay et al. [25].

In the third example, a square stiffened plate with a side length of 1 m is considered. The depth of the plate is 1 cm and the depth of the stiffener is 5 cm. The plate is reinforced by two stiffeners lying along the x_1 axis. The stiffeners, shown in Fig. 5.8, are placed at a distance of 30 cm from the edges of the plate. The distance between

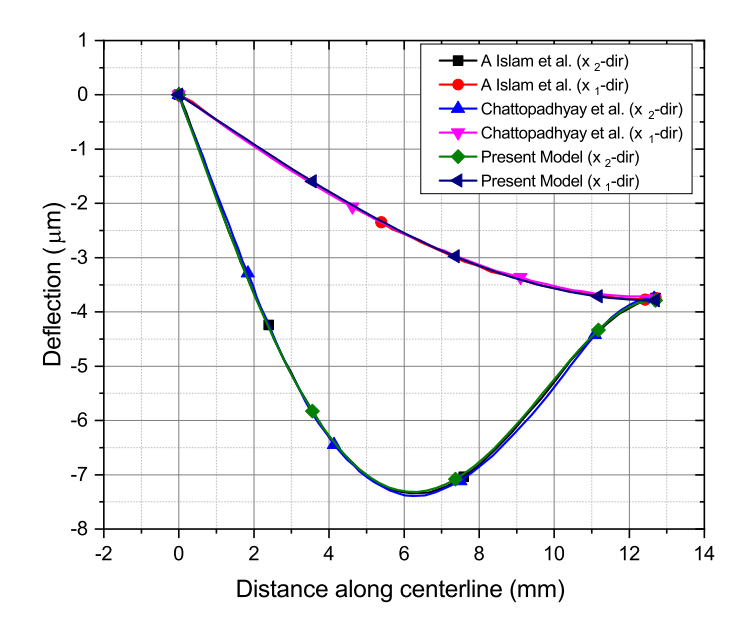


Figure 5.7: Deflections along the centerlines of the plate parallel to the x_1 and x_2 axis

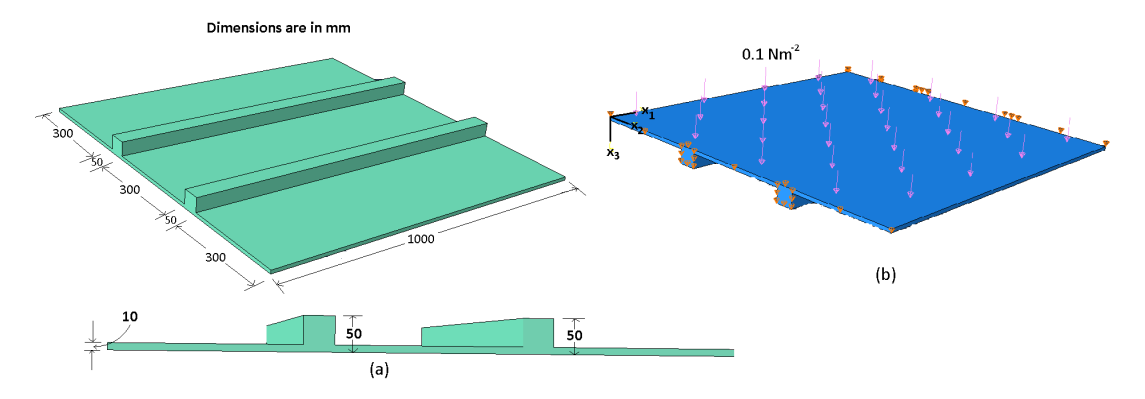


Figure 5.8: (a) Dimensions (b) Loading conditions

the stiffeners is 30 cm. The whole structure is made of homogeneous isotropic material with Young's Modulus of $E=200\times 10^9~Pa$ and Poissons ratio of $\nu=0.3$. The two edges perpendicular to the stiffeners are kept simply supported, and the other two are free. Uniform pressure load $P=0.1~Nm^{-2}$ is applied at the bottom surface of the plate as shown in Fig. 5.8

Fig. 5.9 shows the deformation pattern of the stiffened structure as obtained by the present approach and the 3D FEA.

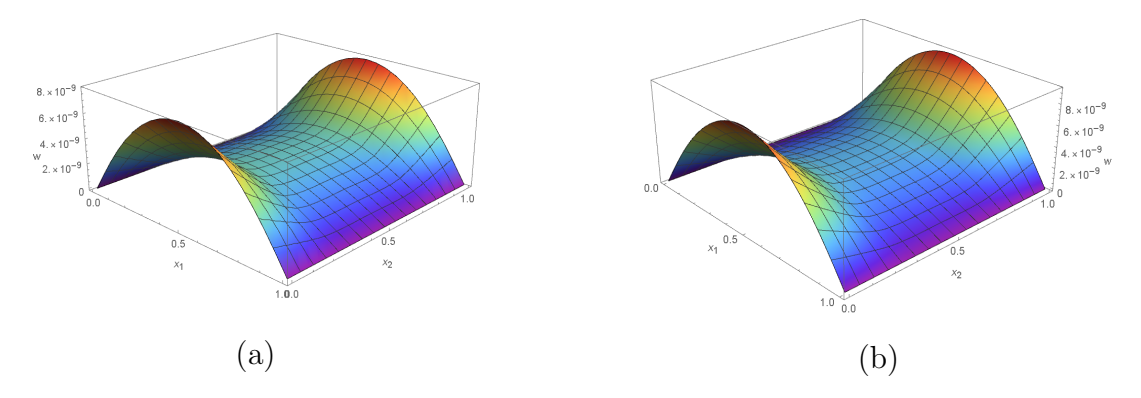


Figure 5.9: Deflection in x_3 direction (a) present work (b) 3-D FEA result

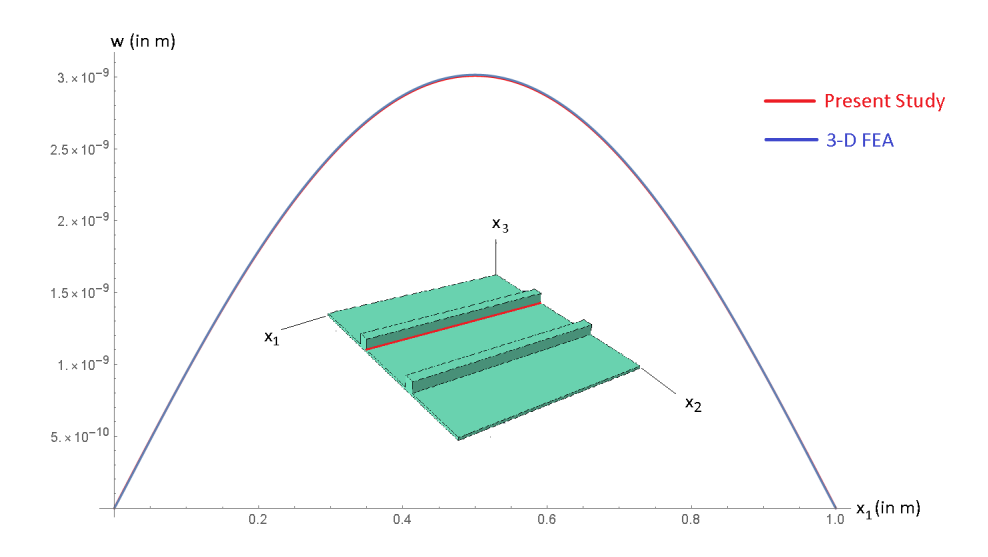


Figure 5.10: Comparison of result with 3-D FEA and present result

The interface deformation response of the structure was studied by the present approach and compared with that obtained by the 3-D FEA. Fig. 5.10 shows the displacement of the stiffened plate in x_3 direction along the path highlighted in red colour.

Fig. 5.11 shows the percentage error in the results obtained by the present approach and the 3-D FEA. Thus the result is in good agreement with that of the 3-D FEA.

In the fourth example, a rectangular stiffened plate with a length of a = 0.21 m and width of b = 0.20 m is considered as shown in Fig. 5.12(a). The depth of the plate h is 2 mm. The plate is reinforced by a stiffener lying along the x_1 axis and placed in the middle of the plate. The depth of the stiffener H is 8 mm as shown in Fig. 5.12(b). The whole structure is made of an anisotropic material with the following material properties

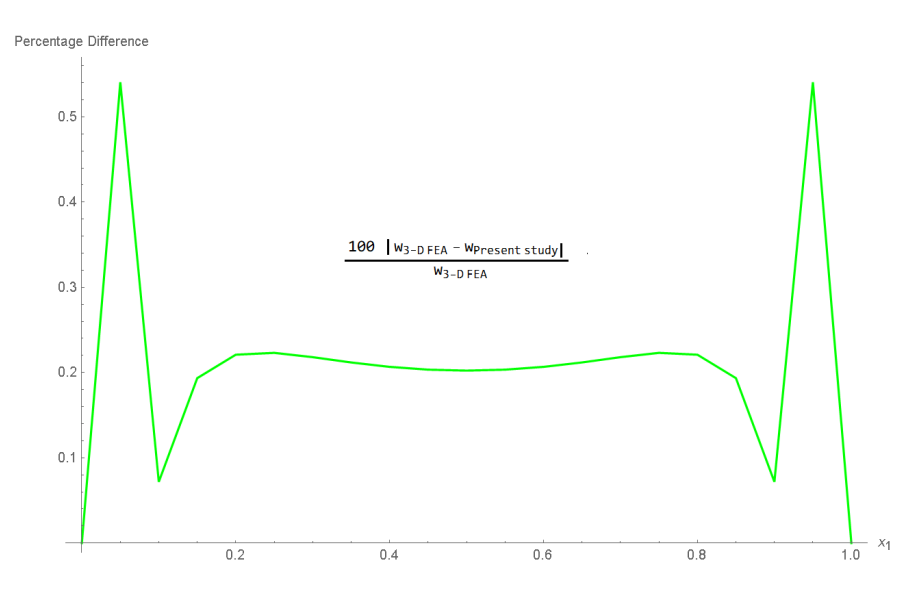


Figure 5.11: Percentage error

[116]:
$$E_L = 25 \times 10^6 \text{ psi } (172.369 \text{ GPa})$$

$$E_T = 1 \times 10^6 \text{ psi } (6.895 \text{ GPa})$$

$$G_{LT} = 0.5 \times 10^6 \text{ psi } (3.337 \text{ GPa})$$

$$G_{TT} = 0.2 \times 10^6 \text{ psi } (1.379 \text{ GPa})$$

$$\nu_{LT} = \nu_{TT} = 0.25$$

$$L : \text{Longitudinal direction } (x_1)$$

$$T : \text{Transverse direction } (x_2, x_3)$$

The plate is clamped at all of its edges as shown in Fig. 5.12(c). Uniform pressure load $P = 500 \text{ Nm}^{-2}$ is applied at the bottom surface of the plate as shown in Fig. 5.12(b).

Fig. 5.13 displays the variation of the displacement component u_3 with respect to x_1 and x_2 for the fourth example. Fig. 5.13(a) was generated using the 3D FEA approach, while Fig. 5.13(b) was produced using the present approach. Fig. 5.14 illustrates the variation of the percentage error in the value of u_3 with respect to x_1 and x_2 . The percentage error (PE) is defined in Eq. (5.3).

$$PE = 100 \left| \frac{u_{3,\text{FEA}} - u_{3,\text{Present}}}{u_{3,\text{FEA}}^{max}} \right|$$
 (5.3)

Where $u_{3,\text{FEA}}$ and $u_{3,\text{Present}}$ are values of u_3 obtained using the 3D FEA and Present approaches. $u_{3,\text{FEA}}^{max}$ is the maximum value of $u_{3,\text{FEA}}$. Figure 5.14 demonstrates that the

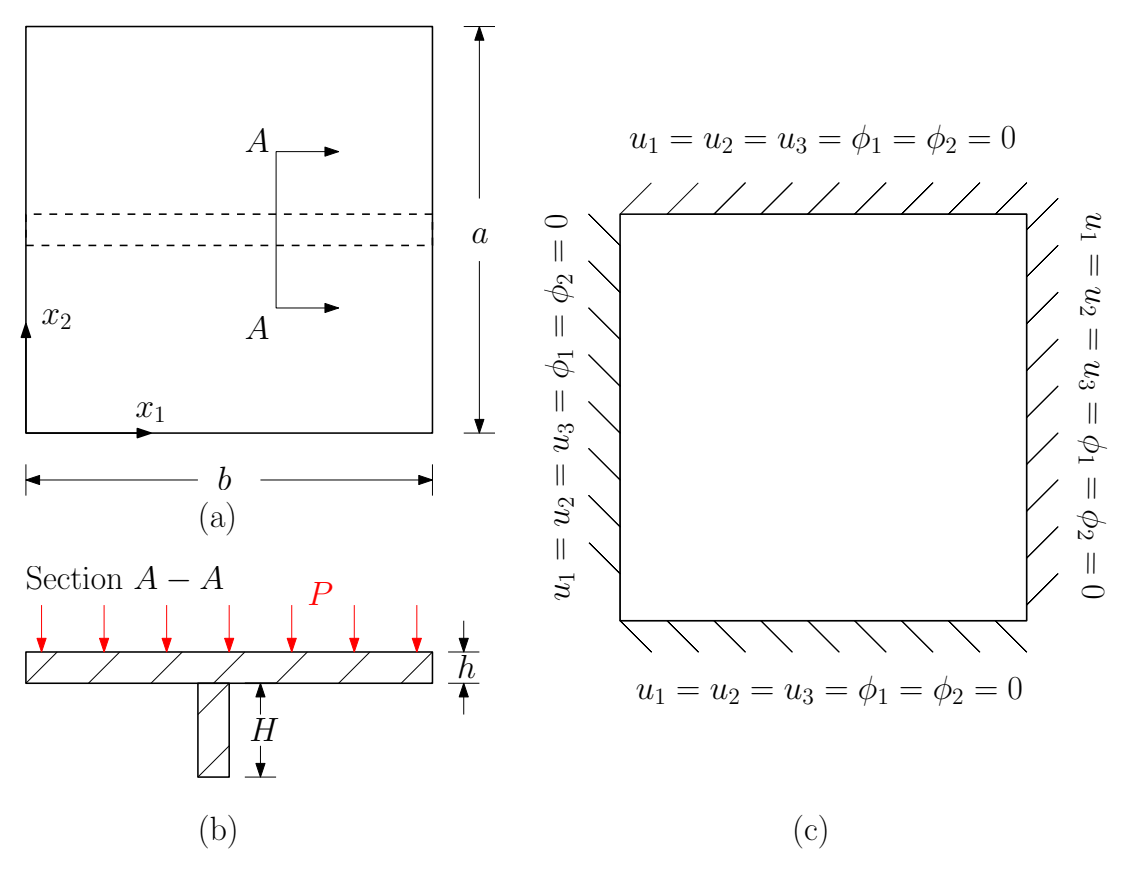


Figure 5.12: Stiffened plate analyzed in the fourth example (a) in plane geometry of the plate (b) through-the-thickness structure of the plate and loading condition (c) boundary conditions

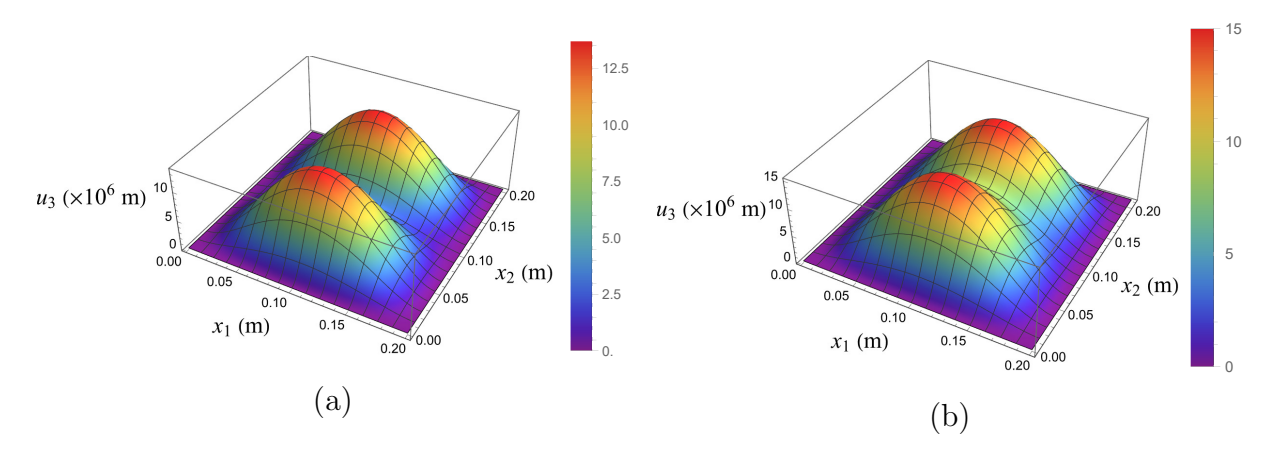


Figure 5.13: Out-of-plane deflection of the plate considered in the fourth example. The results are obtained using (a) 3D FEA approach (b) present approach

CHAPTER 5 5.4. CONCLUSION

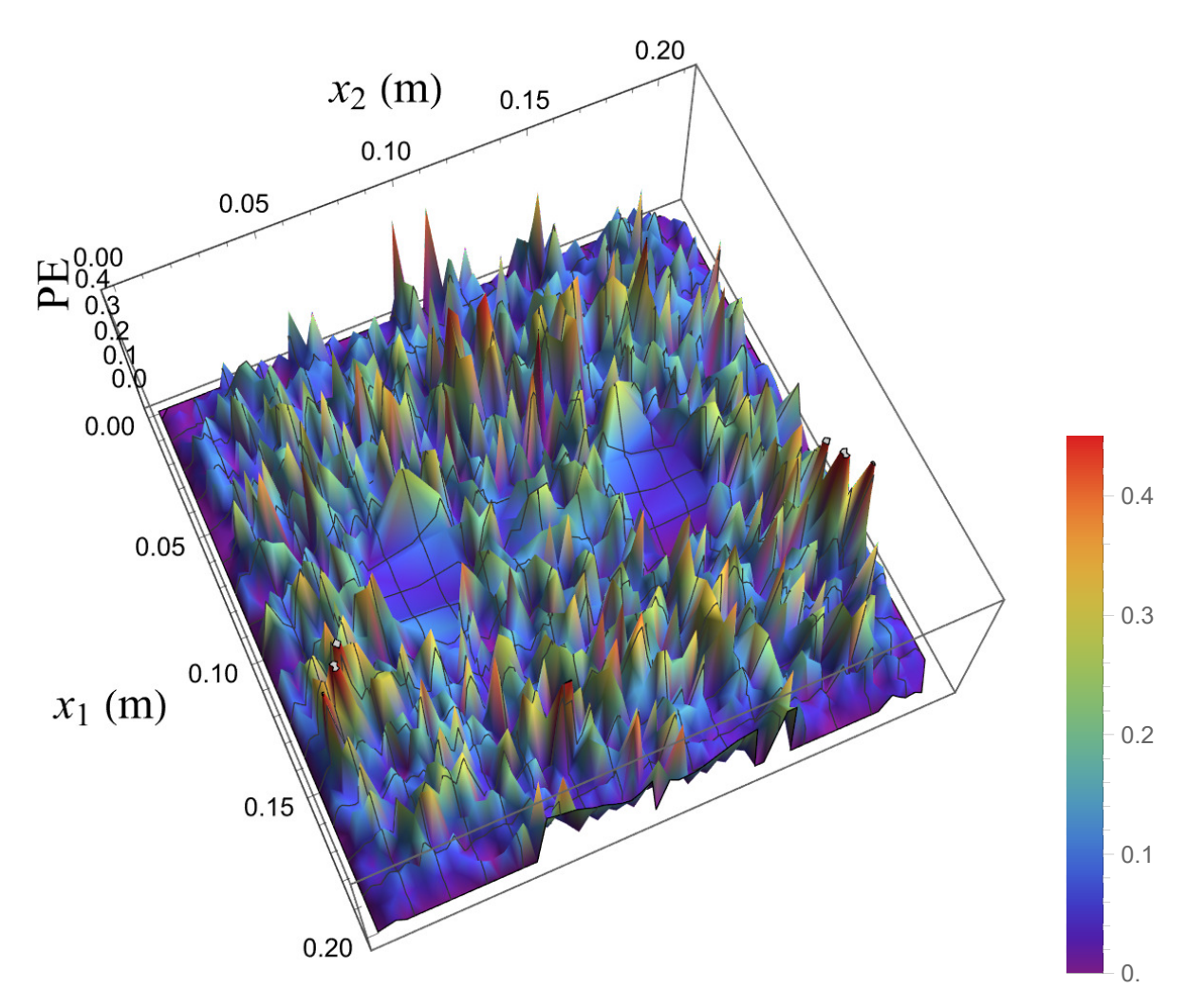


Figure 5.14: Percentage error in the out of plane deflection u_3 for the fourth example results obtained by the 3D FEA and the present approach are in very good agreement.

5.4 Conclusion

This approach treats the stiffened plates as structures with varying through-the-thickness structure. To exploit the thin nature of the structure compared to its in-plane dimensions, the Variational Asymptotic Method (VAM) is employed. This method systematically reduces the dimensionality of the problem, leading to computationally efficient solutions. The good agreement between the results obtained using this approach and those reported in the literature validates its effectiveness.

Chapter 6

Conclusion and Future Scope

This thesis introduces a novel VAM based reduced-order model for geometrically nonlinear analysis of plate-like structures. This reduced-order model efficiently handles structures where one dimension is significantly smaller than the other two. The model's versatility has been demonstrated through successful application to various plate configurations, including anisotropic plates, multilayer composite plates, functionally graded plates, and stiffened plates. Results obtained using the proposed reduced-order model show excellent agreement with benchmark problems from the literature and with those obtained from 3D finite element analysis. A brief summary of the work presented in this thesis is given below.

6.1 Summary

A literature survey has been carried out on stiffened plates and approaches used for their analysis. The following key research gaps were found.

- 1. Most of the reduced order theories are presupposition based and relies on *ad hoc* and *a priori* assumptions.
- 2. A number of Assymptotically correct plate theories are available, however the have folloing shortcomings
 - (a) Relies on pre-assumed kinematics of plate
 - (b) In most of the literature asymptotic expansion is done relying on the assumed orders of relevant quantities.

(c) Higher order derivatives of the primary variables are eliminated following a mathematically complex extremization process done at the expense of the asymptotic correctness of the theory.

A novel, asymptotically accurate equivalent single layer (ESL) theory has been introduced to address limitations in existing theories and analyze the geometrically nonlinear behavior of anisotropic plates. This development lays the foundation for subsequent analyses. The theory developed for anisotropic plates has been extended to analyze multilayered symmetric composite plates. A key aspect is ensuring the continuity of displacements and transverse stresses across layers, which is absent in classical ESL theories. Additionally, a novel approach for calculating shear correction factors is introduced, significantly reducing computational complexity while maintaining high accuracy. Building upon these advancements, the framework was further extended to tackle functionally graded (FG) plates with varying material properties. The optimal reference plane location within the FG plate was determined, and a new ESL theory for FG plates was developed using VAM and the established isoenergetic concept. This approach results in an accurate and computationally efficient ESL plate theory for FG plates. Finally, the developed theoretical frameworks were adapted to analyze both symmetric and asymmetric stiffened plates, presenting a systematic approach for efficient and accurate analysis

6.2 Key highlights of present work

- 1. The dimensional reduction using VAM is based on first principles, avoiding reliance on pre-assumed kinematics of the plate and assumptions regarding the order of different quantities of interest.
- 2. A bound on thickness to length ratio $\left(\frac{h}{l}\right)$ and supnorm of strains has been used for the asymptotic expansion. In the energy functional this translates to asymptotic expansion in powers of (ξ) . The analysis with strain energy accurate up to the order of $(\xi^8\mu)$ results in analytic expressions for displacement vector and strains accurate up to order of (ξ^4h) and (ξ^4) respectively. It is observed from the results that the diminishing value of small parameter $\left(\frac{h}{l}\right)$ improves the accuracy, aligning them more closely with the results obtained from 3D FEA. Therefore it becomes evident that the proposed model is asymptotically accurate and demonstrates satisfactory performance for thin and moderately thick plates.

- 3. It is interesting to observe that the zeroth order solution results in the estimation of 3D displacement field in terms of 2D variables $u_i(x_1, x_2)$. Essentially, this leads to the dimensional reduction of 3D problem to 2D, which is assumed a priori in classical plate theories.
- 4. The reference plane is not chosen *a priori*. It is selected in a mathematically justified manner.
- 5. The higher order 1D through the thickness analysis involves derivatives of $u_i(x_1, x_2)$ w.r.t x_{α} . The complexity involving these derivatives is eliminated through a novel isoenegetic approach and choosing the reference plane suitably resulting in better estimation of the overall deformation.
- 6. It may be noted that most of the plate theories rely on the *ad hoc* assumption of plane stress condition as an integral part of their formulation. However, it is interesting to observe that the plane stress condition is a natural consequence of the mathematical procedure adopted in the present formulation.
- 7. The proposed model as well as the FSDT estimates strains up to the same order of accuracy resulting in comparable levels of computational complexities and cost. However, due to its asymptotic correctness, the current model has the following advantages over FSDT model
 - i. FSDT addresses shear effects by assuming a constant distribution of transverse shear strains throughout the thickness. However, this study reveals that the actual asymptotic distribution of transverse shear strains follows a series of quadratic curves.
 - ii. Unlike FSDT, the present work ensures the continuity of the transverse stresses along the thickness direction and zero tangential traction boundary conditions on the surface of the plate, ensuring excellent agreement with the expected physical behavior.
 - iii. Unlike FSDT there is no need for shear correction factor.

To summarize, this work provides a more refined, accurate, and computationally efficient reduced order theory applicable for thin and moderately thick plate like structures. Comparison with established theories such as CLPT, FSDT, R-TSDT and 3D FEA demonstrates the accuracy of the present work.

6.3 Scope of Future Research

The proposed framework for analyzing plate-like structures has demonstrably yielded successful results across various applications. Based on these implementations, there is significant potential to further refine and broaden the capabilities of present framework for tackling a wider range of engineering problems. Here are some promising avenues for future exploration:

- 1. Extension to Stiffened/Unstiffened Shell Structures: The developed framework can be adapted and extended to analyze shell-type structures, both stiffened and unstiffened. Investigating the behavior of such structures under various loading conditions and geometries would be valuable for practical applications in aerospace, automotive, and maritime industries.
- 2. Handling Material Non-linearity: Extending the analysis to incorporate material non-linearity would be a significant advancement. Investigating the behavior of stiffened/unstiffened plates under non-linear material models such as plasticity, viscoelasticity, or damage mechanics could provide insights into the structural response under realistic loading scenarios.
- 3. Multi-physics Problems: The framework could be extended to handle multiphysics problems, such as the interaction between mechanics, heat transfer, and moisture diffusion. This would be particularly relevant for analyzing composite materials commonly used in aerospace and marine structures.
- 4. Handling Asymmetric Composite Plates: Extending the analysis to handle asymmetric composite plates would further enhance the applicability of this framework.
- 5. Buckling and Dynamic Problems: Addressing buckling and dynamic problems would be crucial for understanding the stability and dynamic response of stiff-ened/unstiffened structures. Developing methodologies to predict critical buckling loads and natural frequencies, as well as studying the dynamic behavior under transient loads, would be valuable for structural design and optimization.

With these future scopes, this work can continue to contribute significantly to the advancement of structural analysis and design, with implications for various engineering applications.

Bibliography

- [1] J. N. Reddy, "Analysis of functionally graded plates," *International Journal for Numerical Methods in Engineering*, vol. 47, no. 1-3, pp. 663–684, Jan. 2000.
- [2] W. Yu, Simplified Formulation of Mechanics of Structure Genome, AIAA Journal, vol. 57, no. 10, pp. 4201–4209, 2019. DOI: https://doi.org/10.2514/1.J057500.
- [3] Amandeep, Abhay Mahajan, and Srikant Padhee, Analysis of Functionally Graded Cylinders for Different Gradation Law under Coupled Thermo-Mechanical Loading, vol. 7, pp. 21-25, Nov. 2018.
- [4] M. M. Alinia and S. A. M. Ghannadpour, *Nonlinear analysis of pressure loaded FGM plates, Compos. Struct.*, vol. 88, no. 3, pp. 354-359, 2009. DOI: https://doi.org/10.1016/j.compstruct.2008.04.013.
- [5] Caliri, Mauricio F., Antonio Joaquim Mendes Ferreira and Volnei Tita, A review on plate and shell theories for laminated and sandwich structures highlighting the finite element method, Composite Structures 156, 63-77, 2016.
- [6] Luciano Demasi, $\infty 6$ Mixed plate theories based on the Generalized Unified Formulation. Part I: Governing equations, Composite Structures, vol. 87, no. 1, pp. 1-11, 2009. DOI: https://doi.org/10.1016/j.compstruct.2008.07.013.
- [7] Erasmo Carrera, Theories and Finite Elements for Multilayered Plates and Shells: A Unified compact formulation with numerical assessment and benchmarking, Arch. Comput. Methods Eng., vol. 10, no. 3, pp. 215-296, 2003. DOI: https://doi.org/10.1007/BF02736224.
- [8] Erasmo Carrera, Angelo Ciuffreda, A unified formulation to assess theories of multilayered plates for various bending problems, Composite Structures, vol. 69, no. 3, pp. 271-293, 2005. DOI: https://doi.org/10.1016/j.compstruct.2004.07.003.
- [9] P. Vidal, L. Gallimard, O. Polit, E. Valot, Analysis of functionally graded plates based on a variable separation method, Mechanics of Advanced Materials and Structures, vol. 29, no. 26, pp. 4890-4901, 2022. DOI: https://doi.org/10.1080/15376494. 2021.1942597.

- [10] Silvia Marzavan, Vasile Nastasescu, Displacement calculus of the functionally graded plates by finite element method, Alexandria Engineering Journal, vol. 61, no. 12, pp. 12075-12090, 2022. DOI: https://doi.org/10.1016/j.aej.2022.06.004.
- [11] M.K. Singha, T. Prakash, M. Ganapathi, Finite element analysis of functionally graded plates under transverse load, Finite Elements in Analysis and Design, vol. 47, no. 4, pp. 453-460, 2011. DOI: https://doi.org/10.1016/j.finel.2010.12.001.
- [12] T.-K. Nguyen, K. Sab, G. Bonnet, First-order shear deformation plate models for functionally graded materials, Composite Structures, vol. 83, no. 1, pp. 25-36, 2008. DOI: https://doi.org/10.1016/j.compstruct.2007.03.004.
- [13] J. Sunil Kumar, M. Sundeep, M. Baddepudi, Analytical study on bending behaviour of plates made of functionally graded materials using higher-order shear, Materials Today: Proceedings, vol. 23, 2023. DOI: https://doi.org/10.1016/j.matpr.2023.06.239.
- [14] Z. Zong, X. Li, M. Li, M. M. Chiaramonte, W. Matusik, E. Grinspun, K. Carlberg, C. Jiang, P. Y. Chen, Neural Stress Fields for Reduced-order Elastoplasticity and Fracture, in Proceedings of the ACM Symposium on Computer Animation, 2023. DOI: https://doi.org/10.1145/3610548.3618207.
- [15] Q. Wang, K. M. Liew, A Theory for Reduced Order Control Design of Plate Systems, Journal of Applied Mechanics, vol. 64, no. 3, pp. 532-537, Sep. 1997. DOI: https://doi.org/10.1115/1.2788925.
- [16] R.C. Batra, M. Porfiri, D. Spinello, Reduced-order models for microelectromechanical rectangular and circular plates incorporating the Casimir force, International Journal of Solids and Structures, vol. 45, no. 11, pp. 3558-3583, 2008. DOI: https://doi.org/10.1016/j.ijsolstr.2008.02.019.
- [17] Islam M. El-Galy, Bassiouny I. Saleh, Mahmoud H. Ahmed, Functionally graded materials classifications and development trends from industrial point of view, SN Applied Sciences, vol. 1, no. 11, Oct. 2019. DOI: https://doi.org/10.1007/ s42452-019-1413-4.
- [18] Amandeep, Satwinder Jit Singh, Srikant Sekhar Padhee, Analytic Solution of Timoshenko-Like Deformation in Bidirectional Functionally Graded Beams, Journal of Engineering Mechanics, vol. 150, no. 2, pp. 04023118, 2024. DOI: https://doi.org/10.1061/JENMDT.EMENG-7317.
- [19] Masayuki Niino, Toshio Hirai, Ryuzo Watanabe, Functionally graded materials Aiming for super heat-resistant materials for spacecraft, Journal of the Japan Society for Composite Materials, vol. 13, no. 6, pp. 257-264, 1987. DOI: https://doi.org/10.6089/jscm.13.257.

- [20] Rasheedat Modupe Mahamood and Esther Titilayo Akinlabi, Types of Functionally Graded Materials and Their Areas of Application, in Functionally Graded Materials, Springer International Publishing, Cham, 2017, pp. 9–21. ISBN: 978-3-319-53756-6. DOI: https://doi.org/10.1007/978-3-319-53756-6_2. URL: https://doi.org/10.1007/978-3-319-53756-6_2.
- [21] Bassiouny Saleh, Jinghua Jiang, Reham Fathi, Tareq Al-hababi, Qiong Xu, Lisha Wang, Dan Song, Aibin Ma, 30 Years of functionally graded materials: An overview of manufacturing methods, Applications and Future Challenges, Composites Part B: Engineering, vol. 201, pp. 108376, 2020. ISSN: 1359-8368. DOI: https://doi.org/10.1016/j.compositesb.2020.108376. URL: https://www.sciencedirect.com/science/article/pii/S1359836820334247.
- [22] Y.A. Çengel and A.J. Ghajar, Heat and Mass Transfer: Fundamentals & Applications, Asia Higher Education Engineering/Computer Science Mechanica series, McGraw Hill Education, 2015. ISBN: 9789814595278. URL: https://books.google.co.uk/books?id=1YPhoAEACAAJ.
- [23] A. Deb, M. Deb, and M. Booton, Analysis of orthotropically modeled stiffened plates, International Journal of Solids and Structures, vol. 27, no. 5, pp. 647-664, 1991. DOI: https://doi.org/10.1016/0020-7683(91)90219-6.
- [24] Richard Arthur Bares and Charles E. Massonnet, Analysis of Beam Grids and Orthotropic Plates, 1966. URL: https://api.semanticscholar.org/CorpusID: 60193167.
- [25] Chattopadhyay B, Sinha PK, Mukhopadhyay M., Finite Element Analysis of Blade-Stiffened Composite Plates under Transverse Loads. Journal of Reinforced Plastics and Composites. 1993;12(1):76-100. doi:10.1177/073168449301200105
- [26] C.M. Wang, J.N. Reddy, and K.H. Lee (Eds.), Shear Deformable Beams and Plates, Elsevier Science Ltd, Oxford, 2000. DOI: https://doi.org/10.1016/B978-008043784-2/50001-0
- [27] Chen et al., Static and dynamic analysis of Isogrid Stiffened Composite Plates (ISCP) using equivalent model based on variational asymptotic method, Thin-Walled Struct., vol. 163, p. 107671, Jun. 2021. DOI: https://doi.org/10.1016/J.TWS. 2021.107671
- [28] J.N. Kamineni and R.G. Burela, Constraint method for laminated composite flat stiffened panel analysis using variational asymptotic method (VAM), Thin-Walled Struct., vol. 145, p. 106374, Dec. 2019. DOI: https://doi.org/10.1016/j.tws. 2019.106374
- [29] G. Qing, J. Qiu, and Y. Liu, Free vibration analysis of stiffened laminated plates, International Journal of Solids and Structures, vol. 43, pp. 1357–1371, 2006.

- [30] E.J. Sapountzakis and J.T. Katsikadelis, A new model for slab and beam structures—comparison with other models, Computers & Structures, vol. 80, no. 5, pp. 459–470, 2002, Elsevier.
- [31] A. Bhar, S.S. Phoenix, and S.K. Satsangi, Finite element analysis of laminated composite stiffened plates using FSDT and HSDT: A comparative perspective, Composites Structures, vol. 92, pp. 312–321, 2010.
- [32] A.K. Ghosh and K.C. Biswal, Free-vibration analysis of stiffened laminated plates using higher-order shear deformation theory, Finite Elem Anal Des, vol. 22, pp. 143–161, 1996.
- [33] K.C. Biswal and A.K. Ghosh, Finite element analysis for stiffened laminated plates using higher order shear deformation theory, Computers & Structures, vol. 53, no. 1, pp. 161–171, 1994.
- [34] E.A. Sadek and S.A. Tawfik, A finite element model for the analysis of stiffened laminated plates, Computers & Structures, vol. 75, no. 4, pp. 369–383, 2000, Elsevier.
- [35] A. Mukherjee and LC. Menghani, Displacement and stress response of laminated beams and stiffened plates using a high-order element, Composites Structures, vol. 28, pp. 93-111, 1994.
- [36] A. Deb, M. Deb, and M. Booton, Analysis of orthotropically modeled stiffened plates, International Journal of Solids and Structures, vol. 27, no. 5, pp. 647-664, 1991. DOI: https://doi.org/10.1016/0020-7683(91)90219-6.
- [37] E. I. Harik and G. L. Salamoun, The analytical strip method of solution for stiffened rectangular plates, Comput. Struc., vol. 29, pp. 283-291, 1988.
- [38] A. H. Sheikh and M. Mukhopadhyay, Analysis of stiffened plate with arbitrary planform by the general spline finite strip method, Computational Structures, vol. 42, pp. 53-67, 1992.
- [39] C. S. Rossow and A. K. Ibrahimkhalil, Constraint method analysis of stiffened plates, Computational Structures, vol. 8, pp. 51-60, 1978.
- [40] M. S. Troitsky, Stiffened Plates: Bending, Stability and Vibrations, New York, 1976.
- [41] J. Clarkson, Tests of Fiat Plated Grillages under Concentrated Loads, Transactions of the Royal Institution of Naval Architects, vol. 101, pp. 129–140, 1959.
- [42] R. Bareš and C.E. Massonnet, Analysis of Beam Grids and Orthotropic Plates by the Guyon-Massonnet-Bareš Method, Lockwood, 1968. URL: https://books.google.co.in/books?id=gC1SAAAAMAAJ.

- [43] S.A. Zaghloul and J.B. Kennedy, Nonlinear Behavior of Symmetrically Laminated Plates, J. Appl. Mech., vol. 42, no. 1, pp. 234–236, Mar. 1975. DOI: 10.1115/1.3423532.
- [44] N.K. Shakya and S.S. Padhee, Computationally efficient optimal design of hygrother-mally stable laminate with bend-twist coupling by analytical and numerical strategy, Composites Part A: Applied Science and Manufacturing, vol. 170, p. 107546, 2023. DOI: 10.1016/j.compositesa.2023.107546.
- [45] F. Gruttmann and W. Wagner, Shear correction factors for layered plates and shells, Computational Mechanics, vol. 59, no. 1, pp. 129–146, 2017. DOI: 10.1007/s00466-016-1339-2.
- [46] J. M. Whitney, Shear Correction Factors for Orthotropic Laminates Under Static Load, Journal of Applied Mechanics, vol. 40, no. 1, pp. 302–304, 1973. DOI: 10.1115/1.3422950.
- [47] P. F. Pai, A new look at shear correction factors and warping functions of anisotropic laminates, International Journal of Solids and Structures, vol. 32, no. 16, pp. 2295–2313, 1995. DOI: 10.1016/0020-7683(94)00258-X.
- [48] S. Wang and Y. Zhang, Buckling, post-buckling and delamination propagation in debonded composite laminates Part 2: Numerical applications, Composite Structures, vol. 88, no. 1, pp. 131-146, 2009. DOI: 10.1016/j.compstruct.2008.02.012.
- [49] P. Madabhusi-Raman and J. F. Davalos, Static shear correction factor for laminated rectangular beams, Composites Part B: Engineering, vol. 27, no. 3, pp. 285-293, 1996. DOI: 10.1016/1359-8368(95)00014-3.
- [50] J. M. Whitney, Stress Analysis of Thick Laminated Composite and Sandwich Plates, J. Compos. Mater., vol. 6, no. 3, pp. 426–440, 1972. DOI: 10.1177/002199837200600301.
- [51] J.N. Reddy and C.M. Wang, An overview of the relationships between solutions of the classical and shear deformation plate theories, Composites Science and Technology, vol. 60, no. 12, pp. 2327-2335, 2000. DOI: 10.1016/S0266-3538(00)00028-2.
- [52] G. R. Cowper, The Shear Coefficient in Timoshenko's Beam Theory, Journal of Applied Mechanics, vol. 33, no. 2, pp. 335-340, Jun. 1966. DOI: 10.1115/1.3625046.
- [53] C.M. Wang, J.N. Reddy, and K.H. Lee, Chapter 6 Theories of Plate Bending, in Shear Deformable Beams and Plates, eds. C.M. Wang, J.N. Reddy, and K.H. Lee, Elsevier Science Ltd, Oxford, 2000, pp. 89-109. DOI: 10.1016/B978-008043784-2/50006-X.
- [54] Jacek Chróścielewski, Wojciech Pietraszkiewicz, and Wojciech Witkowski, On shear correction factors in the non-linear theory of elastic shells, International

- Journal of Solids and Structures, vol. 47, no. 25, pp. 3537-3545, 2010. DOI: 10.1016/j.ijsolstr.2010.09.002.
- [55] Reddy, J. N., & Wang, C. M. (2002). On Shear Deformation Plate Solutions: Relationship to The Classical Solutions. In D. Durban, D. Givoli, & J. G. Simmonds (Eds.), Advances in the Mechanics of Plates and Shells: The Avinoam Libai Anniversary Volume (pp. 259-276). Springer Netherlands. DOI: 10.1007/0-306-46954-517.
- [56] Liew, K. M., Pan, Z. Z., & Zhang, L. W. (2019). An overview of layer-wise theories for composite laminates and structures: Development, numerical implementation and application. *Composites Structures*, 216, 240-259. DOI: 10.1016/j.compstruct.2019.02.074.
- [57] Pathak, Anup Kumar, Singh, Satwinder Jit, and Padhee, Srikant Sekhar. Asymptotically correct isoenergetic formulation of geometrically nonlinear anisotropic plates. Mech. Adv. Mater. Struct., vol. 1-23, 2024. doi: 10.1080/15376494.2024.2319106.
- [58] Shakya, Nishant K., and Padhee, Srikant S., Asymptotic analysis of Timoshenkolike orthotropic beam with elliptical cross-section, European Journal of Mechanics-A/Solids, vol. 102, p. 105100, 2023, Elsevier.
- [59] Mindlin, R. D., Influence of Rotatory Inertia and Shear on Flexural Motions of Isotropic, Elastic Plates, Journal of Applied Mechanics, vol. 18, no. 1, pp. 31-38, April 2021. DOI: 10.1115/1.4010217.
- [60] Basset, A. B., VI. On the extension and flexure of cylindrical and spherical thin elastic shells, Philosophical Transactions of the Royal Society of London. (A.), vol. 181, pp. 433-480, 1890. DOI: 10.1098/rsta.1890.0007.
- [61] Liao, C.-L., Reddy, J.N., Analysis of anisotropic, stiffened composite laminates using a continuum-based shell element, Computers & Structures, vol. 34, no. 6, pp. 805-815, 1990. DOI: 10.1016/0045-7949(90)90351-2.
- [62] Author, Derivation of Plate Theory Accounting Asymptotically Correct Shear Deformation, Journal of Applied Mechanics, vol. 64, no. 4, pp. 905-915, Dec. 1997. DOI: 10.1115/1.2788998.
- [63] Harursampath, D., Harish, A. B., & Hodges, D. H., Model reduction in thin-walled open-section composite beams using variational asymptotic method. Part I: Theory, Thin-Walled Structures, vol. 117, pp. 356-366, 2017. DOI: 10.1016/j.tws.2017.03.018.
- [64] Rajagopal, A., Hodges, D. H., & Yu, W., Asymptotic beam theory for planar deformation of initially curved isotropic strips, Thin-Walled Structures, vol. 50, no. 1, pp. 106-115, 2012. DOI: 10.1016/j.tws.2011.08.012.
- [65] Kim, J.-S. and Cho, M., Enhanced first-order theory based on mixed formulation and transverse normal effect, International Journal of Solids and Structures, vol. 44, no. 3, pp. 1256-1276, 2007. DOI: 10.1016/j.ijsolstr.2006.06.018.

- [66] Bogdanovich, A.E. and Yushanov, S.P., Three-dimensional variational analysis of Pagano's problems for laminated composite plates, Composites Science and Technology, vol. 60, no. 12, pp. 2407-2425, 2000. DOI: 10.1016/S0266-3538(00)00035-X.
- [67] Amandeep, Satwinder J. Singh, and Srikant Sekhar Padhee, Analytic solution of Timoshenko-like Deformation in Bidirectional Functionally Graded Beams, Journal of Engineering Mechanics, pp. 1-15, Nov. 2023. DOI: 10.1016/JENMDT/EMENG-73171.4062223.
- [68] Mark Levinson, An accurate, simple theory of the statics and dynamics of elastic plates, Mech. Res. Commun., vol. 7, no. 6, pp. 343-350, 1980. DOI: https://doi.org/10.1016/0093-6413(80)90049-X.
- [69] Neeraj Grover, D.K. Maiti, and B.N. Singh, A new inverse hyperbolic shear deformation theory for static and buckling analysis of laminated composite and sandwich plates, Composite Structures, vol. 95, pp. 667-675, 2013. DOI: 10.1016/j.compstruct.2012.08.012.
- [70] Veloorillom Madhavan Sreehari, Linju Joseph George, and Dipak Kumar Maiti, Bending and buckling analysis of smart composite plates with and without internal flaw using an inverse hyperbolic shear deformation theory, Composite Structures, vol. 138, pp. 64-74, 2016.
- [71] A.Y.T. Leung, Junchuan Niu, C.W. Lim, and Kongjie Song, A new unconstrained third-order plate theory for Navier solutions of symmetrically laminated plates, Computers & Structures, vol. 81, no. 26, pp. 2539-2548, 2003. DOI: 10.1016/S0045-7949(03)00290-6.
- [72] A. Barut, E. Madenci, and A. Tessler, C0-continuous triangular plate element for laminated composite and sandwich plates using the 2,2 Refined Zigzag Theory, Composite Structures, vol. 106, pp. 835-853, 2013. DOI: 10.1016/j.compstruct.2013.07.024.
- [73] Geoffrey M. Cook and Alexander Tessler, A {3,2}-order bending theory for laminated composite and sandwich beams, Composites Part B-engineering, vol. 29, pp. 565-576, 1998.
- [74] K. H. Lo, R. M. Christensen, and E. M. Wu, A High-Order Theory of Plate Deformation—Part 1: Homogeneous Plates, Journal of Applied Mechanics, vol. 44, no. 4, pp. 663-668, Dec. 1977. DOI: 10.1115/1.3424154.
- [75] L. M. J. S. Dinis, R. M. Natal Jorge, and J. Belinha, An Unconstrained Third-Order Plate Theory Applied to Functionally Graded Plates Using a Meshless Method, Mechanics of Advanced Materials and Structures, vol. 17, no. 2, pp. 108-133, 2010. DOI: 10.1080/15376490903249925.

- [76] J N Reddy and Rafael A Arciniega, Shear Deformation Plate and Shell Theories: From Stavsky to Present, Mechanics of Advanced Materials and Structures, vol. 11, no. 6, pp. 535–582, 2004. DOI: 10.1080/15376490490452777.
- [77] Yuvraj M Ghugal and Ravindra P Shimpi, A Review of Refined Shear Deformation Theories of Isotropic and Anisotropic Laminated Plates, Journal of Reinforced Plastics and Composites, vol. 21, no. 9, pp. 775–813, 2002. DOI: 10.1106/T6CP-EN1F-4EHC-NJ4G.
- [78] NJ Pagano and SJ Hatfield, Elastic Behavior of Multilayered Bidirectional Composites, AIAA Journal, vol. 10, no. 7, pp. 931–933, 1972. DOI: 10.2514/3.50249.
- [79] Abdul Idlbi, Moussa Karama, and Michel Touratier, Comparison of Various Laminated Plate Theories, Composite Structures, vol. 37, no. 2, pp. 173–184, 1997. DOI: 10.1016/S0263-8223(97)80010-4.
- [80] Pravin Kulkarni, Ashwinkumar Dhoble, and Pramod Padole, A review of research and recent trends in analysis of composite plates, Sādhanā, vol. 43, no. 6, p. 96, 2018. DOI: 10.1007/s12046-018-0867-1.
- [81] Nishant Kumar Shakya and Srikant Sekhar Padhee, Asymptotic Analysis of Elastic Coupling in Anisotropic-Homogeneous Beam, Journal of Applied Mechanics, vol. 90, no. 4, p. 044501, Jan. 2023. DOI: 10.1115/1.4056458.
- [82] Amandeep, Satwinder J. Singh, and Srikant Sekhar Padhee, Asymptotically Accurate Analytical Solution for Timoshenko-like Deformation of Functionally Graded Beams, Journal of Applied Mechanics, pp. 1-15, Mar. 2023. DOI: 10.1115/1.4062223.
- [83] T. C. Lim, Improved shear correction factors for deflection of simply supported very thick rectangular auxetic plates, Int. J. Mech. Mater. Eng., vol. 11, no. 1, p. 13, 2016. DOI: 10.1186/s40712-016-0065-z.
- [84] J. M. Whitney and N. J. Pagano, Shear Deformation in Heterogeneous Anisotropic Plates, Journal of Applied Mechanics, vol. 37, no. 4, pp. 1031-1036, Dec. 1970. DOI: 10.1115/1.3408654.
- [85] R. P. Shimpi, H. G. Patel, and H. Arya, New First-Order Shear Deformation Plate Theories, Journal of Applied Mechanics, vol. 74, no. 3, pp. 523-533, May 2006. DOI: 10.1115/1.2423036.
- [86] Wenbin Yu, Dewey H. Hodges, and Vitali V. Volovoi, Asymptotically accurate 3-D recovery from Reissner-like composite plate finite elements, Computers & Structures, vol. 81, no. 7, pp. 439-454, 2003. DOI: 10.1016/S0045-7949(03)00011-7.
- [87] J.L. Mantari, A.S. Oktem, and C. Guedes Soares, A new trigonometric shear deformation theory for isotropic, laminated composite and sandwich plates, International Journal of Solids and Structures, vol. 49, no. 1, pp. 43-53, 2012. DOI: 10.1016/j.ijsolstr.2011.09.008.

- [88] M. Touratier, An efficient standard plate theory, International Journal of Engineering Science, vol. 29, no. 8, pp. 901-916, 1991. DOI: 10.1016/0020-7225(91)90165-Y.
- [89] K. P. Soldatos, A transverse shear deformation theory for homogeneous monoclinic plates, Acta Mech., vol. 94, no. 3, pp. 195–220, 1992. DOI: 10.1007/BF01176650.
- [90] Erasmo Carrera, Mixed layer-wise models for multilayered plates analysis, Composite Structures, vol. 43, no. 1, pp. 57-70, 1998. DOI: 10.1016/S0263-8223(98)00097-X.
- [91] Ireneusz Kreja, A literature review on computational models for laminated composite and sandwich panels, Cent. Eur. J. Eng., vol. 1, no. 1, pp. 59–80, 2011. DOI: 10.2478/s13531-011-0005-x.
- [92] E. Carrera, Theories and finite elements for multilayered, anisotropic, composite plates and shells, Arch. Comput. Methods Eng., vol. 9, no. 2, pp. 87–140, 2002. DOI: 10.1007/BF02736649.
- [93] M. F. Caliri, A. J. M. Ferreira, and V. Tita, A review on plate and shell theories for laminated and sandwich structures highlighting the finite element method, Composite Structures, vol. 156, pp. 63-77, 2016.
- [94] J. Meenen, An Assessment of Classical and Refined Plate Theories Derived From the Principle of Virtual Displacements, in Theories of Plates and Shells: Critical Review and New Applications, Springer Berlin Heidelberg, 2004, pp. 141–148. DOI: 10.1007/978-3-540-39905-6_17.
- [95] A. Eijo, E. Oñate, and S. Oller, Delamination in laminated plates using the 4-noded quadrilateral QLRZ plate element based on the refined zigzag theory, Composite Structures, vol. 108, pp. 456-471, 2014. DOI: 10.1016/j.compstruct.2013.09.052.
- [96] M. Boscolo, Analytical solution for free vibration analysis of composite plates with layer-wise displacement assumptions, Composite Structures, vol. 100, pp. 493-510, 2013. DOI: 10.1016/j.compstruct.2013.01.015.
- [97] R. Khandan, S. Noroozi, P. Sewell, and J. Vinney, *The development of laminated composite plate theories: a review, Journal of Materials Science*, vol. 47, no. 16, pp. 5901–5910, 2012. DOI: 10.1007/s10853-012-6329-y.
- [98] Metin Aydogdu, A new shear deformation theory for laminated composite plates, Composite Structures, vol. 89, no. 1, pp. 94–101, 2009.
- [99] G.M. Kulikov and S.V. Plotnikova, Exact 3D stress analysis of laminated composite plates by sampling surfaces method, Composite Structures, vol. 94, no. 12, pp. 3654-3663, 2012. DOI: 10.1016/j.compstruct.2012.06.006.
- [100] Serge Abrate and Marco Di Sciuva, Equivalent single layer theories for composite and sandwich structures: A review, Composite Structures, vol. 179, pp. 482-494, 2017. DOI: 10.1016/j.compstruct.2017.07.090.

- [101] J. N. Reddy and D. H. Robbins Jr, Theories and Computational Models for Composite Laminates, Applied Mechanics Reviews, vol. 47, no. 6, pp. 147-169, 1994. DOI: 10.1115/1.3111076.
- [102] Huu-Tai Thai and Seung-Eock Kim, A review of theories for the modeling and analysis of functionally graded plates and shells, Composite Structures, vol. 128, pp. 70-86, 2015. DOI: 10.1016/j.compstruct.2015.03.010.
- [103] Y.B. Cho and R.C. Averill, First-order zig-zag sublaminate plate theory and finite element model for laminated composite and sandwich panels, Composite Structures, vol. 50, no. 1, pp. 1-15, 2000. DOI: 10.1016/S0263-8223(99)00063-X.
- [104] Erasmo Carrera, Historical review of Zig-Zag theories for multilayered plates and shells, Appl. Mech. Rev., vol. 56, no. 3, pp. 287–308, 2003. DOI: 10.1115/1.1557614.
- [105] Ugo Icardi and Federico Sola, Assessment of recent zig-zag theories for laminated and sandwich structures, Composites Part B: Engineering, vol. 97, pp. 26-52, 2016. DOI: 10.1016/j.compositesb.2016.04.058.
- [106] Ahmed K. Noor and W. Scott Burton, Assessment of Shear Deformation Theories for Multilayered Composite Plates, Applied Mechanics Reviews, vol. 42, no. 1, pp. 1-13, 1989. DOI: 10.1115/1.3152418.
- [107] V.L. Berdichevsky, Variational-asymptotic method of shell theory construction, Journal of Applied Mathematics and Mechanics, vol. 43, no. 4, pp. 664–687, 1979.
- [108] Wenbin Yu, Mathematical construction of a Reissner-Mindlin plate theory for composite laminates, International Journal of Solids and Structures, vol. 42, no. 26, pp. 6680–6699, 2005. DOI: 10.1016/j.ijsolstr.2005.02.049.
- [109] Dewey H. Hodges, Ali R. Atilgan, and D. A. Danielson, A geometrically nonlinear theory of elastic plates, J. Appl. Mech. Trans. ASME, vol. 60, no. 1, pp. 109–116, 1993. DOI: 10.1115/1.2900732.
- [110] S. Keshava Kumar, Review of Laminated Composite Plate Theories, with Emphasis on Variational Asymptotic Method, AIAA J., vol. 57, no. 10, pp. 4182–4188, 2019. DOI: 10.2514/1.J057552.
- [111] Ali R. Atilgan and Dewey H. Hodges, On the strain energy of laminated composite plates, International Journal of Solids and Structures, vol. 29, no. 20, pp. 2527-2543, 1992. DOI: 10.1016/0020-7683(92)90007-G.
- [112] Vladislav G. Sutyrin and Dewey H. Hodges, On asymptotically correct linear laminated plate theory, International Journal of Solids and Structures, vol. 33, no. 25, pp. 3649-3671, 1996. DOI: 10.1016/0020-7683(95)00208-1.

- [113] Wenbin Yu, Dewey H. Hodges, and Vitali V. Volovoi, Asymptotic construction of Reissner-like composite plate theory with accurate strain recovery, International Journal of Solids and Structures, vol. 39, no. 20, pp. 5185-5203, 2002. DOI: 10.1016/S0020-7683(02)00410-9.
- [114] Wenbin Yu, Dewey H. Hodges, and Jimmy C Ho, Variational asymptotic beam sectional analysis An updated version, Int. J. Eng. Sci., vol. 59, pp. 40–64, 2012.
- [115] Dineshkumar Harursampath, Ajay B. Harish, and Dewey H. Hodges, Model reduction in thin-walled open-section composite beams using Variational Asymptotic Method. Part II: Applications, Thin-Walled Structures, vol. 117, pp. 367-377, 2017. DOI: 10.1016/j.tws.2017.03.021.
- [116] S.R. Atashipour, U.A. Girhammar, and M. Al-Emrani, Exact Lévy-type solutions for bending of thick laminated orthotropic plates based on 3-D elasticity and shear deformation theories, Composite Structures, vol. 163, pp. 129-151, 2017. DOI: 10.1016/j.compstruct.2016.12.026.
- [117] H. Hadavinia, K. Gordnian, J. Karwatzki, and A. Aboutorabi, Deriving shear correction factor for thick laminated plates using the energy equivalence method, Structural Durability & Health Monitoring, vol. 2, no. 4, p. 197, 2006.
- [118] Guangyu Shi, A new simple third-order shear deformation theory of plates, International Journal of Solids and Structures, vol. 44, no. 13, pp. 4399-4417, 2007. DOI: 10.1016/j.ijsolstr.2006.11.031.
- [119] J. N. Reddy, Mechanics of Laminated Composite Plates and Shells: Theory and Analysis, Second Edition, 2nd ed. Boca Raton: CRC Press, 2003.
- [120] A. E. H. Love, The Small Free Vibrations and Deformation of a Thin Elastic Shell, Philosophical Transactions of the Royal Society of London. A, vol. 179, pp. 491–546, 1888. URL: http://www.jstor.org/stable/90527.
- [121] Eric Reissner, The Effect of Transverse Shear Deformation on the Bending of Elastic Plates, Journal of Applied Mechanics, vol. 12, no. 2, pp. A69-A77, 2021. DOI: 10.1115/1.4009435.
- [122] J. N. Reddy, A Simple Higher-Order Theory for Laminated Composite Plates, Journal of Applied Mechanics, vol. 51, no. 4, pp. 745-752, 1984. DOI: 10.1115/1.3167719.
- [123] Stefanos Vlachoutsis, Shear correction factors for plates and shells, International Journal for Numerical Methods in Engineering, vol. 33, no. 7, pp. 1537-1552, 1992. DOI: 10.1002/nme.1620330712.
- [124] K.C. Le, An asymptotically exact first-order shear deformation theory for functionally graded plates, International Journal of Engineering Science, vol. 190, p. 103875, 2023. DOI: 10.1016/j.ijengsci.2023.103875.

- [125] D. H. Hodges, Geometrically Exact, Intrinsic Theory for Dynamics of Curved and Twisted Anisotropic Beams, AIAA Journal, vol. 41, no. 6, pp. 1131-1137, 2003. DOI: 10.2514/2.2054.
- [126] D. Harursampath and D. H. Hodges, Asymptotic analysis of the non-linear behavior of long anisotropic tubes, International Journal of Non-Linear Mechanics, vol. 34, no. 6, pp. 1003-1018, 1999. DOI: 10.1016/S0020-7462(98)00070-5.
- [127] D. H. Hodges, Nonlinear Composite Beam Theory, Progress in Astronautics and Aeronautics, American Institute of Aeronautics and Astronautics, 2006. URL: https://books.google.co.in/books?id=FEFKAQAAIAAJ.
- [128] M. E. Gurtin, E. Fried, and L. Anand, The Mechanics and Thermodynamics of Continua, Cambridge University Press, 2010. URL: http://dx.doi.org/10.1017/ CB09780511762956.
- [129] A. Amandeep, A. K. Pathak, and S. S. Padhee, Closed-Form Expressions of Shear Correction Factor for Functionally Graded Beams, Journal of Applied Mechanics, vol. 91, no. 3, p. 034501, 2023. DOI: 10.1115/1.4063817.
- [130] A. Maji and P. K. Mahato, Development and applications of shear deformation theories for laminated composite plates: An overview, Journal of Thermoplastic Composite Materials, vol. 35, no. 12, pp. 2576-2619, 2022. DOI: 10.1177/0892705720930765.
- [131] B. D. Agarwal, L. J. Broutman, and K. Chandrashekhara, *Analysis and Performance of Fiber Composites*, Wiley, 2017. URL: https://books.google.co.in/books?id=Pqg7DwAAQBAJ.
- [132] The Editors of Encyclopaedia Britannica, *Monoclinic System*, 2018. URL: https://www.britannica.com/science/monoclinic-system.
- [133] L. W. Rehfield and R. R. Valisetty, A simple, refined theory for bending and stretching of homogeneous plates, AIAA Journal, vol. 22, no. 1, pp. 90-95, 1984. DOI: 10.2514/3.8344.
- [134] R. P. Shimpi and H. G. Patel, A two variable refined plate theory for orthotropic plate analysis, International Journal of Solids and Structures, vol. 43, no. 22, pp. 6783-6799, 2006. DOI: 10.1016/j.ijsolstr.2006.02.007.
- [135] P. Schneider and R. Kienzler, A Reissner-type plate theory for monoclinic material derived by extending the uniform-approximation technique by orthogonal tensor decompositions of nth-order gradients, Meccanica, vol. 52, no. 9, pp. 2143-2167, 2017. DOI: 10.1007/s11012-016-0573-1.
- [136] S Keshava Kumar, Dineshkumar Harursampath, Erasmo Carrera, Maria Cinefra, and Stefano Valvano, *Modal analysis of delaminated plates and shells using Carrera Unified Formulation MITC9 shell element, Mech. Adv. Mater. Struct.*, vol. 25, no. 8, pp. 681–697, Jun. 2018. DOI: 10.1080/15376494.2017.1302024.

- [137] Ankit Deo and Wenbin Yu, Equivalent 3D properties of thin-walled composite structures using mechanics of structure genome, Mech. Adv. Mater. Struct., vol. 30, no. 9, pp. 1737–1748, 2023. DOI: 10.1080/15376494.2022.2042755.
- [138] Vinyas Mahesh and Dineshkumar Harursampath, Nonlinear deflection analysis of CNT/magneto-electro-elastic smart shells under multi-physics loading, Mech. Adv. Mater. Struct., vol. 29, no. 7, pp. 1047–1071, Mar. 2022. DOI: 10.1080/15376494.2020.1805059.
- [139] Padmanav Dash and B N Singh, Static Response of Geometrically Nonlinear Laminated Composite Plates Having Uncertain Material Properties, Mech. Adv. Mater. Struct., vol. 22, no. 4, pp. 269–280, Apr. 2015. DOI: 10.1080/15376494.2012.736056.
- [140] M Petrolo and A Lamberti, Axiomatic/asymptotic analysis of refined layer-wise theories for composite and sandwich plates, Mech. Adv. Mater. Struct., vol. 23, no. 1, pp. 28–42, Jan. 2016. DOI: 10.1080/15376494.2014.924607.
- [141] Yanchuan Hui, Qun Huang, Gabriele De Pietro, Gaetano Giunta, Heng Hu, Salim Belouettar, and Erasmo Carrera, Hierarchical beam finite elements for geometrically nonlinear analysis coupled with Asymptotic Numerical Method, Mech. Adv. Mater. Struct., vol. 28, no. 24, pp. 2487–2500, Dec. 2021. DOI: 10.1080/15376494.2020.1743898.
- [142] Chien H Thai Loc V. Tran T. Nguyen-Thoi and H Nguyen-Xuan, An Edge-Based Smoothed Discrete Shear Gap Method Using the C0-Type Higher-Order Shear Deformation Theory for Analysis of Laminated Composite Plates, Mech. Adv. Mater. Struct., vol. 22, no. 4, pp. 248–268, 2015. DOI: 10.1080/15376494.2012.736055.
- [143] Wu Zhen, Chen Jian, and Chen Wanji, Reddy-type zig-zag model for multilayered composite plate based on the HW variational theorem, Mech. Adv. Mater. Struct., vol. 25, no. 11, pp. 964–974, Aug. 2018. DOI: 10.1080/15376494.2017.1323142.
- [144] Y Urthaler and J N Reddy, A Mixed Finite Element for the Nonlinear Bending Analysis of Laminated Composite Plates Based on FSDT, Mech. Adv. Mater. Struct., vol. 15, no. 5, pp. 335–354, Apr. 2008. DOI: 10.1080/15376490802045671.
- [145] Abdelouahed Tounsi Rabha Menaa, Fethi Mouaici, Ismail Mechab, Mohamed Zidi, and El Abbas Adda Bedia, Analytical Solutions for Static Shear Correction Factor of Functionally Graded Rectangular Beams, Mechanics of Advanced Materials and Structures, vol. 19, no. 8, pp. 641-652, 2012. DOI: 10.1080/15376494.2011.581409.
- [146] K. Sab T.-K. Nguyen and G. Bonnet, Shear Correction Factors for Functionally Graded Plates, Mech. Adv. Mater. Struct., vol. 14, no. 8, pp. 567–575, 2007. DOI: 10.1080/15376490701672575.
- [147] Ning Liu and Wenbin Yu, Evaluation of smeared properties approaches and mechanics of structure genome for analyzing composite beams, Mech. Adv. Mater. Struct., vol. 25, no. 14, pp. 1171–1185, Oct. 2018. DOI: 10.1080/15376494.2017.1330977.

- [148] Prasanta Sahoo Anirban Mitra and Kashinath Saha, Nonlinear Vibration Analysis of Simply Supported Stiffened Plate by a Variational Method, Mechanics of Advanced Materials and Structures, vol. 20, no. 5, pp. 373-396, 2013. DOI: 10.1080/15376494.2011.627640.
- [149] G H Nie C K Chan and T T He, Asymptotic Solution for Post-Buckling of a Circular Delamination with Non-Linear Fiber Bridging in 3D Orthotropic Materials, Mech. Adv. Mater. Struct., vol. 19, no. 5, pp. 367–375, Jul. 2012. DOI: 10.1080/15376494.2010.528165.
- [150] Maria Cinefra, Alessandro Lamberti, Ashraf M Zenkour, and Erasmo Carrera, Axiomatic/Asymptotic Technique Applied to Refined Theories for Piezoelectric Plates, Mech. Adv. Mater. Struct., vol. 22, no. 1-2, pp. 107–124, Jan. 2015. DOI: 10.1080/15376494.2014.908043.
- [151] Dineshkumar Harursampath Renuka Sahu and Sathiskumar A Ponnusami, Continuum modeling of nonlinear buckling behavior of CNT using variational asymptotic method and nonlinear FEA, Mech. Adv. Mater. Struct., vol. 0, no. 0, pp. 1–18, 2023. DOI: 10.1080/15376494.2023.2211971.
- [152] H R H KABIR, BENDING OF A SIMPLY SUPPORTED RECTANGULAR PLATE WITH ARBITRARY LAMINATION, Mech. Compos. Mater. Struct., vol. 3, no. 4, pp. 341–358, 1996. DOI: 10.1080/10759419608945871.
- [153] 10.1080/15376494.2021.1956028, Layer-wise solutions for variable stiffness composite laminated sandwich plate using curvilinear fibers, Mech. Adv. Mater. Struct., vol. 29, no. 26, pp. 5460–5477, 2022. DOI: 10.1080/15376494.2021.1956028.
- [154] Sherrill B Biggers T. Baranski Andrzej, *Postbuckling Analysis of Laminated Composite Plates Using a Higher-Order Zig-Zag Theory*, *Mech. Compos. Mater. Struct.*, vol. 7, no. 3, pp. 285–314, Jul. 2000. DOI: 10.1080/10759410050031149.
- [155] Luciano Demasi and Wenbin Yu, Assess the Accuracy of the Variational Asymptotic Plate and Shell Analysis Using the Generalized Unified Formulation, Mech. Adv. Mater. Struct., vol. 20, no. 3, pp. 227–241, Mar. 2013. DOI: 10.1080/15376494.2011.584150.
- [156] M. Faghih Shojaei and R. Ansari, Variational differential quadrature: A technique to simplify numerical analysis of structures, Appl. Math. Model., vol. 49, pp. 705–738, 2017. DOI: 10.1016/j.apm.2017.02.052.
- [157] R. Hassani, R. Ansari, and H. Rouhi, Large deformation analysis of 2D hyper-elastic bodies based on the compressible nonlinear elasticity: A numerical variational method, Int. J. Non. Linear. Mech., vol. 116, pp. 39–54, 2019. DOI: 10.1016/j.ijnonlinmec.2019.05.003.

- [158] Y. Gholami, R. Ansari, and R. Gholami, Three-dimensional nonlinear primary resonance of functionally graded rectangular small-scale plates based on strain gradient elasticity theory, Thin-Walled Struct., vol. 150, p. 106681, 2020. DOI: 10.1016/j.tws.2020.106681.
- [159] R. Ansari, R. Hassani, R. Gholami, and H. Rouhi, Thermal postbuckling analysis of FG-CNTRC plates with various shapes and temperature-dependent properties using the VDQ-FEM technique, Aerosp. Sci. Technol., vol. 106, p. 106078, 2020. DOI: 10.1016/j.ast.2020.106078.
- [160] E. Viola, F. Tornabene, and N. Fantuzzi, General higher-order shear deformation theories for the free vibration analysis of completely doubly-curved laminated shells and panels, Compos. Struct., vol. 95, pp. 639–666, 2013. DOI: 10.1016/j.compstruct.2012.08.005.
- [161] Y. Gholami, R. Ansari, R. Gholami, and H. Rouhi, Nonlinear bending analysis of nanoplates made of FGMs based on the most general strain gradient model and 3D elasticity theory, Eur. Phys. J. Plus, vol. 134, no. 4, p. 167, 2019. DOI: 10.1140/epjp/i2019-12501-x.
- [162] Gero Friesecke, Richard D James, and Stefan Müller, A theorem on geometric rigidity and the derivation of nonlinear plate theory from three-dimensional elasticity, Commun. Pure Appl. Math., vol. 55, no. 11, pp. 1461–1506, 2002. DOI: 10.1002/cpa.10048.
- [163] Roberto Paroni, Second-Order Structured Deformations: Approximation Theorems and Energetics BT Multiscale Modeling in Continuum Mechanics and Structured Deformations, in: Gianpetro Del Piero and David R Owen (eds.), Multiscale Modeling in Continuum Mechanics and Structured Deformations, Springer Vienna, Vienna, 2004, pp. 177–202. DOI: 10.1007/978-3-7091-2770-4-5.
- [164] Antonio Gaudiello, Régis Monneau, Jacqueline Mossino, François Murat, and Ali Sili, *Junction of elastic plates and beams*, *ESAIM COCV*, vol. 13, no. 3, pp. 419–457, Jul. 2007. DOI: 10.1051/cocv:2007036.
- [165] Marco Picchi Scardaoni and Roberto Paroni, Linear Models of a Stiffened Plate via Γ -Convergence, J. Elast., vol. 151, no. 2, pp. 237–272, 2022. DOI: 10.1007/s10659-022-09935-y.
- [166] Paolo Podio-Guidugli, Validation of Classical Beam and Plate Models by Variational Convergence, in: George Jaiani and Paolo Podio-Guidugli (eds.), IUTAM Symp. Relations Shell Plate Beam 3D Model., Springer Netherlands, Dordrecht, 2008, pp. 177–188. DOI: 10.1007/978-1-4020-8774-5₁6.
- [167] Roberto Paroni, Paolo Podio-Guidugli, and Giuseppe Tomassetti, A JUSTIFI-CATION OF THE REISSNER-MINDLIN PLATE THEORY THROUGH VARI-

- ATIONAL CONVERGENCE, Anal. Appl., vol. 05, no. 02, pp. 165–182, Apr. 2007. DOI: 10.1142/S0219530507000936.
- [168] Francesco Tornabene, Nicholas Fantuzzi, Francesco Ubertini, and Erasmo Viola, Strong Formulation Finite Element Method Based on Differential Quadrature: A Survey, Appl. Mech. Rev., vol. 67, no. 2, pp. 20801, 2015. DOI: 10.1115/1.4028859.
- [169] R Ansari, R Hassani, R Gholami, and H Rouhi, Nonlinear bending analysis of arbitrary-shaped porous nanocomposite plates using a novel numerical approach, Int. J. Non. Linear. Mech., vol. 126, pp. 103556, 2020. DOI: 10.1016/j.ijnonlinmec.2020.103556.
- [170] Jiangchao Chen, HSDT mesh-free method for free vibration analysis of sandwich structures, Mech. Adv. Mater. Struct., vol. 0, no. 0, pp. 1–15, Taylor & Francis, 2023. DOI: 10.1080/15376494.2023.2271913.
- [171] Qing Xia, Ping Xiang, Lizhong Jiang, Jianwei Yan, and Linxin Peng, Bending and free vibration and analysis of laminated plates on Winkler foundations based on meshless layerwise theory, Mech. Adv. Mater. Struct., vol. 29, no. 27, pp. 6168–6187, Taylor & Francis, Dec. 2022. DOI: 10.1080/15376494.2021.1972497.
- [172] Andrea Braides, Gamma-Convergence for Beginners, Oxford University Press, 2002. DOI: 10.1093/acprof:oso/9780198507840.001.0001.
- [173] G. A. Athanassoulis and K. A. Belibassakis, A consistent couple-mode theory for the propagation of small amplitude water waves over variable bathymetry regions, J. Fluid Mech., 389 (1999), 275-301.
- [174] J. A. Bailard, J. W. DeVries and J. T. Kirby, Consideration in using Bragg reflection for storm erosion protection, J. Waterway, Port, Coastal, and Ocean Eng., 118(1) (1992), 62-74.
- [175] H. Lamb, *Hydrodynamics*, Camb. Univ. Press, 1932.
- [176] C. C. Mei and J. L. Black, Scattering of surface waves by rectangular obstacles in waters of finite depth, J. Fluid Mech., 38 (3) (1969), 499-511.
- [177] C. C. Mei, T. Hara and M. Nachari, Note on Bragg scattering of water waves by parallel bars in the sea bed, J. Fluid Mech., 186 (1988), 147-162.
- [178] C. C. Mei and B. Le Méhauté, Note on the equations of long waves over an uneven bottom, J. Geophysical Res., 71 (1966), no. 2, 393-400.
- [179] J. W. Miles, Surface-wave scattering matrix for a shelf, J. Fluid Mech., 28 (1967) 755-767.
- [180] J. W. Miles, *Integral Transforms in Applied Mathematics*, Cambridge University Press, Cambridge, 1971.

- [181] J. W. Miles, Oblique surface wave diffraction by a cylindrical obstacle, Dyn. Atms. and Oceans, 6 (1981), 121-123.
- [182] J. W. Miles, Variational approximations for gravity waves in water of variable depth, J. Fluid Mech., 232 (1991), 681-688.
- [183] J. W. Miles, On gravity-wave scattering by non-secular changes in depth, J. Fluid Mech., 376 (1998), 53-60.
- [184] J. W. Miles and P. G. Chamberlain, Topographical scattering of gravity waves, J. Fluid Mech., 361 (1998), 175-188.
- [185] M. Nachari and C. C. Mei, Bragg scattering of water waves by doubly periodic sea bed, J. Fluid Mech., 192 (1988), 51-74.
- [186] A. Nachbin and G. C. Papanicolaou, Water waves in shallow channels of rapidly varying depth, J. Fluid Mech., 241 (1992), 311-332.
- [187] D. Porter, The Mild-Slope Equations, J. Fluid Mech., 494 (2003), 51-63.

Expressions g_2 , g_3 , f_2 and f_3

As we keep on perturbing the solution for increased accuracy, we encounter bulky expressions containing higher order derivatives of u_1, u_2 and u_3 . These bulky expressions are replaced in Chapter 2 with two-dimensional functions f_2, f_3, g_2 and g_3 . This is done to make the equations concise. Also, this replacement does not reduce the completeness of the chapter as the chapter does not go into the details of these expressions and removes them from the final reduced order plate model using the concept of isoenergetics. The details of these replacements are included in this appendix.

As shown in Chapter 2, the third-order solution results in the following Euler-Lagrange equations.

$$2C_{55}f_2 + 6C_{55}x_3g_2 + 2C_{45}f_3 + 6C_{45}x_3g_3 = C_{55}\frac{\partial^2 v_1^3}{\partial x_3^2} + C_{45}\frac{\partial^2 v_2^3}{\partial x_3^2}$$

$$2C_{45}f_2 + 6C_{45}x_3g_2 + 2C_{44}f_3 + 6C_{44}x_3g_3 = C_{45}\frac{\partial^2 v_1^3}{\partial x_3^2} + C_{44}\frac{\partial^2 v_2^3}{\partial x_3^2}$$

$$C_{33}\frac{\partial^2 v_3^3}{\partial x_3^2} = 0$$
(G.1)

Where f_2 , f_3 , g_2 and g_3 are functions of x_1 and x_2 . The expressions for these functions in terms of derivatives of u_i w.r.t. x_j and the material constants are given below

$$\begin{split} g_2 &= \frac{1}{6C_{33}(C_{45}^2 - C_{44}C_{55})} \Bigg[(-C_{26}C_{33}C_{44} + C_{23}C_{36}C_{44} \\ &- C_{23}^2C_{45} + C_{22}C_{33}C_{45}) \frac{\partial^3 u_3}{\partial x_1^3} + 3 \frac{\partial^3 u_3}{\partial x_1\partial x_2^2} - (C_{13}C_{23}C_{44} \\ &- C_{12}C_{33}C_{44} + 2C_{36}^2C_{44} + 3C_{26}C_{33}C_{45} - 3C_{23}C_{36}C_{45} - C_{23}C_{45}^2 \\ &+ C_{23}C_{44}C_{55} - 2C_{33}C_{44}C_{66}) \frac{\partial^3 u_3}{\partial x_1^2\partial x_2} + (-3C_{16}C_{33}C_{44} \\ &+ 3C_{13}C_{36}C_{44} - C_{13}C_{23}C_{45} + C_{12}C_{33}C_{45} - 2C_{36}^2C_{45} - 2C_{36}C_{45}^2 \\ &+ 2C_{36}C_{44}C_{55} + 2C_{33}C_{45}C_{66}) \frac{\partial^3 u_3}{\partial x_1\partial x_2^2} + (C_{13}^2C_{44} - C_{11}C_{33}C_{44} \\ &+ C_{16}C_{33}C_{45} - C_{13}C_{45}(C_{36} + C_{45}) + C_{13}C_{44}C_{55}) \frac{\partial^3 u_3}{\partial x_2^3} \Bigg] \\ g_3 &= \frac{1}{6C_{33}(C_{45}^2 - C_{44}C_{55})} \Bigg[(C_{26}C_{33}C_{45} - C_{23}C_{45}(C_{36} + C_{45}) \\ &- C_{22}C_{33}C_{55} + C_{23}(C_{23} + C_{44})C_{55}) \frac{\partial^3 u_3}{\partial x_1^3} + 3 \frac{\partial^3 u_3}{\partial x_1\partial x_2^2} \\ &- (-C_{13}C_{23}C_{45} + C_{12}C_{33}C_{45} - 2C_{36}^2C_{45} - 2C_{36}C_{45}^2 \\ &- 3C_{26}C_{33}C_{55} + 3C_{23}C_{36}C_{55} + 2C_{36}C_{44}C_{55} \\ &+ 2C_{33}C_{45}C_{66}) \frac{\partial^3 u_3}{\partial x_1^2\partial x_2} + (3C_{16}C_{33}C_{45} - C_{55}(C_{12}C_{33} \\ &- C_{13}C_{45}(3C_{36} + C_{45}) + C_{13}(C_{23} + C_{44})C_{55} - C_{55}(C_{12}C_{33} \\ &- 2C_{36}^2 + 2C_{33}C_{66})) \frac{\partial^3 u_3}{\partial x_1\partial x_2^2} - (-C_{13}^2C_{45} + C_{11}C_{33}C_{45} \\ &- C_{16}C_{33}C_{55} + C_{13}C_{36}C_{55}) \frac{\partial^3 u_3}{\partial x_1\partial x_2^2} \\ &- (-C_{13}C_{24}C_{45} + C_{11}C_{33}C_{45} \\ &- C_{16}C_{33}C_{55} + C_{13}C_{36}C_{55}) \frac{\partial^3 u_3}{\partial x_1\partial x_2^2} \\ &- (-C_{13}C_{24}C_{45} + C_{11}C_{33}C_{45} \\ &- C_{16}C_{33}C_{55} + C_{13}C_{36}C_{55}) \frac{\partial^3 u_3}{\partial x_1\partial x_2^2} \\ &- (-C_{13}C_{45}C_{45} + C_{11}C_{33}C_{45} \\ &- C_{16}C_{33}C_{55} + C_{13}C_{36}C_{55}) \frac{\partial^3 u_3}{\partial x_1\partial x_2^2} \\ &- (-C_{13}C_{45}C_{45} + C_{11}C_{33}C_{45} \\ &- C_{16}C_{33}C_{55} + C_{13}C_{36}C_{55}) \frac{\partial^3 u_3}{\partial x_1\partial x_2^2} \\ &- (-C_{13}C_{45}C_{45} + C_{11}C_{33}C_{45} \\ &- C_{16}C_{33}C_{55} + C_{13}C_{36}C_{55}) \frac{\partial^3 u_3}{\partial x_1\partial x_2^2} \\ &- C_{16}C_{33}$$

$$\begin{split} f_2 &= \frac{1}{2C_{33}(C_{45}^2 - C_{44}C_{55})} \left[-C_{36}^2C_{44} - C_{26}C_{33}C_{45} \right. \\ &+ C_{23}C_{36}C_{45} + C_{33}C_{44}C_{66} \frac{\partial^2 u_1}{\partial x_1^2} + \frac{\partial^2 u_1}{\partial x_2^2} + (C_{26}C_{33}C_{44} \right. \\ &- C_{23}C_{36}C_{44} + C_{23}^2C_{45} - C_{22}C_{33}C_{45}) \frac{\partial^2 u_2}{\partial x_1^2} + \frac{\partial^2 u_2}{\partial x_2^2} \\ &+ 2C_{16}C_{33}C_{44} \frac{\partial^2 u_1}{\partial x_1\partial x_2} - 2C_{13}C_{36}C_{44} \frac{\partial^2 u_1}{\partial x_1\partial x_2} \\ &+ C_{13}C_{23}C_{45} \frac{\partial^2 u_1}{\partial x_1\partial x_2} - C_{12}C_{33}C_{45} \frac{\partial^2 u_1}{\partial x_1\partial x_2} \\ &+ C_{36}^2C_{45} \frac{\partial^2 u_1}{\partial x_1\partial x_2} + C_{36}C_{45}^2 \frac{\partial^2 u_1}{\partial x_1\partial x_2} - C_{36}C_{44}C_{55} \frac{\partial^2 u_1}{\partial x_1\partial x_2} \\ &- C_{33}C_{45}C_{66} \frac{\partial^2 u_1}{\partial x_1\partial x_2} - C_{13}C_{23}C_{44} \frac{\partial^2 u_2}{\partial x_1\partial x_2} \\ &+ C_{12}C_{33}C_{44} \frac{\partial^2 u_2}{\partial x_1\partial x_2} - C_{36}^2C_{44} \frac{\partial^2 u_2}{\partial x_1\partial x_2} \\ &- 2C_{26}C_{33}C_{45} \frac{\partial^2 u_2}{\partial x_1\partial x_2} + 2C_{23}C_{36}C_{45} \frac{\partial^2 u_2}{\partial x_1\partial x_2} \\ &+ C_{23}C_{45}^2 \frac{\partial^2 u_2}{\partial x_1\partial x_2} - C_{23}C_{44}C_{55} \frac{\partial^2 u_2}{\partial x_1\partial x_2} \\ &+ C_{33}C_{44}C_{66} \frac{\partial^2 u_2}{\partial x_1\partial x_2} - C_{13}C_{44}C_{55} \frac{\partial^2 u_2}{\partial x_1\partial x_2} \\ &+ C_{33}C_{44}C_{66} \frac{\partial^2 u_2}{\partial x_1\partial x_2} - C_{13}C_{44}C_{55} \frac{\partial^2 u_1}{\partial x_1\partial x_2} \\ &- C_{16}C_{33}C_{45} \frac{\partial^2 u_1}{\partial x_1\partial x_2} + C_{13}C_{36}C_{45} \frac{\partial^2 u_1}{\partial x_1\partial x_2} + C_{13}C_{45} \frac{\partial^2 u_1}{\partial x_1^2} \\ &- C_{16}C_{33}C_{45} \frac{\partial^2 u_1}{\partial x_1^2} + C_{13}C_{36}C_{45} \frac{\partial^2 u_1}{\partial x_1^2} + C_{13}C_{45} \frac{\partial^2 u_1}{\partial x_1^2} \\ &- C_{16}C_{33}C_{45} \frac{\partial^2 u_1}{\partial x_1^2} + C_{13}C_{36}C_{45} \frac{\partial^2 u_1}{\partial x_1^2} + C_{13}C_{45} \frac{\partial^2 u_1}{\partial x_1^2} \\ &- C_{13}C_{44}C_{55} \frac{\partial^2 u_1}{\partial x_1^2} + (C_{16}C_{33}C_{44} - C_{13}C_{36}C_{44} \\ &+ C_{36}C_{45}(C_{36} + C_{45}) - C_{36}C_{44}C_{55} - C_{33}C_{45}C_{66}) \frac{\partial^2 u_2}{\partial x_1^2} \\ &- C_{13}C_{45}C_{45}(C_{36} + C_{45}) - C_{36}C_{44}C_{55} - C_{33}C_{45}C_{66}) \frac{\partial^2 u_2}{\partial x_1^2} \\ &- C_{13}C_{45}C_{45}(C_{36} + C_{45}) - C_{36}C_{45}C_{55}(C_{45}C_{55}) \frac{\partial^2 u_1}{\partial x_1^2} \\ &- C_{13}C_{45}C_{45}(C_{36} + C_{45}) - C_{36}C_{45}C_{45}(C_{36} + C_{45}) - C_{36}C_{45}C_{45}(C_{36}) \frac{\partial^2 u_1}{\partial x_1^2} \\ &- C$$

$$f_{3} = \frac{1}{2C_{33}(C_{45}^{2} - C_{44}C_{55})} \left[(C_{36}C_{45}(C_{36} + C_{45}) + C_{26}C_{33}C_{55} - C_{36}(C_{23} + C_{44})C_{55} - C_{33}C_{45}C_{66}) \frac{\partial^{2}u_{1}}{\partial x_{1}^{2}} + \frac{\partial^{2}u_{1}}{\partial x_{2}^{2}} - (C_{26}C_{33}C_{45} - C_{23}C_{45}(C_{36} + C_{45}) + C_{22}C_{33}C_{55} - C_{23}(C_{23} + C_{44})C_{55}) \frac{\partial^{2}u_{2}}{\partial x_{1}^{2}} + \frac{\partial^{2}u_{2}}{\partial x_{2}^{2}} - 2C_{16}C_{33}C_{45} \frac{\partial^{2}u_{1}}{\partial x_{1}\partial x_{2}} + 2C_{13}C_{36}C_{45} \frac{\partial^{2}u_{1}}{\partial x_{1}\partial x_{2}} + C_{13}C_{45} \frac{\partial^{2}u_{1}}{\partial x_{1}\partial x_{2}} - C_{13}C_{23}C_{55} \frac{\partial^{2}u_{1}}{\partial x_{1}\partial x_{2}} + C_{12}C_{33}C_{55} \frac{\partial^{2}u_{1}}{\partial x_{1}\partial x_{2}} - C_{13}C_{23}C_{55} \frac{\partial^{2}u_{1}}{\partial x_{1}\partial x_{2}} + C_{33}C_{55} \frac{\partial^{2}u_{1}}{\partial x_{1}\partial x_{2}} + C_{33}C_{55}C_{66} \frac{\partial^{2}u_{1}}{\partial x_{1}\partial x_{2}} + C_{13}C_{23}C_{45} \frac{\partial^{2}u_{2}}{\partial x_{1}\partial x_{2}} - C_{12}C_{33}C_{45} \frac{\partial^{2}u_{2}}{\partial x_{1}\partial x_{2}} + C_{36}C_{45} \frac{\partial^{2}u_{2}}{\partial x_{1}\partial x_{2}} + C_{36}C_{45} \frac{\partial^{2}u_{2}}{\partial x_{1}\partial x_{2}} + C_{36}C_{45} \frac{\partial^{2}u_{2}}{\partial x_{1}\partial x_{2}} + 2C_{26}C_{33}C_{55} \frac{\partial^{2}u_{2}}{\partial x_{1}\partial x_{2}} - 2C_{23}C_{36}C_{55} \frac{\partial^{2}u_{2}}{\partial x_{1}\partial x_{2}} - C_{36}C_{44}C_{55} \frac{\partial^{2}u_{2}}{\partial x_{1}\partial x_{2}} - C_{33}C_{45}C_{66} \frac{\partial^{2}u_{2}}{\partial x_{1}\partial x_{2}} + C_{13}^{2}C_{45} \frac{\partial^{2}u_{1}}{\partial x_{1}^{2}} - C_{13}C_{36}C_{55} \frac{\partial^{2}u_{1}}{\partial x_{1}^{2}} - C_{11}C_{33}C_{45} \frac{\partial^{2}u_{1}}{\partial x_{1}^{2}} + C_{16}C_{33}C_{55} \frac{\partial^{2}u_{1}}{\partial x_{1}^{2}} - C_{13}C_{36}C_{55} \frac{\partial^{2}u_{1}}{\partial x_{1}^{2}} + (-C_{16}C_{33}C_{45} + C_{13}C_{36}C_{45} - C_{36}^{2}C_{55} + C_{33}C_{55}C_{66}) \frac{\partial^{2}u_{2}}{\partial x_{1}^{2}} + (-C_{16}C_{33}C_{45} + C_{13}C_{36}C_{45} - C_{36}^{2}C_{55} + C_{33}C_{55}C_{66}) \frac{\partial^{2}u_{2}}{\partial x_{1}^{2}} \right]$$

Appendix H

Comparison of strain components

Chapter 2 derives a new plate theory named ACI-ESP plate theory. It is worth noting the differences in strains obtained from various plate theories. The normal strains given by different well-known plate theories are compared in Table H.1. Tables H.2 and H.3 compare the transverse and in-plane shear strains. This comparison shows that the ACI-ESP plate theory has the same expressions for the in-plane normal and shear stresses as those provided by the FSDT plate theory. However, in contrast to the FSDT plate theory, the present theory predicts the transverse shear stresses with similar accuracy to that of higher-order plate theories.

Table H.1: Comparison of normal strains $\sigma_{\alpha\alpha}$ in different plate models for cases involving small displacements and rotations only

Plate Model	Normal strain (E_{11})	Normal strain (E_{22})
CLPT [100]	$\frac{\partial u_1}{\partial x_1} - x_3 \frac{\partial^2 u_3}{\partial x_1^2}$	$\frac{\partial u_2}{\partial x_2} - x_3 \frac{\partial^2 u_3}{\partial x_2^2}$
FSDT [100]	$\frac{\partial u_1}{\partial x_1} + x_3 \frac{\partial \phi_1}{\partial x_1}$	$\frac{\partial u_2}{\partial x_2} + x_3 \frac{\partial \phi_2}{\partial x_2}$
ACI-ESL	$\frac{\partial u_1}{\partial x_1} + x_3 \frac{\partial \phi_1}{\partial x_1}$	$\frac{\partial u_2}{\partial x_2} + x_3 \frac{\partial \phi_2}{\partial x_2}$
R-TSDT	$\frac{\partial u_1}{\partial x_1} + x_3 \frac{\partial \phi_1}{\partial x_1}$	$\frac{\partial u_2}{\partial x_2} + x_3 \frac{\partial \phi_2}{\partial x_2}$
[122]	$ -\frac{4}{3} \frac{x_3^2}{h^2} \left(\frac{\partial \phi_1}{\partial x_1} + \frac{\partial^2 u_3}{\partial x_1^2} \right) $	$-\frac{4}{3}\frac{x_3^2}{h^2}\left(\frac{\partial\phi_2}{\partial x_2}+\frac{\partial^2 u_3}{\partial x_2^2}\right)$
G-TSDT	$\frac{\partial u_1}{\partial x_1} + x_3 \frac{\partial \phi_1}{\partial x_1}$	$\frac{\partial u_2}{\partial x_2} + x_3 \frac{\partial \phi_2}{\partial x_2}$
[118]	$+\left(\frac{x_3}{4}-\frac{5x_3^3}{3h^2}\right)\left(\frac{\partial\phi_1}{\partial x_1}+\frac{\partial^2u_3}{\partial x_1^2}\right)$	$+\left(\frac{x_3}{4}-\frac{5x_3^3}{3h^2}\right)\left(\frac{\partial\phi_2}{\partial x_2}+\frac{\partial^2u_3}{\partial x_2^2}\right)$

Appendix H 165

Table H.2: Comparison of transverse shear strains $\sigma_{\alpha 3}$ in different plate models for cases involving small displacements and rotations only

Plate Model	Shear strain $(2E_{23})$	Shear strain $(2E_{13})$
CLPT [100]	0	0
FSDT [100]	$\left(\phi_2 + \frac{\partial u_3}{\partial x_2}\right)$	$\left(\phi_1 + \frac{\partial u_3}{\partial x_1}\right)$
ACI-ESL	$\frac{5(h^2 - 4x_3^2)}{4h^2} \left(\phi_2 + \frac{\partial u_3}{\partial x_2}\right)$	$\frac{5(h^2-4x_3^2)}{4h^2}\left(\phi_1+\frac{\partial u_3}{\partial x_1}\right)$
R-TSDT	$\frac{(h^2 - 4x_3^2)}{h^2} \left(\phi_2 + \frac{\partial u_3}{\partial x_2} \right)$	$\frac{(h^2-4x_3^2)}{h^2}\left(\phi_1+\frac{\partial u_3}{\partial x_1}\right)$
[122]	$\frac{1}{h^2} \left(\phi_2 + \frac{1}{\partial x_2} \right)$	$\frac{1}{h^2} \left(\varphi_1 + \frac{1}{\partial x_1} \right)$
G-TSDT	$5(h^2-4x_3^2)$ $\left(\begin{array}{ccc} 1 & 1 & \partial u_3 \end{array}\right)$	$5(h^2-4x_3^2)$ $\left(\begin{array}{ccc} 1 & 1 & \partial u_3 \end{array}\right)$
[118]	$\frac{5(h^2 - 4x_3^2)}{4h^2} \left(\phi_2 + \frac{\partial u_3}{\partial x_2}\right)$	$\frac{5(h^2 - 4x_3^2)}{4h^2} \left(\phi_1 + \frac{\partial u_3}{\partial x_1} \right)$

Table H.3: Comparison of in-plane shear strains σ_{12} in different plate models for cases involving small displacements and rotations only

Plate Model	Shear strain $(2E_{12})$
CLPT [100]	$\frac{\partial u_1}{\partial x_2} + \frac{\partial u_2}{\partial x_1} - x_3 \left(\frac{\partial^2 u_3}{\partial x_1 \partial x_2} \right)$
FSDT [100]	$\frac{\partial u_1}{\partial x_2} + \frac{\partial u_2}{\partial x_1} + x_3 \left(\frac{\partial \phi_1}{\partial x_2} + \frac{\partial \phi_2}{\partial x_1} \right)$
ACI-ESL	$\frac{\partial u_1}{\partial x_2} + \frac{\partial u_2}{\partial x_1} + x_3 \left(\frac{\partial \phi_1}{\partial x_2} + \frac{\partial \phi_2}{\partial x_1} \right)$
R-TSDT [122]	$ \frac{\partial u_1}{\partial x_2} + \frac{\partial u_2}{\partial x_1} \\ + x_3 \left(\frac{\partial \phi_1}{\partial x_2} + \frac{\partial \phi_2}{\partial x_1} \right) \\ - \frac{4}{3} \frac{x_3^2}{h^2} \left(\frac{\partial \phi_1}{\partial x_2} + \frac{\partial^2 u_3}{\partial x_1 \partial x_2} \right) \\ - \frac{4}{3} \frac{x_3^2}{h^2} \left(\frac{\partial \phi_2}{\partial x_1} + \frac{\partial^2 u_3}{\partial x_1 \partial x_2} \right) $
G-TSDT [118]	$ \frac{\partial u_1}{\partial x_2} + \frac{\partial u_2}{\partial x_1} \\ + x_3 \left(\frac{\partial \phi_1}{\partial x_2} + \frac{\partial \phi_2}{\partial x_1} \right) \\ + \left(\frac{x_3}{4} - \frac{5x_3^3}{3h^2} \right) \left(\frac{\partial \phi_1}{\partial x_2} + \frac{\partial^2 u_3}{\partial x_1 \partial x_2} \right) \\ + \left(\frac{x_3}{4} - \frac{5x_3^3}{3h^2} \right) \left(\frac{\partial \phi_2}{\partial x_1} + \frac{\partial^2 u_3}{\partial x_1 \partial x_2} \right) $

Expressions g_2^r , g_3^r , f_2^r and f_3^r

As we continue to perturb the solution for increased accuracy, we encounter bulky expressions containing higher-order derivatives of u_1, u_2 and u_3 . These bulky expressions are replaced in Chapter 3 with two-dimensional functions f_2^r, f_3^r, g_2^r and g_3^r . This is done to make the equations more concise. The details of these replacements are provided in this appendix.

As shown in Chapter 3, the third-order solution results in the following Euler-Lagrange equations.

$$C_{55}^{r} \left(\frac{\partial}{\partial x_{3}}\right)^{2} {}^{3}v_{1}^{r} + C_{45}^{r} \left(\frac{\partial}{\partial x_{3}}\right)^{2} {}^{3}v_{2}^{r} = 2C_{55}^{r} f_{2}^{r} + 6C_{55}^{r} x_{3} g_{2}^{r} + 2C_{45}^{r} f_{3}^{r} + 6C_{45}^{r} x_{3} g_{3}^{r}$$

$$C_{45}^{r} \left(\frac{\partial}{\partial x_{3}}\right)^{2} {}^{3}v_{1}^{r} + C_{44}^{r} \left(\frac{\partial}{\partial x_{3}}\right)^{2} {}^{3}v_{2}^{r} = 2C_{45}^{r} f_{2}^{r} + 6C_{45}^{r} x_{3} g_{2}^{r} + 2C_{44}^{r} f_{3}^{r} + 6C_{44}^{r} x_{3} g_{3}^{r}$$

$$C_{33}^{r} \left(\frac{\partial}{\partial x_{3}}\right)^{2} {}^{3}v_{2}^{r} = 0$$
(I.1)

Where f_2^r , f_3^r , g_2^r and g_3^r are functions of x_1 and x_2 . The expressions for these functions in terms of derivatives of u_i w.r.t. x_j and the material constants are given below

$$\begin{split} g_2^r &= \frac{1}{6C_{33}^r \{(C_{45}^r)^2 - C_{44}^r C_{55}^r\}} \left[\left\{ -C_{26}^r C_{33}^r C_{44}^r + C_{23}^r C_{36}^r C_{44}^r \right. \right. \\ &- (C_{23}^r)^2 (C_{45}^r)^2 + C_{22}^r C_{33}^r (C_{45}^r)^2 \right\} \frac{\partial^3 u_3}{\partial x_1^3} + 3 \frac{\partial^3 u_3}{\partial x_1 \partial x_2^2} \\ &- \left\{ C_{13}^r C_{23}^r C_{44}^r - (C_{12}^r)^2 C_{33}^r C_{44}^r + 2(C_{36}^r)^2 C_{44}^r + 3 C_{26}^r C_{33}^r C_{45}^r \right. \\ &- 3 C_{23}^r C_{36}^r C_{45}^r - (C_{23}^r)^2 (C_{45}^r)^2 + C_{23}^r C_{44}^r C_{55}^r - 2 C_{33}^r C_{44}^r (C_{66}^r) \right\} \frac{\partial^3 u_3}{\partial x_1^2 \partial x_2} \\ &+ \left\{ - 3 C_{16}^r C_{33}^r C_{44}^r + 3 C_{13}^r C_{36}^r C_{44}^r - C_{13}^r (C_{23}^r)^2 C_{45}^r + (C_{12}^r)^2 C_{33}^r C_{45}^r \right. \\ &- 2 (C_{36}^r)^2 C_{45}^r - 2 C_{36}^r (C_{45}^r)^2 + 2 C_{36}^r C_{44}^r C_{55}^r + 2 C_{33}^r C_{45}^r C_{66}^r \right\} \frac{\partial^3 u_3}{\partial x_1 \partial x_2^2} \\ &+ \left\{ C_{13}^r (C_{13}^r)^2 C_{44}^r - (C_{11}^r)^2 C_{33}^r C_{44}^r + C_{16}^r C_{33}^r C_{45}^r - C_{13}^r C_{45}^r (C_{36}^r + C_{45}^r) \right. \\ &+ \left. C_{13}^r C_{44}^r C_{55}^r \right\} \frac{\partial^3 u_3}{\partial x_2^3} \right] \\ g_3^r &= \frac{1}{6 C_{33}^r \{(C_{45}^r)^2 - C_{44}^r C_{55}^r \}} \left[\left\{ - C_{26}^r C_{33}^r C_{45}^r + C_{23}^r C_{45}^r (C_{36}^r + C_{45}^r) \right. \\ &- \left. C_{12}^r C_{13}^r C_{15}^r + C_{23}^r (C_{23}^r + C_{44}^r) C_{55}^r \right\} \frac{\partial^3 u_3}{\partial x_1^3} + 3 \frac{\partial^3 u_3}{\partial x_1 \partial x_2^2} \\ &- \left\{ - C_{13}^r C_{23}^r C_{45}^r + (C_{12}^r)^2 C_{33}^r C_{45}^r - 2(C_{36}^r)^2 C_{45}^r - 2C_{36}^r C_{45}^r^2 - C_{36}^r C_{45}^r \right. \\ &- \left. 3 C_{26}^r C_{33}^r C_{55}^r + 3 C_{23}^r C_{36}^r C_{55}^r + 2 C_{36}^r C_{44}^r C_{55}^r \right. \\ &- \left. 2 C_{13}^r C_{45}^r C_{16}^r \right\} \frac{\partial^3 u_3}{\partial x_1^2 \partial x_2} + \left\{ 3 C_{16}^r C_{33}^r C_{45}^r - C_{15}^r C_{12}^r C_{33}^r C_{45}^r - C_{15}^r C_{15}^$$

$$\begin{split} f_2^r &= \frac{1}{2C_{33}^r \left\{ (C_{45}^r)^2 - C_{44}^r C_{55}^r \right\}} \left[- (C_{36}^r)^2 C_{44}^r - C_{26}^r C_{33}^r C_{45}^r \right. \\ &+ C_{23}^r C_{36}^r C_{45}^r + C_{33}^r C_{44}^r C_{66}^r \frac{\partial^2 u_1}{\partial x_1^2} + \frac{\partial^2 u_1}{\partial x_2^2} + \left\{ C_{26}^r C_{33}^r C_{44}^r \right. \\ &- C_{23}^r C_{36}^r C_{44}^r + (C_{23}^r)^2 C_{45}^r - C_{22}^r C_{33}^r C_{45}^r \right\} \frac{\partial^2 u_2}{\partial x_1^2} + \frac{\partial^2 u_2}{\partial x_2^2} \\ &+ 2C_{16}^r C_{33}^r C_{44}^r \frac{\partial^2 u_1}{\partial x_1 \partial x_2} - 2C_{13}^r C_{36}^r C_{44}^r \frac{\partial^2 u_1}{\partial x_1 \partial x_2} \\ &+ C_{13}^r C_{23}^r C_{45}^r \frac{\partial^2 u_1}{\partial x_1 \partial x_2} - C_{12}^r C_{33}^r C_{45}^r \frac{\partial^2 u_1}{\partial x_1 \partial x_2} \\ &+ C_{36}^r C_{45}^r \frac{\partial^2 u_1}{\partial x_1 \partial x_2} - C_{12}^r C_{33}^r C_{45}^r \frac{\partial^2 u_1}{\partial x_1 \partial x_2} \\ &+ C_{36}^r C_{45}^r \frac{\partial^2 u_1}{\partial x_1 \partial x_2} + C_{36}^r (C_{45}^r)^2 \frac{\partial^2 u_1}{\partial x_1 \partial x_2} - C_{36}^r C_{44}^r C_{55}^r \frac{\partial^2 u_1}{\partial x_1 \partial x_2} \\ &- C_{33}^r C_{45}^r C_{66}^r \frac{\partial^2 u_1}{\partial x_1 \partial x_2} - C_{13}^r C_{23}^r C_{44}^r \frac{\partial^2 u_2}{\partial x_1 \partial x_2} \\ &+ C_{12}^r C_{33}^r C_{45}^r \frac{\partial^2 u_2}{\partial x_1 \partial x_2} - (C_{36}^r)^2 C_{44}^r \frac{\partial^2 u_2}{\partial x_1 \partial x_2} \\ &+ C_{12}^r C_{33}^r C_{45}^r \frac{\partial^2 u_2}{\partial x_1 \partial x_2} + 2C_{23}^r C_{36}^r C_{45}^r \frac{\partial^2 u_2}{\partial x_1 \partial x_2} \\ &+ C_{23}^r (C_{45}^r)^2 \frac{\partial^2 u_2}{\partial x_1 \partial x_2} - C_{23}^r C_{44}^r C_{55}^r \frac{\partial^2 u_2}{\partial x_1 \partial x_2} \\ &+ C_{33}^r C_{44}^r C_{66}^r \frac{\partial^2 u_2}{\partial x_1 \partial x_2} - (C_{13}^r)^2 C_{44}^r \frac{\partial^2 u_1}{\partial x_1^2} + C_{17}^r C_{33}^r C_{44}^r \frac{\partial^2 u_1}{\partial x_1^2} \\ &+ C_{36}^r C_{44}^r C_{66}^r \frac{\partial^2 u_2}{\partial x_1 \partial x_2} - (C_{13}^r)^2 C_{44}^r \frac{\partial^2 u_1}{\partial x_1^2} + C_{17}^r C_{33}^r C_{44}^r \frac{\partial^2 u_1}{\partial x_1^2} \\ &- C_{16}^r C_{33}^r C_{45}^r \frac{\partial^2 u_1}{\partial x_1^2} + C_{13}^r C_{36}^r C_{45}^r \frac{\partial^2 u_1}{\partial x_1^2} + C_{13}^r C_{45}^r \frac{\partial^2 u_1}{\partial x_1^2} \\ &- C_{16}^r C_{33}^r C_{45}^r \frac{\partial^2 u_1}{\partial x_1^2} + \left\{ C_{16}^r C_{33}^r C_{44}^r - C_{13}^r C_{36}^r C_{44}^r \right\} \\ &- C_{13}^r C_{44}^r C_{55}^r \frac{\partial^2 u_1}{\partial x_1^2} + \left\{ C_{16}^r C_{33}^r C_{44}^r - C_{13}^r C_{36}^r C_{44}^r \right\} \\ &- C_{13}^r C_{45}^r C_{45}^r C_{45}^r C_{45}^r C_{45}^r C_{45}^r C_{45}^r C_{45}^r$$

$$\begin{split} f_3^r &= \frac{1}{2C_{33}^r \left\{ (C_{45}^r)^2 - C_{44}^r C_{55}^r \right\}} \left[(C_{36}^r C_{45}^r (C_{36}^r + C_{45}^r) + C_{26}^r C_{33}^r C_{55}^r \right. \\ &- C_{36}^r (C_{23}^r + C_{44}^r) C_{55}^r - C_{33}^r C_{45}^r C_{66}^r) \frac{\partial^2 u_1}{\partial x_1^2} + \frac{\partial^2 u_1}{\partial x_2^2} \\ &- (C_{26}^r C_{33}^r C_{45}^r - C_{23}^r C_{45}^r (C_{36}^r + C_{45}^r) + (C_{22}^r)^2 C_{33}^r C_{55}^r \\ &- C_{23}^r (C_{23}^r + C_{44}^r) C_{55}^r) \frac{\partial^2 u_2}{\partial x_1^2} + \frac{\partial^2 u_2}{\partial x_2^2} - 2C_{16}^r C_{33}^r C_{45}^r \frac{\partial^2 u_1}{\partial x_1 \partial x_2} \\ &+ 2C_{13}^r C_{36}^r C_{45}^r \frac{\partial^2 u_1}{\partial x_1 \partial x_2} + (C_{13}^r)^2 C_{45}^r \frac{\partial^2 u_1}{\partial x_1 \partial x_2} \\ &- C_{13}^r C_{23}^r C_{55}^r \frac{\partial^2 u_1}{\partial x_1 \partial x_2} + (C_{12}^r)^2 C_{33}^r C_{55}^r \frac{\partial^2 u_1}{\partial x_1 \partial x_2} \\ &- (C_{36}^r)^2 C_{55}^r \frac{\partial^2 u_1}{\partial x_1 \partial x_2} - C_{13}^r C_{44}^r C_{55}^r \frac{\partial^2 u_1}{\partial x_1 \partial x_2} + C_{33}^r C_{55}^r (C_{66}^r)^2 \frac{\partial^2 u_1}{\partial x_1 \partial x_2} \\ &+ C_{13}^r C_{23}^r C_{45}^r \frac{\partial^2 u_2}{\partial x_1 \partial x_2} - (C_{12}^r)^2 C_{33}^r C_{45}^r \frac{\partial^2 u_2}{\partial x_1 \partial x_2} + (C_{36}^r)^2 C_{45}^r \frac{\partial^2 u_2}{\partial x_1 \partial x_2} \\ &+ C_{13}^r C_{23}^r C_{45}^r \frac{\partial^2 u_2}{\partial x_1 \partial x_2} - C_{12}^r C_{23}^r C_{45}^r \frac{\partial^2 u_2}{\partial x_1 \partial x_2} + (C_{36}^r)^2 C_{45}^r \frac{\partial^2 u_2}{\partial x_1 \partial x_2} \\ &+ C_{36}^r C_{45}^r (C_{36}^r + C_{45}^r) \frac{\partial^2 u_2}{\partial x_1 \partial x_2} - C_{36}^r C_{44}^r C_{55}^r \frac{\partial^2 u_2}{\partial x_1 \partial x_2} - C_{33}^r C_{45}^r \frac{\partial^2 u_2}{\partial x_1 \partial x_2} \\ &- 2C_{23}^r C_{36}^r C_{55}^r \frac{\partial^2 u_2}{\partial x_1 \partial x_2} - C_{36}^r C_{44}^r C_{55}^r \frac{\partial^2 u_2}{\partial x_1 \partial x_2} - C_{33}^r C_{45}^r (C_{66}^r)^2 \frac{\partial^2 u_2}{\partial x_1 \partial x_2} \\ &+ (C_{13}^r)^2 C_{45}^r \frac{\partial^2 u_1}{\partial x_1^2} - (C_{11}^r)^2 C_{33}^r C_{45}^r \frac{\partial^2 u_1}{\partial x_1^2} + C_{16}^r C_{33}^r C_{55}^r \frac{\partial^2 u_1}{\partial x_1^2} \\ &- C_{13}^r C_{36}^r C_{55}^r \frac{\partial^2 u_1}{\partial x_1^2} + \left\{ - (C_{16}^r C_{33}^r C_{45}^r + C_{13}^r C_{36}^r C_{45}^r \\ &- (C_{36}^r)^2 C_{55}^r + C_{33}^r C_{55}^r (C_{66}^r)^2 \right\} \frac{\partial^2 u_2}{\partial x_1^2} \\ &- (C_{36}^r)^2 C_{55}^r + C_{33}^r C_{55}^r (C_{66}^r)^2 \right\} \frac{\partial^2 u_2}{\partial x_1^2} \end{aligned}$$